Cell Journal (Yakhteh)

Guide for Authors

Aims and Scope: The "Cell Journal (Yakhteh)" is a peer review and monthly English publication of Royan Institute of Iran. The aim of the journal is to disseminate information through publishing the most recent scientific research studies on exclusively Cellular, Molecular and other related topics. **Cell J**, has been certified by the Ministry of Culture and Islamic Guidance since 1999 and also accredited as a scientific and research journal by HBI (Health and Biomedical Information) Journal Accreditation Commission since 2000 which is an open access journal. **This journal holds the membership of the Committee on Publication Ethics (COPE).**

1. Types of articles

The articles in the field of Cellular and Molecular can be considered for publications in **Cell J.** These articles are as below:

A. Original articles

Original articles are scientific reports of the original research studies. The article consists of English Abstract (structured), Introduction, Materials and Methods, Results, Discussion, Conclusion, Acknowledgements, Author's Contributions, and References **(Up to 40).**

B. Review articles

Review articles are the articles written by well experienced authors and those who have excellence in the related fields. The corresponding author of the review article must be one of the authors of at least three published articles appearing in the references. The review article consists of English Abstract (unstructured), Introduction, Conclusion, Author's Contributions, and References **(Up to 70).**

C. Systematic Reviews

Systematic reviews are a type of literature review that collect and critically analyzes multiple research studies or papers. The Systematic reviews consist of English Abstract (unstructured), Introduction, Materials and Methods, Results, Discussion, Conclusion, Acknowledgements, Author's Contributions, and References **(Up to 70).**

D. Short communications

Short communications are articles containing new findings. Submissions should be brief reports of ongoing researches. The short communication consists of English Abstract (unstructured), the body of the manuscript (should not hold heading or subheading), Acknowledgements, Author's Contributions, and References **(Up to 30).**

E. Case reports

Case reports are short discussions of a case or case series with unique features not previously described which make an important teaching point or scientific observation. They may describe novel techniques or use equipment, or new information on diseases of importance. It consists of English Abstracts (Unstructured), Introduction, Case Report, Discussion, Acknowledgements, Author's Contributions, and References **(Up to 30).**

F. Editorial

Editorials are articles should be written in relevant and new data of journals' filed by either the editor in chief or the editorial board.

G. Imaging in biology

Images in biology should focus on a single case with an interesting illustration such as a photograph, histological specimen or investigation. Color images are welcomed. The text should be brief and informative.

H. Letter to the editors

Letter to the editors are in response to previously published **Cell J** articles, and may also include interesting cases that do not meet the requirement of being truly exceptional, as well as other brief technical or clinical notes of general interest.

I. Debate

Debates are articles which show a discussion of the positive and negative view of the author concerning all aspect of the issue relevant to scientific research.

2. Submission process

It is recommended to see the guidelines for reporting different kinds of manuscripts. This guide explains how to prepare the

manuscript for submission. Before submitting, we suggest authors to familiarize themselves with **Cell J** format and content by reading the journal via the website (www.celljournal.com). The corresponding author ensures that all authors are included in the author list and agree with its order, and they must be aware of the manuscript submission.

A. Author contributions statements

It is essential for authors to include a statement of responsibility in the manuscript that specifies the contribution of every one of them. This participation must include conception and design of the manuscript, data acquisition or data analysis and interpretation, drafting of the manuscript and/or revising it for critically important intellectual content, revision and final approval of the manuscript and statistical analysis, obtaining funding, administrative, technical, or material support, or supervision. Authors who do not meet the above criteria should be acknowledged in the **Acknowledgments section.**

B. Cover letter and copyright

Each manuscript should be accompanied by a cover letter, signed by all authors specifying the following statement: "The manuscript has been seen and approved by all authors and is not under active consideration for publication. It has neither been accepted for publication nor published in another journal fully or partially (except in abstract form). **Also, no manuscript would be accepted in case it has been pre-printed or submitted to other websites.** I hereby assign the copyright of the enclosed manuscript to **Cell J.**" Corresponding author must confirm the proof of the manuscript before online publishing. Also, it is needed to suggest three peer reviewers in the field of their manuscript.

C. Manuscript preparation

Authors whose first language is not English encouraged to consult a native English speaker in order to confirm his manuscripts to American or British (not a mixture) English usage and grammar. It is necessary to mention that we will check the plagiarism of your manuscript by iThenticate Software. The manuscript should be prepared in accordance with the "International Committee of Medical Journal Editors (ICMJE)". Please send your manuscript in two formats word and PDF (including: title, name of all the authors with their degree, abstract, full text, references, tables and figures) and also send tables and figures separately in the site. The abstract and text pages should have consecutive line numbers in the left margin beginning with the title page and continuing through the last page of the written text. Each abbreviation must be defined in the abstract and text when they are mentioned for the first time. Avoid using abbreviation in the title. Please use the international and standard abbreviations and symbols

It should be added that an essential step toward the integration and linking of scientific information reported in published literature is using standardized nomenclature in all fields of science and medicine. Species names must be italicized (*e.g., Homo sapiens*) and also the full genus and species written out in full, both in the title of the manuscript and at the first mention of an organism in a paper.

It is necessary to mention that genes, mutations, genotypes, and alleles must be indicated in italics. Please use the recommended name by consulting the appropriate genetic nomenclature database, e.g., HUGO for human genes. In another words; if it is a human gene, you must write all the letters in capital and italic (*e.g., OCT4, c-MYC*). If not, only write the first letter in capital and italic (*e.g., Oct4, c-Myc*). **In addition, protein designations are the same as the gene symbol but are not italicized.**

Of note, Cell J will only consider publishing genetic association study papers that are novel and statistically robust. Authors are advised to adhere to the recommendations outlined in the STREGA statement (http://www.strega-statement.org). The following criteria must be met for all submissions:

1. Hardy-Weinberg Equilibrium (HWE) calculations must be carried out and reported along with the P-values if applicable [see Namipashaki et al. 2015 (Cell J, Vol 17, N 2, Pages: 187-192) for a discussion].

2. Linkage disequilibrium (LD) structure between SNPs (if multiple SNPs are reported) must be presented.

3. Appropriate multiple testing correction (if multiple independent SNPs are reported) must be included.

Submissions that fail to meet the above criteria will be rejected before being sent out for review.

Each of the following manuscript components should begin in the following sequence:

Authors' names and order of them must be carefully considered (full name(s), highest awarded academic degree(s), email(s), and institutional affiliation(s) of all the authors in English. Also, you must send mobile number and full postal address of the corresponding author).

Changes to Authorship such as addition, deletion or rearrangement of author names must be made only before the manuscript has been accepted in the case of approving by the journal editor. In this case, the corresponding author must explain the reason of changing and confirm them (which has been signed by all authors of the manuscript). If the manuscript has already been published in an online issue, an erratum is needed.

Title is providing the full title of the research (do not use abbreviations in title).

Running title is providing a maximum of 7 words (no more than 50 characters).

Abstract must include Objective, Materials and Methods, Results, and Conclusion (no more than 300 words).

Keywords, three to five, must be supplied by the authors at the foot of the abstract chosen from the Medical Subject Heading (MeSH). Therefore; they must be specific and relevant to the paper.

The following components should be identified after the abstract:

Introduction: The Introduction should provide a brief background to the subject of the paper, explain the importance of the study, and state a precise study question or purpose.

Materials and Methods: It includes the exact methods or observations of experiments. If an apparatus is used, its manufacturer's name and address should be stipulated in parenthesis. If the method is established, give reference but if the method is new, give enough information so that another author can perform it. If a drug is used, its generic name, dose, and route of administration must be given. Standard units of measurements and chemical symbols of elements do not need to be defined.

Statistical analysis: Type of study and statistical methods should be mentioned and specified by any general computer program used.

Ethical considerations*:* Please state that informed consent was obtained from all human adult participants and from the parents or legal guardians of minors and include the name of the appropriate institutional review board that approved the project. It is necessary to indicate in the text that the maintenance and care of experimental animals complies with National Institutes of Health guidelines for the humane use of laboratory animals, or those of your Institute or agency.

Clinical trial registration: All of the Clinical Trials performing in Iran must be registered in Iranian Registry of Clinical Trials (www.irct.ir). The clinical trials performed abroad, could be considered for publication if they register in a registration site approved by WHO or www.clinicaltrials.gov. If you are reporting phase II or phase III randomized controlled trials, you must refer to the CONSORT Statement for recommendations to facilitate the complete and transparent reporting of trial findings. Reports that do not conform to the CONSORT guidelines may need to be revised before peer-reviewing.

Results: They must be presented in the form of text, tables, and figures. Take care that the text does not repeat data that are presented in tables and/or figures. Only emphasize and summarize the essential features of the main results. Tables and figures must be numbered consecutively as appeared in the text and should be organized in separate pages at the end of the manuscript while their location should be mentioned in the main text.

Tables and figures: If the result of your manuscript is too short, it is better to use the text instead of tables & figures. Tables should have a short descriptive heading above them and also any footnotes. Figure's caption should contain a brief title for the whole figure and continue with a short explanation of each part and also the symbols used (no more than 100 words). All figures must be prepared based on cell journal's guideline in color (no more than 6 Figures and Tables) and also in TIF format with 300 DPI resolution.

Of Note: Please put the tables & figures of the result in the results section not any other section of the manuscript.

Supplementary materials would be published on the online version of the journal. This material is important to the understanding and interpretation of the report and should not repeat material within the print article. The amount of supplementary material should be limited. Supplementary material should be original and not previously published and will undergo editorial and peer review with the main manuscript. Also, they must be cited in the manuscript text in parentheses, in a similar way as when citing a figure or a table. Provide a caption for each supplementary material submitted.

Discussion: It should emphasize the present findings and the variations or similarities with other researches done by other researchers. The detailed results should not be repeated in the discussion again. It must emphasize the new and important aspects of the study.

Conclusion: It emphasizes the new and important aspects of the study. All conclusions are justified by the results of the study.

Acknowledgements: This part includes a statement thanking those who contributed substantially with work relevant to the study but does not have authorship criteria. It includes those who provided technical help, writing assistance and name of departments that provided only general support. You must mention financial support in the study. Otherwise; write this sentence "There is no financial support in this study".

Conflict of interest: Any conflict of interest (financial or otherwise) and sources of financial support must be listed in the Acknowledgements. It includes providers of supplies and services from a commercial organization. Any commercial affiliation must be disclosed, regardless of providing the funding or not.

Of Note: If you have already any patent related to the subject of your manuscript, or you are going to apply for such a patent, it must be mentioned in this part.

References: The references must be written based on the Vancouver style. Thus the references are cited numerically in the text and listed in the bibliography by the order of their appearance. The titles of journals must be abbreviated according to the style used in the list of Journals Indexed in PubMed. Write surname and initials of all authors when there are six or less. In the case of seven or more authors, the names of the first six authors followed by "et al." must be listed. You can download Endnote file for Journal references style: endnote file

The reference of information must be based on the following order:

Article:

Surname(s) and first letter of name &middle name(s) of author(s) .Manuscript title. Journal title (abbr).publication date (year); Volume & Issue: Page number.

Example: Manicardi GC, Bianchi PG, Pantano S, Azzoni P, Bizzaro D, Bianchi U, et al. Presence of endogenous nicks in DNA of ejaculated human spermatozoa and its relationship to chromomycin A3 accessibility. Biol Reprod. 1995; 52(4): 864-867.

Book:

Surname(s) and first letter of name & middle name(s) of author(s).Book title. Edition. Publication place: publisher name; publication date (year); Page number.

Example: Edelman CL, Mandle CL. Health promotion throughout the lifespan. 2nd ed. ST Louis: Mosby; 1998; 145-163.

Chapter of book:

Surname(s) and first letter of name & middle name(s) of author(s).Chapter title. In: Surname(s) and first letter of name & middle name(s) of editor(s), editors. Book title. Edition. Publication place: publisher name; publication date (year); Page number.

Example: Phillips SJ, Whisnant JP. Hypertension and stroke. In: Laragh JH, Brenner BM, editors. Hypertension: pathophysiology, diagnosis, and management. 2nd ed. New York: Raven Press; 1995; 465-478.

Abstract book:

Example: Amini rad O.The antioxidant effect of pomegranate juice on sperm parameters and fertility potential in mice. Cell J. 2008;10 Suppl 1:38.

Thesis:

Name of author. Thesis title. Degree. City name. University. Publication date (year).

Example: Eftekhari Yazdi P. Comparison of fragment removal and co-culture with Vero cell monolayers on development of human fragmented embryos. Presented for the Ph.D., Tehran. Tarbiyat Modarres University. 2004.

Internet references

Article:

Example: Jahanshahi A, Mirnajafi-Zadeh J, Javan M, Mohammad-Zadeh M, Rohani M. Effect of low-frequency stimulation on adenosineA1 and A2A receptors gene expression in dentate gyrus of perforant path kindled rats. Cell J. 2008; 10 (2): 87-92. Available from: http://www.celljournal.org. (20 Oct 2008).

Book:

Example: Anderson SC, Poulsen KB. Anderson's electronic atlas of hematology.[CD-ROM]. Philadelphia: Lippincott Williams & Wilkins; 2002.

D. Proofs are sent by email as PDF files and should be checked and returned within 72 hours of receipt. It is the authors' responsibility to check that all the text and data as contained in the page proofs are correct and suitable for publication. **We are requested to pay particular attention to author's names and affiliations as it is essential that these details be accurate when the article is published.**

E. Pay for publication: Publishing an article in **Cell J** requires Article Processing Charges (APC) that will be billed to the submitting author following the acceptance of an article for publication. For more information please see www.celljournal.org.

F. Ethics of scientific publication: Manuscripts that have been published elsewhere with the same intellectual material will refer to duplicate publication. If authors have used their own previously published work or work that is currently under review, as the basis for a submitted manuscript, they are required to cite the previous work and indicate how their submitted manuscript offers novel contributions beyond those of the previous work. Research and publication misconduct is considered a serious breach of ethics.

The Journal systematically employs iThenticate, plagiarism detection and prevention software designed to ensure the originality of written work before publication. Plagiarism of text from a previously published manuscript by the same or another author is a serious publication offence. Some parts of text may be used, only where the source of the quoted material is clearly acknowledged.

3. General information

A. You can send your manuscript via online submission system which is available on our website. If the manuscript is not prepared according to the format of **Cell J**, it will be returned to authors.

B. The order of article appearance in the Journal is not demonstrating the scientific characters of the authors.

C. Cell J has authority to accept or reject the manuscript.

D. The received manuscript will be evaluated by associate editor. **Cell J** uses a single-blind peer review system and if the manuscript suits the journal criteria, we select the reviewers. If three reviewers pass their judgments on the manuscript, it will be presented to the editorial board of **Cell J.** If the editorial board has a positive judgment about the manuscript, reviewers' comments will be presented to the corresponding author (the identification of the reviewers will not be revealed). The executive member of journal will contact the corresponding author directly within 3-4 weeks by email. If authors do not receive any reply from journal office after the specified time, they can contact journal office. Finally, executive manager will respond promptly to authors' request.

The Final Checklist

The authors must ensure that before submitting the manuscript for publication, they have to consider the following parts:

1. The first page of manuscript should contain title, name of the author/coauthors, their academic qualifications, designation & institutions they are affiliated with, mailing address for future correspondence, email address, phone, and fax number.

2. Text of manuscript and References prepared as stated in the "guide for authors" section.

3. Tables should be on a separate page. Figures must be sent in color and also in JPEG (Jpg) format.

4. Cover Letter should be uploaded with the signature of all authors.

5. An ethical committee letter should be inserted at the end of the cover letter.

The Editor-in-Chief: Ahmad Hosseini, Ph.D.

Cell Journal *(Yakhteh)*

P.O. Box: 16635-148, Iran

Tel/Fax: + 98-21-22510895

Emails: Celljournal@royaninstitute.org

info@celljournal.org

IN THE NAME OF GOD

Dr. Saeed Kazemi Ashtiani

Gone But not Forgotten

In the memory of the late Director of Royan Institute, Founder of Stem Cells Research in Iran and Chairman of ***Cell Journal*** *(Yakhteh)*. May he rest in peace.

PUBLISHED & SPONSORED BY:
Publication of Royan Institute (ACECR)

Indexed in:
1. Thomson Reuters (ISI)
2. PubMed
3. PubMed Central (PMC)
4. National Library Medicine (NLM)
5. Biosis Preview
6. Index Medicus for the Eastern Mediterranean Region (IMEMR)
7. Regional Information Center for Sciences and Technology (RICeST)
8. Index Copernicus International
9. Cambridge Scientific Abstract (CSA)
10. EMBASE
11. Scopus
12. Cinahl Database
13. Google Scholar
14. Chemical Abstract Service (CAS)
15. Proquest
16. Directory of Open Access Journals (DOAJ)
17. Open Academic Journals Index (OAJI)
18. Directory of Research Journals Indexing (DRJI)
19. Scientific Information Database (SID)
20. Iranmedex
21. Islamic World Science Citation Center (ISC)
22. Magiran
23. Science Library Index
24. Biological Abstracts
25. Essential Science Indicators
26. EuroPub

ACECR

Editorial Office Address (Dr. Ahmad Hosseini):
Royan Institute, P.O.Box: 16635-148,
Tehran, Iran
Tel & Fax: (+9821)22510895
Website: www.celljournal.org
Emails: info@celljournal.org
celljournal@royaninstitute.org

Printing Company:
Naghshe e Johar Co.
No. 103, Fajr alley, Tehranpars Street,
Tehran, Iran.

Cell Journal$_{(Yakhteh)}$, Vol 24, No 5, May 2022, Serial Number: 100, Pages: 215-284

CONTENTS

Original Articles

Original Article

^{188}Rhenium Treatment Induces *DACT2* Expression in Hepatocellular Carcinoma Cells

Samieh Asadian, M.Sc.[1, 2, 3], Abbas Piryaei, Ph.D.[4, 5], Zahra Farzaneh, Ph.D.[2, 3], Bagher Aziz Kalantari, M.Sc.[6], Mehdi Azad, Ph.D.[1], Sahar Moghbeli Nejad, Ph.D.[1], Mohamad Reza Davarpanah, M.Sc.[7], Morteza Mohamadi, M.Sc.[7], Anastasia Shpichka, Ph.D.[8, 9, 10], Nematolah Gheibi, Ph.D.[1]*, Peter Timashev, Ph.D.[8, 9, 10], Massoud Vosough, M.D., Ph.D.[2, 3]*

1. Cellular and Molecular Research Center, Research Institute for Prevention of Non-Communicable Diseases, Qazvin University of Medical Sciences, Qazvin, Iran
2. Department of Regenerative Medicine, Cell Science Research Center, Royan Institute for Stem Cell Biology and Technology, ACECR, Tehran, Iran
3. Department of Stem Cells and Developmental Biology, Cell Science Research Center, Royan Institute for Stem Cell Biology and Technology, ACECR, Tehran, Iran
4. Department of Biology and Anatomical Sciences, School of Medicine, Shahid Beheshti University of Medical Sciences, Tehran, Iran
5. Department of Tissue Engineering and Applied Cell Sciences, School of Advanced Technologies in Medicine, Shahid Beheshti University of Medical Sciences, Tehran, Iran
6. Department of Organic Chemistry, Karaj Branch, Islamic Azad University, Karaj, Iran
7. Department of Physical Chemistry, Faculty of Science, University of Tehran, Tehran, Iran
8. Institute for Regenerative Medicine, Sechenov First Moscow State Medical University, Moscow, Russia
9. World-Class Research Center "Digital biodesign and personalized healthcare", Sechenov First Moscow State Medical University, Moscow, Russia
10. Chemistry Department, Lomonosov Moscow State University, Moscow, Russia

***Corresponding Addresses: Cellular and Molecular Research Center, Research Institute for Prevention of Non-Communicable Diseases, Qazvin University of Medical Sciences, Qazvin, Iran**
P.O.Box: 16635-148, Department of Regenerative Medicine, Cell Science Research Center, Royan Institute for Stem Cell Biology and Technology, ACECR, Tehran, Iran
Emails: ngheibi@qums.ac.ir, masvos@Royaninstitute.org*

Received: 10/December/2020, Accepted: 19/April/2021

Abstract

Objectives: Epigenetic alterations, including any change in DNA methylation pattern, could be the missing link of understanding radiation-induced genomic instability. Dapper, Dishevelled-associated antagonist of β-catenin homolog 2 (*DACT2*) is a tumor suppressor gene regulating Wnt/β-catenin. In hepatocellular carcinoma (HCC), *DACT2* is hypermethylated, while methylation status of its promoter regulates the corresponding expression. Radionuclides have been used to reduce proliferation and induce apoptosis in cancerous cells. Epigenetic impact of radionuclides as therapeutic agents for treatment of HCC is still unknown. The aim of this study was to evaluate epigenetic impact of ^{188}Rhenium perrhenate ($^{188}ReO_4$) on HCC cells.

Material and Methods: In this *in vitro* experimental study, HepG2 and Huh7 cells were treated with $^{188}ReO_4$, receiving 55 and 73 Mega Becquerel (MBq) exposures, respectively. For cell viability measurement, live/dead staining was carried out 18, 24, and 48 hours post-exposure. mRNA expression level of *β-Catenin*, *Wnt1*, *DNMT1*, *DACT2* and *WIF-1* genes were quantified by quantitative reverse transcription-polymerase chain reaction **(**qRT-PCR). Then, possible regulatory impact of *DACT2* upregulation was investigated through evaluating methylation-specific PCR (MS-PCR).

Results: Results showed that viability of both cells was reduced after treatment with $^{188}ReO_4$ at three time points post-exposure compared to the control groups. The qRT-PCR results showed that *DACT2* mRNA level was significantly increased at 24, and 48 hours post-exposure in HepG2 cells compared to the control group, while, no significant change was observed in Huh7 cells. Methylation pattern of *DACT2* promoter remained unchanged in HepG2 and Huh7 cells.

Conclusion: Treatment with $^{188}ReO_4$ reduced viability of HepG2 and Huh7 cells. Although *DACT2* expression was increased after $^{188}ReO_4$ exposure in HepG2 cells, methylation pattern of its promoter remained unchanged. This study assessed impacts of the $^{188}ReO_4$ β-irradiation on expression and induction of *DACT2* epigenetic aberrations as well as the correlation of this agent with viability of cells.

Keywords: DNA Methylation, Epigenetics, Hepatocellular Carcinoma, Radionuclide

Cell Journal(Yakhteh), Vol 24, No 5, May 2022, Pages: 215-221

Citation: **Asadian S, Piryaei A, Farzaneh Z, Aziz Kalantari B, Azad M, Moghbeli Nejad S, Davarpanah MR, Mohamadi M, Shpichka A, Gheibi N, Timashev P, Vosough M. ^{188}rhenium treatment induces DACT2 expression in hepatocellular carcinoma cells. Cell J. 2022; 24(5): 215-221. doi: 10.22074/cellj.2022.7894.**

Introduction

Hepatocellular carcinoma (HCC) is a common malignancy, globally (1). Tumorigenesis is followed by deviations of gene expression and protein function initiated by genetic and epigenetic modifications. The molecular pathways contributing to hepatocarcinogenesis are a multi-stage process involved in progressive accumulation of molecular aberrations determining different molecular, cellular and histopathological events (2).

Activation of the Wnt/β-catenin signaling pathway is commonly associated with initiation and progression of HCC, colorectal cancer and other different types of cancer (3). The association of alterations in Wnt signaling

pathway with cancer development was signified after reporting that highlighted the activation of int1 (*Wnt1*), either by pro-viral insertion into the *Wnt1* locus or transgenic overexpression in mice model, resulted in mammary malignancies (4).

The Wnt/β-catenin pathway regulates cell proliferation and plays a crucial role in the carcinogenesis of HCC. Genetic mutations or abnormal activation of the Wnt/β-catenin pathway are key players in the tumor development within up to 50% of HCC cases. Mutations of the *Catenin* gene are thought to be the prominent genetic aberration initiating development of HCC (5).

The first proof of crucial impact of epigenetic changes in cancer development and progression was reported in 1983, by Feinberg and Vogelstein. They showed shifted methylation pattern of genes in colorectal tumors (6). Epigenetic alterations play crucial roles in the pathogenesis of many human diseases, including cancer (7), particularly HCC (8). In this regard, recent studies showed that methylation in the promoter region of dapper, dishevelled-associated antagonist of β-catenin homolog 2 *(DACT2)* gene, as an antagonist of β-catenin, was correlated with loss or reduction of dapper, while Wnt inhibitory factor 1 **(***WIF-1*) promotor hypermethylation activates Wnt/β-catenin pathway (9). Dapper was identified by screening proteins that interact with dishevelled, a critical factor in the Wnt signaling. Dapper and dishevelled were co-localized intracellularly and formed a complex with Axin, GSK3 and β-catenin to continue the pathway (10). Researchers found that *DACT2* expression was downregulated in certain colorectal cancers (11). Similarly, it was reported that mRNA expression of *DACT2* was downregulated in human HCC (12). Therefore, *DACT2* was considered as a tumor suppressor gene in many types of tumors. Researchers demonstrated that tumor size was larger (>5 cm) in HCC patients with downregulated *DACT2*, compared to those with high *DACT2* expression. Thus, this gene may play a substantial role in the growth and development of HCC cells (13). Several studies evaluated potential correlation of mRNA expression level with promoter methylation of *DACT2* in different tumors (14). Likewise, to the previous reports in different types of cancers, *DACT2* expression was regulated by hypermethylation of the corresponding gene promoter. The promoter hypermethylation might be a crucial mechanism of *DACT2* gene silencing transcriptional level in HCC cells (13).

WIF-1 is an endogenous antagonist for Wnt. It inhibits Wnt pathway through binding to Wnt proteins in the extracellular space (15). Recent studies showed association of *WIF-1* promoter hypermethylation with the corresponding gene silencing in HCC (16). This loss of gene expression could be restored after treatment with epigenetic modification drugs (17).

Among the targeted therapies, using radionuclides introduced as a potential intra-tumoral radiation-based treatment approach for HCC. In this approach, administration of radionuclides into the hepatic artery targets cancer cells within tumor mass, whereas the non-cancerous surrounding tissue remains unaffected (18, 19). In this regard, various radionuclides have been reported including Yttrium-90 microspheres, Rhenium-188 lipiodol, Iodine-131 lipiodol, Rhenium-188 microspheres, Holmium-166 chitosan and Holmium-166 microspheres for intra-arterial therapy of liver carcinoma (20).

Recent *in vivo* studies demonstrated that radionuclides could have a remarkable impact on the epigenetic status, particularly in DNA methylation pattern (21). Notably, continuous and chronic exposure induced epigenetic changes such as non-coding area hypermethylation associated with genomic instability up to 20 consecutive passages post-irradiation (22). It has been suggested that an external epigenetic driver could be involved in this phenomenon, such as ROS-radicals, methylation changes or microRNA mediated signaling (23). ROS production due to ionizing radiation is linked with alterations in DNA methylation pattern (24). Hydroxyl radical-induced DNA damage (25) have been shown to induce DNA hypomethylation by interfering with DNA methyltransferases (DNMTs) and therefore resulting in whole genomic hypomethylation (26). In addition, oxidative stress induced by ROS can induce gene silencing by abnormal hypermethylation of promoter regions in tumor suppressor genes. Thus, it might lead to cancer progression.

Epigenetic alterations are dynamic and usually work as an adaptation mechanism to different changes of environmental factors. Even though there is growing evidences on the importance of epigenetics and biological processes induced by radiotherapy in various cancer types including HCC, specific epigenetic effects of radionuclides on *DACT2*, as an important inhibitor of Wnt/β-catenin signaling, are not revealed completely at the molecular level.

In this study, we investigated apoptosis induction capacity of ^{188}Rhenium perrhenate ($^{188}ReO_4$) on HepG2 and Huh7 cells, as well as normal fibroblasts. After 18, 24 and 48 hours post-irradiation by $^{188}ReO_4$, cell viability was measured through live/dead assay. Gene expression of particular genes and promotor methylation pattern were evaluated to investigate possible epigenetic changes.

Material and Methods

Ethical approval

The Ethical Committee of Royan institute (IR.ACECR.ROYAN.REC.1397.052) approved this study.

Cell culture and treatment

In this *in vitro* experimental study, HepG2 and Huh7 cells were obtained from Royan Cell Bank (Royan Institute, Iran). The cells were cultured in high-glucose Dulbecco's modified Eagle's medium (HGDMEM, Gibco, USA) at

37˚C in a humidified cell culture incubator with 5% CO_2. The culture medium was enriched with 10% fetal bovine serum (FBS), 2 mM L-glutamine, 1 mM non-essential amino acids and 1% penicillin/streptomycin (Pen/Strep, all from Gibco, USA). Cells were sub-cultured by trypsin/EDTA (0.25%, Gibco, USA). The culture media were refreshed every day. Expression level of all genes was normalized to the expression levels at time zero. All viability values were presented in percentage and normalized to the viability values at the time zero.

Cell viability assay

After 18, 24 and 48 hours post-treatment with 55 and 73 MBq of $^{188}ReO_4$, HepG2 and Huh7 cells (initial cell seeding number: 2500 cells) were suspended in PBS and mixed with LIVE/DEAD® viability/cytotoxicity kit (Invitrogen, USA), consisting of live/dead staining solution (0.2 µM calcein-AM and 0.1 µM ethidium homodimer-1). The cancer cells were incubated for 20 minutes at room temperature with the reagent. Cell viability was shown by green or red fluorescence labelled cells representative for live and dead cells, respectively. Live and dead cells were observed by counting green and red fluorescent signals using fluorescence microscope (Olympus, Japan).

Image analysis was conducted to preliminary recognition of pixels with the given color channel intensity (red or green), and then counting live and dead cells using ImageJ (Imagej.nih.gov). To validate cell viability measurements, non-overlapping images (three pictures) from a coverslip were used to analyze mean value for each single coverslip, which represented one experimental measurement. Number of experiment repeats is indicated as "n". The student's two-tailed t test, ANOVA and post hoc Bonferroni test were used in terms of statistical analysis.

Quantitative reverse transcription–polymerase chain reaction

In order to study expression levels of *DNMT1*, *Wnt1*, *β-Catenin*, *WIF-1* and *DACT2* using quantitative reverse transcription-polymerase chain reaction (qRT-PCR), we designed primers. mRNA expression level of the genes were quantified in HepG2 and Huh7 cells that treated with 55 and 73 MBq of $^{188}ReO_4$ and the control groups. To evaluate Wnt/*β*-catenin signaling pathway in HepG2 cells, qRT-PCR was performed for *β-Catenin*, *Wnt1*, *DNMT1*, *DACT2* and *WIF-1* genes. RNA extraction was performed using TRIzol (Invitrogen®, USA), and cDNA was synthesized using PrimeScript™ Reverse Transcriptase Kit (Takara Bio, Japan) according to the manufacturer's instructions. qRT-PCR reactions were performed using a real-time PCR system (Applied Biosystems StepOne instrument, USA) using SYBR Green Master Mix (Takara Bio) and the results were analyzed by StepOne software (Applied Biosystems). The samples were collected from three independent biological replicates for each group. Finally, mRNA expression level of each gene was normalized to *GAPDH* and calculated relative to HepG2 and Huh7 in the adherent culture. Analysis was performed by the comparative CT Method, $2^{-\Delta\Delta Ct}$. The primers are listed in the Table 1.

Table 1: List of the primers used for qRT-PCR and MS-PCR in this study

Gene	Primer sequence (5´-3´)
GAPDH	F: CAATGACCCCTTCATTGACC
	R: TGGAAGATGGTGATGGGATT
β-Catenin	F: CATCTACACAGTTTGATGCTGCT
	R: GCAGTTTTGTCAGTTCAGGGA
Wnt1	F: GGGCATCGTGAACATAGCCTCCTCC
	R: CGGCGGAGGTGATTGCGAAGATAAA
DNMT1	F: CCGACTACATCAAAGGCAGC
	R: AGGTTGATGTCTGCGTGGTA
DACT2	F: GGCTGAGACAACAGGACATCG
	R: GACCGTCGCTCATCTCGTAAAA
WIF-1	F: TATGGATCGATGCTCACCAG
	R: CAGAGGGACATTGACGGTTG
DACT2	F: GATTTTAGTTTATTTTGGCGATTTGC
	R: CACATCTCCCGAACAAAATCCCG
DACT2	F: TAGATTTTAGTTTATTTTGGTGATTTGT
	R: TCCACATCTCCCAAACAAAATCCCA

qRT-PCR; Quantitative reverse transcription-polymerase chain reaction and MS-PCR; Methylation-specific PCR.

Methylation-specific PCR

Genomic DNA from test and control group of HepG2 and Huh7 cells were extracted using the Proteinase-K method. After chloroform/phenol extraction, DNA precipitation was performed in ethanol. DNA was dissolved in low Tris/EDTA (TE) buffer and stored at -20°C (27). Genomic DNA was extracted from treated and untreated cells, followed by reacting with bisulfite to perform MS-PCR. The MS-PCR primers were designed considering the genomic sequences, flanking the presumed transcription start site (TSS). The primer sequences were oligo-synthesized (Invitrogen, USA) in order to perform MS-PCR for *DACT2* and detect bisulfite-induced changes affecting unmethylated and methylated alleles. The *DACT2* primers were used in MS-PCR listed in the Table 1.

Statistical analyses

Statistical analysis was performed using SPSS version 20 (IBM Co., USA) and PRISM 6.0 software package (GraphPad Software

Co., USA). Statistical analysis was performed using one-way ANOVA and independent-sample t test. The $P<0.05$ was considered statistically significant. Data was presented as mean ± standard deviation (mean ± SD). Samples were collected from three independent biological replicates.

Results

Cell viability after treatment of HepG2 and Huh7 cells with $^{188}ReO_4$

To quantify cell viability, HepG2 and Huh7 cells were treated with 55 and 73 MBq of $^{188}ReO_4$. They were evaluated at three time points, including 18, 24 and 48 hours post-exposure. Then, live/dead assay was performed as mentioned in material and methods. As shown in Figure 1A, 55 MBq of $^{188}ReO_4$, produced a reasonable impairment of cell viability, and viability at the three time points were 66.45%, 62.73% and 49.92%, respectively, as shown in Figure 1B. For Huh7 cells, treatment with 73 MBq of $^{188}ReO_4$ resulted in reduced viability up to 42%, 50%, and 54% at the three time points. After 48 hours exposure with 55 MBq of $^{188}ReO_4$, statistically significant cell death occurred in comparison with the control group ($P<0.05$). This data suggested that exposure to $^{188}ReO_4$ made a significant impact on the cell viability in the both cell lines.

Quantitative reverse transcription-polymerase chain reaction

Downregulation of *DNMT1* was observed at all of the three time points; however it was significant only at the 18 hours post-exposure compared to the control group (Fig.1C). mRNA expression of *β-catenin* was upregulated after treatment with $^{188}ReO_4$, compared to the control group. The mentioned upregulations were significant at the 18 and 24 hours post-exposure. There was not significant diffrence in the expression of *β-catenin* between the treated HepG2 cells and control group 48 hours after treatment (Fig.1D). To further analyze impact of $^{188}ReO_4$ on Wnt/β-catenin signaling pathway, relative mRNA expression of *Wnt1* was measuered by qRT-PCR. Data showed no significant difference between the treated cells and control HepG2 cells at all of the time points (Fig.1E). qRT-PCR data showed a significant upregulation in *WIF1* level, 48 hours post-treatment compared to the control cells (Fig.1F), while there was not any significant change in the other time points. Expression of *DACT2* was upregulated at all of the time points. However, in HepG2 cells the mRNA expression was significantly higher than control group, 24 and 48 hours after exposure (Fig.1G).

Methylation status of *DACT2* promoter in HCC cell lines didn't change after exposure

The results showed that *DACT2* transcript was upregulated in HepG2 cells, 24 and 48 hours after treatment with 55 MBq of $^{188}ReO4$ (Fig.1G). To evaluate whether upregulation of *DACT2* is correlated with epigenetic alteration of the promoter methylation status after treatment with $^{188}ReO_4$, we carried out MS-PCR. The results indicated that *DACT2* promoter in the HepG2 cells remained methylated at thje 18, 24, and 48 hours post-treatment with $^{188}ReO_4$ (Fig.1H, I). The same experiment was performed for Huh7 cells treated with $^{188}ReO_4$ at the three time points, resulted in the same findings. These data proposed that mRNA expression level changes of *DACT2* are not associated with epigenetic changes in methylation status of its promotor.

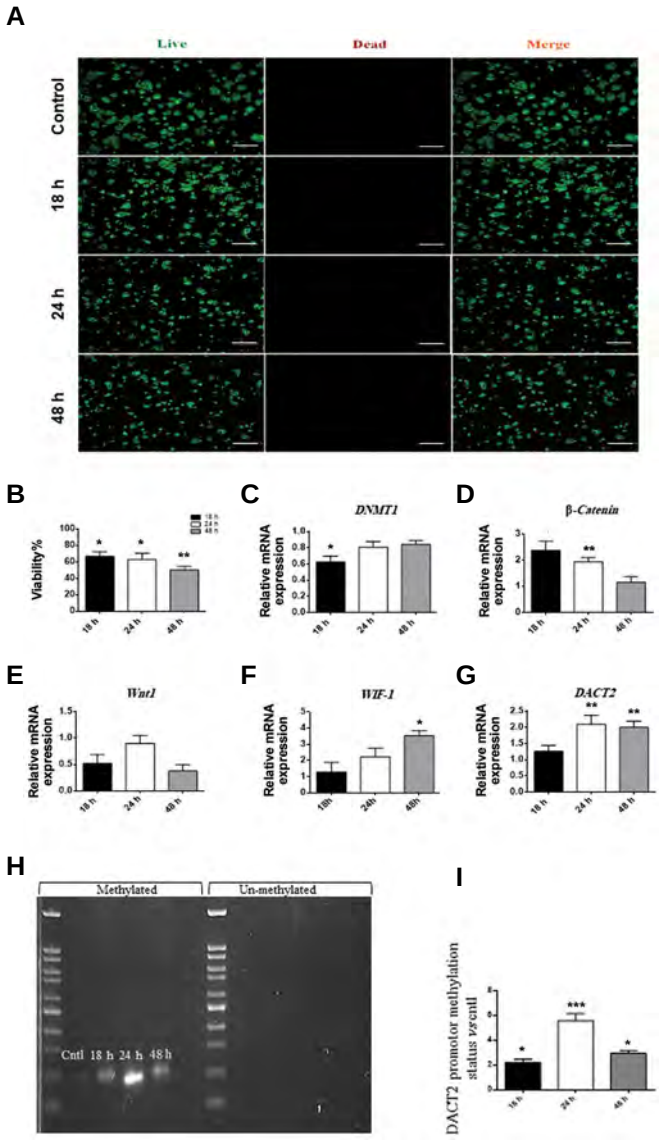

Fig.1: Molecular modifications after treatment of cells with $^{188}ReO4$. **A.** Live/dead cell viability assay of HepG2 cells treated with 55 MBq 188 ReO4, and untreated HepG2 cells (control group). The cells were evaluated at 18, 24 and 48 hours after treatment. The live and dead cells were visualized in green and red fluorescence, respectively (scale bar: 500 µm). **B.** Viability percent vs. control after treatment with 55 MBq at three time points 18, 24 and 48 hours. **C-G.** qRT-PCR analysis for *DNMT1*, β-*catenin, WNT1, WIF-1* and *DACT2*, to evaluate relative mRNA expression in HepG2 cells treated with 55 MBq of 188ReO4 vs. control after 18, 24 and 48 hours post-exposure. **H.** MS-PCR test results. Methylation status of the DACT2 promotor was evaluated by MS-PCR in HepG2 cells after 18, 24, and 48 hours post-exposure. **I.** Promoter methylation status of DACT2 was quantified by ImageJ in HepG2 cell line at three time points after treatment. Data are presented as the mean ± SD, n=3 (*; $P<0.05$, **; $P<0.01$, ***; $P<0.001$). h; Hour.

Exposure impact on normal cells and Huh7 cells

To evaluate the impact of treatment with $^{188}ReO_4$ on normal cells, the same experiment was performed on human dermal fibroblasts (HDF). Viability of HDF cells did not show any significant difference after treatment with various exposures at the three time points. Percentage of dead cells are also illustrated at different time points (Fig.2A).

DACT2 mRNA expression did not show any significant change in the three time points compared to the control group of Huh7 cells. *β-catenin* expression in Huh7 cells showed a similar trend to HepG2 cells, however, 48 hours post treatment, downregulation was significant compared to the control group (Fig.2B).

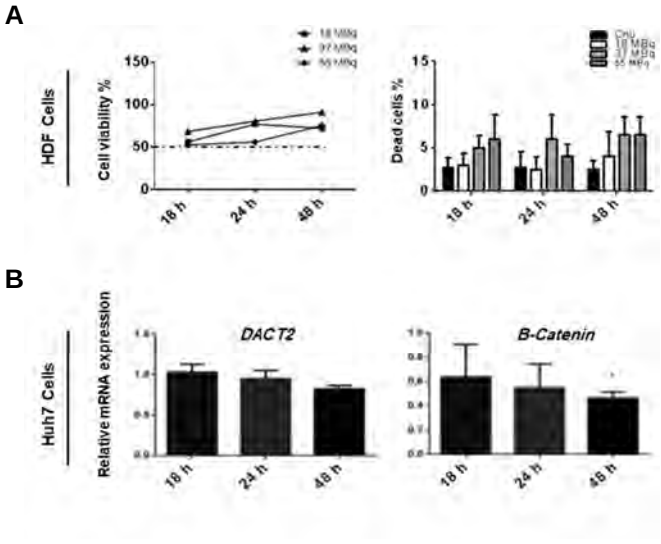

Fig.2: The exposure impact on normal cells and Huh7 cells. **A.** Evaluation of viability after treatment with $^{188}ReO_4$ in HDF cells. Viability of the HDF cells were visualized and compared to the control (untreated) cells after treatment with 18, 37 and 55 MBq $^{188}ReO_4$ at 18, 24 and 48 hours. Mean viability percent *vs.* control after treatment with 18, 37 and 55 MBq in HDF cells after 18, 24 and 48 hours exposure. Percentage of the dead cells treated with the same condition were presented here. Data are expressed as the mean ± SD, n=3 (*; P<0.05) vs. control group. **B.** The bar graphs show quantification of the qRT-PCR analysis for *DACT2* and *β-catenin* in Huh7 cells treated with $^{188}ReO4$ and received 73 MBq vs. control after 18, 24 and 48 hours post-exposure. Data are presented as the mean ± SD, n=3, (*; P<0.05) .

Discussion

DNA methylation status change is a crusial feature of epigenetic modification, which initialy occurs in the CpG islands of gene promoter regions. Activation of multiple DNMTs are required to establish and maintain DNA methylation patterns (28). Some studies showed that DNA methylation response secondery to irradiation is the same to the common biological stimulations (29). In the current study, we showed that mRNA expression level of *DACT2* was upregulated in HepG2 cells, at the 24 and 48 hours post-exposure to $^{188}ReO_4$. These results were in correlation with decreased cell viability at the 18, 24, and 48 hours post-exposure. Therefore, *DACT2* may play critical role in the viability of cancer cells and progression of HCC (13). Aberrant activation of Wnt signaling is a significant cause for intiation and progression of cancer, which could be originated from genetic or epigenetic changes (30). Frequency in methylation status of Wnt signaling antagonists proposes a vital role in the activation of this pathway during carcinogenesis (31). *DACT2* accelerates dishevelled (Dvl/Dsh) degradation in the lysosome-dependent pathway. This inhibits LEF1 binding to β-catenin.

Restoring expression of *DACT2* induces transcriptional activation of T cell factor-4 and the downstream Wnt signaling, which plays a suppressive role for them (32). *DACT2* inhibits cell proliferation, induces breakage in G2-M phase in cell lines and inhibits tumor growth in the xenograft nude mice (11). *DACT2* expression was silenced by hypermethylation of its promoter in HCC, suggesting that the transcriptional silencing of *DACT2* may be one of the main factors in the progression of HCC (15). Moreover, previous studies showed another antagonist of Wnt signaling, *WIF-1*, which is downregulated and hypermethylated in the HCCs compared to the normal liver tissue (33).

Possible association of *DACT2* expression with radionuclide therapy has not yet been studied in human cancer. Studies highlighted implication of such therapies that restore tumor suppressive function of *DACT2* and *WIF1* in HCC patient; however, therapeutic impact of the radionuclides on HCC cells as well as the increased expression of *DACT2* and *WIF-1* have been remained to be explored. The role of *DACT2* as a tumor suppressor, its downregulation in cancer and correlation of *DACT2* expression with the methylation status of its promotor have been studied in colorectal cancer. In colon cancer, restoring *DACT2* expression repressed malignant cell growth by inducing apoptosis and proliferation inhibition both *in vitro* and *in vivo* models (11). Additionally, aberrant promoter hypermethylation of *DACT2* was reported in the other types of cancer, indicating significant reduction of *DACT2* expression (34). These findings led us to study potential correlation of expression level and promoter methylation status of *DACT2* gene in HCC cells after treatment with radionuclides.

It has been reported that radiation could induce epigenetic alterations post-irradiation (35, 36). Particularly, reactgive oxygen species (ROS) production is associated with alterations in DNA methylation patterns. Moreover, ROS derivatives contribute to DNA hypomethylation by interfering with the DNMTs and therfore resulting in decreased methylation (26).

The present study was conducted to investigate possible correlation of β-irradiation with $^{188}ReO_4$, as a novel therapeutic agent, on HCC cells and remodeling of *DACT2* promotor methylation status. This study showed that viability of HepG2 and Huh7 cells was declined noticeably after exposure to β-irradiation. We showed for the first time that *DACT2* and *WIF-1* were upregulated in HepG2 cells, 24 and 48 hours after treatment. This

data suggested that viability changes might be due to the impaired Wnt/β-catenin pathway. We carried out qRT-PCR to determine whether $^{188}ReO_4$ induced upregulation of *Wnt1* and *β-catenin* expression levels. Expression of *Wnt1* was significantly upregulated in HCC cells and it had a key role in the survival of the HCC cells (37). Our data showed no significant reduction of *Wnt1* and *β-catenin* expression in mRNA level. Further investigations showed that expression level of *DNMT1* was not changed significantly in HepG2 cells after treatment with $^{188}ReO_4$, compared to the control group. Additionally, to find out possible correlation of *DACT2* upregulation and epigenetic alterations on its promotor after treatment with $^{188}ReO_4$, promotor methylation status of the *DACT2* was evaluated by MS-PCR in the both cell lines. Our data suggested that *DACT2* upregulation is not associated with promoter hypomethylation after exposure to $^{188}ReO_4$ in HepG2 and Huh7 cells.

Comparison of our results with previous studies showed that radiation did not significantly change the activity of Wnt/β-catenin pathway (38). However, previous studies showed that low-dose radiation induced upregulation of *Wnt1*, *Wnt3a*,*Wnt5a* and *β-catenin* (39). In our study, there were significant *β-catenin* upregulations at 18 and 24 hours post-exposure of HepG2 cells while there was no change in *Wnt1* expression. Few studies showed that sirtuin 2 (SIRT2) in response to radiation-induced stress directly interacted with β-catenin and inhibited Wnt signaling (40). This study did not show any correlation between epigenetic status of *DACT2* promotor after treatment with $^{188}ReO_4$ and alteration in mRNA expression level in the both lines.

Conclusion

$^{188}ReO_4$ treatment reduced viability of HepG2 and Huh7 cells. This exposure increased expression of *DACT2* in HepG2, but it did not affect epigenetic status of its promotor. However, Huh7 cells did not show any change in the *DACT2* expression level and epigenetic status of the coressponding gene promotor. Further work is needed to find the exact impact of β-irradiation on epigenetic modifications of the Wnt/β-catenin pathway.

Aknowledgments

The authors would like to express their gratitude to their colleagues at Regenerative Medicine Department of Royan Institute (Tehran, Iran). "The study was partly supported by i. National Cancer Control Charity Foundation, registration number 41476, Tehran, IRAN, ii. Ghazvin University of Medical Science, and iii. The Ministry of Science and Higher Education of the Russian Federation within the framework of state support for the creation and development of World-Class Research Centers "Digital biodesign and personalized healthcare" (N. 075-15-2020-926). The authors declare no conflict of interest.

Authors' Contributions

S.A.; Performed the experiments, as part of her thesis, drafting the manuscript and drawing the figures. A.P., Z.F., M.A., A.S., P.T., S.M.N.; Helped and involved in study design, analyses and drafting the manuscript. B.A.K., M.R.D., M.M.; Prepared the radionucleid and involved in study design and revising the manuscript. P.T., N.G., M.V.; Designed the study, performed the analysis, writing and revising the manuscript as well as proofreading. All authors read and approved the final manuscript.

References

1. Siegel RL, Miller KD, Jemal A. Cancer statistics, 2019. CA Cancer J Clin. 2019; 69(1): 7-34.
2. Dhanasekaran R, Bandoh S, Roberts LRJF. Molecular pathogenesis of hepatocellular carcinoma and impact of therapeutic advances. F1000Res. 2016; 5.
3. Zhan T, Rindtorff N, Boutros M. Wnt signaling in cancer. Oncogene. 2017; 36(11): 1461-1473.
4. Tsukamoto AS, Grosschedl R, Guzman RC, Parslow T, Varmus HEJC. Expression of the int-1 gene in transgenic mice is associated with mammary gland hyperplasia and adenocarcinomas in male and female mice. Cell. 1988; 55(4): 619-625.
5. Khalaf AM, Fuentes D, Morshid AI, Burke MR, Kaseb AO, Hassan M, et al. Role of Wnt/β-catenin signaling in hepatocellular carcinoma, pathogenesis, and clinical significance. J Hepatocell Carcinoma. 2018; 5: 61-73.
6. Feinberg AP, Vogelstein BJN. Hypomethylation distinguishes genes of some human cancers from their normal counterparts. Nature. 1983; 301(5895): 89-92.
7. Dawson MA, Kouzarides T. Cancer epigenetics: from mechanism to therapy. Cell. 2012; 150(1): 12-27.
8. Tsang DP, Wu WK, Kang W, Lee YY, Wu F, Yu Z, et al. Yin Yang 1-mediated epigenetic silencing of tumour-suppressive microRNAs activates nuclear factor-κB in hepatocellular carcinoma. J Pathol. 2016; 238(5): 651-664.
9. Jia Y, Yang Y, Brock MV, Zhan Q, Herman JG, Guo M. Epigenetic regulation of DACT2, a key component of the Wnt signalling pathway in human lung cancer. J Pathol. 2013; 230(2): 194-204.
10. Cheyette BN, Waxman JS, Miller JR, Takemaru KI, Sheldahl LC, Khlebtsova N, et al. Dapper, a Dishevelled-associated antagonist of β-catenin and JNK signaling, is required for notochord formation. Dev Cell. 2002; 2(4): 449-461.
11. Wang S, Dong Y, Zhang Y, Wang X, Xu L, Yang S, et al. DACT2 is a functional tumor suppressor through inhibiting Wnt/β-catenin pathway and associated with poor survival in colon cancer. Oncogene. 2015; 34(20): 2575-2585.
12. Xiang T, Fan Y, Li C, Li L, Ying Y, Mu J, et al. DACT2 silencing by promoter CpG methylation disrupts its regulation of epithelial-to-mesenchymal transition and cytoskeleton reorganization in breast cancer cells. Oncotarget. 2016;7(43):70924-70935.
13. Gao S, Yang Z, Zheng ZY, Yao J, Zhang F, Wu LM, et al. Reduced expression of DACT2 promotes hepatocellular carcinoma progression: involvement of methylation-mediated gene silencing. World J Surg Oncol. 2013; 11: 57.
14. Yu Y, Yan W, Liu X, Jia Y, Cao B, Yu Y, et al. DACT2 is frequently methylated in human gastric cancer and methylation of DACT2 activated Wnt signaling. Am J Cancer Res. 2014; 4(6): 710-724.
15. Zhang X, Yang Y, Liu X, Herman JG, Brock MV, Licchesi JD, et al. Epigenetic regulation of the Wnt signaling inhibitor DACT2 in human hepatocellular carcinoma. Epigenetics. 2013; 8(4): 373-382.
16. Deng Y, Yu B, Cheng Q, Jin J, You H, Ke R, et al. Epigenetic silencing of WIF-1 in hepatocellular carcinomas. J Cancer Res Clin Oncol. 2010; 136(8): 1161-1167.
17. Liu YL, Yang HP, Gong L, Tang CL, Wang HJJM. Hypomethylation effects of curcumin, demethoxycurcumin and bisdemethoxycurcumin on WIF-1 promoter in non-small cell lung cancer cell lines. Mol Med Rep. 2011; 4(4): 675-679.
18. Guidoccio F, Boni G, Volterrani D, Mariani G. Radionuclide therapy for tumors of the liver and biliary tract. Nuclear Medicine Textbook. Springer: 2019; 859-879.
19. Asadian S, Mirzaei H, Kalantari BA, Davarpanah MR, Mohamadi M, Shpichka A, et al. β-radiating radionuclides in cancer treatment, novel insight into promising approach. Pharmacol Res. 2020; 105070.
20. Bozkurt MF, Salanci BV, Uğur Ö. Intra-arterial radionuclide therapies for liver tumors. Semin Nucl Med. 2016; 46(4): 324-339.

21. Gombeau K, Pereira S, Ravanat JL, Camilleri V, Cavalie I, Bourdineaud J-P, et al. Depleted uranium induces sex-and tissue-specific methylation patterns in adult zebrafish. J Environ Radioact. 2016; 154: 25-33.
22. Kaup S, Grandjean V, Mukherjee R, Kapoor A, Keyes E, Seymour CB, et al. Radiation-induced genomic instability is associated with DNA methylation changes in cultured human keratinocytes. Mutat Res. 2006; 597(1-2): 87-97.
23. Tamminga J, Kovalchuk O. Role of DNA damage and epigenetic DNA methylation changes in radiation-induced genomic instability and bystander effects in germline in vivo. Curr Mol Pharmacol. 2011; 4(2): 115-125.
24. Donkena KV, Young CY, Tindall DJ. Oxidative stress and DNA methylation in prostate cancer. Obstet Gynecol Int. 2010; 2010: 302051.
25. Christman JK, Sheikhnejad G, Marasco CJ, Sufrin JR. 5-Methyl-2'-deoxycytidine in single-stranded DNA can act in cis to signal de novo DNA methylation. Proc Natl Acad Sci USA. 1995; 92(16): 7347-7351.
26. Franco R, Schoneveld O, Georgakilas AG, Panayiotidis MI. Oxidative stress, DNA methylation and carcinogenesis. Cancer Lett. 2008; 266(1): 6-11.
27. Rust S, Funke H, Assmann G. Mutagenically separated PCR (MS-PCR): a highly specific one step procedure for easy mutation detection. Nucleic Acids Res. 1993; 21(16): 3623-3629.
28. Denis H, Ndlovu MN, Fuks FJ. Regulation of mammalian DNA methyltransferases: a route to new mechanisms. EMBO Rep. 2011; 12(7): 647-656.
29. Antwih DA, Gabbara KM, Lancaster WD, Ruden DM, Zielske SP. Radiation-induced epigenetic DNA methylation modification of radiation-response pathways. Epigenetics. 2013; 8(8): 839-848.
30. Baylin SB, Ohm JE. Epigenetic gene silencing in cancer–a mechanism for early oncogenic pathway addiction? Nat Rev Cancer. 2006; 6(2): 107-116.
31. Jia Y, Yang Y, Liu S, Liu S, Herman JG, Lu F, et al. SOX17 antagonizes WNT/β-catenin signaling pathway in hepatocellular carcinoma. Epigenetics. 2010; 5(8): 743-749.
32. Kim DH, Kim EJ, Kim DH, Park SW. Dact2 is involved in the regulation of epithelial-mesenchymal transition. Biochem Biophys Res Commun. 2020; 524(1): 190-197.
33. Huang L, Li MX, Wang L, Li BK, Chen GH, He LR, et al. Prognostic value of Wnt inhibitory factor-1 expression in hepatocellular carcinoma that is independent of gene methylation. Tumour Biol. 2011; 32(1): 233-240.
34. Jiang X, Tan J, Li J, Kivimäe S, Yang X, Zhuang L, et al. DACT3 is an epigenetic regulator of Wnt/β-catenin signaling in colorectal cancer and is a therapeutic target of histone modifications. Cancer Cell. 2008; 13(6): 529-541.
35. Aypar U, Morgan WF, Baulch JE. Radiation-induced epigenetic alterations after low and high LET irradiations. Mutat Res. 2011; 707(1-2): 24-33.
36. Danielsson A, Barreau K, Kling T, Tisell M, Carén H. Accumulation of DNA methylation alterations in paediatric glioma stem cells following fractionated dose irradiation. Clin Epigenetics. 2020; 12(1): 26.
37. Wei W, Chua MS, Grepper S, So SK. Blockade of Wnt-1 signaling leads to anti-tumor effects in hepatocellular carcinoma cells. Mol Cancer. 2009; 8: 76.
38. Hai B, Yang Z, Shangguan L, Zhao Y, Boyer A, Liu F. Concurrent transient activation of Wnt/β-catenin pathway prevents radiation damage to salivary glands. Int J Radiat Oncol Biol Phys. 2012; 83(1): e109-e116.
39. Albuquerque C, Pebre Pereira L. Wnt signalling-targeted therapy in the CMS2 tumour subtype: a new paradigm in CRC treatment? Adv Exp Med Biol. 2018; 1110: 75-100.
40. Nguyen P, Lee S, Lorang-Leins D, Trepel J, Smart DK. SIRT2 interacts with β-catenin to inhibit Wnt signaling output in response to radiation-induced stress. Mol Cancer Res. 2014; 12(9): 1244-1253.

Original Article

LncRNA DS Cell Adhesion Molecule Antisense RNA 1 Facilitates Oral Squamous Cell Carcinoma Progression through The microRNA-138-5p/ Enhancer of Zeste 2 Polycomb Repressive Complex 2 Subunit Axis

Yanbo Zhang, M.M., Xuefeng Wang, M.M., Peng Wang, M.B., Xingle Zhang, M.M., Shangzhi Han, M.M., Feng Huo, M.B.*

Department of Stomatology, Affiliated Hospital of Chengde Medical College, Chengde, Hebei Province, China

***Corresponding Address: Department of Stomatology, Affiliated Hospital of Chengde Medical College, Chengde, Hebei Province, China**
Email: taofu9496@163.com*

Received: 26/August/2020, Accepted: 29/December/2020

Abstract

Objective: A lot of lncRNAs are implicated in oral squamous cell carcinoma (OSCC) progression. The study aimed at investigating lncRNA DS cell adhesion molecule antisense RNA 1 (DSCAM-AS1)'s functional role and molecular mechanism in OSCC.

Materials and Methods: In this experimental study, a total of 46 pairs of OSCC samples and para-cancerous tissues were collected during surgery. In OSCC tissues and cell lines, quantitative real time polymerase chain reaction (qRT-PCR) was performed for detecting DSCAM-AS1 and microRNA-138-5p (miR-138-5p) expression levels. Western blot was conducted to examine the enhancer of zeste 2 polycomb repressive complex 2 subunit (EZH2) expression level. Then, DSCAM-AS1 was knocked down with siRNA in OSCC cells and MTT and EdU assays were conducted to evaluate OSCC cell proliferation. Transwell assay was utilized for detecting OSCC cell migration and invasion capacities. Besides, the relationships among DSCAM-AS1, miR-138-5p, and EZH2 were explored through RNA immunoprecipitation, dual-luciferase reporter assay, qRT-PCR, and Western blot.

Results: DSCAM-AS1 expression was remarkably increased in OSCC tissues and cell lines, and DSCAM-AS1 knockdown could significantly restrain OSCC cell proliferation, migration, and invasion. MiR-138-5p was identified as a target of DSCAM-AS1, and its inhibitor could reverse the suppressive effects of DSCAM-AS1 knockdown on OSCC progression. EZH2 was verified as a target of miR-138-5p, and EZH2 knockdown could counteract the promotional impact of miR-138-5p inhibitor on OSCC progression. Additionally, DSCAM-AS1, as a ceRNA, could regulate EZH2 expression via miR-138-5p.

Conclusion: DSCAM-AS1 can play a tumor-promoting role in OSCC via miR-138-5p/EZH2 axis.

Keywords: DSCAM-AS1, Oral Squamous Cell Carcinoma, Proliferation

Cell Journal(Yakhteh), Vol 24, No 5, May 2022, Pages: 222-229

Citation: **Zhang Y, Wang X, Wang P, Zhang X, Han Sh, Huo F. LncRNA DS cell adhesion molecule antisense RNA 1 facilitates oral squamous cell carcinoma progression through the microRNA-138-5p/ enhancer of zeste 2 polycomb repressive complex 2 subunit axis. Cell J. 2022; 24(5): 222-229. doi: 10.22074/cellj.2022.7763.**

Introduction

Oral squamous cell carcinoma (OSCC) is a common malignancy occurring in the head and neck, accounting for more than 90% of cases of oral malignant diseases (1). There are more than 350,000 new cases each year and about 180,000 death cases worldwide (2). Although great progress has been made in surgery, chemotherapy, and radiotherapy, OSCC patients' five-year survival rate is merely 40-50% due to metastasis and chemotherapy/ radiotherapy resistance (3). In such a context, a full understanding of the molecular mechanism underlying OSCC progression is urgently needed to uncover new therapeutic targets.

LncRNAs can take part in modulating various biological processes, such as cell proliferation, migration, and apoptosis (4). Previous research have shown that many lncRNAs, as tumor suppressors or promoters, partake in OSCC tumorigenesis and development, such as urothelial cancer associated 1 (5), homeobox A11 antisense RNA (6), and TINCR ubiquitin domain containing (7). DS cell adhesion molecule antisense RNA 1 (DSCAM-AS1) expression is reported to be up-regulated in several tumors, for example, breast cancer (8), hepatocellular carcinoma (9), etc. However, its expression characteristics and functional role in OSCC are unclear.

MicroRNAs (miRs or miRNAs) target the 3′-UTR of mRNA to regulate gene expressions (10). The aberrant expression of miRNAs is linked with the pathogenesis of OSCC (11). Reportedly, miR-138-5p is underexpressed in OSCC, and it inhibits OSCC cell proliferation and invasion via targeting ISG15 ubiquitin like modifier (12); additionally, enhancer of zeste 2 polycomb repressive complex 2 subunit (EZH2) is reported as a target gene of miR-138-5p (13).

A large amount of research have demonstrated that the ceRNA network is involved in regulating tumor occurrence and development (14). Interestingly, bioinformatics analysis suggested that the sequence of DSCAM-AS1

contained the potential binding site for miR-138-5p. Given that EZH2 is a target gene of miR-138-5p, we supposed that DSCAM-AS1 could probably be a ceRNA to regulate miR-138-5p and EZH2 expressions.

Materials and Methods

Cell culture and transfection

Normal human oral epithelial cell line (NHOK) was purchased from the Cell Bank of the Chinese Academy of Sciences (Shanghai, China); OSCC cell lines (HSC-3, SCC-15, SCC-4, and CAL-27) were bought from the American Type Culture Collection (ATCC, Manassas, VA, USA). The above cell lines were cultured in RPMI-1640 medium (Sigma-Aldrich, St. Louis, MO, USA) with 100 U/ml penicillin, 100 μg/ml streptomycin, and 10% fetal bovine serum (FBS, Sigma-Aldrich, St. Louis, MO, USA) at 37°C in 5% CO_2.

Three small interference RNAs (siRNAs) against DSCAM-AS1 (si-DSCAM-AS1), scrambled siRNA control (si-NC), miR-138-5p mimics (miR-138-5p mi), negative control mimics (miR-NC), miR-138-5p inhibitor (miR-138-5p in), and EZH2 siRNA (si-EZH) were bought from the GenePharma (Shanghai, China). Lipofectamine™ 3000 (Invitrogen, Carlsbad, CA, USA) was adopted for transfecting them into cells.

Clinical sample collection

From March 2013 to January 2019, para-cancerous tissues and tumor tissues of 46 patients diagnosed with OSCC in the Affiliated Hospital of Chengde Medical College were collected during surgery, and two pathologists completed the pathological diagnosis. The tissues were immediately maintained in liquid nitrogen after the collection until RNA extraction. The subjects had not received any anti-tumor therapies such as radiotherapy and chemotherapy before the surgery.

Ethical approval

This study was reviewed, discussed, and endorsed by the Ethics Committee of the Affiliated Hospital of Chengde Medical College (Approval No. 201301006), and all of the subjects offered the signed informed consent before this study was performed.

Quantitative real time polymerase chain reaction

Total RNA of cell lines and tissues was extracted by TRIzol reagent (Invitrogen, Carlsbad, CA, USA), and cDNA Reverse Transcription Kit (TaKaRa, Ltd., Dalian, China) was employed for reversely transcribing RNA into cDNA. Subsequently, the SYBR Premix Ex Taq™ kit (TaKaRa, Otsu, Shiga, Japan) was utilized for amplification, and eventually, the relative RNA expression was obtained through the $2^{-\Delta\Delta Ct}$ method. *U6* and *GAPDH* served as the internal references. Below are the quantitative real time polymerase chain reaction (qRT-PCR) primer sequences:

DSCAM-AS1-

F: 5′- GATCGGGAAAGCCAACCA-3′
R: 5′-TGGAGGAGGGACAGAGAAGG-3′

miR-138-5p-

F: 5′-AGCTGGTGTTGTGAATCAGGCCG-3′
R: 5′-TGGTGTCGTGGAGTCG-3′

EZH2-

F: 5′-CCCTGACCTCTGTCTTACTTGTGGA-3′
R: 5′-ACGTCAG ATGGTGCCAGCAATA-3′

GAPDH-

F: 5′-TGCACCACCAACTGCTTAGC-3′
R: 5′-GGCATGGAC TGTGGTCATGAG-3′

U6-

F: 5′-CTCGCTTCGGCAGCACA-3′
R: 5′-AACGCTTCACGAATTTGC GT-3′

MTT assay

The measurement of transfected cell proliferation was conducted with a MTT kit (Roche, Basel, Switzerland). After the cells were attached to the bottom of the wells and grew stably, 20 μL of MTT solution (5 mg/ml) was added to each well, and then the cells were incubated for 4 hours. Subsequently, 150 μL of dimethyl sulfoxide was added to each well, and the plate was shaken for 10 minutes to dissolve the formazan crystals. After that, a microplate reader (Bio-Rad, Hercules, CA, USA) was utilized to detect the absorbance of the cells at 490 nm. With the same method, the absorbance values were detected on the 24 hours, 48 hours, and 72 hours, respectively.

EdU assay

EdU Kit (RiboBio, Guangzhou, China) was used for EdU assay to detect the proliferation of the transfected cells. OSCC cells were transferred into 96-well plates, and then EdU staining solution was added to each well before the cells were incubated. 2 hours later, cells were fixed for 30 minutes with 4% paraformaldehyde and then incubated with glycine (ThermoFisher Scientific, Waltham, MA, USA) for 10 minutes. Next, Apollo Dye Solution was adopted for staining the cells, and DAPI solution (Beyotime, Shanghai, China) was used to stain the nuclei of the cells. Ultimately, a fluorescence microscope (Nikon, Tokyo, Japan) was employed to observe and count the EdU-positive cells.

Western blot

RIPA buffer (Sigma-Aldrich, Darmstadt, Germany) was used to lyse the transfected cells. Then SDS-PAGE was used to separate the protein samples in each group. Next, the proteins were transferred to PVDF membranes (GE Healthcare Life Sciences, Little Chalfont, UK). After blocking with 5% skimmed milk at 37°C for 2 hours, the PVDF membranes were incubated overnight with

primary antibodies (anti-EZH2 antibody: cat. no. 4905, 1:1000, Cell Signaling Technology, USA; anti-GAPDH: ab181602, 1:5000, Abcam, UK) at 4°C and subsequently incubated with the secondary antibody (Proteintech, Rosemont, IL, USA) for 1 hour at room temperature. The protein detection was performed by the enhanced chemiluminescence (ECL) substrate kit (Amersham Biosciences, Little Chalfont, UK).

Transwell assay

The migration and invasion of transfected cells were assessed by the Transwell chambers (8 μm pore size; Corning, Corning, NY, USA). For the invasion assay, the membranes were pre-coated with Matrigel (BD, Bedford, MA, USA), and this procedure was not performed in the migration assay. OSCC cells (2×10^4/well) were transferred into the upper compartments with serum-free medium and RPMI-1640 medium was added to the bottom compartments (with 10% FBS). Following the incubation at 37°C for 24 hours, cells that passed through the filter to the bottom surface of the membrane were stained with crystal violet solution and then counted by a microscope (Nikon, Tokyo, Japan).

Dual-luciferase reporter assay

DSCAM-AS1 or *EZH2* 3′-UTR sequence with wild type (WT) or mutant (MUT) binding sites for *miR-138-5p* was respectively inserted into pmirGLO luciferase reporter plasmids (Promega, Madison, WI, USA). Then, Lipofectamine 3000 (Invitrogen, Carlsbad, CA, USA) was employed to co-transfect the above-mentioned reporter vectors and *miR-138-5p* mimics or miR-NC into 293T cells. 36 hours after the transfection, the luciferase activity was detected by the dual-luciferase reporter assay system (Promega, Madison, WI, USA).

RIP assay

The Magna RIP Kit (Millipore, Billerica, MA, USA) was used for the RIP assay. In brief, RIP lysis buffer was utilized for lysing the transfected cells, which were incubated with magnetic beads (Millipore, Billerica, MA, USA) coated with Ago2 antibody (Anti-Ago2) or IgG antibody (Anti-IgG). Then the immunoprecipitated RNA was isolated with the TRIzol method and reversely transcribed into cDNA. Subsequently, the enrichment of *DSCAM-AS1* and *miR-138-5p* in the immunoprecipitate was analyzed by qRT-PCR.

Statistical analysis

The experiments were performed in triplicate, and the data were statistically analyzed by SPSS 19.0 software (SPSS Inc., Chicago, IL, USA) and expressed as mean ± standard deviation. The student's *t*-test was conducted for the difference analysis between two groups, and the Chi-square test was conducted for examining the relationship between DSCAM-AS1 expression and clinicopathological characteristics. $P<0.05$ signified statistical significance.

Results

DSCAM-AS1 and *EZH2* expressions were increased in OSCC cell lines and tissues

qRT-PCR was used for detecting the expression of *DSCAM-AS1* in 46 OSCC patients' tumor tissues and para-cancerous tissues. It was revealed that *DSCAM-AS1* expression was remarkably increased in OSCC tissues compared to that in the paracancerous tissues (Fig.1A). Similarly, it was also uncovered that *DSCAM-AS1* expression was markedly enhanced in OSCC cell lines, including CAL-27, HSC-3, SCC-15, and SCC-4, in comparison with those in the cell line NHOK (Fig.1B, Fig.S1, See Supplementary Online Information at www.celljournal.org). Similarly, *EZH2* mRNA expression level was increased in OSCC tissues (Fig.1C) that was reflected at the protein level confirmed by the western blot analysis (Fig.1D). Then the 46 OSCC samples were averagely divided into high expression group and low expression group (n=23 in each group). We analyzed the association between *DSCAM-AS1* expression and OSCC patients' pathological features and found that high *DSCAM-AS1* expression was significantly correlated with lymph node metastasis and advanced clinical stage (Table 1). Therefore, *DSCAM-AS1* is likely to be a vital regulator in the OSCC progression.

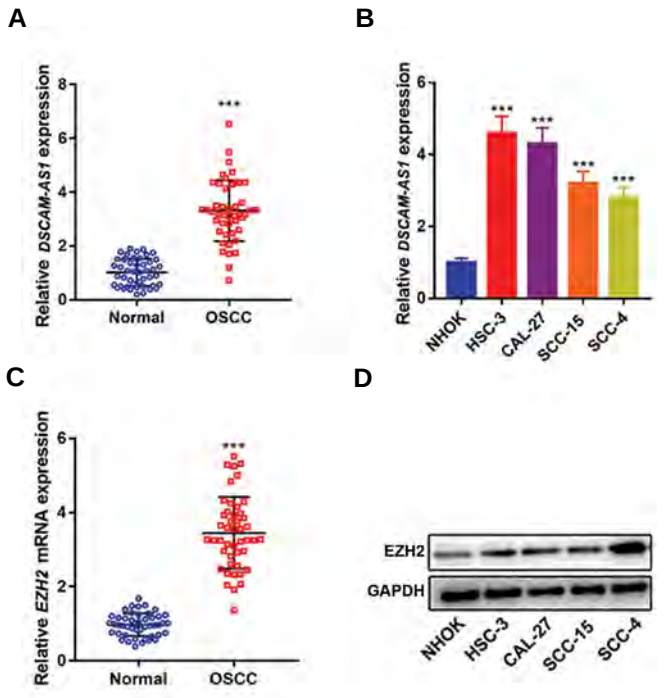

Fig.1: *DSCAM-AS1* and *EZH2* expressions were up-regulated in OSCC tissues and cell lines. **A.** qRT-PCR showed that *DSCAM-AS1* expression was upregulated in OSCC tissues. **B.** qRT-PCR showed that *DSCAM-AS1* expression was upregulated in OSCC cell lines. **C.** qRT-PCR showed that *EZH2* mRNA expression was upregulated in OSCC tissues. **D.** Western blot showed that EZH2 expression was upregulated in OSCC cell lines. The experiments were performed in triplicate. ***; P<0.001, OSCC; Oral squamous cell carcinoma, and qRT-PCR; Quantitative real time polymerase chain reaction.

Table 1: Correlation between *DSCAM-AS1* expression and pathological characteristics

Parameter	The number of patients	DSCAM-AS1 expression		P value
		High (n=23)	Low (n=23)	
Age (Y)				
≥ 60	28	11	17	0.069
< 60	18	12	6	
Gender				
Male	24	11	13	0.554
Female	22	12	10	
Tumor size (cm)				
≥ 5	34	16	18	0.501
< 5	12	7	5	
Clinical stage				
III-IV	22	17	5	0.0003
I-II	24	6	18	
Lymphatic metastasis				
Negative	25	16	9	0.038
Positive	21	7	14	

DSCAM-AS1; DS cell adhesion molecule antisense RNA 1.

Knocking down *DSCAM-AS1* could inhibit OSCC cell proliferation, migration, and invasion

To investigate *DSCAM-AS1*'s biological functions in OSCC progression, three siRNAs (si-*DSCAM-AS1*#1, #2, and #3) were used to knock down *DSCAM-AS1* expression in CAL-27 and HSC-3 cell lines. As shown in Figure 2, transfection of these *DSCAM-AS1* siRNAs notably decreased *DSCAM-AS1* expression, and *DSCAM-AS1* expression in the si-*DSCAM-AS1*#1 group was the lowest, thus si-*DSCAM-AS1*#1 was used for the subsequent experiments (Fig.2A). MTT assay showed that knocking down *DSCAM-AS1* markedly inhibited the proliferation of HSC-3 and CAL-27 cells (Fig.2B, C). EdU staining was used to detect proliferating cells, and DAPI staining the cell nuclei of alive cells (15). EdU assay showed that the percentage of EDU-positive cells was markedly decreased in the si-*DSCAM-AS1*#1 group. In addition, the Transwell assay manifested that silencing of *DSCAM-AS1* could dramatically inhibit HSC-3 and CAL-27 cell migration and invasion (Fig.2E, F).

MiR-138-5p was a target of *DSCAM-AS1*

To expound the potential mechanism by which DSCAM-AS1 participated in OSCC progression, the StarBase v2.0 database (http://starbase.sysu.edu.cn/) was used to retrieve possible target miRNAs of *DSCAM-AS1*, and it was unmasked that *DSCAM-AS1* contained a binding site for *miR-138-5p* (Fig.3A). Subsequently, we used the luciferase reporter assay for examining the binding relationship between them and found that *miR-138-5p* mimics could significantly reduce WT reporter's luciferase activity but would not affect MUT reporter's luciferase activity (Fig.3B). In addition, the RIP assay also confirmed that *DSCAM-AS1* was able to interact with *miR-138-5p* directly (Fig.3C, D). qRT-PCR indicated that *miR-138-5p* expression was markedly down-regulated in OSCC tissues and cell lines (Fig.3E, F). Notably, *DSCAM-AS1* knockdown in HSC-3 and CAL-27 cell lines induced a significant increase of *miR-138-5p* expression (Fig.3G). Therefore, it was concluded that *DSCAM-AS1* could sponge *miR-138-5p* and repress its expression.

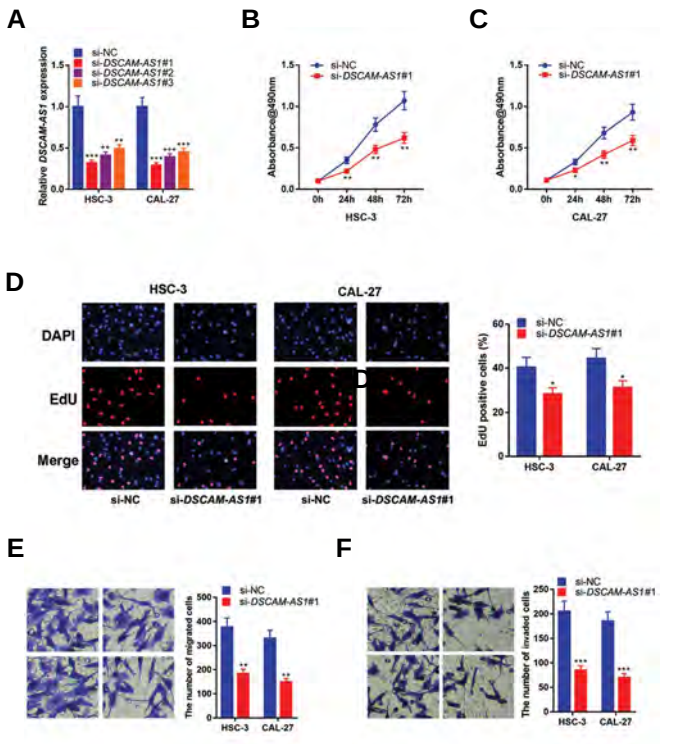

Fig.2: Knockdown of *DSCAM-AS1* inhibited OSCC cell proliferation, migration, and invasion. **A.** After transfection of *DSCAM-AS1* siRNA, *DSCAM-AS1* was downregulated in HSC-3 and CAL-27 cells, which was verified by qRT-PCR. **B, C.** MTT assay showed that OSCC cell proliferation was lower in the si-*DSCAM-AS1*#1 group. **D.** EdU assay showed that detect OSCC cell proliferation level was lower in the si-*DSCAM-AS1*#1 group. **E, F.** Transwell assay showed that OSCC cell migration and invasion abilities were decreased in the si-*DSCAM-AS1*#1 group. The experiments were performed in triplicate. *; P<0.05, **; P<0.01, ***; P<0.001, OSCC; Oral squamous cell carcinoma, qRT-PCR; Quantitative real time polymerase chain reaction, siRNA; Small interfering RNA, MTT; 3-(4,5-dimethylthiazol-2-yl)-2,5-diphenyltetrazolium bromide, and EdU; 5-ethynyl-2'-deoxyuridine.

DSCAM-AS1 played a role in OSCC cells through *miR-138-5p*

Next, *miR-138-5p* inhibitors were transfected into HSC-3 and CAL-27 cells, and MTT, EdU, and Transwell assays were performed. The results elucidated that *miR-138-5p* inhibition markedly facilitated OSCC cell proliferation, migration, and invasion capabilities (Fig.4A-E). To confirm that *DSCAM-AS1* was involved in OSCC progression through repressing *miR-138-5p* expression, rescue experiments were performed. The

results suggested that *miR-138-5p* inhibitors were able to significantly abolish *DSCAM-AS1* knockdown-induced inhibitory impact on OSCC cell proliferation, migration, and invasion (Fig.4F, J). These findings suggested that *DSCAM-AS1* could promote OSCC progression via suppressing *miR-138-5p* expression.

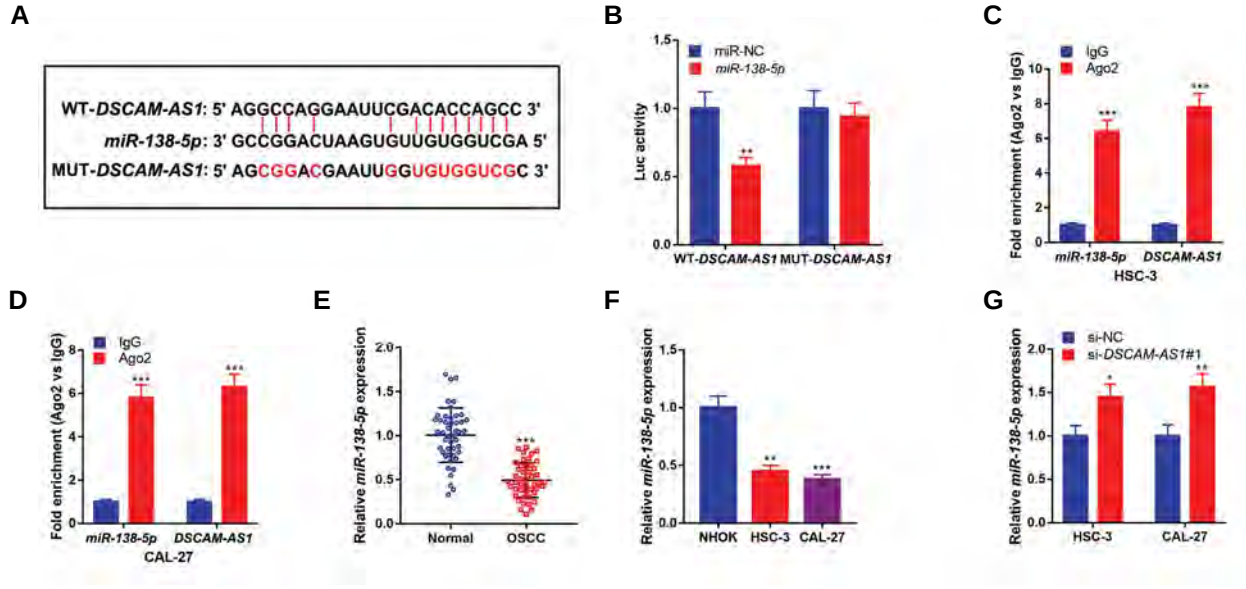

Fig.3: *MiR-138-5p* was a target of *DSCAM-AS1*. **A.** StarBase database predicted that *DSCAM-AS1* contained the complementary binding site for *miR-138-5p*. **B.** Luciferase reporter assay confirmed that the *DSCAM-AS1* and *miR-138-5p* could bind directly to each other. **C, D.** RIP assay verified the direct interaction between *miR-138-5p* and *DSCAM-AS1*. **E, F.** qRT-PCR showed that the expression of *miR-138-5p* was downregulated in the OSCC tissues and cell lines. **G.** qRT-PCR showed that *miR-138-5p* expression was upregulated in OSCC cell lines transfected with *DSCAM-AS1* siRNA. The experiments were performed in triplicate. *; P<0.05, **; P<0.01, ***; P<0.001, RIP; RNA immunoprecipitation, qRT-PCR; Quantitative real time polymerase chain reaction, OSCC; Oral squamous cell carcinoma, and siRNA; Small interfering RNA.

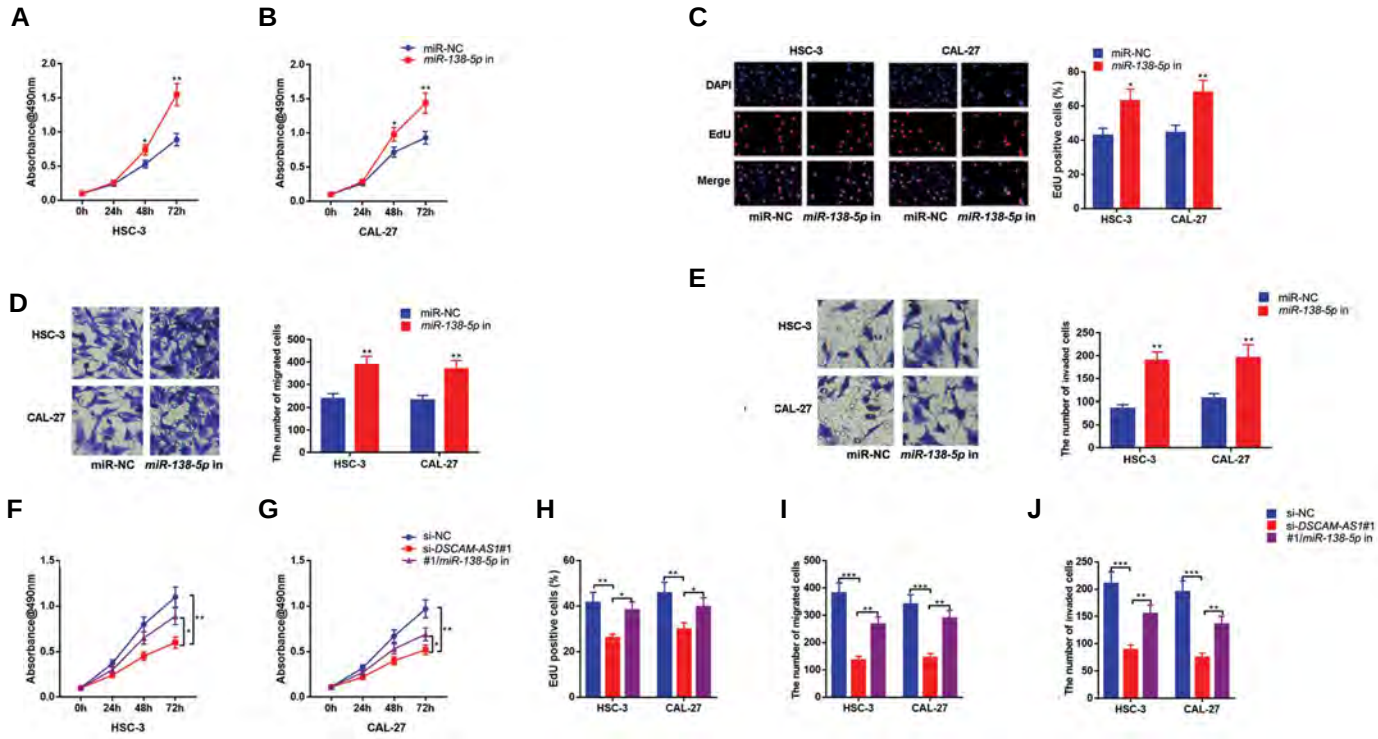

Fig.4: *DSCAM-AS1* played a role in OSCC cells via regulating *miR-138-5p* expression. **A-C.** MTT assay and EdU assay showed that OSCC cell proliferation was increased in OSCC cells transfected with *miR-138-5p* inhibitor. **D, E.** Transwell assay showed that cell migration and invasion abilities were increased in OSCC cells transfected with *miR-138-5p* inhibitor. **F-H.** MTT and EDU assay showed that OSCC cell proliferation was increased in the OSCC cells co-transfected with *DSCAM-AS1* siRNA and *miR-138-5p* inhibitors compared with OSCC cells transfected with *DSCAM-AS1* siRNA. **I, J.** Transwell assay showed that OSCC cell migration and invasion abilities were increased in the OSCC cells co-transfected with *DSCAM-AS1* siRNA and *miR-138-5p* inhibitors compared with OSCC cells transfected with *DSCAM-AS1* siRNA. The experiments were performed in triplicate. *; P<0.05, **; P<0.01, ***; P<0.001, OSCC; Oral squamous cell carcinoma, MTT; 3-(4,5-dimethylthiazol-2-yl)-2,5-diphenyltetrazolium bromide, EdU; 5-ethynyl-2'-deoxyuridine, and siRNA; Small interfering RNA.

MiR-138-5p could directly target *EZH2* to inhibit OSCC progression

Next, we use 5 online databases (microT, TargetScan, PicTar, miRmap, and miRanda) to search the potential targets of *miR-138-5p*, and a Venn diagram depicted that there were 85 genes predicted by all of the bioinformatics tools, and *EZH2* was among them (Fig.5A). Subsequently, dual-luciferase reporter assay showed that *miR-138-5p* mimics notably reduced the luciferase activity of the WT *EZH2* reporter vector but had no impact on the MUT *EZH2* reporter (Fig.5B). In addition, the RIP assay showed that *miR-138-5p* and *EZH2* mRNA were directly interacted (Fig.5C, D). Moreover, rescue experiments revealed that *EZH2* siRNA could partly counteract the *miR-138-5p* inhibitor-induced promoting impact on OSCC cell proliferation, migration, and invasion (Fig.5E-I). The aforementioned evidence confirmed that *miR-138-5p* could regulate OSCC progression by inhibiting *EZH2*.

DSCAM-AS1 regulated *EZH2* expression via *miR-138-5p*

Eventually, to substantiate the regulatory effects of *DSCAM-AS1* on *miR-138-5p* and *EZH2* expressions in OSCC cells, we transfected *DSCAM-AS1* siRNA or *DSCAM-AS1* siRNA+*miR-138-5p* inhibitors into HSC-3 and CAL-27 cell lines, respectively. Our data demonstrated that knocking down *DSCAM-AS1* observably inhibited *EZH2* expression, and the co-transfection of *miR-138-5p* inhibitors partially abolished the inhibiting impact of *DSCAM-AS1* knockdown on the *EZH2* expression (Fig.5J, K). Hence, it was concluded that *DSCAM-AS1* could regulate *EZH2* expression through repressing *miR-138-5p* expression.

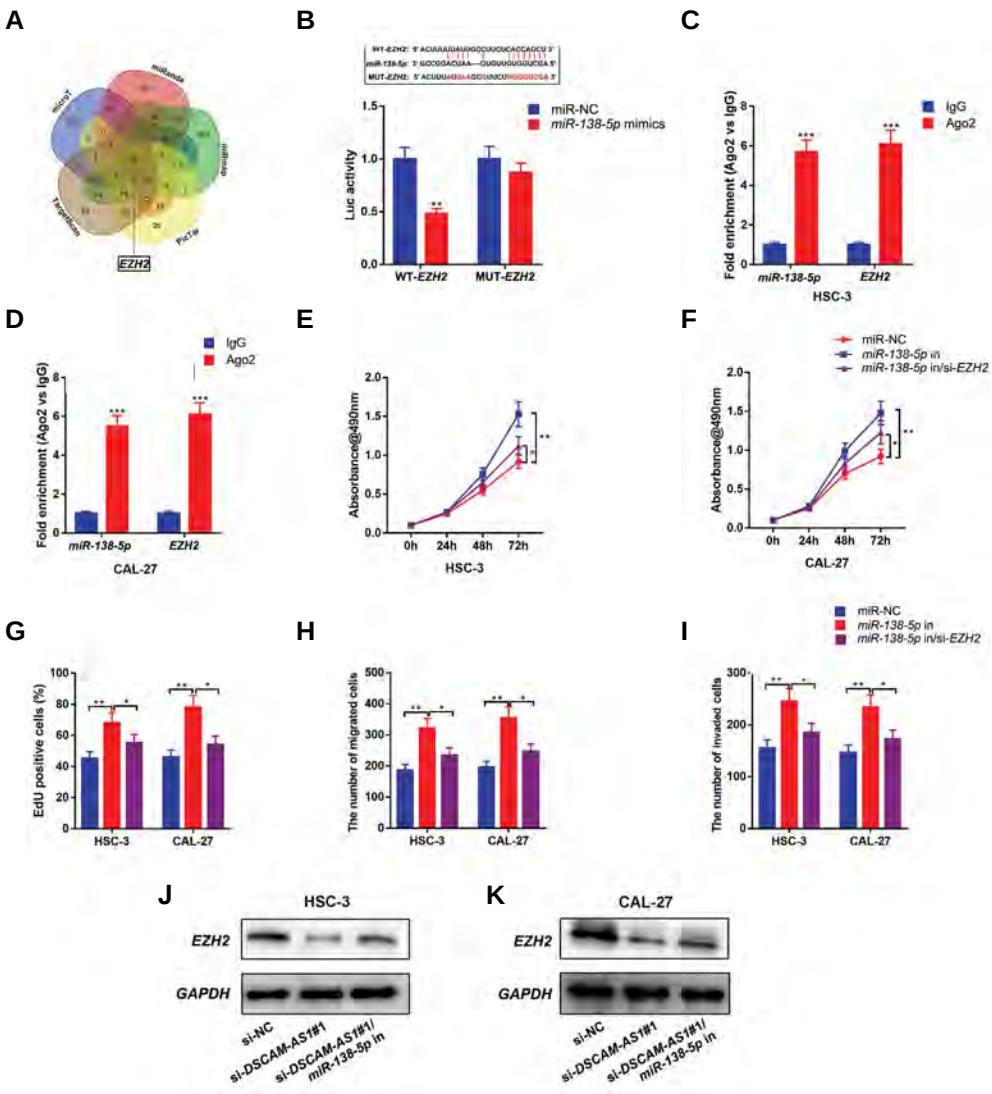

Fig.5: *MiR-138-5p* could directly target *EZH2* to inhibit OSCC progression. **A.** The targets of *miR-138-5p* were predicted by five online databases. **B.** StarBase predicted that the 3´UTR of *EZH2* contained a binding site for *miR-138-5p*, and dual-luciferase reporter assay confirmed that *miR-138-3p* and the 3´UTR of *EZH2* could directly bind to each other. **C, D.** RIP assay verified the relationship between *miR-138-5p* and *DSCAM-AS1*. **E-G.** MTT and EdU assay showed that OSCC cell proliferation was decreased in OSCC cells co-transfected with *miR-138-5p* inhibitors and *EZH2* siRNA compared with OSCC cells transfected with *miR-138-5p* inhibitors. **H, I.** Transwell assay showed that OSCC cell proliferation was decreased in OSCC cells co-transfected with *miR-138-5p* inhibitors and *EZH2* siRNA compared with OSCC cells transfected with *miR-138-5p* inhibitors. **J, K.** Western blot showed that the expression of EZH2 in OSCC cell lines was increased in the OSCC cells co-transfected with DSCAM-AS1 siRNA and miR-138-5p inhibitors compared with OSCC cells transfected with DSCAM-AS1 siRNA. The experiments were performed in triplicate. *; P<0.05, **; P<0.01, ***; P<0.001, OSCC; Oral squamous cell carcinoma, siRNA; Small interfering RNA, RIP; RNA immunoprecipitation, MTT; 3-(4,5-dimethylthiazol-2-yl)-2,5-diphenyltetrazolium bromide, and EdU; 5-ethynyl-2'-deoxyuridine.

Discussion

LncRNAs feature prominently in cancer biology. Accumulating studies confirmed that DSCAM-AS1 contributes to promoting the carcinogenesis and disease progression of multiple cancers. For example, DSCAM-AS1 can enhance ribonucleotide reductase regulatory subunit M2 expression via inhibiting miR-204-5p expression, thus promoting breast cancer cell proliferation (8). DSCAM-AS1 expression is remarkably elevated in hepatocellular carcinoma cell lines and tissues, and DSCAM-AS1 promotes hepatocellular carcinoma cell proliferation and migration through targeting miR-338-3p (9). In this study, it was found that DSCAM-AS1 expression was significantly up-regulated in OSCC tumor tissues and cell lines; high DSCAM-AS1 expression was linked to unfavorable pathological characteristics of OSCC patients; *In vitro* experiments confirmed that knocking down DSCAM-AS1 significantly inhibited OSCC cell proliferation, migration, and invasion. Such findings exhibited that DSCAM-AS1 could probably play a role as a cancer-promoting factor in OSCC.

LncRNAs can act as ceRNAs by sponging miRNAs to affect the expression of mRNAs and thus play a role in OSCC (16). For example, lncRNA nuclear paraspeckle assembly transcript 1 can absorb miR-365 as a molecular sponge to regulate regulator of G protein signaling 20, thus promoting OSCC cell proliferation and invasion (17). LncRNA relaxin 1, as a ceRNA of miR-138, regulates EZH2 and promotes OSCC cell proliferation and invasion (13). HOXA11-AS adsorbs miR-98-5p to up-regulate the expression of Y-box binding protein 2, thereby facilitating OSCC development (18). To delve deeper into the underlying mechanism of DSCAM-AS1 in OSCC, we used the StarBase database to predict the miRNAs that were potentially regulated by DSCAM-AS1, and then miR-138-5p was selected for further research. As a tumor suppressor, miR-138-5p participates in the development of multiple tumors. For instance, miR-138-5p expression is significantly reduced in colorectal cancer cell lines and tissues, and miR-138-5p can inhibit cell proliferation by inhibiting programmed cell death 1 ligand 1 (19). In OSCC, it's been shown that miR-138 expression is notably down-regulated in cancer tissues and cell lines, and miR-138 is able to suppress cell proliferation, migration, and invasion via modulating ISG15 (12). Another study reported that lncRNA H19 imprinted maternally expressed transcript suppresses the expression of EZH2 by inhibiting miR-138 expression to play a cancer-promoting role in OSCC (13). In this work, we demonstrated that DSCAM-AS1 and miR-138-5p were able to bind directly to each other, miR-138-5p expression was markedly reduced in OSCC cell lines and tissues, and miR-138-5p could repress the malignant biological behaviors of OSCC cells. Furthermore, DSCAM-AS1 knockdown in OSCC cells elevated miR-138-5p expression, and miR-138-5p inhibitors partly abolished the inhibitory effect of DSCAM-AS1 knockdown on the malignancy of OSCC cells. Therefore, our findings unearthed that miR-138-5p was likely to suppress OSCC expression, miR-138-5p was a downstream target of DSCAM-AS1, and DSCAM-AS1 played a cancer-promoting role in OSCC by inhibiting miR-138-5p expression.

Given that lncRNA acts as a ceRNA to eliminate the inhibitory effect of miRNA on target genes, the target genes of miRNA are important parts of the ceRNA network. In the present work, EZH2 was proven to be a target of miR-138-5p, which is consistent with the previous report (13). As the core part of the polycomb repressive complex 2, EZH2 plays a cancer-promoting role in many tumors. A previous study verified that EZH2 can inhibit cyclin dependent kinase inhibitor 1A expression to promote the proliferation of gastric cancer cells (20); in the head and neck squamous cell carcinoma, EZH2 participates in tumor progression by regulating EMT (21). In the current study, we uncovered that EZH2 expression was markedly enhanced in OSCC cell lines and tissues. Besides, knocking down EZH2 could partially counteract the promotional impact of miR-138-5p inhibition on OSCC progression. These findings indicated that miR-138-5p repressed OSCC development via suppressing EZH2 expression. Further experiments showed that EZH2 expression was modulated by DSCAM-AS1/miR-138-5p axis. The above-mentioned evidence confirmed that the DSCAM-AS1/miR-138-5p/EZH2 axis participated in regulating OSCC progression.

Conclusion

We identified a novel oncogenic lncRNA, DSCAM-AS1, in OSCC. It was demonstrated that DSCAM-AS1 increases OSCC cell proliferation, migration, and invasion through modulating miR-138-5p/EZH2 axis. DSCAM-AS1 may be a potential biomarker and target for OSCC diagnosis and therapies.

Acknowledgements

We thank Hubei Yican Health Industry Co., Ltd for its linguistic assistance during the preparation of this manuscript. The data used to support the findings of this study are available from the corresponding author upon request. There is no financial support and conflict of interest in this study.

Authors' Contributions

Y.Z., F.H.; Participated in study design and drafting the manuscript. Y.Z., X.W., P.W.; Contributed extensively in interpretation of the data and the conclusion. Y.Z., X.W., X.Z., S.H.; Performed data collection and experiments. All authors performed editing read and approved the final manuscript.

References

1. Bhatia N, Lalla Y, Vu AN, Farah CS. Advances in optical adjunctive

AIDS for visualisation and detection of oral malignant and potentially malignant lesions. Int J Dent. 2013; 2013: 194029.
2. Bray F, Ferlay J, Soerjomataram I, Siegel RL, Torre LA, Jemal A. Global cancer statistics 2018: GLOBOCAN estimates of incidence and mortality worldwide for 36 cancers in 185 countries. CA Cancer J Clin. 2018; 68(6): 394-424.
3. Warnakulasuriya S. Global epidemiology of oral and oropharyngeal cancer. Oral Oncol. 2009; 45(4-5): 309-316.
4. Ponting CP, Oliver PL, Reik W. Evolution and functions of long noncoding RNAs. Cell. 2009; 136(4): 629-641.
5. Fang Z, Zhao J, Xie W, Sun Q, Wang H, Qiao B. LncRNA UCA1 promotes proliferation and cisplatin resistance of oral squamous cell carcinoma by sunppressing miR-184 expression. Cancer Med. 2017; 6(12): 2897-2908.
6. Wang X, Li H, Shi J. LncRNA HOXA11-as promotes proliferation and cisplatin resistance of oral squamous cell carcinoma by suppression of miR-214-3p expression. Biomed Res Int. 2019; 2019: 8645153.
7. Chen F, Qi S, Zhang X, Wu J, Yang X, Wang R. lncRNA PLAC2 activated by H3K27 acetylation promotes cell proliferation and invasion via the activation of Wnt/βcatenin pathway in oral squamous cell carcinoma. Int J Oncol. 2019; 54(4): 1183-1194.
8. Liang WH, Li N, Yuan ZQ, Qian XL, Wang ZH. DSCAM-AS1 promotes tumor growth of breast cancer by reducing miR-204-5p and up-regulating RRM2. Mol Carcinog. 2019; 58(4): 461-473.
9. Ji D, Hu G, Zhang X, Yu T, Yang J. Long non-coding RNA DSCAM-AS1 accelerates the progression of hepatocellular carcinoma via sponging miR-338-3p. Am J Transl Res. 2019 Jul 15;11(7):4290-4302. Retraction in: Am J Transl Res. 2021; 13(12): 14238.
10. Karatas OF, Oner M, Abay A, Diyapoglu A. MicroRNAs in human tongue squamous cell carcinoma: from pathogenesis to therapeutic implications. Oral Oncol. 2017; 67: 124-130.
11. Zhang Q, He Y, Nie M, Cai W. Roles of miR-138 and ISG15 in oral squamous cell carcinoma. Exp Ther Med. 2017; 14(3): 2329-2334.
12. Hong Y, He H, Sui W, Zhang J, Zhang S, Yang D. Long non-coding RNA H1 promotes cell proliferation and invasion by acting as a ceRNA of miR138 and releasing EZH2 in oral squamous cell carcinoma. Int J Oncol. 2018; 52(3): 901-912.
13. Salmena L, Poliseno L, Tay Y, Kats L, Pandolfi PP. A ceRNA hypothesis: the Rosetta Stone of a hidden RNA language? Cell. 2011; 146(3): 353-358.
14. Angelozzi M, de Charleroy CR, Lefebvre V. EdU-based assay of cell proliferation and stem cell quiescence in skeletal tissue sections. Methods Mol Biol. 2021; 2230: 357-365.
15. Ye J, Jiao Y. LncRNA FAL1 promotes the development of oral squamous cell carcinoma through regulating the microRNA-761/CRKL pathway. Eur Rev Med Pharmacol Sci. 2019; 23(13): 5779-5786.
16. Huang G, He X, Wei XL. lncRNA NEAT1 promotes cell proliferation and invasion by regulating miR365/RGS20 in oral squamous cell carcinoma. Oncol Rep. 2018; 39(4): 1948-1956.
17. Niu X, Yang B, Liu F, Fang Q. LncRNA HOXA11-AS promotes OSCC progression by sponging miR-98-5p to upregulate YBX2 expression. Biomed Pharmacother. 2020; 121: 109623.
18. Zhao L, Yu H, Yi S, Peng X, Su P, Xiao Z, et al. The tumor suppressor miR-138-5p targets PD-L1 in colorectal cancer. Oncotarget. 2016; 7(29): 45370-45384.
19. Zhao L, Yu H, Yi S, Peng X, Su P, Xiao Z, et al. The tumor suppressor miR-138-5p targets PD-L1 in colorectal cancer. Oncotarget. 2016; 7(29): 45370-45384.
20. Chang JW, Gwak SY, Shim GA, Liu L, Lim YC, Kim JM, et al. EZH2 is associated with poor prognosis in head-and-neck squamous cell carcinoma via regulating the epithelial-to-mesenchymal transition and chemosensitivity. Oral Oncol. 2016; 52: 66-74.
21. Zheng M, Cao MX, Luo XJ, Li L, Wang K, Wang SS, et al. EZH2 promotes invasion and tumour glycolysis by regulating STAT3 and FoxO1 signalling in human OSCC cells. J Cell Mol Med. 2019; 23(10): 6942-6954.

Original Article

GUSBP11 Inhibited The Progression of Triple Negative Breast Cancer via Targeting The *miR-579-3p/SPNS2* Axis

Guangbin Wu, M.Sc., Peilong Sun, Ph.D., Chunzhi Qin, Ph.D.*

Department of General Surgery, Jinshan Hospital, Fudan University, Shanghai, China

Corresponding Address: Department of General Surgery, Jinshan Hospital, Fudan University, Shanghai, China
Email: zhiao060863@163.com

Received: 29/March/2021, Accepted: 22/August/2021

Abstract

Objective: Growing evidences have exposed the important roles of long noncoding RNAs (lncRNAs) in the triple negative breast cancer (TNBC) inhibition. The function of glucuronidase beta pseudogene 11 (*GUSBP11*) in the TNBC occurrence remains obscure. To detect the function of GUSBP11 in TNBC progression and explore its downstream molecular mechanism.

Materials and Methods: In this experimental study, using quantitative reverse transcription real-time polymerase chain reaction (RT-qPCR), we measured the *GUSBP11* expression in the TNBC cell lines. Gain-of-function assays, including colony formation, flow cytometry, and western blot were used to identify the probable effects of *GUSBP11* overexpression on the malignant behaviors of TNBC cell lines. Moreover, mechanism assays, including RNA immunoprecipitation (RIP), RNA pull down and luciferase reporter assays were taken to measure the possible mechanism of *GUSBP11* in the TNBC cell lines.

Results: *GUSBP11* expressed at a low RNA level in the TNBC cell lines. Overexpression of *GUSBP11* RNA expression inhibited the proliferation, migration, epithelial-to-mesenchymal transition (EMT) and stemness while elevated the apoptosis of the TNBC cell lines. *GUSBP11* positively regulated the expression of sphingolipid transporter 2 (*SPNS2*) via acting as a competing endogenous RNA (ceRNA) of *miR-579-3p*, thereby suppressing the development of TNBC cell lines.

Conclusion: *GUSBP11* impedes TNBC progression via modulating the *miR-579-3p*/*SPNS2* axis.

Keywords: *GUSBP11*, *miR-579-3p, SPNS2*, Triple-Negative Breast Cancer

Cell Journal(Yakhteh), Vol 24, No 5, May 2022, Pages: 230-238

Citation: Wu G, Sun OP, Qin C. GUSBP11 inhibited the progression of triple negative breast cancer via targeting the miR-579-3p/SPNS2 axis. Cell J. 2022; 24(5): 230-238. doi: 10.22074/cellj.2022.8024.

Introduction

Breast cancer (BC) is one of the most frequent cancers, which mostly occur in the females. The incidence rate is increasing, accompanied by the young age of BC patients in recent years (1, 2). Triple-negative breast cancer (TNBC) is a subtype of BC, which is featured by the absence of estrogen receptor (ER), progesterone receptor (PR), and human epidermal growth factor receptor-2 (HER2) (3). Despite of improvements in the screening, operation, and chemo-radiotherapy methods, the TNBC patient's prognosis is still not optimistic (4, 5). Hence, it is necessary to explore novel potential therapeutic targets.

Non-coding RNAs (ncRNAs) mainly include long non-coding RNAs (lncRNAs) and microRNAs (miRNAs) (6, 7). In recent years, lncRNAs have been reported to act as important regulators in various biological processes of human cancers via various approaches, such as the regulation of transcription, translation, protein modification, and the formation of RNA-protein or protein-protein complexes (8). A large amount of evidence has suggested that lncRNAs act as tumor promoters or tumor suppressors in the TNBC development (9). In addition, many lncRNAs are identified as potential therapeutic targets for TNBC treatment (10). Even so, there are some lncRNAs underlying TNBC remain to be explored. In the current study, we mainly focused on the role of a novel lncRNA glucuronidase beta pseudogene 11 (*GUSBP11*) in the TNBC.

MicroRNAs (miRNAs) are crucial regulators in the TNBC development (11). For example, *miR-29b-3p* contributes to the TNBC progression through the TRAF3 regulating (12); *miR-613* represses cell migration and invasion via inhibiting Daam1 in the TNBC (13). Besides, miRNAs can exert functions post-transcriptionally via degrading mRNA or inhibiting the translation via binding to the 3′ untranslated region (3′UTR) of the targeted genes (14). The controller role of *miR-579-3p* in the melanoma progression has been revealed in a previous study (15), but we still don't know whether it can function in the TNBC and its underlying mechanism remain to be unveiled. In this study, we uncovered the involvement of *miR-579-3p* in the *GUSBP11*-mediated TNBC progression.

Our research group focused on the role of sphingolipid transporter 2 (*SPNS2*) in the TNBC progression. We speculated that *GUSBP11* inhibited TNBC cell malignancy via *miR-579-3p*/*SPNS2* axis. Therefore, we analyzed the expression pattern of the genes in the TNBC cell lines and examined the related biological functions. Collectively, this study was aimed to investigate the impacts of the *GUSBP11*/*miR-579-3p*/*SPNS2* axis in the TNBC progression.

Materials and Methods

Cell culture

In this experimental study, human BC cell lines (MDA-MB-231, MDA-MB-436, MDA-MB-453, SKBR3, MCF-7, BT-474, AU565, T-47D, ZR-75-1), HEK293T cell line and human breast non-tumorigenic epithelial cell line (MCF-10A) were all obtained from the American Type Culture Collection (ATCC, Manassas, VA, USA). Human BC cell lines (CAL-120, SUM190 and SUM1315) were obtained from COBIOER (Nanjing, China). The HEK293T cell line was cultured in the ATCC-formulated Eagle's Minimum Essential Medium (EMEM, M0200, Sigma-Aldrich, St. Louis, MO, USA). MDA-MB-231, MDA-MB-436, MDA-MB-453 cell lines were cultured in the Leibovitz's L-15 Medium (11415049, Thermo Fisher Scientific, Rockford, IL, USA). The MCF-10A cell line was grown in the MEBM (CC-2151, LONZA, Basel, Switzerland). The SKBR3 cell line was grown in the McCoy's 5a Medium (16600108, Thermo Fisher Scientific, Rockford, IL, USA). MCF-7 and CAL-120 cell lines were grown in the Dulbecco's Minimum Essential Medium (A4192101, Gibco, Rockville, MD, USA). The BT-474 cell line was grown in the Hybri-Care Medium (ATCC46-X, ATCC, Manassas, VA, USA). AU565, T-47D, ZR-75-1 and SUM190 cell lines were cultured in the RPMI-1640 Medium (A4192301, Gibco, Rockville, MD, USA). The SUM1315 cell line was cultured in the Ham's F-12 medium (88424, Thermo Fisher Scientific, Rockford, IL, USA). All the culture mediums were treated with 10% fetal bovine serum (FBS, 16140071, Thermo Fisher Scientific, Rockford, IL, USA) and mixed with 1% penicillin and streptomycin (15140148, Thermo Fisher Scientific, Rockford, IL, USA). Cell culture was achieved in the 5% CO_2 at 37°C. The culture mediums were changed after 3-4 days of cultivation, and the cell lines went through passage every 7 days.

Cell transfection

For overexpression, the full-length cDNA sequences of *GUSBP11* were inserted into the pcDNA3.1 vectors (15042907, Sigma-Aldrich, St. Louis, MO, USA) to construct pcDNA3.1/*GUSBP11* plasmids. Likewise, the whole length of YY1, p300 and HDAC2 was separately inserted into pcDNA3.1 vectors to generate their overexpression vectors. Empty pcDNA3.1 vector was used as the negative control (NC) for all overexpression vectors. Besides, *miR-579-3p* and NC mimics, the specific shRNAs to *SPNS2* and nonspecific shRNAs (sh/NC) were purchased from GenePharma (Shanghai, China). Transfections were conducted using Lipofectamine 3000 (Invitrogen) and terminated after 48 hours. For rescue assays, we severally transfected pcDNA3.1, pcDNA3.1/GUSBP11, pcDNA3.1/*GUSBP11*+*miR-579-3p* mimics and pcDNA3.1/GUSBP11+sh/*SPNS2*#1 into MDA-MB-231 and MDA-MB-453 cell lines.

Quantitative reverse transcription real-time polymerase chain reaction

Total RNA was extracted from the cell lines using TRIzol Reagent (15596026, Thermo Fisher Scientific, Rockford, IL, USA). Next, PrimeScript RT master mix (RR036Q, Takara, Japan) was employed for reverse transcription of RNA. Then, SYBR Premix Ex TaqTM II (4309155, Applied Biosystems, Foster city, CA, USA) was utilized to examine the gene expression based on $2^{-\Delta\Delta Ct}$ method. *GAPDH* or *U6* was used as the internal reference. Samples were assayed in triplicate and results were obtained from three independent experiments.

Colony formation assay

Transfected TNBC cell lines (500 cells per well) were planted into 6-well plates. After 12 days, the culture medium was discarded and the cell lines were fixed with a Methanol solution (67-56-1, Bojing Chemical Co., Ltd, Shanghai, China) for 15 minutes, and stained by 0.5% crystal violet (V5265, Sigma-Aldrich, St. Louis, MO, USA) for 10 minutes at room temperature. The number of colonies was manually counted. Samples were assayed in triplicate and results were obtained from three independent experiments.

5-Ethynyl-2′-deoxyuridine

5-Ethynyl-2′-deoxyuridine (EdU) staining was performed using a BeyoClick™ Cell Proliferation Kit (C0075L, Beyotime, Guangzhou, China). Transfected TNBC cell lines were added with EdU and incubated for 2 hours at room temperature. After washing, cell lines were fixed with 4% paraformaldehyde. The nucleus was stained by DAPI (D9542, Sigma-Aldrich, St. Louis, MO, USA) and images were captured via using an inverted microscope (Olympus, Japan). Samples were assayed in triplicate and results were obtained from three independent experiments.

Terminal-deoxynucleoitidyl Transferase Mediated Nick End labeling (TUNEL)

TUNEL reagent (12156792910, Roche, Basel, Switzerland) was commercially acquired for TUNEL experiment. Transfected cell lines (1×10^4) were planted into the 96-well plates, fixed by 4% paraformaldehyde, permeabilized with 0.1% Triton-X100, and then treated with TUNEL kit (Merck KGaA, Darmstadt, Germany) for 1 hour. Finally, cell nucleus was subjected to DAPI staining and observed using fluorescence microscope (DMI8, Leica, Wetzlar, Germany). Samples were assayed in triplicate and results were obtained from three independent experiments.

Flow cytometry analysis

Transfected cell lines were collected and placed into the 6-well plates. Flow cytometer was used following the instruction (17-344, Sigma-Aldrich, St. Louis, MO, USA), and the Annexin V-FITC/PI double staining kit

(APOAF, Sigma-Aldrich, St. Louis, MO, USA) was purchased from Invitrogen. After staining for 15 minutes, cell lines were reaped for flow cytometry. Samples were assayed in triplicate and results were obtained from three independent experiments.

Transwell assay

Cell lines (5×10^4) were seeded into the upper chamber of the insert (pore size 8 μm; 3428, Corning, NY, USA) and incubated in the serum-free DMEM medium. The DMEM medium containing 10% FBS was added to the lower chamber. After incubation for 24 hours in the 5% CO_2 at 37°C, the upper membrane cells were wiped, and the migrated cells through the membrane were fixed with 4% paraformaldehyde (E672002, Sangon Biotech, Shanghai, China) and stained with 0.1% crystal violet (V5265, Sigma-Aldrich, St. Louis, MO, USA). The images were observed via an inverted microscope (DMi1, Leica, Wetzlar, Germany). Samples were assayed in triplicate and results were obtained from three independent experiments.

Sphere formation assay

Cell lines were cultured in the serum-free DMEM medium treated with insulin (12643, Sigma-Aldrich, St. Louis, MO, USA), 20 ng/mL human recombinant epidermal growth factor (EGF, GF144, Sigma-Aldrich, St. Louis, MO, USA) and 10 ng/mL basic fibroblast growth factor (bFGF, 2255, Sigma-Aldrich, St. Louis, MO, USA). After 14 days of culture, the sphere formation was observed using a microscope (DMi1, Leica, Wetzlar, Germany). Samples were assayed in triplicate and results were obtained from three independent experiments.

ChIP assay

Following the protocol, an EZ ChIP Chromatin Immunoprecipitation kit (17-295; Millipore, Billerica, MA, USA) was applied to ChIP assay. Chromatin was cross-linked and sonicated to 200-1000-bp fragments, followed by immunoprecipitation with anti-YY1 or anti-IgG antibody (401455-2ML-M, Millipore, Billerica, MA, USA) which was selected as the NC. RT-qPCR was eventually carried out for enrichment detection. Samples were assayed in triplicate and results were obtained from three independent experiments.

Subcellular fractionation

RNA was separated from the nuclear or cytoplasmic fraction via a PARIS Kit (AM1921, Thermo Fisher Scientific, Rockford, IL, USA), followed by quantification with RT-qPCR. Here, *GAPDH* and *U6* were served as cytoplasmic and nuclear marker, respectively. Samples were assayed in triplicate and results were obtained from three independent experiments.

Fluorescence in situ hybridization

The cellular localization of *GUSBP11* was detected via a FISH kit (F32952, Invitrogen, Carlsbad, CA, USA). The cell lines were cultured with the Digoxigenin-labeled *GUSBP11* probe (Ribobio, Guangzhou, China) in hybridization solution (H7782, Sigma-Aldrich, St. Louis, MO, USA). Nuclei were counterstained with DAPI (D9542, Sigma-Aldrich, St. Louis, MO, USA), and the cell lines were finally observed under a confocal laser-scanning microscope. Briefly, adding a few drops of DAPI dye to the prepared slides for 10 minutes. Then, the slides were gently rinsed with running water, and excess water absorbed by filter paper. Next, a drop of antifade mounting medium was added and the slides were observed under a fluorescence microscope. Samples were assayed in triplicate and results were obtained from three independent experiments.

RNA immunoprecipitation

RNA immunoprecipitation (RIP) assay was implemented via an RNA-binding protein immunoprecipitation kit (17-704, Sigma-Aldrich, St. Louis, MO, USA). Transfected cell lines were lysed, and then hatched with RIP buffer containing magnetic beads conjugated with anti-Ago2 antibody. After being washed and purified, the immunoprecipitated RNA was analyzed via RT-qPCR. Samples were assayed in triplicate and results were obtained from three independent experiments.

RNA pull down assay

GUSBP11 biotin probe (Ribobio, Guangzhou, China) or wild-type or mutant-type of *miR-579-3p* were transcribed into the cell lines. Transfected cell lysates were hatched with Dynabeads M-280 Streptavidin (11206D, Thermo Fisher Scientific, Rockford, IL, USA) overnight at 4°C according to the manufacturer's requirements. Then, the beads were washed and eluted. RNAs were extracted by TRIzol reagent (15596026, Thermo Fisher Scientific, Rockford, IL, USA) and evaluated by RT-qPCR. Samples were assayed in triplicate and results were obtained from three independent experiments.

Luciferase reporter assays

The sequence of *GUSBP11* promoter was sub-cloned into pGL3 vector (Promega, Madison, WI, USA). And, overexpression plasmids were co-transfected into the cell lines to evaluate the activity of *GUSBP11* transcription.

The *GUSBP11* fragment or *SPNS2* 3'UTR fragment covering the *miR-579-3p* binding site was inserted into the pmirGLO vector (Promega, Madison, WI, USA). And then, the cell lines were severally co-transfected with luciferase reporter vectors containing *GUSBP11*-Wt/Mut or *SPNS2* 3′UTR-WT/Mut and *miR-579-3p* mimics/NC mimics using Lipofectamine 3000 (L3000075, Invitrogen, Carlsbad, CA, USA). The Firefly and Renilla luciferase activity was measured at 48 hours after transfection with a dual-luciferase reporter assay kit (E1910, Promega, Madison, WI, USA). Samples were assayed in triplicate and results were obtained from three

independent experiments.

Statistical analysis

All experimental data were shown as mean ± standard deviation (SD) of three independent experiments and analyzed by GraphPad Prism 5.0 (San Diego, CA, USA). The significant difference of the groups was assessed using Student's t test and one-way analysis of variance (ANOVA). Also, $P<0.05$ indicated statistically significant data.

Results

Overexpression of *GUSBP11* in the RNA level suppresses the TNBC cell growth

Searching online database (http://gepia2.cancer-pku.cn), lncRNA *GUSBP11* was determined to be down-regulated in the all types of BC tissues in comparison with the normal tissues (Fig.1A-E). To further explore the potential role of *GUSBP11* in the specific cancer types, we evaluated its RNA level in the all subtypes of BC cell lines. In comparison with the human normal mammary cell line (MCF-10A), *GUSBP11* expression was only obvious down-regulated in the TNBC cell lines, including MDA-MB-436, MDA-MB-453 and MDA-MB-231 (Fig.1F), suggesting that *GUSBP11* down-regulation might be correlated with the TNBC progression. Next, we designed gain-of-function assays to identify the functional role of *GUSBP11* overexpression in the TNBC. At first, pcDNA3.1/*GUSBP11* was transfected into the MDA-MB-231 and MDA-MB-453 cell lines which presented the lowest RNA level of *GUSBP11* (Fig.1G). It was observed in the colony formation experiments that the number of colonies in the TNBC cell lines was decreased after the overexpression of *GUSBP11* (Fig.1H). Consistently, the EdU positive stained cells were lessened up to 30% when *GUSBP11* was up-regulated (Fig.1I). On the contrary, a rise of about 7% in the apoptosis rate was observed in MDA-MB-231 and MDA-MB-453 cell lines due to *GUSBP11* up-regulation (Fig.1J, K). All these data suggested that *GUSBP11* was down-regulated in the TNBC cells and its overexpression impeded cell growth.

GUSBP11 up-regulation represses invasion, migration and stemness of the TNBC cell lines

We continued to detect the effects of *GUSBP11* on other biological properties of the TNBC cell lines. Through Transwell assays, we found that the invasive and migratory abilities of TNBC cell lines were repressed by *GUSBP11* elevation (Fig.2A, B). Consistently, we observed that the overexpression of *GUSBP11* led to an increase in the protein expression of E-cadherin while a decrease in the protein expression of MMP2, MMP7, N-cadherin and Vimentin, which indicated that *GUSBP11* up-regulation repressed the epithelial-mesenchymal transition, namely epithelial-to-mesenchymal transition (EMT) process in the TNBC cell lines (Fig.2C). Up-regulation of *GUSBP11* significantly suppressed sphere formation in the MDA-MB-453 and MDA-MB-231 cell lines, in different aspects including number and size (Fig.2D). Moreover, we also examined the RNA as well as protein levels of stemness markers using RT-qPCR and western blot. It was uncovered that the levels of *NANOG*, *OCT4* and *SOX2* were all decreased under *GUSBP11* overexpression (Fig.2E, F).

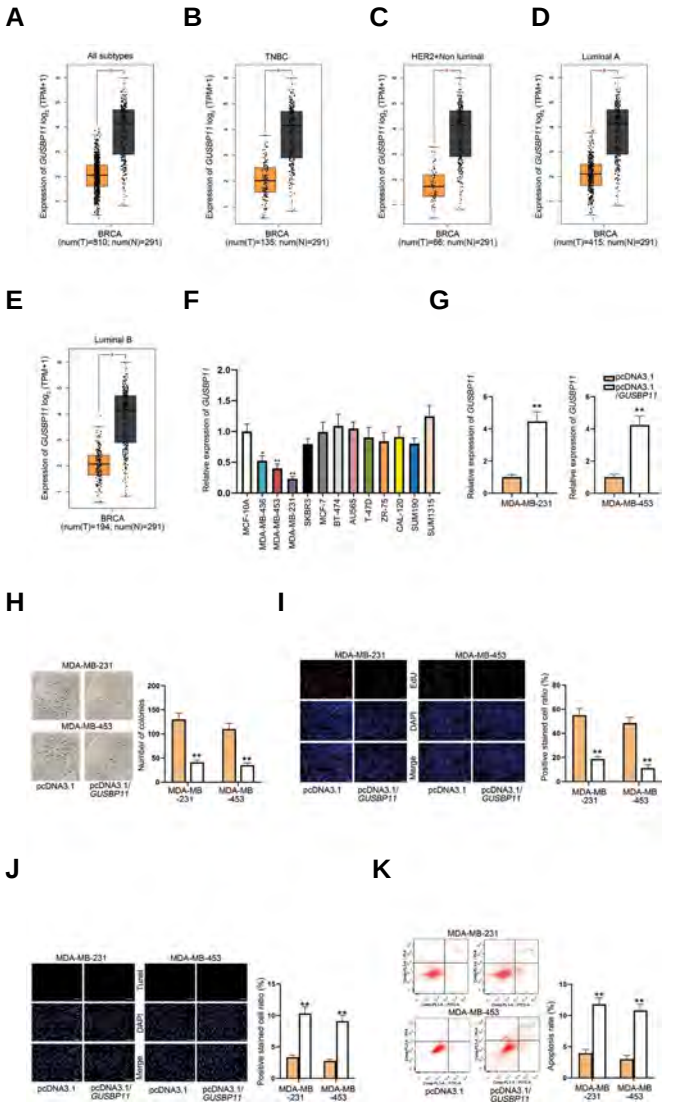

Fig.1: *GUSBP11* suppresses the TNBC cell lines growth. **A-E.** Box plot from GEPIA 2 database indicated the expression of *GUSBP11* in the different subtypes of breast cancer tissues. **F.** The expression of *GUSBP11* in the various types of breast cancer cell lines in comparison with human normal mammary cell line (MCF-10A). **G.** *GUSBP11* expression was enhanced in the TNBC cell lines via the transfection of pcDNA3.1/*GUSBP11*. **H.** The number of colonies in the pcDNA3.1/*GUSBP11*-transfected TNBC cell lines. **I.** The proliferation of the TNBC cell lines after *GUSBP11* elevation was evaluated by EdU assays (scale bar: 50 µm). **J,** and **K.** TUNEL assay, along with flow cytometry was taken to assess the apoptosis of the TNBC cell lines upon *GUSBP11* elevation (scale bar: 50 µm). Three independent experiments were conducted (n=3). TNBC; Triple negative breast cancer, *; $P<0.05$, and **; $P<0.01$.

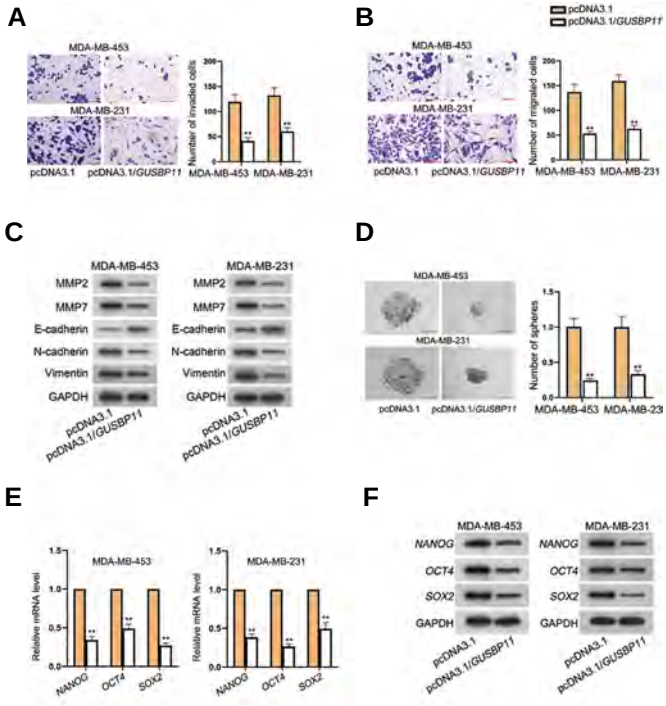

Fig.2: *GUSBP11* up-regulation represses cell migration, EMT and stemness in the TNBC cell lines. **A, B.** Transwell assays were performed to analyze the migration and invasion of the TNBC cell lines after *GUSBP11* overexpression (scale bar: 50 μm). **C.** Protein levels of EMT markers as well as cell invasion-related factors were tested in the TNBC cell lines after *GUSBP11* overexpression. **D.** The sphere formation assay was taken to measure the effect of *GUSBP11* elevation on the stemness of the TNBC cell lines (scale bar: 100 μm). **E, F.** The RNA level and protein level of stemness markers after *GUSBP11* overexpression. Three independent experiments were conducted (n=3). EMT; Epithelial-to-mesenchymal transition, TNBC; Triple negative breast cancer, and **; P<0.01.

YY1/p300/HDAC2 complex induces transcription inhibition of *GUSBP11* and suppresses its expression

To explore the upstream molecular mechanism of *GUSBP11* RNA in the TNBC, we used UCSC, an online database (http://genome.ucsc.edu/), and found that YY1 and p300 are two transcription factors that acted on the *GUSBP11* promoter. Through further screening in the JASPAR (http://jaspar.genereg.net/), we obtained three binding sequences of YY1 in the *GUSBP11* promoter (Fig.3A). Therefore, we constructed these three mutated sequences in order and then, verified the specific binding sites through luciferase reporter assay. Data revealed that YY1 might bind to the site 2 of *GUSBP11* promoter, where the luciferase activity of the HEK293T cell line showed an enhancement in the Site2-MUT group (Fig.3B). Through ChIP assay, it was verified that YY1 was enriched in the *GUSBP11* promoter in contrast to the control IgG group (Fig.3C). It has been reported that the YY1, p300 and HDAC2 can form a complex that regulates the development of colorectal cancer (16). Therefore, we conducted ChIP assay to verify the interaction of YY1/p300/HDAC2 axis and the *GUSBP11* promoter in the TNBC cell lines. Intriguingly, we uncovered that the enrichment of *GUSBP11* RNA in the immunoprecipitates conjugated to anti-YY1 was higher after overexpression of those three factors (Fig.3D). Similarly, the result of luciferase reporter assay in the HEK293T cell line showed that the activity of *GUSBP11* promoter was decreased a lot after overexpression of YY1, HDAC2 and p300, whereas this decreased tendency was more obvious when they were all overexpressed (Fig.3E). Finally, the expression level of *GUSBP11* was found to be reduced after individually overexpression of YY1, p300 or HDAC2, while this tendency of *GUSBP11* expression was more evident after the co-overexpression of them (Fig.3F).

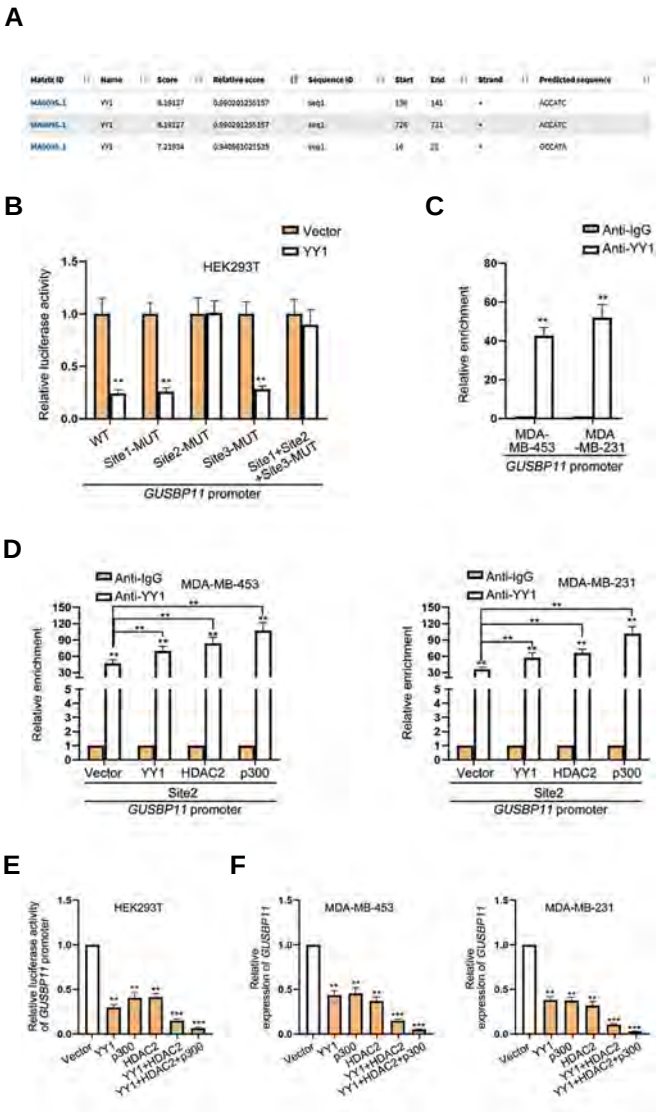

Fig.3: The YY1/p300/HDAC2 complex induces transcription inhibition of *GUSBP11* and suppresses its expression. **A.** Three binding sequences of YY1 in the *GUSBP11* promoter were obtained from JASPAR. **B.** The luciferase reporter assay was carried out to verify whether YY1 might bind to *GUSBP11* promoter. **C.** The affinity of YY1 in the *GUSBP11* promoter was verified by ChIP assay. **D.** ChIP assay was performed to measure the enticement of YY1 upon YY1, HDAC2 and p300 overexpression. **E.** The luciferase reporter assay was performed in the HEK293T cell line when YY1, HDAC2 or p300 was overexpressed alone or whey were overexpressed at the same time. **F.** RT-qPCR analysis of *GUSBP11* expression in the TNBC cell lines with individual or common overexpression of YY1, p300 and HDAC2. Three independent experiments were conducted (n=3). TNBC; Triple negative breast cancer, RT-qPCR; Quantitative reverse transcription real-time polymerase chain reaction, **; P<0.01, and ***; P<0.001.

GUSBP11 positively regulates *SPNS2* expression in the TNBC cell lines

In this part, we tried to verify the interaction between *GUSBP11* and *SPNS2*. According to GEPIA 2 database, we discovered that *SPNS2* expression was markedly declined in the TNBC tissues in contrast to normal tissues (Fig.4A). Meanwhile, a positive correlation between the *GUSBP11* expression and the *SPNS2* expression was observed (Fig.4B). Applying RT-qPCR, it was revealed that *SPNS2* was down-regulated in the TNBC cell lines in comparison with the MCF-10A cell line (Fig.4C). Afterwards, we explored whether *GUSBP11* and *SPNS2* could regulate each other. We found that *SPNS2* expression was up-regulated in the MDA-MB-231 and MDA-MB-453 cell lines transfected with pcDNA3.1/*GUSBP11* at both RNA and protein levels (Fig.4D). However, *SPNS2* overexpression did not affect the RNA expression of *GUSBP11* (Fig.4E, Fig.S1A, See Supplementary Online Information at www.celljournal.org). To further probe the potential mechanism of *GUSBP11* on the regulating *SPNS2* expression in the TNBC cell lines, we performed subcellular fractionation and FISH assays to determine the subcellular localization of *GUSBP11* in the TNBC cell lines. The results indicated that *GUSBP11* was majorly distributed in the cytoplasm, implying that *GUSBP11* regulated *SPNS2* at post-transcriptional level (17, 18, Fig.4F, G). To strengthen our hypothesis, we conducted luciferase reporter assay and determined that *GUSBP11* had no effect on the activity of the *SPNS2* promoter in RNA level (Fig.4H). As competitive endogenous RNA (ceRNA) mechanism is known as a common post-transcriptional regulatory method, we decided to explore whether *GUSBP11* may modulate the *SPNS2* expression through acting as a ceRNA to target certain miRNA in the TNBC cell lines. According to the result of RIP assays, both *GUSBP11* and *SPNS2* were highly enriched in the anti-Ago2 groups (Fig.4I), which supported the ceRNA model. Furthermore, a series of functional assays were taken to verify the effects of *SPNS2* overexpression in the TNBC cell lines, and results showed that increased *SPNS2* expression led to suppress cell proliferation, along with attenuated migration, invasion and EMT in the TNBC cell lines (Fig.S1B-J, See Supplementary Online Information at www.celljournal.org).

GUSBP11 positively regulates the *SPNS2* expression via interacting with *miR-579-3p*

We searched starBase (http://starbase.sysu.edu.cn) website to look for possible miRNAs combined with both *GUSBP11* and *SPNS2*. As illustrated in the Figure 5A, two miRNAs (*miR-579-3p* and *miR-664b-3p*) were observed at the intersection. Through RNA pull down assays, it was shown that *miR-579-3p* was abundantly enriched in the *GUSBP11* biotin probe groups, while the other candidate *miR-664b-3p* showed no obvious change (Fig.5B). Therefore, *miR-579-3p* was chosen for further analyses. RIP data validated that *GUSBP11*, *miR-579-3p* and *SPNS2* were effectively abundant in the anti-Ago2 groups, indicating that these three RNAs co-existed in the RISCs (Fig.5C). Besides, we uncovered that the enrichment of *GUSBP11* and *SPNS2* was enhanced in the wild type of *miR-579-3p* group, while no obvious change was seen in the control group or the mutant group (Fig.5D). The respective binding sites of *GUSBP11* and *SPNS2* on the *miR-579-3p* were predicted via StarBase website (Fig.5E). We overexpressed *miR-579-3p* expression via the transfection of *miR-579-3p* mimics in the TNBC cell lines (Fig.5F), and it was then manifested from luciferase reporter assays that *miR-579-3p* mimics declined the luciferase activity of *GUSBP11*-WT and *SPNS2* 3′UTR-WT groups, while barely affected the *GUSBP11*-Mut and *SPNS2* 3′UTR-Mut groups (Fig.5G).

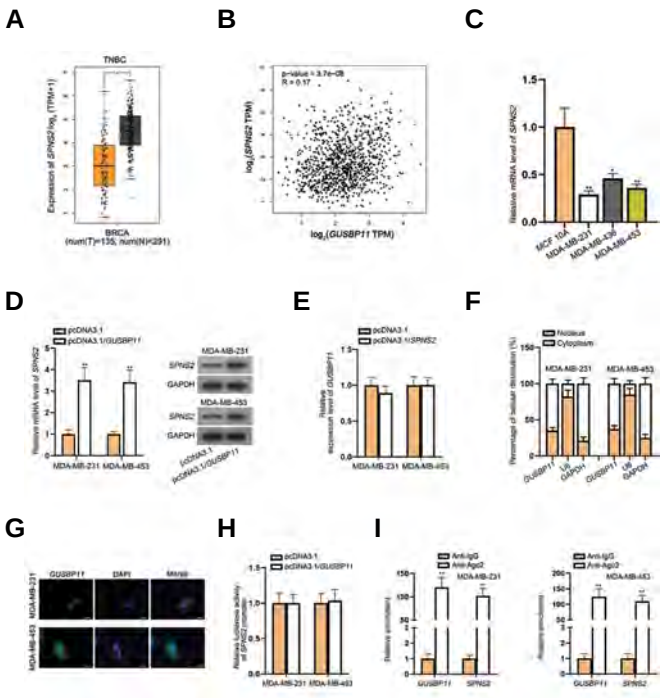

Fig.4: *GUSBP11* acts as a ceRNA to positively regulate *SPNS2* expression in the TNBC cell lines. **A.** Box plot from GEPIA 2 database indicated the expression of *SPNS2* in the 135 tumor TNBC tissues and 291 normal tissues. **B.** The correlation between *GUSBP11* and *SPNS2* expression was presented via GEPIA 2 database. **C.** The mRNA level of *SPNS2* in the TNBC cell lines MDA-MB-231, MDA-MB-436 and MDA-MB-453 in comparison with the MCF-10A cell line. **D.** *SPNS2* expression at both RNA and protein levels in the TNBC cell lines transfected with pcDNA3.1/*GUSBP11*. **E.** The *GUSBP11* RNA level in the TNBC cell lines with *SPNS2* overexpression. **F, G.** The cellular location of *GUSBP11* in the TNBC cell lines was determined by subcellular fractionation and FISH experiments (scale bar: 10 µm). **H.** The luciferase activity of *SPNS2* promoter in the *GUSBP11*-overexpressed TNBC cell lines. **I.** The enrichment of *GUSBP11* and *SPNS2* in the Anti-Ago2 groups in contrast to the control IgG group was measured by RIP assays. Three independent experiments were conducted (n=3). TNBC; Triple negative breast cancer, *; P<0.05, and **; P<0.01.

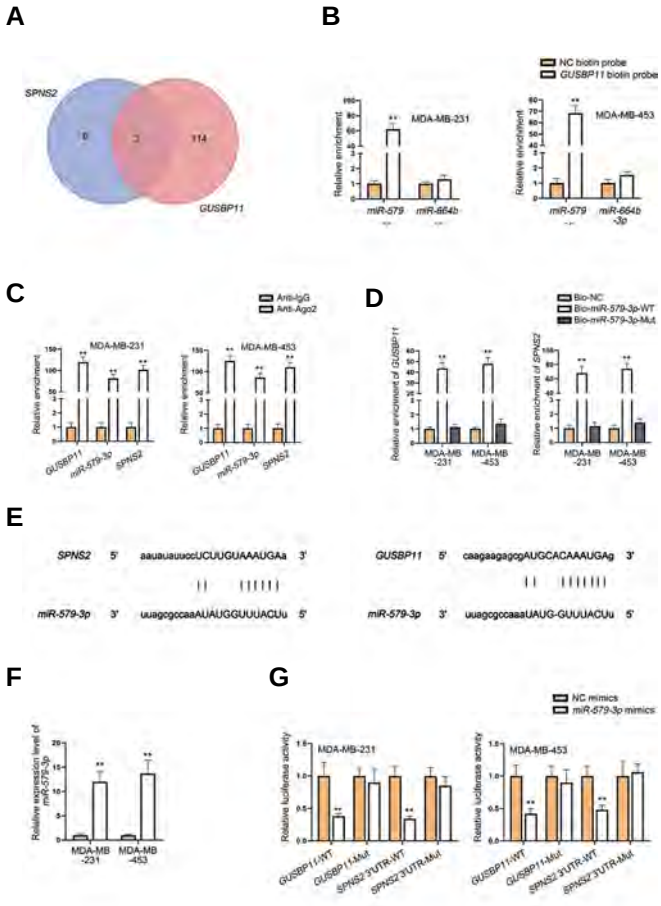

Fig.5: *GUSBP11* regulates *SPNS2* expression via interacting with the *miR-579-3p* in the TNBC cell lines. **A.** Potential miRNAs combined with the *GUSBP11* and *SPNS2* were predicted through starBase. **B.** The abundance of *miR-579-3p* and *miR-664b-3p* in the *GUSBP11* biotin probe groups was measured by RNA pull down assays. **C.** The enrichment of *GUSBP11*, *miR-579-3p* and *SPNS2* in the Anti-Ago2 groups was examined via RIP assays. **D.** The enrichment of *GUSBP11* and *SPNS2* in the bio-*miR-579-3p*-WT or bio-*miR-579-3p*-Mut groups was measured by RNA pull down assays. **E.** Respective binding sites of *GUSBP11* and *SPNS2* on the *miR-579-3p* were predicted via starBase website. **F.** *MiR-579-3p* expression in the TNBC cell lines transfected with *miR-579-3p* mimics. **G.** The luciferase activity of *GUSBP11*-WT/Mut or *SPNS2* 3′UTR-WT/Mut in the TNBC cell lines when *miR-579-3p* was up-regulated. Three independent experiments were conducted (n=3). TNBC; Triple negative breast cancer and **; P<0.01.

GUSBP11 restrains cell proliferation and promotes cell apoptosis in the TNBC cell lines via sponging *miR-579-3p* to elevate *SPNS2* expression

We knocked down *SPNS2* in the MDA-MB-231 and MDA-MB-453 cell lines via the transfection of sh/*SPNS2*#1/2 (Fig.6A). After that, a series of rescue assays were taken to verify the regulatory mechanism of *GUSBP11*/*miR-579-3p*/*SPNS2* axis on the TNBC cell lines proliferation and apoptosis. As shown in the colony formation and EdU assays, overexpression of *GUSBP11* reduced the proliferation of the TNBC cell lines, while such effect was partially reversed by the co-transfection of *miR-579-3p* mimics or sh/*SPNS2*#1 (Fig.6B, C). In the TUNEL assays and flow cytometry analyses, the enhanced apoptosis rate induced by *GUSBP11* up-regulation was abolished after co-transfection of *miR-579-3p* mimics or sh/*SPNS2*#1 (Fig.6D, E).

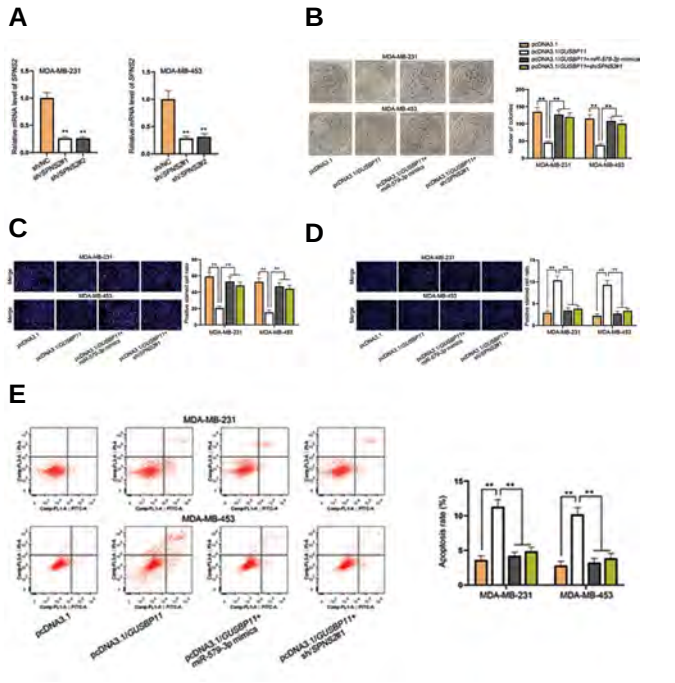

Fig.6: *GUSBP11* impedes the TNBC cell lines progression by targeting *miR-579-3p* to up-regulate the *SPNS2* expression. **A.** The mRNA level of *SPNS2* in the TNBC cell lines transfected with shRNAs targeting *SPNS2*. Rescue experiments were conducted in the TNBC cell lines transfected with different plasmids (pcDNA3.1, pcDNA3.1/*GUSBP11*, pcDNA3.1/*GUSBP11*+*miR-579-3p* mimics and pcDNA3.1/*GUSBP11*+sh/*SPNS2*#1. **B, C.** Colony formation and EdU (scale bar: 50 μm) assay were taken to analyze the proliferation of the TNBC cell lines under different transfection conditions. **D, E.** TUNEL (scale bar: 50 μm), together with flow cytometry was performed to measure the apoptosis of the TNBC cell lines in different groups. Three independent experiments were conducted (n=3). TNBC; Triple negative breast cancer and **; P<0.01.

GUSBP11 represses cell migration, EMT and stemness in the TNBC cell lines via interacting with *miR-579-3p* to increase *SPNS2* expression

The impacts of the *GUSBP11*/*miR-579-3p*/*SPNS2* axis on the cell migration, EMT and stemness were also determined. In Transwell assays, we found that the overexpression of *miR-579-3p* or the silencing of *SPNS2* could countervail the repressive cell migration and invasion in the TNBC caused by *GUSBP11* up-regulation (Fig.S2A, B, See Supplementary Online Information at www.celljournal.org). Meanwhile, the repressed EMT caused by GUSBP11 overexpression was offset after the co-transfection of miR-579-3p mimics or sh/SPNS2#1 (Fig.S2C, See Supplementary Online Information at www.celljournal.org). Additionally, *miR-579-3p* elevation or *SPNS2* deletion could restore the reduced number of spheres that was mediated by the *GUSBP11* up-regulation (Fig.S2D, See Supplementary Online Information at www.celljournal.org). Meanwhile, the levels of stemness markers reduced by *GUSBP11* silencing were recovered after overexpression of *miR-579-3p* or knockdown of *SPNS2* (Fig.S2E, F, See Supplementary Online Information at www.celljournal.org).

Discussion

Recently, emerging evidences have shown that lncRNAs

are implicated in the development of TNBC (19). Thus, a better understanding of lncRNAs might contribute to effective treatment of the TNBC patients. According to recent studies, *GUSBP11* has been registered to be closely linked to gastric cancer (20) and neck squamous cell carcinoma (21). Nonetheless, the function of *GUSBP11* in the TNBC occurrence remains largely obscure. In our research, we discovered that *GUSBP11* was down-regulated in the TNBC cell lines. Overexpression of *GUSBP11* obviously inhibited cell growth, migration, EMT and stemness in the TNBC cell lines. All these data demonstrated that *GUSBP11* exerted anti-oncogenic functions on the TNBC progression.

Transcriptional regulation is a mechanism that can regulate RNA expression. Previous studies have reported that lncRNAs can be activated by their upstream transcription factors and thus up-regulating lncRNAs in the human cancers (22, 23). Additionally, lncRNAs can be down-regulated by their upstream transcription suppressors (24). Here, we also investigated the upstream mechanism of *GUSBP11* in the TNBC cell lines. YY1/p300/HDAC2 complex has been reported to be efficient in the gene transcription suppressing (25), so in our research, we predicted that YY1 and p300 may be two potential upstream regulatory factors for *GUSBP11*. Through mechanism experiments, we demonstrated that down-regulation of *GUSBP11* in the TNBC cell lines was induced by the YY1/p300/HDAC2 complex affinity to its promoter region.

Competitive endogenous RNA (ceRNA) mechanism is known as a common post-transcriptional regulatory method and lncRNAs have been extensively reported to affect cancer development via ceRNA model (26, 27). Accumulating evidence have pointed that lncRNAs can compete for miRNA response elements (MREs) with the driver genes to be involved in cancer development by acting as a ceRNA to interact with miRNA (28). Our study also demonstrated that *GUSBP11* functioned as a ceRNA to positively regulate *SPNS2* expression in the TNBC cell lines. As reported previously, *SPNS2* enhances proliferation, migration and invasion colorectal cancer cell line via controlling S1P/S1PR1/3 axis and Akt and ERK pathway (29). *SPNS2* plays crucial roles in repressing the migratory ability in the non-small cell lung cancer cell line (30). However, we found that *SPNS2* presented a low RNA level in the TNBC cell lines, and it was further validated that overexpression of *SPNS2* significantly suppressed the malignant cell behaviors in the TNBC. As known, miRNA is a key part of ceRNA mechanism and numerous miRNAs exert important roles in the TNBC progression (31). *MiR-221/222* enhances the Wnt/β-catenin signaling to facilitate TNBC aggressiveness (32). *MiR-211-5p* inhibits tumor cell growth and metastasis in the TNBC cell lines as well as the TNBC xenograft model via targeting SETBP1 (33). In this study, we found that *miR-579-3p* was a common miRNA combined with *GUSBP11* and *SPNS2*. It has been documented that *miR-579-3p* is down-regulated in the squamous cell lung carcinoma cell line, while its overexpression represses this progression (34). Moreover, *miR-579-3p* is related to melanoma progression and resistance to target treatments (15). In our study, we confirmed that *GUSBP11* inhibited the progression of TNBC via targeting the *miR-579-3p*/*SPNS2* axis.

However, due to the limited time and materials, there still existed several limitations in this study which required for further verification. Also, clinical data should be complemented to enrich the significance of our current study. We will make further clinical investigation in our future research.

Conclusion

GUSBP11 restrains cell proliferation and promotes cell apoptosis in the TNBC cell lines via sponging miR-579-3p to elevate SPNS2 expression.

Acknowledgements

We appreciate the support of laboratory. This research was funded by the Basic Research Programs of Science and Technology Commission of Shanghai Jin Shang district (2017-3-02). There is no conflict of interest in this study.

Authors' Contribution

G.W.; Participated in study design, data collection and evaluation, drafting and statistical analysis. P.S.; Contributed to all experimental work, data and statistical analysis, and interpretation of data. C.Q.; Drafted the manuscript. All authors have read and approved the manuscript.

References

1. DeSantis C, Siegel R, Bandi P, Jemal A. Breast cancer statistics, 2011. CA Cancer J Clin. 2011; 61(6): 409-418.
2. Woolston C. Breast cancer. Nature. 2015; 527(7578): S101.
3. Kumar P, Aggarwal R. An overview of triple-negative breast cancer. Arch Gynecol Obstet. 2016; 293(2): 247-269.
4. Fahad Ullah M. Breast cancer: current perspectives on the disease status. Adv Exp Med Biol. 2019; 1152: 51-64.
5. Maughan KL, Lutterbie MA, Ham PS. Treatment of breast cancer. Am Fam Physician. 2010; 81(11): 1339-1346.
6. Wang J, Zhu S, Meng N, He Y, Lu R, Yan GR. ncRNA-encoded peptides or proteins and cancer. Mol Ther. 2019; 27(10): 1718-1725.
7. Anastasiadou E, Jacob LS, Slack FJ. Non-coding RNA networks in cancer. Nat Rev Cancer. 2018; 18(1): 5-18.
8. Ferrè F, Colantoni A, Helmer-Citterich M. Revealing protein-lncRNA interaction. Brief Bioinform. 2016; 17(1): 106-116.
9. Li J, Li L, Yuan H, Huang XW, Xiang T, Dai S. Up-regulated lncRNA GAS5 promotes chemosensitivity and apoptosis of triple-negative breast cancer cells. Cell Cycle. 2019; 18(16): 1965-1975.
10. Song X, Liu Z, Yu Z. LncRNA NEF is downregulated in triple negative breast cancer and correlated with poor prognosis. Acta Biochim Biophys Sin (Shanghai). 2019; 51(4): 386-392.
11. Weng YS, Tseng HY, Chen YA, Shen PC, Al Haq AT, Chen LM, et al. MCT-1/miR-34a/IL-6/IL-6R signaling axis promotes EMT progression, cancer stemness and M2 macrophage polarization in triple-negative breast cancer. Mol Cancer. 2019; 18(1): 42.
12. Zhang B, Shetti D, Fan C, Wei K. miR-29b-3p promotes progression of MDA-MB-231 triple-negative breast cancer cells through downregulating TRAF3. Biol Res. 2019; 52(1): 38.
13. Xiong H, Yan T, Zhang W, Shi F, Jiang X, Wang X, et al. miR-613

inhibits cell migration and invasion by downregulating Daam1 in triple-negative breast cancer. Cell Signal. 2018; 44: 33-42.
14. Fabian MR, Sonenberg N, Filipowicz W. Regulation of mRNA translation and stability by microRNAs. Annu Rev Biochem. 2010; 79: 351-379.
15. Fattore L, Mancini R, Acunzo M, Romano G, Laganà A, Pisanu ME, et al. miR-579-3p controls melanoma progression and resistance to target therapy. Proc Natl Acad Sci USA. 2016; 113(34): E5005-13.
16. Tang W, Zhou W, Xiang L, Wu X, Zhang P, Wang J, et al. The p300/YY1/miR-500a-5p/HDAC2 signalling axis regulates cell proliferation in human colorectal cancer. Nat Commun. 2019; 10(1): 663.
17. Uchida Y, Chiba T, Kurimoto R, Asahara H. Post-transcriptional regulation of inflammation by RNA-binding proteins via cis-elements of mRNAs. J Biochem. 2019; 166(5): 375-382.
18. Boyce AKJ, Epp AL, Nagarajan A, Swayne LA. Transcriptional and post-translational regulation of pannexins. Biochim Biophys Acta Biomembr. 2018; 1860(1): 72-82.
19. Fu J, Dong G, Shi H, Zhang J, Ning Z, Bao X, et al. LncRNA MIR503HG inhibits cell migration and invasion via miR-103/OLFM4 axis in triple negative breast cancer. J Cell Mol Med. 2019; 23(7): 4738-4745.
20. Zheng R, Liang J, Lu J, Li S, Zhang G, Wang X, et al. Genome-wide long non-coding RNAs identified a panel of novel plasma biomarkers for gastric cancer diagnosis. Gastric Cancer. 2019; 22(4): 731-741.
21. Cao W, Liu JN, Liu Z, Wang X, Han ZG, Ji T, et al. A three-lncRNA signature derived from the Atlas of ncRNA in cancer (TANRIC) database predicts the survival of patients with head and neck squamous cell carcinoma. Oral Oncol. 2017; 65: 94-101.
22. Wang H, Huo X, Yang XR, He J, Cheng L, Wang N, et al. STAT3-mediated upregulation of lncRNA HOXD-AS1 as a ceRNA facilitates liver cancer metastasis by regulating SOX4. Mol Cancer. 2017; 16(1): 136.
23. Tian Y, Ma R, Sun Y, Liu H, Zhang H, Sun Y, et al. SP1-activated long noncoding RNA lncRNA GCMA functions as a competing endogenous RNA to promote tumor metastasis by sponging miR-124 and miR-34a in gastric cancer. Oncogene. 2020; 39(25): 4854-4868.
24. Wang C, Tan C, Wen Y, Zhang D, Li G, Chang L, et al. FOXP1-induced lncRNA CLRN1-AS1 acts as a tumor suppressor in pituitary prolactinoma by repressing the autophagy via inactivating Wnt/β-catenin signaling pathway. Cell Death Dis. 2019; 10(7): 499.
25. Tang W, Zhou W, Xiang L, Wu X, Zhang P, Wang J, et al. The p300/YY1/miR-500a-5p/HDAC2 signalling axis regulates cell proliferation in human colorectal cancer. Nat Commun. 2019; 10(1): 663.
26. Li K, Ma YB, Tian YH, Xu XL, Gao Y, He YQ, et al. Silencing lncRNA SNHG6 suppresses proliferation and invasion of breast cancer cells through miR-26a/VASP axis. Pathol Res Pract. 2019; 215(10): 152575.
27. Tay Y, Rinn J, Pandolfi PP. The multilayered complexity of ceRNA crosstalk and competition. Nature. 2014; 505(7483): 344-352.
28. Qi X, Zhang DH, Wu N, Xiao JH, Wang X, Ma W. ceRNA in cancer: possible functions and clinical implications. J Med Genet. 2015; 52(10): 710-718.
29. Gu X, Jiang Y, Xue W, Song C, Wang Y, Liu Y, et al. SPNS2 promotes the malignancy of colorectal cancer cells via regulating Akt and ERK pathway. Clin Exp Pharmacol Physiol. 2019; 46(9): 861-871.
30. Bradley E, Dasgupta S, Jiang X, Zhao X, Zhu G, He Q, et al. Critical role of Spns2, a sphingosine-1-phosphate transporter, in lung cancer cell survival and migration. PLoS One. 2014; 9(10): e110119.
31. Yang R, Xing L, Zheng X, Sun Y, Wang X, Chen J. The circRNA circAGFG1 acts as a sponge of miR-195-5p to promote triple-negative breast cancer progression through regulating CCNE1 expression. Mol Cancer. 2019; 18(1): 4.
32. Liu S, Wang Z, Liu Z, Shi S, Zhang Z, Zhang J, et al. miR-221/222 activate the Wnt/β-catenin signaling to promote triple-negative breast cancer. J Mol Cell Biol. 2018; 10(4): 302-315.
33. Chen LL, Zhang ZJ, Yi ZB, Li JJ. MicroRNA-211-5p suppresses tumour cell proliferation, invasion, migration and metastasis in triple-negative breast cancer by directly targeting SETBP1. Br J Cancer. 2017; 117(1): 78-88.
34. Wu RR, Zhong Q, Liu HF, Liu SB. Role of miR-579-3p in the development of squamous cell lung carcinoma and the regulatory mechanisms. Eur Rev Med Pharmacol Sci. 2019; 23(21): 9464-9470.

Original Article

FHL1 Overexpression as A Inhibitor of Lung Cancer Cell Invasion via Increasing *RhoGDIß* mRNA Expression

Min-ke Shi, M.D.#, Yu-long Xuan, M.D.#, Xiao-feng He, M.D.*

Department of Thoracic Surgery, Nanjing Drum Tower Hospital, The Affiliated Hospital of Nanjing University Medical School, Nanjing, PR. China

#These authors contributed equally to this work.

Corresponding Address: Department of Thoracic Surgery, Nanjing Drum Tower Hospital, The Affiliated Hospital of Nanjing University Medical School, Nanjing, PR. China
Email: 261459450@qq.com

Received: 31/March/2021, Accepted: 26/June/2021

Abstract

Objective: Four and a half Lin-11, Isl-1, Mac-3 (LIM) protein 1 (FHL1) is one of the FHL protein family, which is regarded as a tumor suppressor in the multiple malignant tumors. In this study, we aimed to explore the regulatory effects and mechanisms of FHL1 on lung cancer cell invasion.

Materials and Methods: In this experimental study, bioinformatics analysis of *FHL1* transcripts in human lung adenocarcinomas of TCGA database was performed. Quantitative real-time polymerase chain reaction (PCR) was performed to detect *FHL1* mRNA expression in 15 paired human lung cancer tissues and their adjacent normal lung tissues, or lung cancer cell lines (A549 and H1299) in comparison with human bronchial epithelial cell line (Beas-2B). Moreover, western blot was used to analyze FHL1 and rho GDP-dissociation inhibitor beta (RhoGDIβ) protein expression in the indicated cell lines. Also, transwell assays were employed to measure the migrated, and invaded of indicated cell lines.

Results: *FHL1* transcripts were downregulated in the human lung adenocarcinoma. The impaired *FHL1* transcripts were positively correlated with advanced tumor node metastasis (TNM) stage. Moreover, as compared to the adjacent normal lung tissues, *FHL1* mRNA was low expressed in 15 paired human lung cancer tissues than their adjacent normal lung tissues. Besides, *FHL1* mRNA and protein expression were also reduced in H1299 and A549 cell lines in comparison with Beas-2B cell line. Overexpressed FHL1 protein inhibited the invasive ability of H1299 and A549 cell lines. Mechanically, FHL1 protein overexpression increased the RhoGDIβ protein and mRNA abundance, while knockdown of RhoGDIβ protein, completely restored the invasion ability of A549 (Flag-FHL1) cell line.

Conclusion: Our findings indicated that as a key FHL1 downstream regulator, RhoGDIβ is in charge of FHL1 inhibiting lung cancer cell invasion abilities, providing a critical insight into understanding the role of FHL1 for lung cancer development.

Keywords: FHL1, Invasion, Gene Expression, Lung Cancer, rho GDP-Dissociation Inhibitor Beta

Cell Journal(Yakhteh), Vol 24, No 5, May 2022, Pages: 239-244

Citation: **Shi Mk, Xuan Yl, He Xf. FHL1 overexpression as a inhibitor of lung cancer cell invasion via increasing RhoGDIβ mRNA expression. Cell J. 2022; 24(5): 239-244. doi: 10.22074/cellj.2022.8031.**

Introduction

Lung cancer, one of the most common cancers, has received a lot of attention. While its morbidity and mortality are increasing year by year, the poor 5-year survival for non-small-cell lung cancer is merely about 15% (1, 2). Furthermore, based on traditional pathological and clinical parameters, non-small-cell lung cancer outcomes could not be determined (3). Due to the poor understanding of lung cancer mechanisms, tumorigenesis and progression, the advances of effective treatments remain limited. Therefore, development of novel molecular targets, biomarkers and novel therapeutic strategies are necessary.

Four and a half Lin-11, Isl-1, Mac-3 (LIM) protein 1 (FHL1) belongs to the FHL protein family, which comprises of four LIM domains and an N-terminal half LIM domain (4, 5). Multiple investigations on clinical samples have revealed that FHL1 protein expression inhibition in the several types of tumors, including lung (6), liver (7), breast (8), gastric (9), and prostate cancer (10). Researches on human totally lung cancer patients who received radiotherapy have indicated that the downregulation of FHL1 protein has resulted in significantly lower disease-free survival (6). Recently, They reported the inhibitory effects of FHL1 protein on lung cancer cell growth. FHL1 protein overexpression induced G1 and G2/M cell cycle arrest through inhibiting protein expression of Cyclin A, Cyclin B1 and Cyclin D, as well as inducing the expression of p21 and p27 protein, suggesting the tumor suppressor effect of FHL1 on human lung cancer cell growth. Moreover, SRC protein promoted the phosphorylation of FHL1 protein, then increased the directly binding with BCLAF1 protein in the nucleus, and finally promoted tumor cell growth (11), revealing that the role of FHL1 and its mechanism in the cancer progression is complicated.

RhoGDIβ protein belongs to the family of RHO guanosine diphosphate dissociation inhibitors (12, 13). Rho GTPases widely participate in a number of cellular responses, particularly in the cell motility (14).

Several investigations have indicated that RhoGDIβ is an aggressive human cancer marker (15). The protein and mRNA expression of RhoGDIβ was reported to be downregulated in both adenocarcinoma and squamous lung cell carcinoma (16). A reduction of tumor versican was observed upon overexpression of RhoGDIβ protein, and thereby suppressed lung metastasis *in vivo* mouse models (17). However, other researchers have revealed the oncogenic function of RhoGDIβ. For instance, RhoGDIβ has been shown to mediate ATG7-induced bladder cancer invasion (18). RhoGDIβ prevented the lung colonization of bladder cancer through unexpected targeting RhoC protein and reducing the activation of RhoC (19).

Based on the above, the therapeutic targeting of these FHL1/RhoGDIβ may appear to be a promising anti-cancer strategy. Therefore, we intended to figure out the relationship between FHL1 protein expression and human lung cancer cell invasion, and study the mechanism that involved in this progress, especially the function of RhoGDIβ.

Materials and Methods

Ethical considerations

This study was permitted by the Ethics Committee of Nanjing Drum Tower Hospital, The Affiliated Hospital of Nanjing University Medical School (2020-103-27). Written informed consents were obtained from all participants.

Plasmids, reagents and antibodies

In this study, shRNA specific targeting RhoGDIβ (shRhoGDIβ) were obtained from BioVector NTCC Inc. (Cat No. 58897, Shanghai, China). The PCR-amplified FHL1 fragment was inserted into the pcDNA3.1 vector (Cat No. P8990, Miaolinbio, China) to construct the Flag-tagged FHL1 plasmid. Before the transfection, the plasmid preparation kit (Cat No. D0003, Beyotime, China) was used to pretreating the plasmids. The TRIzol reagent (Cat No.15596026) and SuperScriptTM First-Strand Synthesis system (Cat No. 11904018) were acquired from Invitrogen (China). The antibodies specific against FHL1(Cat No. ab255828), Flag (Cat No. ab205606), and GAPDH (Cat No. ab9485) were purchased from Abcam (China). Antibodies against RhoGDIα (Cat No. sc-373724), RhoGDIβ (Cat No. sc-271108) and β-Actin (Cat No. sc-8432), were purchased from Santa Cruz (China).

Cell culture and transfection

Human lung cancer cell line A549 (BFN60800665, BLUEFBIO™, China), H1299 (BFN60804058, BLUEFBIO™, China) and human bronchial epithelial cell line Beas-2B (BFN608009328, BLUEFBIO™, China) were cultured in Dulbecco's modified Eagle's medium (DMEM, Cat No. C11995500BT, Gibco, China), supplemented with 2 μM of L-glutamine (Cat No. 25030149, Gibco, China), 25 μg/ml of gentamycin (Cat No. 15710-049, Thermo Fisher Scientific, China), and 10% heat-inactivated fetal bovine serum (FBS, Cat No. 10099-141C, Gibco, China). Cell transfections were performed by using PolyJetTM DNA In Vitro Transfection Reagent(Cat No. SL100468, SignaGen Laboratories, USA), according to the manufacturer's instruction and described in the previous studies (18). For the transfection of pcDNA3.1/Flag-FHL1 into A549 and H1299 cell lines, 2 μg of plasmids were used, and the stable transfectants were generated by G418 selection (500 g/ml). For the transfection of shRhoGDIβ into A549 (Flag-FHL1), 2 μg of plasmids were used, and the stable transfectants were generated by puromycin selection (2 μg/ml).

Western blot analysis

Beas-2B, A549 and H-1299 cell lines and their transfectants were cultured at 37°C in 5% CO_2 and 10% FBS medium for 12 hours till to 70-80% concentration. After 12 hours for culturing cells in 0.1% FBS medium, the 10% FBS DMEM medium was used for another 12 hours. Afterward, whole cell extracts were prepared with the cell lysis buffer [10 mM Tris-HCl (Cat No. T1090), pH=7.4, 1% sodium dodecyl sulfate (SDS, Cat No. S8010), and 1 mM Na3VO4 (Cat No. IS0210)] (all of them from the Solarbio Life Science, China) and then were subjected to Western Blot analysis according to the previous study (20).

Quantitative real-time polymerase chain reaction

A Fast SYBR Green Master Mix kit (Cat No. 4385614, Applied Biosystems, China) was used to detect the mRNA expression. The primers were:

human *FHL1*-

F: 5′CTG CTG CCT GAA A-3′
R: 5′-TCT CCT GCC ACA AT-3′

human *RhoGDIβ*-

F: 5′-ACC CGG CTC ACC CTG GTT TGT-3′
R: 5′-ACC CCA GTC CTG TAG GTG TGC TG-3′

human *β-Actin*-

F: 5′-CTC CAT CCT GGC CTC GCT GT-3′
R: 5′-GCT GTC ACC TTC ACC GTT CC-3′

Cell migration and invasion assay

For migration assays, three transwell chambers (Cat No. 353097, Corning, USA) were used for each individual cell group. The invasion kit (Cat No. 354480, BD Biosciences, USA) was used for each individual cell group. The stable transfectants which were under selected for 3-4 weeks with the indicated antibiotics , puromycin (Cat No. A1113803, Gibco, China), or G418 (Cat No. 10131027, Gibco, China). And then the stable transfectants were used to do the cell migration and

invasion assays and the normalized invasion rate was calculated according to the manufactures' instruments. According to the previous study (21), six photographs of each chamber were taken using the microscope, Olympus DP71 [Model No. DP71, Olympus (China) Co., Ltd, China], and the number of the migrated or invaded cells was counted using the "Image J"software. Based on the number of migrated or invaded cells, the migration rate was normalized with the nonsense control cells, while the invasion rate was firstly calculated by dividing the number of migrated cells, and then were normalized with nonsense control cells (18). The presented data are representative of three independent experiments.

Human lung cancer tissue specimens

All human lung cancer tissue specimens (15 pairs of human lung cancer tissues and their paired adjacent normal lung tissues) were obtained from patients who received surgery at the Affiliated Hospital of Nanjing University Medical School (Nanjing, China) during 2020-2021.

Bioinformatics analysis of TCGA database

Because of the aberrant silencing attribution of FHL1 in human cancers, the bioinformatics analysis was initially performed on *FHL1* transcripts with 574 lung cancer patients from TCGA database. UALCAN (http://ualcan.path.uab.edu) (22) was used to perform the bioinformatics analysis of *FHL1* transcripts in human lung cancer tissues.

Statistical analysis

GraphPad Prism 6.0 Software (GraphPad Software, USA) was employed for statistical analysis. All data demonstrated mean ± SD of triplicate assays. Student's t test was used to detect the significance of differences between groups. One-way ANOVA test was performed to detect the significant differences of multiple comparisons. The differences were considered significant at $P<0.05$.

Results

FHL1 protein expression was inhibited in the human lung cancer tissues and cell lines

The bioinformatics results revealed that the FHL1 transcripts were downregulated in the human lung cancer tissues when compared with the normal tissue samples (Fig.1A). Furthermore, the impaired FHL1 transcripts were positively correlated with advanced TNM stage (Fig.1B). Analysis of the *FHL1* mRNA expression showed a downregulation in the human lung cancers (Fig.1C). Next, the protein and mRNA expression of *FHL1* was examined among Beas-2B, A549 and H1299 cell lines. The result showed that *FHL1* mRNA and protein expression were decreased in the H1299 and A549 cell lines in comparison with Beas-2B cell lines (Fig.1D, E). Our data showed that *FHL1* mRNA and protein expression were inhibited in human lung cancers.

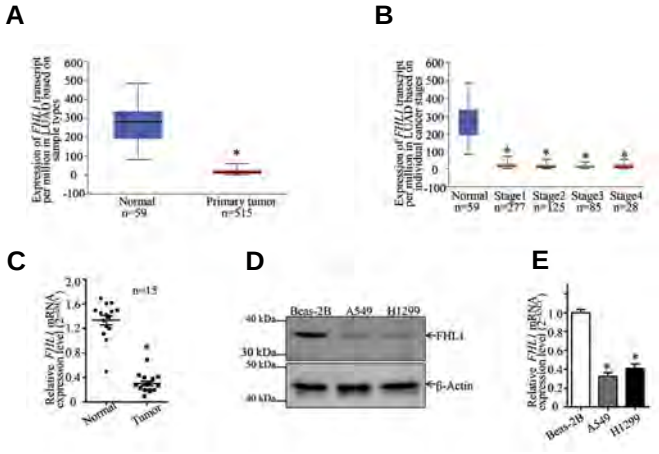

Fig.1: FHL1 was downregulated in human lung cancer tissues and cell lines. **A, B.** Bioinformatics analysis was performed on the *FHL1* transcript with 574 lung adenocarcinoma (LUAD) patients from the TCGA database. The *FHL1* transcripts were reduced in lung cancer tissues, in comparison with the normal lung tissues. The expression of *FHL1* transcript was downregulated in lung cancer patients with an advanced stage. **C.** *FHL1* mRNA expression was detected in 15 paired lung cancer tissues and their adjacent normal tissues. Student's t test was used to detect the P value, $P<0.05$. **D.** Expression of FHL1 in Beas-2B, A549, and H1299 cell lines was determined by western blot assay. β-Actin was used as a protein loading control. **E.** *FHL1* mRNA expression was determined by real-time polymerase chain reaction (PCR), and the asterisk (*) represents a notable decrease from normal Beas-2B cells ($P<0.05$).

FHL1 inhibition was essential for human lung cancer cell invasion

In order to investigate the relevance between FHL1 protein and human lung cancer development, the Flag-tagged FHL1 overexpression plasmid was stably transfected into A549 cell line (Fig.2A). Furthermore, the result revealed that FHL1 protein overexpression suppressed the invasion of these cells (Fig.2B, C). We stably transfected Flag-FHL1 into H1299 cell line (Fig.3A), and also, found that FHL1 overexpression inhibited the invasion of H1299 cell line (Fig.3B, C). Our results showed a new negative regulatory effect of FHL1 on human lung cancer invasion.

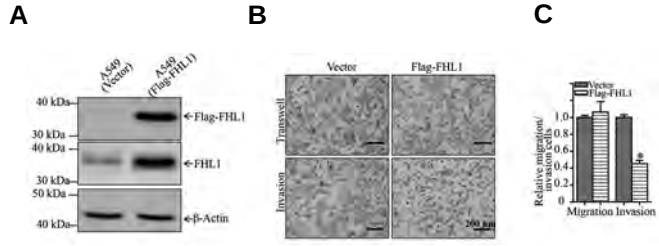

Fig.2: FHL1 overexpression inhibited the invasion of A549 cell line. **A.** The Flag-tagged FHL1 plasmid was stably transfected into A549 cell line. **B.** The invasive ability was determined using the Biocoat™ matrigel® invasion chamber, while the migration ability was detected using the same system without the matrigel (scale bar: 200 μm), **C.** The invasive ability was normalized to the insert control. The asterisk (*) represents a significant reduction as compared to A549 (Vector) cell lines ($P<0.05$).

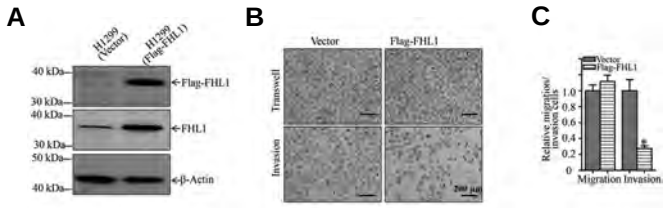

Fig.3: FHL1 overexpression inhibited the invasion of H1299 cell line**. A.** The Flag-tagged FHL1 plasmid was stably transfected into the H1299 cell line. **B.** The invasive ability was determined using the Biocoat™ matrigel® invasion chamber, while the migration ability was detected using the same system without the matrigel (scale bar: 200 μm). **C.** The invasive ability was normalized to the insert control. The asterisk (*) represents a significant reduction as compared to H1299 (Vector) cell lines (P<0.05).

FHL1 protein suppression of lung cancer invasion was regulated by decreasing *RhoGDI*β mRNA expression

In order to investigate the mechanism of FHL1 protein in regulating lung cancer invasion, western blot was carried out to select the potential FHL1 downstream effectors. The results showed that the overexpression of FHL1 only increased RhoGDIβ protein abundance, and had no remarkable effect on RhoGDIα protein expression in both A549 and H1299 cell lines (Fig.4A, B), indicating that FHL1 overexpression exerts a promotion effect on the RhoGDIβ protein expression in human lung cancer cells. Additionally, in order to investigate the mechanism underlying the FHL1 upregulating RhoGDIβ protein, we firstly detected a *RhoGDIβ* mRNA abundance. As shown in Figure 4C, D, the *RhoGDIβ* mRNA level was significant increased in the FHL1 overexpression transfectants. Therefore, it was anticipated that RhoGDIβ might be responsible for the FHL1 inhibition in human lung cancer cell invasion. Following, shRhoGDIβ#1 and shRhoGDIβ#2 were stably transfected into A549 (Flag-FHL1) cells (Fig.5A). Subsequently, invasion assay was performed and the data revealed that *RhoGDIβ* knockdown enhanced the invasion ability of A549 (Flag-FHL1) cells, in comparison to those observed in their scramble nonsense transfectants A549 (Flag-FHL1/Nonsense) cells (Fig.5B, C), demonstrating that RhoGDIβ protein is the FHL1 downstream mediator that is responsible for its inhibitory role in the human lung cancer cell invasion. Collectively, these present results demonstrate that FHL1 suppression leads to *RhoGDIβ* mRNA level decrease and protein expression inhibition, and finally promotes human lung cancer cell invasion.

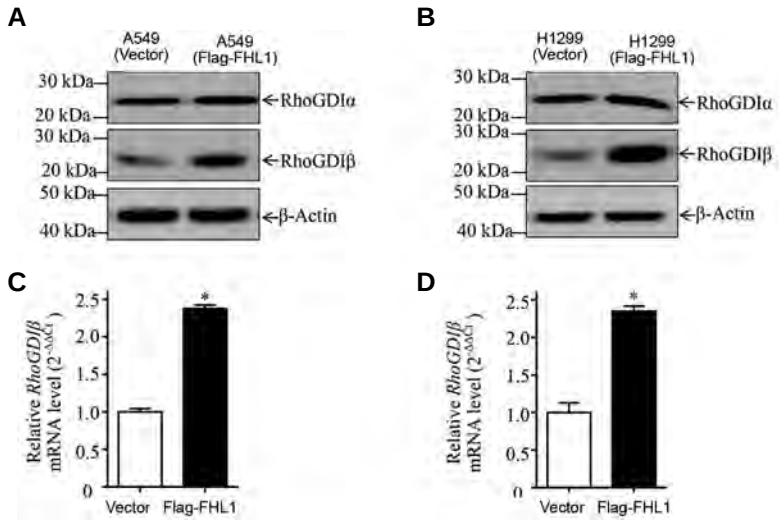

Fig.4: FHL1 ectopic expression promoted the protein and mRNA expression of *RhoGDI*β. **A, B.** The Flag-tagged FHL1 plasmid was transfected into A549 and H1299 cell lines stably. The western blot assay was utilized to detect the expression of RhoGDIα and RhoGDIβ protein. β-Actin was used as a protein loading control. **C, D.** *RhoGDI*β mRNA expression was determined by real-time polymerase chain reaction (PCR). The bars indicate the mean ± standard deviation (SD) of 3 independent experiments. The asterisk (*) represents a notable enhancement in comparison with vector control cells (P<0.05).

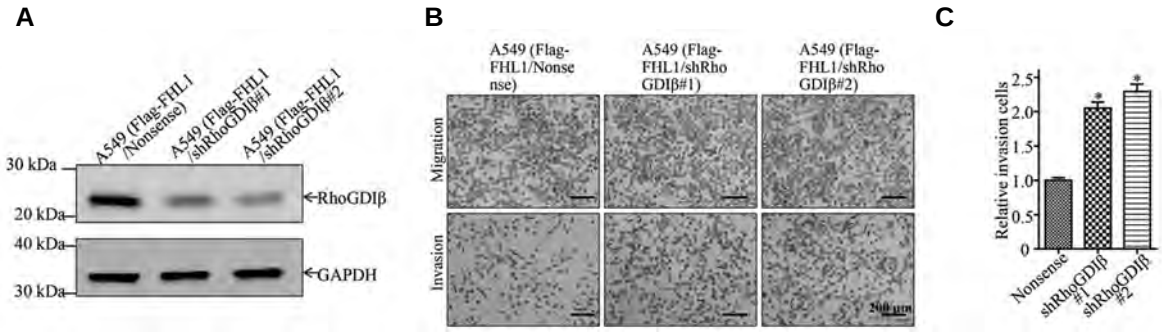

Fig.5: RhoGDIβ acted as a FHL1 downstream mediator responsible for the FHL1-inhibited human lung cancer invasion. **A.** The RhoGDIβ knockdown constructs were transfected into A549 (Flag-FHL1) cell lines stably. **B.** The invasion abilities of A549 (Flag-FHL1/Nonsense), A549 (Flag-FHL1/shRhoGDIβ#1), and A549 (Flag-FHL1/shRhoGDIβ#2) cell lines were detected (scale bar: 200 μm). **C.** The bars indicate mean ± SD of 3 independent experiments. Student's t test was used to detect the P value. The asterisk (*) represents a significant increase as compared to A549 (Flag-FHL1/Nonsense) transfectants (P<0.05).

Discussion

The results of several investigations revealed that FHL1 protein expression is suppressed in a number of tumors, including breast cancer (8), gastric cancer (23), kidney cancer (24), prostate cancer (25), and liver cancer (26, 27). Niu et al. (6) found lower expression FHL1 level in the 27 lung tumors (n=30, 27/30) by using western blot. Their immunohistochemistry results showed that 100% of non-tumor lungs (80/80) expressed FHL1, while only 26.3% (21/80) of cancerous tissues stained positive for FHL1. Our results were similar to the previous studies that reported FHL1 protein is lower expressed in human lung cancers.

FHL1 exerts a tumor suppressor effect on the multiple cancers. For example, FHL1 promotes paclitaxel resistance through regulating the caspase-3 activation in the hepatic carcinoma cells (27). FHL1 overexpression gives rise to G1 and G2/M cell cycle arrest and finally decreases lung cancer cell growth (6). FHL1 influences TGF-β-like signaling pathway activation, which leads to the inhibition of human hepatoma cell line anchorage-dependent and -independent growth *in vitro* and tumor formation in nude mice (7). All the above researches illustrated the tumor suppressor function of FHL1 in the cancer cell growth. However, other malignant functions of FHL1 is still not fully understood. In glioblastoma, FHL1 was highly expressed, and overexpression of FHL1 protein promoted the growth, migration, and invasion of glioblastoma cells *in vivo* and *in vitro* through regulating EGFR protein expression (28). In this study, the ectopic overexpression of FHL1 inhibited the invasion abilities of human lung cancer cell lines, while the migration ability was not affected.

Cell migration is the property of the live cells that is important for cell homeostasis, while cancer cell invasion means the function to migrate through the extracellular matrices and penetrate into new tissues (29). We supposed that the ectopic overexpression of FHL1 protein regulated multiple upstream factor gene expression and protein-protein interactions of cell migration. Their effects on the cell migration were finally neutralized, eventually overexpression of FHL1 showed no effect on cell migration. Moreover, we found that FHL1 overexpression promoted the mRNA and protein expression of RhoGDIβ, but not RhoGDIα protein expression. FHL1 overexpression might regulate the mRNA level, protein translation, or protein degradation levels of RhoGDIα, that ultimately had no effect on the its protein expression. In comparison with normal FHL1 overexpression human lung cancer cells, knockdown of RhoGDIβ protein reversed the invasion ability inhibition of FHL1 overexpression cells. Our results indicate that FHL1 might exert an essential role in the lung cancer progression and development.

RhoGDIβ is a member of the family of RHO guanosine diphosphate dissociation inhibitors (RhoGDIs), plays a tumor suppressor role in the diverse tumors and has been considered as an aggressive human cancer marker (15, 30). Altered RhoGDIβ expression has been observed in the multiple human cancers, including bladder cancers (18, 31), ovarian cancers (32) and lung cancer (33, 34). It has been reported that knockdown of RhoGDIβ promotes the lung cancer cell migration and invasion by regulating the PI3K/Akt pathway and MMP-9 protein expression (34). In this study, FHL1 overexpression upregulated RhoGDIβ protein expression, but had no effect on the RhoGDIα expression, excluding its role on the FHL1-inhibited human lung cancer invasion. Knockdown of RhoGDIβ expression completely restored the invasive ability of invasion-deficient A549 (Flag-FHL1) cells, suggesting that RhoGDIβ is a FHL1 downstream mediator responsible for its negative regulation of human lung cancer cell invasion. Due to the limitation of our study, we did not show the results of H1299 (Flag-FHL1/shRhoGDIβ) cells to illustrate the role of RhoGDIβ for the FHL1 inhibition in human lung cancer cell invasion. In conclusion, our results showed that RhoGDIβ exerted oncogenic functions in the lung cancer cell invasion. Additionally, we also discovered that overexpression FHL1 promoted the mRNA profile of *RhoGDIβ*. We suppose that *RhoGDIβ* mRNA stability or its transcription level will be regulated, and the underlying mechanism of FHL1 in regulating *RhoGDIβ* mRNA expression is still investigating in our group.

In addition, the reason underlying lower expression of FHL1 protein expression in human lung cancer is still unclear, and the molecular mechanism is worth to study in the next programme. Moreover, PI3K/Akt/mTOR pathway has been reported to be responsible for RhoGDIβ exerting oncogenic role in human lung cancer metastasis (16). Herein, we proposed a potential regulation between FHL1 and RhoGDIβ protein in the lung cancer invasion. However, it is still unknown that the downstream pathway involved in the FHL1/RhoGDIβ inhibiting lung cancer invasion.

Conclusion

FHL1 protein was found to be downregulated in the human lung cancer patients and cell lines, which exerts a critical role in the lung cancer cell invasion. Furthermore, it was found that RhoGDIβ protein is the FHL1 protein downstream effector and is responsible for its reduction of lung cancer cell invasion. These new discoveries appear to be a potential chance to design a FHL1/RhoGDIβ-based-specific therapeutic strategy for human lung cancer treatment.

Acknowledgments

The authors would like to thank Junlan Zhu for her technical support in invasion experiment and for the detecting the *FHL1* mRNA expression in human lung cancer tissues. There is no financially support and conflict of interest in this study.

Authors' Contributions

X.H.; Conceived and designed the study. M.S., Y.X.;

Detected the cells' biological function, conducted the RT-PCR assays, carried out the Western blot assays, and performed the statistical analysis. X.H., M.S.; Drafted the manuscript. All authors read and approved the final version of the manuscript.

Reference

1. Awad R,Nott L. Radiation recall pneumonitis induced by erlotinib after palliative thoracic radiotherapy for lung cancer: Case report and literature review. Asia Pac J Clin Oncol. 2016; 12(1): 91-95.
2. Tang F, Tang S, Guo X, Yang C,Jia K. CT45A1 siRNA silencing suppresses the proliferation, metastasis and invasion of lung cancer cells by downregulating the ERK/CREB signaling pathway. Mol Med Rep. 2017; 16(5): 6708-6714.
3. Herbst R S, Morgensztern D,Boshoff C. The biology and management of non-small cell lung cancer. Nature. 2018; 553(7689): 446-454.
4. Chu P H, Ruiz-Lozano P, Zhou Q, Cai C,Chen J. Expression patterns of FHL/SLIM family members suggest important functional roles in skeletal muscle and cardiovascular system. Mech Dev. 2000; 95(1-2): 259-265.
5. Kadrmas J L,Beckerle M C. The LIM domain: from the cytoskeleton to the nucleus. Nat Rev Mol Cell Biol. 2004; 5(11): 920-931.
6. Niu C, Liang C, Guo J, Cheng L, Zhang H, Qin X, et al. Downregulation and growth inhibitory role of FHL1 in lung cancer. Int J Cancer. 2012; 130(11): 2549-2556.
7. Ding L, Wang Z, Yan J, Yang X, Liu A, Qiu W, et al. Human four-and-a-half LIM family members suppress tumor cell growth through a TGF-beta-like signaling pathway. J Clin Invest. 2009; 119(2): 349-361.
8. Ding L, Niu C, Zheng Y, Xiong Z, Liu Y, Lin J, et al. FHL1 interacts with oestrogen receptors and regulates breast cancer cell growth. J Cell Mol Med. 2011; 15(1): 72-85.
9. Xu Y, Liu Z,Guo K. Expression of FHL1 in gastric cancer tissue and its correlation with the invasion and metastasis of gastric cancer. Mol Cell Biochem. 2012; 363(1-2): 93-99.
10. Li X, Jia Z, Shen Y, Ichikawa H, Jarvik J, Nagele R G, et al. Coordinate suppression of Sdpr and Fhl1 expression in tumors of the breast, kidney, and prostate. Cancer Sci. 2008; 99(7): 1326-1333.
11. Wang X, Wei X, Yuan Y, Sun Q, Zhan J, Zhang J, et al. Src-mediated phosphorylation converts FHL1 from tumor suppressor to tumor promoter. J Cell Biol. 2018; 217(4): 1335-1351.
12. DerMardirossian C,Bokoch G M. GDIs: central regulatory molecules in Rho GTPase activation. Trends Cell Biol. 2005; 15(7): 356-363.
13. Moissoglu K, McRoberts K S, Meier J A, Theodorescu D,Schwartz M A. Rho GDP dissociation inhibitor 2 suppresses metastasis via unconventional regulation of RhoGTPases. Cancer Res. 2009; 69(7): 2838-2844.
14. Simons P, Bondu V, Wandinger-Ness A,Buranda T. Small-volume flow cytometry-based multiplex analysis of the activity of small GTPases. Methods Mol Biol. 2018; 1821: 177-195.
15. Liu S, Cui H, Li Q, Zhang L, Na Q,Liu C. RhoGDI2 is expressed in human trophoblasts and involved in their migration by inhibiting the activation of RAC1. Biol Reprod. 2014; 90(4): 88.
16. Niu H, Li H, Xu C,He P. Expression profile of RhoGDI2 in lung cancers and role of RhoGDI2 in lung cancer metastasis. Oncol Rep. 2010; 24(2): 465-471.
17. Said N, Sanchez-Carbayo M, Smith SC,Theodorescu D. RhoGDI2 suppresses lung metastasis in mice by reducing tumor versican expression and macrophage infiltration. J Clin Invest. 2012; 122(4): 1503-1518.
18. Zhu J, Tian Z, Li Y, Hua X, Zhang D, Li J, et al. ATG7 promotes bladder cancer invasion via autophagy-mediated increased ARHGDIB mRNA stability. Adv Sci (Weinh). 2019; 6(8): 1801927.
19. Griner EM, Dancik GM, Costello JC, Owens C, Guin S, Edwards MG, et al. RhoC is an unexpected target of rhogdi2 in prevention of lung colonization of bladder cancer. Mol Cancer Res. 2015; 13(3): 483-492.
20. Taylor SC, Posch A. The design of a quantitative western blot experiment. Biomed Res Int. 2014; 2014: 361590.
21. Zhu J, Li Y, Chen C, Ma J, Sun W, Tian Z, et al. NF-kappaB p65 overexpression promotes bladder cancer cell migration via fbw7-mediated degradation of rhogdialpha protein. Neoplasia. 2017; 19(9): 672-683.
22. Chandrashekar DS, Bashel B, Balasubramanya SAH, Creighton CJ, Ponce-Rodriguez I, Chakravarthi BVSK, et al. UALCAN: a portal for facilitating tumor subgroup gene expression and survival analyses. Neoplasia. 2017; 19(8): 649-658.
23. Asada K, Ando T, Niwa T, Nanjo S, Watanabe N, Okochi-Takada E, et al. FHL1 on chromosome X is a single-hit gastrointestinal tumor-suppressor gene and contributes to the formation of an epigenetic field defect. Oncogene. 2013; 32(17): 2140-2149.
24. Hubbi ME, Gilkes DM, Baek JH, Semenza GL. Four-and-a-half LIM domain proteins inhibit transactivation by hypoxia-inducible factor 1. J Biol Chem. 2012; 287(9): 6139-6149.
25. Zhang S, Zheng C, Yao S, Wang Z, Xu L, Yang R, et al. Proteomic analysis of human prostate cancer PC-3M-1E8 cells and PC-3M-2B4 cells of same origin but with different metastatic potential. PLoS One. 2018; 13(10): e0206139.
26. Wang J, Huang F, Huang J, Kong J, Liu S,Jin J. Epigenetic analysis of FHL1 tumor suppressor gene in human liver cancer. Oncol Lett. 2017; 14(5): 6109-6116.
27. Zhou L, Ding L, Liu J, Zhang Y, Luo X, Zhao L, et al. Four-and-a-half LIM protein 1 promotes paclitaxel resistance in hepatic carcinoma cells through the regulation of caspase-3 activation. J Cancer Res Ther. 2018; 14 Supplement: S767-S773.
28. Sun L, Chen L, Zhu H, Li Y, Chen C C,Li M. FHL1 promotes glioblastoma aggressiveness through regulating EGFR expression. FEBS Lett. 2021; 595(1): 85-98.
29. Martin TA, Ye L, Sanders AJ, Lane J, Jiang WG. Cancer invasion and metastasis: molecular and cellular perspective. 2013. Available from: https://www.ncbi.nlm.nih.gov/books/NBK164700/ (31 Mar 2021).
30. Xu R, Dong Y, Wang L, Tao X, Sun A,Wei D. TAT-RhoGDI2, a novel tumor metastasis suppressor fusion protein: expression, purification and functional evaluation. Appl Microbiol Biotechnol. 2014; 98(23): 9633-9641.
31. Huang H, Jin H, Zhao H, Wang J, Li X, Yan H, et al. RhoGDIbeta promotes Sp1/MMP-2 expression and bladder cancer invasion through perturbing miR-200c-targeted JNK2 protein translation. Mol Oncol. 2017; 11(11): 1579-1594.
32. Stevens EV, Banet N, Onesto C, Plachco A, Alan JK, Nikolaishvili-Feinberg N, et al. RhoGDI2 antagonizes ovarian carcinoma growth, invasion and metastasis. Small GTPases. 2011; 2(4): 202-210.
33. Niu H, Wu B, Jiang H, Li H, Zhang Y, Peng Y, et al. Mechanisms of RhoGDI2 mediated lung cancer epithelial-mesenchymal transition suppression. Cell Physiol Biochem. 2014; 34(6): 2007-2016.
34. Niu H, Wu B, Peng Y, Jiang H, Zhang Y, Wang J, et al. RNA interference-mediated knockdown of RhoGDI2 induces the migration and invasion of human lung cancer A549 cells via activating the PI3K/Akt pathway. Tumour Biol. 2015; 36(1): 409-419.

Original Article

Hsa_circ_0006427 Suppresses Multiplication, Migration and Invasion of Non-Small Cell Lung Cancer Cells through miR-346/VGLL4 Pathway

Jiacheng Sun, M.D.[1], Lei Wang, M.D.[2], Xinhai Zhu, M.M.[3]*, Molei Shen, M.D.[1]*

1. Department of Thoracic Surgery, Pinghu First People's Hospital, Pinghu City, Jiaxing, Zhejiang, China
2. Department of Anesthesiology, Pinghu First People's Hospital, Pinghu City, Jiaxing, Zhejiang, China
3. Department of Thoracic Surgery, Zhejiang Hospital, Xihu District, Hangzhou, Zhejiang, China

Corresponding Addresses: Department of Thoracic Surgery, Zhejiang Hospital, Xihu District, Hangzhou, Zhejiang, China
Department of Thoracic Surgery, Pinghu First People's Hospital, Pinghu City, Jiaxing, Zhejiang, China
Emails: dr-zxh@163.com, dutangxi661@163.com

Received: 29/September/2020, Accepted: 11/January/2021

Abstract

Objective: Circular RNAs (circRNAs) are identified as key modulators in cancer biology. Nonetheless, the role of *circ_0006427* in non-small cell lung cancer (NSCLC) and its modulatory mechanism are undefined. This study aimed to investigate the potential function and mechanism of *circ_0006427* in NSCLC.

Materials and Methods: In this experimental study, *circ_0006427*, *miR-346* and vestigial like family member 4 (*VGLL4*) mRNA expressions were analyzed in NSCLC tissues and cells, using quantitative reverse transcription polymerase chain reaction (qRT-PCR). Multiplication, migration and invasion of NSCLC cells were examined using the CCK-8 method and Transwell experiment, respectively. Dual-luciferase reporter gene experiments were conducted to identify the paring relationship between *circ_0006427* and *miR-346*. Western blot was employed to determine expressions of *VGLL4* and epithelial-mesenchymal transition (EMT) markers on protein levels. Immuno-histochemistry (IHC) method was adopted to assess VGLL4 protein expression in NSCLC tissues.

Results: *Circ_0006427* expression was down-regulated in NSCLC tissues and cells, and *circ_0006427* suppressed multiplication, migration, invasion and EMT of NSCLC cells. *miR-346* expression was upregulated in NSCLC tissues and cells, and *miR-346* worked as a target of *circ_0006427*. *VGLL4* was down-regulated in NSCLC tissues and cells, and knockdown of *VGLL4* accelerated multiplication, migration, invasion and EMT of NSCLC cells. *Circ_0006427* enhanced *VGLL4* expression by competitively binding with *miR-346*.

Conclusion: *Circ_0006427/miR-346/VGLL4* axis regulated NSCLC progression.

Keywords: circRNA, microRNA, Non-Small Cell Lung Cancer, Vestigial-Like Family Member 4

Cell Journal(Yakhteh), Vol 24, No 5, May 2022, Pages: 245-254

Citation: Sun JC, Wang L, Zhu XH, Shen ML. Hsa_circ_0006427 suppresses multiplication, migration and invasion of non-small cell lung cancer cells through miR-346/VGLL4 pathway. Cell J. 2022; 24(5): 245-254. doi: 10.22074/cellj.2022.7795.

Introduction

Lung cancer takes up approximately 20% of all cancer-related deaths (1). Non-small cell lung cancer (NSCLC) is the main pathological type of lung cancer, composed of about 85% of all lung cancer cases (2). Despite the significant diagnostic and therapeutic progress, 5-year overall survival rate of NSCLC patients is still below 20%, due to metastasis and recurrence of malignancy (3). Therefore, it is imperative to better comprehend the underlying molecular mechanisms involved in NSCLC progression to develop novel and effective therapies and to improve prognosis.

Circular RNA (circRNA) is a kind of non-coding RNA (ncRNA) widely found in eukaryocytes (4). Unlike linear RNAs, circRNAs are covalently closed loop molecules that do not have a 5' or 3' end; so they are resistant to degradation and more stable than linear RNAs (5). circRNAs not only function as competitive endogenous RNAs (ceRNAs) to modulate the availability of microRNAs (miRNAs), but also modulate gene transcription and translation via interacting with proteins (6-8). Reportedly, circRNA partakes in regulating multiplication, cell cycle, apoptosis and metastasis of cancer cells (9-11). *Circ_0006427* is a newly discovered circRNA, linked to tumorigenesis. Its expression is downregulated in lung adenocarcinoma tissues and cell lines, and it can impede disease progression by modulating *miR-6783-3p/DKK1* axis (12). Nevertheless, function of *circ_0006427* in NSCLC progression and the potential mechanisms remain to be further elucidated.

miRNAs are crucial regulators in cancer biology (13, 14). *miR-346* is reported to accelerate hepatocellular carcinoma progression by suppressing *BRMS1* expression (15). Furthermore, expression of *miR-346* is validated to be upregulated in NSCLC, and *miR-346* facilitates growth and metastasis of NSCLC cells by modulating the XPC/ERK/Snail/E-cadherin pathway (16). Vestigial-like family member 4 (*VGLL4*) is a tumor suppressor that competitively binds to TEA domain-containing transcription factors (TEADs) to block its interaction with Yes kinase-associated protein (YAP), and suppresses lung cancer progression (17, 18). In this study, we aimed to investigate the effect of circ_0006427 on NSCLC cell proliferation, migration and invasion, and to explore the

mechanism of its interaction with the miR-346/VGLL4 axis in NSCLC.

Materials and Methods

Clinical specimens

In this experimental study, NSCLC tissues and matched paracancerous tissues (n=50) were obtained from Zhejiang hospital (Hangzhou, China). All subjects were pathologically diagnosed after surgery and all of the patients signed the informed consent form. This study was endorsed by the Research Ethics Committee of Zhejiang Hospital (ZJH20170133), and the procedures were designed according to the guidance of the Declaration of Helsinki. Tissue samples were obtained during surgery and preserved in liquid nitrogen until RNA extraction.

Cell culture and transfection

Normal human bronchial epithelial cell (HNBEC) line, BEAS-2B, and lung cancer cell lines (L9981, A549, H292, NCI-H460, and H460) were obtained from the China Center for Type Culture Collection (CCTCC, Wuhan, China). All cells were maintained in Dulbecco's Modified Eagle's Medium (DMEM, Hyclone, USA) containing 10% fetal bovine serum (FBS, Sijiqing, China), 100 U/ml penicillin and 100 U/ml streptomycin (Hyclone, USA) at 37˚C in 5% CO_2.

For *circ_0006427* overexpression, the pcDNA 3.1 vectors (pcDNA, Invitrogen, USA), containing the fragment of *circ_0006427*, were constructed by RiboBio (Guangzhou, China), namely *circ_0006427*/pcDNA 3.1 *(circ_0006427*). shRNA against *VGLL4* (*VGLL4* shRNA, sh-*VGLL4*) and the corresponding negative control (sh-NC), as well as miR-346 mimic and the negative control (NC-mimic) were available from GenePharma (Shanghai, China). NSCLC cells were transfected using Lipofectamine 3000 (Invitrogen, USA) according to the manufacturer's instructions.

Quantitative reverse transcription polymerase chain reaction

Total RNA was extracted from NSCLC tissues and cells using TRIzol reagent (Takara, Japan). Next, 1 µg total RNA was reversely transcribed into cDNA using PrimeScript RT Master Mix (Takara, Japan). Quantitative reverse transcription polymerase chain reaction (qRT-PCR) was executed on ABI 7500 system (Applied Biosystems, USA) employing TransStart Tip Green qPCRSuperMix (Transgen Biotech, China). *β-ACTIN* was the endogenous control for *circ_0006427* and *VGLL4*, while *U6* was the endogenous control for *miR-346*. $2^{-\Delta\Delta Ct}$ method was utilized to calculate relative expression of the genes. The specific primer sequences were as follows:

circ_0006427-

F: 5′-ACAGCTACCGGATGAATGCT-3′
R: 5′-AGGGCTTCAGCTGTTTCTCA-3′

VGLL4-

F: 5′-AACTGCAACCTCTCGCACTG-3′
R: 5′-GCTCGGGCTCCTTGTAATTCT-3′

miR-346-

F: 5′-TGTCTGCCCGCATGCCT-3′
R: 5′-AGTGCAGGGTCCGAGGTATT-3′

β-ACTIN-

F: 5′-CTGTCACCTTCACCGTTCCAGTTT-3′
R: 5′-AGGGGCCATCCACAGTCTTC-3′

U6-

F: 5′-GCTTCGGCAGCACATATACTAAAAT-3′
R: 5′-CGCTTCACGAATTTGCGTGTCAT-3′

Subcellular fractionation assay

Cytoplasmic and nuclear RNA purification kit (Thermo Fisher Scientific, USA) was used to isolate and extract cytoplasmic and nuclear RNA from A549 and H292 cells. Then, expression of *circ_0006427* in the cytoplasm and nucleus of A549 and H292 cells was measured by qRT-PCR. *β-ACTIN* and *U6* were used as cytoplasmic and nuclear controls, respectively.

Cell multiplication experiment

NSCLC cells were transfected for 48 hours, and then their cell viability was detected by cell counting kit-8 (CCK-8, Beyotime, China) assay. In brief, NSCLC cells were inoculated in 96-well plates (3×10^3 cells/well). After 12 hours, 24 hours, 48 hours, 72 hours and 96 hours of culture, 10 µl CCK-8 solution was supplemented to each well and incubated at 37°C for 2 hours. Cell viability of NSCLC cells was subsequently assessed at 450 nm using a spectrophotometer (Bio-Rad, USA).

Transwell experiment

NSCLC cells were resuspended with fresh medium containing 1% FBS. To detect cell migration, NSCLC cells were inoculated in the upper compartment of the Transwell system (Costar, USA). DMEM containing 10% FBS was replenished to the bottom compartment. After culturing the cells were for 24 hours, the remained NSCLC cells on the top surface of filter were removed by a cotton swab. The cells on the below surface of filter were fixed and stained, followed by observing under a microscope. To detect cell invasion, the filters were pre-coated with Matrigel (Millipore, USA) before the inoculation of cells, and the other procedures were performed the same as the migration assay.

Western blot

NSCLC cells were lysed in RIPA lysis buffer (Beyotime, China). The proteins were separated via SDS-PAGE and electrophoretically transferred to PVDF membranes (Millipore, USA). The membranes were then blocked with 5% skimmed milk for 2 hours and they were incubated

with the primary antibodies including anti-*VGLL4* (Abcam, China, 1:1000), E-cadherin (Abcam, China, 1:1000), Vimentin (Abcam, China, 1:1000), and *β-ACTIN* (Abcam, China, 1:1000) at 4°C overnight, respectively. Following that, the membranes were rinsed with TBST buffer and incubated with horseradish peroxidase (HRP)-coupled secondary antibodies (Beyotime, China) for 2 hours. Ultimately, development of protein bands was performed with ECL kit (Amersham Pharmacia Biotech, UK), and the grayscale values of each protein were analyzed using Image J.

Bioinformatics analysis

The binding sites between *circ_0006427* and *miR-346*, or *miR-346* and *VGLL4* were predicted using CircInteractome database (https://circinteractome.nia.nih.gov/) and StarBase (http://starbase.sysu.edu.cn/) database.

Dual-luciferase reporter experiment

The wild-type (WT) or mutant (MUT) *circ_0006427* and *VGLL4* 3′UTR sequences containing the binding site for *miR-346* were cloned into the pGL3 vector (Promega, USA) to construct the reporter vectors: *circ_0006427*-WT, *VGLL4*-WT, *circ_0006427*-MUT and *VGLL4*-MUT. A549 and H292 cells were co-transfected with *miR-346* mimics or NC-mimics with the reporter vectors, respectively. 48 hours after the transfection, luciferase activity of the cells in each group was examined with a dual-luciferase reporter gene reporter system (Promega, USA).

IHC experiment

In brief, samples were fixed in formalin and embedded in paraffin. Xylene was used for paraffin section dewaxing. After rehydrating the sections, antigen repair was performed. Next, the sections were incubated with anti-*VGLL4* antibody (Abcam, China, 1:100) overnight at 4°C. After rinsing with PBS 5 times, secondary antibody IgG (Beyotime, China, 1:400) was supplemented, with which the sections were incubated for 30 minutes. Then, the sections were rinsed with PBS three times. Next, the tissue sections were stained with DAB solution. Finally, staining intensity was photographed using an Olympus BX51 microscope (Olympus, Japan) and scored by two independent pathologists. The scoring system was based on the staining intensity and staining extent. The staining intensity was classified as 0 (negative), 1 (weak), 2 (medium) and 3 (strong). The degree of staining extent depended on the percentage of positive cells, classified into 0 (<5%), 1 (5-25%), 2 (26-50%), 3 (51-75%) and 4 (>75%). Then, these two scores were multiplied and IHC results were classified as 0-3 (negative) and 4-12 (positive).

Statistical analysis

Each experiment was conducted in triplicate. Statistical analysis was implemented using SPSS (version 25.0, SPSS Inc., USA). All data were expressed as mean ± standard deviation (SD). Student's t tests or one-way ANOVA and post-hoc Dunnett's test were applied to analyze the differences. Pearson's correlation analysis was employed to analyze the correlations among *circ_0006427*, *miR-346* and *VGLL4* in NSCLC samples. Correlations between *circ_0006427* expression and clinicopathological parameters were analyzed using the Chi-square test. $P<0.05$ was considered to be statistically significant.

Results

circ_0006427 was downregulated in NSCLC tissues and cells

To assess expression of *circ_0006427* in NSCLC tissues and cells, qRT-PCR was employed. The data displayed that *circ_0006427* was markedly downregulated in NSCLC tissues relative to that in paracancerous tissues (Fig.1A). Similarly, *circ_0006427* expression was unveiled to be downregulated in NSCLC cell lines compared to that in HNBEC line BEAS-2B (Fig.1B). Furthermore, the subcellular distribution of *circ_0006427* was analyzed. Findings showed that *circ_0006427* was mainly located in the cytoplasm of A549 and H292 cells (Fig.1C). Additionally, the relationship between *circ_0006427* expression and clinicopathologic indicators of NSCLC was analyzed by the Chi-square test. The data manifested that reduced level of *circ_0006427* in NSCLC tissues was associated with larger tumor size and positive lymph node metastasis (Table S1, See Supplementary Online Information at www.celljournal.org).

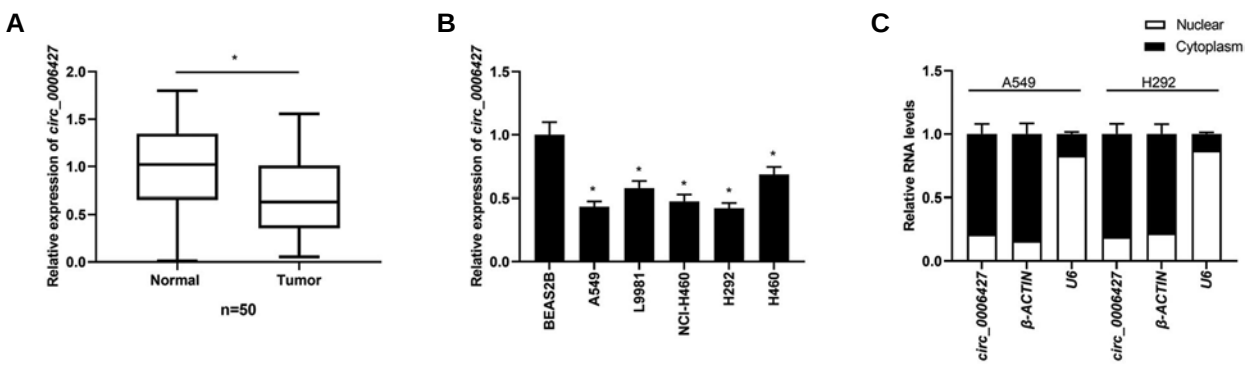

Fig.1: *circ_0006427* was down-regulated in NSCLC. **A.** *circ_0006427* expression in NSCLC tissues and paracancerous tissues was examined by qRT-PCR. **B.** *circ_0006427* expression in NSCLC cells and BEAS-2B cells was detected by qRT-PCR. **C.** Subcellular fractionation assay was used to measure the expression levels of *circ_0006427*, *U6* and *β-ACTIN* in the nuclear and cytoplasm of A549 and H292 cells. All experiments were repeated thrice with triplicate samples in each experiment. *; P<0.05, NSCLC; Non-small cell lung cancer, and qRT-PCR; Quantitative reverse transcription polymerase chain reaction.

Upregulation of *circ_0006427* expression repressed multiplication, migration, invasion and EMT of NSCLC cells

To elucidate the biological function of *circ_0006427* in NSCLC, A549 and H292 cells with the *circ_0006427* lowest expression were transfected with over-expressed *circ_0006427* plasmid to construct an overexpressed model of *circ_0006427* (Fig.2A). The multiplication of NSCLC cells was examined by CCK-8 method, and cell migration and invasion were detected by Transwell experiment. The data implied that upregulation of *circ_0006427* remarkably impeded the multiplication, migration and invasion of NSCLC cells (Fig.2B-F). Moreover, EMT-related protein expression in NSCLC cells was assessed by Western blot, and the data unmasked that upregulation of *circ_0006427* markedly augmented E-cadherin protein expression and inhibited Vimentin protein expression (Fig.2G, H). These data suggested that *circ_0006427* overexpression impeded multiplication, migration, invasion and EMT process of NSCLC cells.

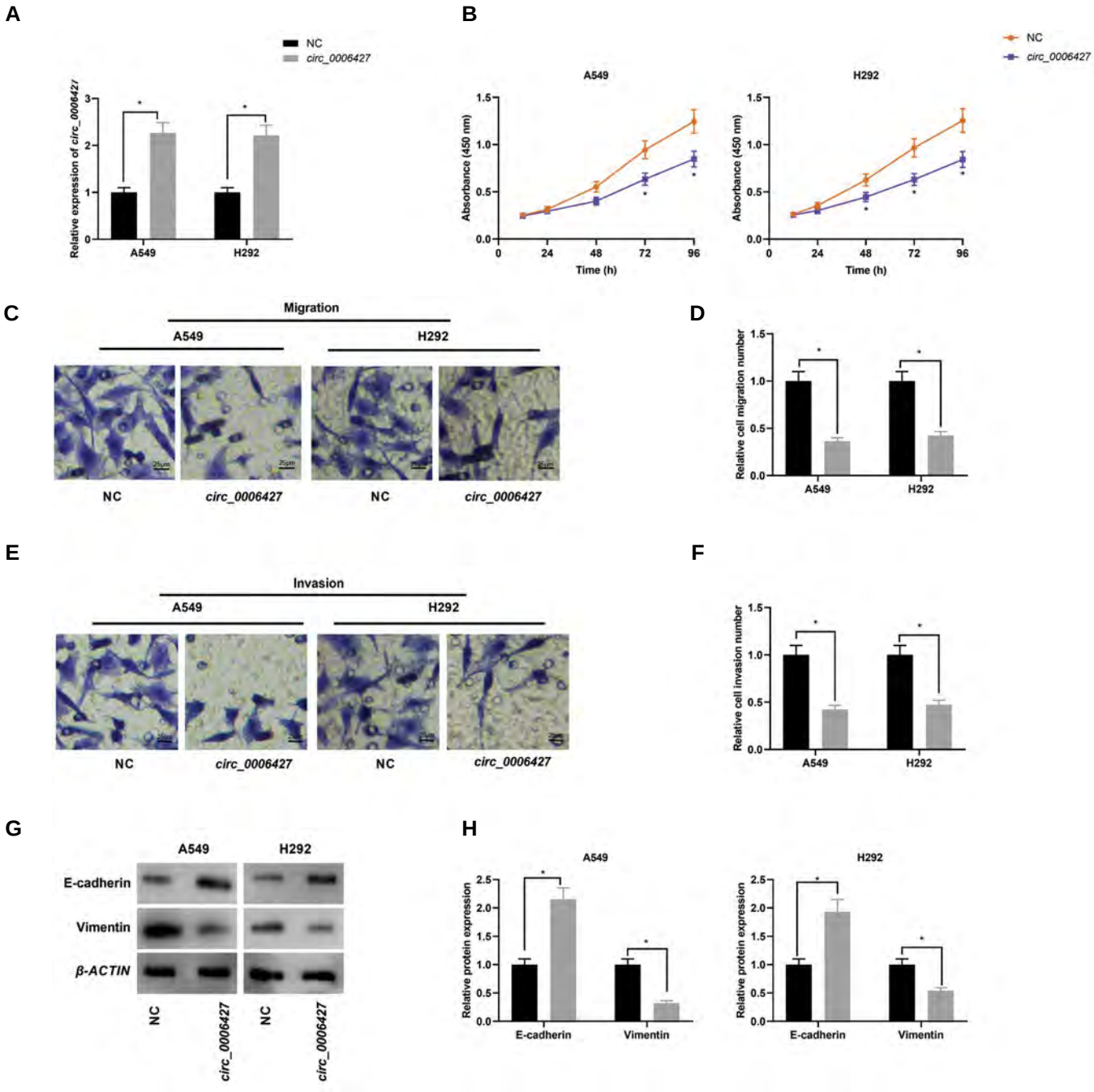

Fig.2: *circ_0006427* overexpression restrained multiplication, migration, invasion and EMT of NSCLC cells. **A.** *circ_0006427* expression in A549 and H292 cells after *circ_0006427* overexpression was detected using qRT-PCR. **B.** The CCK-8 method was employed to detect NSCLC cell multiplication. **C-F.** Transwell experiments were utilized to detect NSCLC cell migration and invasion. **G** and **H.** Western blot was performed to determine E-cadherin and Vimentin protein expressions in NSCLC cells. Original blots are shown in Figure S2 (See Supplementary Online Information at www.celljournal.org), Figure 2G. All experiments were repeated thrice with triplicate samples in each experiment. *; P<0.05, EMT; Epithelial-mesenchymal transition, NSCLC; Non-small cell lung cancer, and NC; Negative control.

circ_0006427 acted as a molecular sponge for *miR-346* in NSCLC cells

The potential binding sites between *circ_0006427* and *miR-346* were projected by bioinformatics analysis (Fig.3A). Subsequently, the relationship between *circ_0006427* and *miR-346* was examined by dual-luciferase reporter gene experiments, the data of which demonstrated that *miR-346* mimics substantially diminished the luciferase activity of *circ_0006427* WT reporter, while did not notably repress the luciferase activity of *circ_0006427* MUT reporter (Fig.3B). Moreover, *miR-346* was remarkably overexpressed in NSCLC tissues and cell lines (Fig.3C, D). Findings of qRT-PCR uncovered that *miR-346* expression was markedly downregulated by *circ_0006427* overexpression in NSCLC tissues (Fig.3E). Additionally, *circ_0006427* expression in NSCLC tissues was negatively associated with *miR-346* expression (Fig.3F). Collectively, these data implied that *circ_0006427* negatively regulated *miR-346* in NSCLC.

miR-346 overexpression reversed the functions of *circ_0006427* in NSCLC cells

To delve into whether *circ_0006427* is involved in NSCLC progression through repressing *miR-346* expression, *miR-346* mimics or NC-mimics were transfected into overexpressed *circ_0006427* cells, A549 and H292 cells respectively (Fig.4A). Cell multiplication, migration and invasion were further examined by CCK-8 method and Transwell experiment. Findings demonstrated that suppressing effects of *circ_0006427* overexpression on cell multiplication, migration and invasion were partially attenuated by *miR-346* mimics (Fig.4B-D). Furthermore, Western blot demonstrated that E-cadherin expression was decreased and Vimentin expression was increased in *circ_0006427*+NC-mimics group remarkably compared to those in *circ_0006427*+*miR-346* group (Fig.4E, F). These results substantiated that *circ_0006427* participated in modulating multiplication, migration, invasion and EMT of NSCLC cells through suppressing *miR-346* expression.

Knockdown of *VGLL4* enhanced NSCLC cell multiplication, migration, invasion and EMT

As a tumor suppressor protein, *VGLL4* associated with lung cancer progression (18). This work examined *VGLL4* expression in NSCLC tissues and paracancerous tissues through IHC and qRT-PCR analyses. Consistently, our data unearthed that *VGLL4* was markedly down-regulated in NSCLC tissues (Fig.5A, B). Similarly, *VGLL4* expression was remarkably reduced in NSCLC cell lines compared to the BESA-2B cells (Fig.5C, D). To fathom tumor-suppressive function of *VGLL4* in NSCLC progression, sh-*VGLL4* was transfected into A549 and H292 cells. As shown, *VGLL4* expression was markedly repressed in NSCLC cells transfected with sh-*VGLL4* (Fig.5E). Data of CCK-8 and Transwell experiments showed knockdown of *VGLL4* remarkably enhanced multiplication, migration and invasion of A549 and H292 cells (Fig.5F-I). Moreover, Western blot revealed that knockdown of *VGLL4* repressed E-cadherin expression in A549 and H292 cells, but upregulated Vimentin expression (Fig.5J, K). These findings elucidated that *VGLL4* played a tumor-suppressive role in NSCLC.

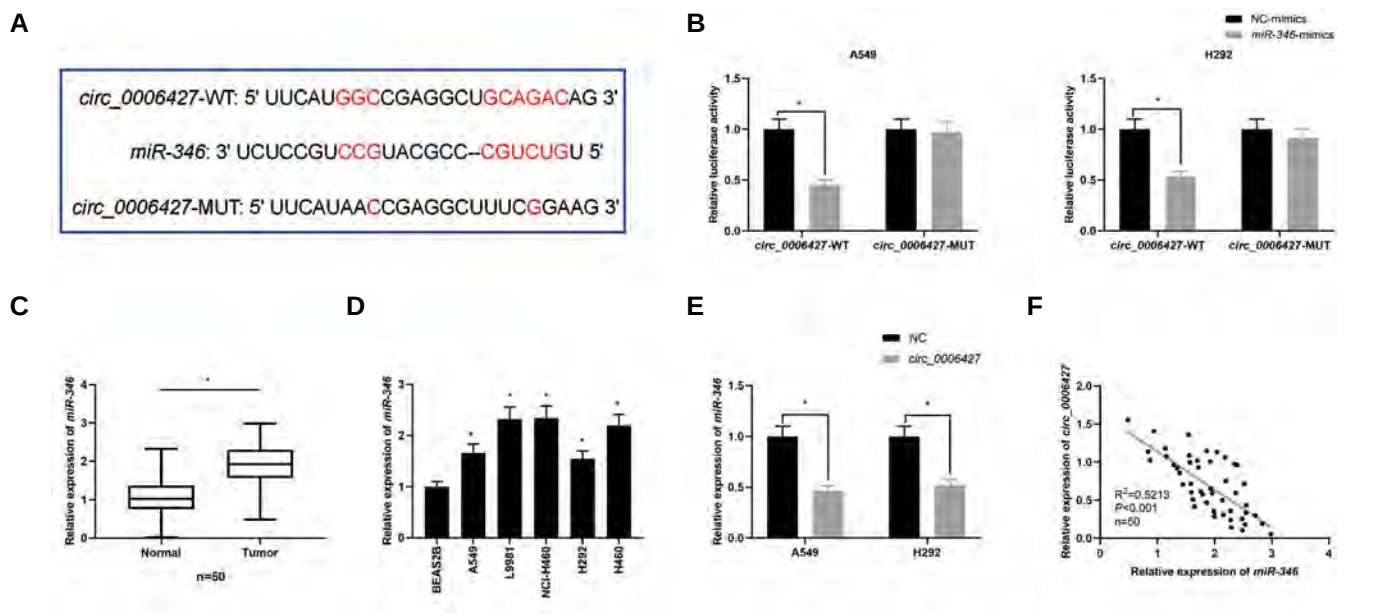

Fig.3: *miR-346* was target of *circ_0006427*. **A.** Bioinformatics analysis predicted binding sequence between *miR-346* and circ_0006427. **B.** Dual-luciferase reporter gene experiments were employed to verify binding relationship between *miR-346* and *circ_0006427*. **C, D.** *miR-346* expression in NSCLC tissues and cells was detected by qRT-PCR. **E.** *miR-346* expression in NSCLC cells overexpressing *circ_0006427* was detected by qRT-PCR. **F.** Pearson's correlation analysis was adopted to analyze the correlation between *miR-346* expression and *circ_0006427* expression in NSCLC tissues. All experiments were repeated thrice with triplicate samples in each experiment. *; P<0.05, NSCLC; Non-small cell lung cancer, qRT-PCR; Quantitative reverse transcription polymerase chain reaction, WT; Wild type, MUT; Mutant, NC-mimics; Mimics negative control, and NC; Negative control.

Circ_0006427 elevated *VGLL4* expression by competitively repressing *miR-346* expression in NSCLC cells

Next, bioinformatics analysis indicated that *VGLL4* 3′UTR contained a binding site of *miR-346* (Fig.6A). Subsequent dual-luciferase reporter gene experiments validated this binding relationship (Fig.6B). Effects of the *circ_0006427/miR-346* axis on *VGLL4* expression were then investigated. Data of qRT-PCR analysis and Western blot suggested that *circ_0006427* overexpression up-regulated *VGLL4* mRNA and protein expressions in NSCLC cells. This upregulation was remarkably reversed by the co-transfection of *miR-346* mimics (Fig.6C, D). Furthermore, the expression of *VGLL4* mRNA in NSCLC tissues was positively associated with *circ_0006427* expression and negatively correlated with *miR-346* expression (Fig.6E, F). From these data, we concluded that *circ_0006427* could upregulate *VGLL4* expression in NSCLC cells through repressing *miR-346* expression.

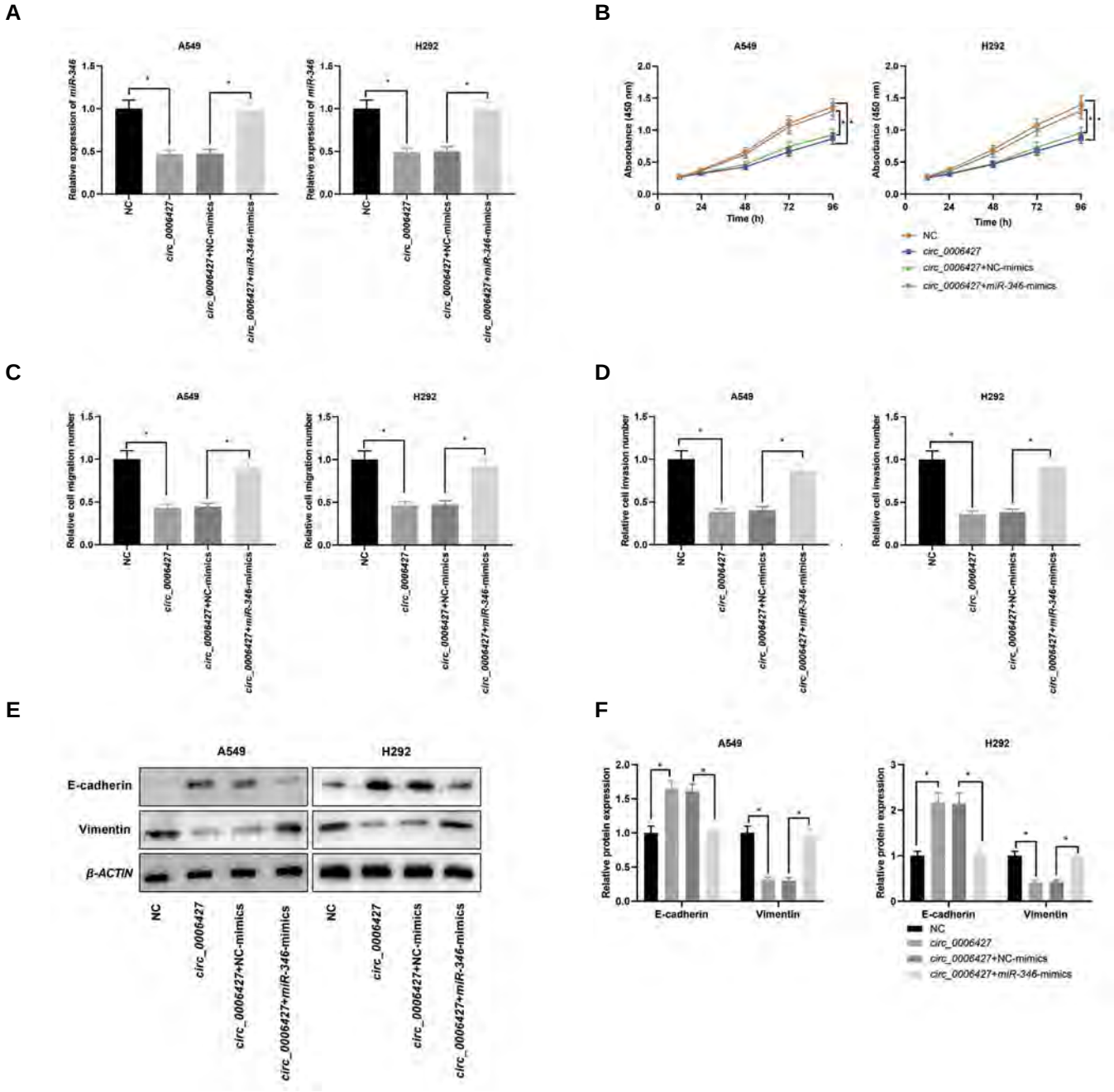

Fig.4: *circ_0006427* targeted *miR-346* and modulated multiplication, migration, invasion and EMT of NSCLC cells. **A.** *miR-346* expression in A549 and H292 cells transfected with *circ_0006427* overexpression plasmid or co-transfected with *miR-346* mimics was detected by qRT-PCR. **B.** CCK-8 assay was utilized to detect the multiplication of NSCLC cells after the transfection. **C, D.** Transwell experiments were exploited to detect migration and invasion of NSCLC cells after the transfection. **E** and **F.** Western blot was applied to determine E-cadherin and Vimentin protein expressions in NSCLC cells. Original blots are shown in Figure S2 (See Supplementary Online Information at www.celljournal.org), Figure 4E. All experiments were repeated thrice with triplicate samples in each experiment. *; P<0.05, EMT; Epithelial-mesenchymal transition, NSCLC; Non-small cell lung cancer, qRT-PCR; Quantitative reverse transcription PCR, NC; Negative control, and NC-mimics; Mimics negative control.

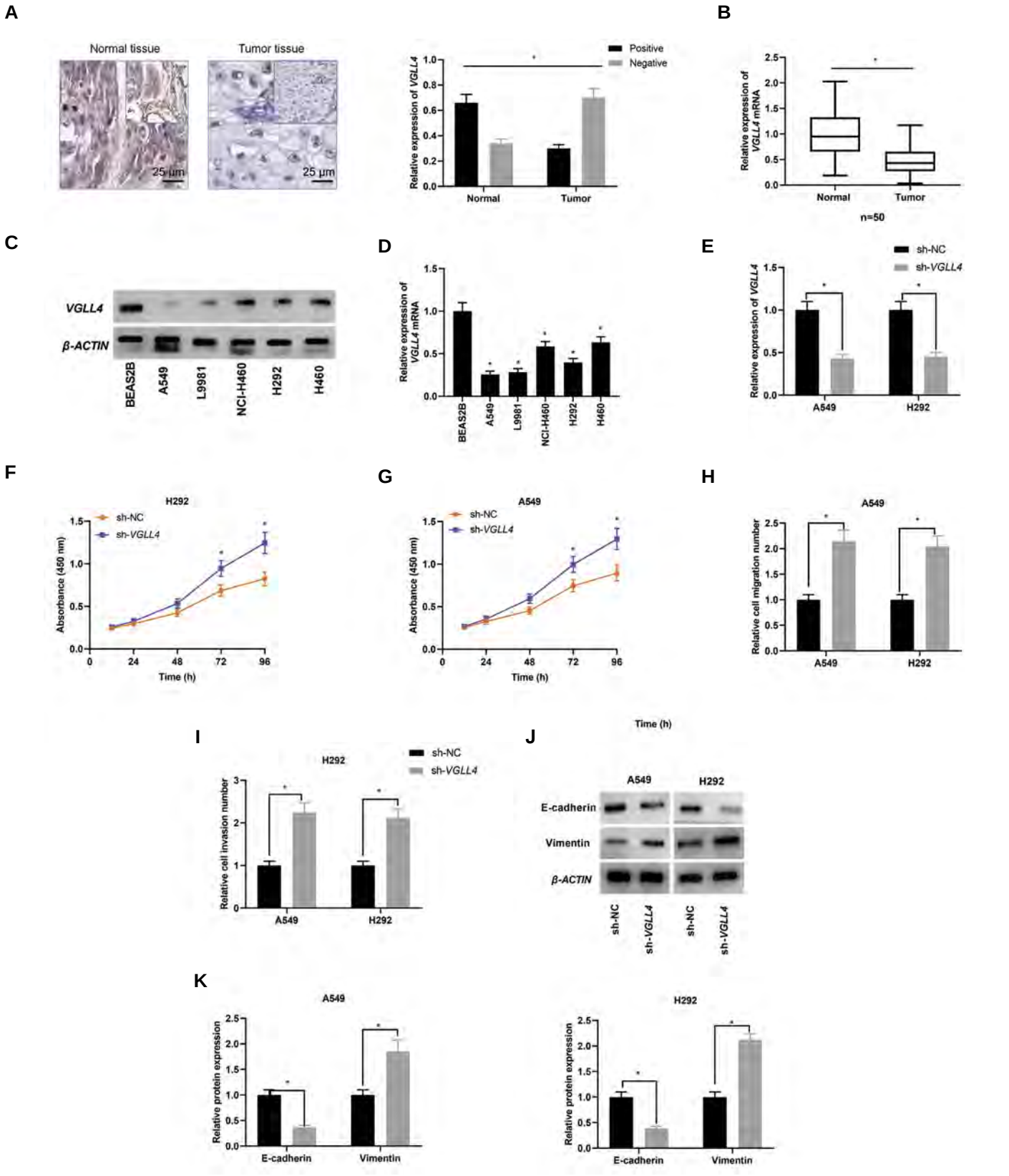

Fig.5: Knockdown of *VGLL4* impeded multiplication, migration, invasion and EMT of NSCLC cells. **A, B.** IHC and qRT-PCR methods were employed to detect *VGLL4* protein and mRNA expressions in NSCLC tissues and paracancerous tissues. **C, D.** Western blot and qRT-PCR were implemented to detect VGLL4 protein and mRNA expressions in NSCLC cells and BEAS2B cells. Original blots are shown in Figure S2 (See Supplementary Online Information at www.celljournal.org), Figure 5C. **E.** *VGLL4* expression in NSCLC cells transfected with sh-*VGLL4* was detected by qRT-PCR. **F, G.** CCK-8 assay was employed to monitor NSCLC cell multiplication. **H, I.** Transwell experiments were executed to detect NSCLC cell migration and invasion. **J, K.** Western blot was used to determine E-cadherin and Vimentin protein expressions in NSCLC cells transfected with sh-VGLL4. Original blots are shown in Figure S2 (See Supplementary Online Information at www.celljournal.org), Figure 5J. All experiments were repeated thrice with triplicate samples in each experiment. *; P<0.05, EMT; Epithelial-mesenchymal transition, NSCLC; Non-small cell lung cancer, IHC; Immunohistochemical, and qRT-PCR; Quantitative reverse transcription polymerase chain reaction.

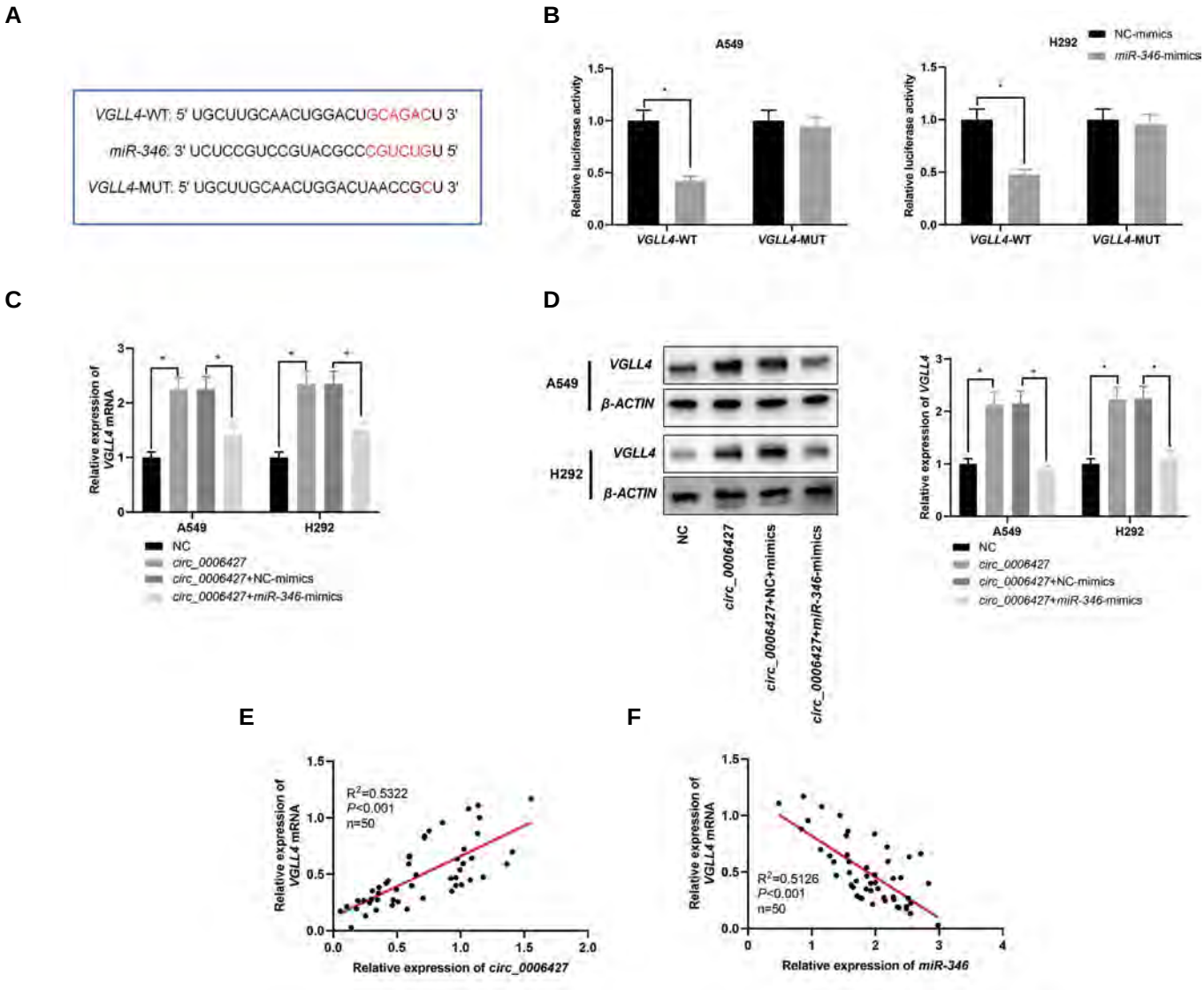

Fig.6: *VGLL4* was the target of *miR-346* in NSCLC cells and positively regulated by *circ_0006427*. **A.** Bioinformatics analysis predicted binding sequence between *miR-346* and *VGLL4*. **B.** Binding relationship between *miR-346* and *VGLL4* was verified using the dual-luciferase reporter gene assay. **C, D.** *VGLL4* mRNA and protein expressions in A549 and H292 cells transfected with *circ_0006427* overexpression plasmid or co-transfected with *miR-346* mimics were detected by qRT-PCR and Western blot. Original blots are shown in Figure S2 (See Supplementary Online Information at www.celljournal.org), Figure 6D. **E** and **F.** Pearson's correlation analysis was applied to determine correlation of *VGLL4* mRNA with *circ_0006427* or *miR-346* expression in NSCLC tissues. All experiments were repeated thrice with triplicate samples in each experiment. *; P<0.05, NSCLC; Non-small cell lung cancer, qRT-PCR; Quantitative reverse transcription polymerase chain reaction, WT; Wild type, MUT; Mutant, NC-mimics; Mimics negative control, and NC; Negative control.

Discussion

circRNAs figure prominently in the regulation of diverse biological processes (19, 20). In recent years, circRNAs are proven to participate in the tumorigenesis and development of several cancers, including NSCLC (21). For example, *circ_0008305* restrains TGF-β-induced NSCLC cell invasion and EMT by modulating *TIF1γ* expression (22); downregulation of *circ_0067934* expression suppresses multiplication, migration and invasion of NSCLC cells. It is linked to unfavorable prognosis of patients (23). Notably, *circ_0006427* expression is downregulated in lung adenocarcinoma, and *circ_0006427* overexpression represses multiplication, migration, invasion and EMT of lung adenocarcinoma cells (12). Consistently, in this work, *circ_0006427* was unearthed to be remarkably under-expressed in both NSCLC tissues and cell lines; *circ_0006427* low expression was related to larger tumor size and positive LNM of NSCLC patients. Functionally, *circ_0006427* was verified to be tumor-suppressive in NSCLC progression by restraining cell multiplication, migration, invasion and EMT.

The role of miRNAs in tumor progression is extensively studied (24, 25). For instance, *miR-421* is highly expressed in NSCLC. It accelerates cell multiplication and cell cycle progression (26). Similarly, *miR-619-5p* in tumor-derived exosome facilitates growth and metastasis of NSCLC cells by impeding *RCAN1.4* expression (27). Accumulating research demonstrated that circRNAs can play "molecular sponge" role by antagonizing miRNAs to modulate expression of the target genes, thus playing an essential regulatory role in tumor progression. For

instance, *circ-ZKSCAN1* facilitates NSCLC progression by targeting *miR-330-5p* to regulate *FAM83A* expression and inactivate the MAPK signaling pathway (28); *circ_0000003* enhances multiplication and metastasis of NSCLC cells by regulating *miR-338-3p*/*IRS2* axis (29). In this work, it was revealed that there was a pairing relationship between *circ_0006427* and *miR-346* in NSCLC progression and *circ_0006427* could work as a molecular sponge for *miR-346*. Meanwhile, *miR-346* expression was markedly upregulated in NSCLC tissues and cell lines, which is consistent with the previous reports (16). Additionally, *miR-346* overexpression remarkably attenuated tumor-suppressive effect caused by *circ_0006427* overexpression. These results implied that *circ_0006427* could exert tumor-suppressive effects in NSCLC progression via sponging *miR-346*.

VGLL4, a member of the VGLL family, is an antagonist of the proto-oncogenic protein YAP (17). Unlike the other VGLL family proteins, *VGLL4* has two TDU domains (18). The N-terminal of *VGLL4* protein can bind to ubiquitin-specific protease 11, thus improving stability of the *VGLL4* protein by facilitating its deubiquitination (30). The role of *VGLL4* varies among cells and tissues. *VGLL4* overexpression is reported to enhance the colony-formation ability of human embryonic stem cells (31). Absence of *VGLL4* impedes *PD-L1* expression and tumor immune escape (32). Additionally, aberrant expression of *VGLL4* occurs frequently in diverse cancers and *VGLL4* is closely related to cell multiplication, migration, invasion and EMT. This can suppress cancer progression by modulating multiple signaling pathways, such as YAP and Wnt/β-catenin (33, 34). Importantly, *VGLL4* is tumor-suppressive in lung cancer, competing with YAP for binding to *TEAD4* and repressing transcription of *TEAD4* downstream genes (18, 35). In this work, we demonstrated that *VGLL4* expression was remarkably downregulated in NSCLC tissues and cells. Simultaneously, knockdown of *VGLL4* markedly enhanced multiplication, migration, invasion and EMT of NSCLC cells. Interestingly, *VGLL4* expression is validated to be linked to multiple miRNAs, such as *miR-130b*, *miR-222* and *miR-130a* (35-37). In this work, *VGLL4* was uncovered to be a direct target of *miR-346* in NSCLC cells. Further experimental data demonstrated that *circ_0006427* could modulate *VGLL4* expression by competitively binding to *miR-346*. Hence, we concluded that *circ_0006427/miR-346/VGLL4* axis could probably take part in NSCLC development.

Conclusion

This work revealed that *circ_0006427* was remarkably downregulated in NSCLC tissues and cells. *Circ_0006427* overexpression restrains multiplication, migration, invasion and EMT of NSCLC cells. Mechanistically, *circ_0006427* modulates *VGLL4* expression via sponging *miR-346*. These data implicated that *circ_0006427/miR-346/VGLL4* regulatory axis could be an essential factor in NSCLC progression.

Acknowledgment

We thank Hubei Yican Health Industry Co., Ltd for its linguistic assistance during the preparation of this manuscript. There is no financial support and conflict of interest in this study.

Authors' Contributions

X.Z., M.Sh.; Conceived and designed the experiments. J.S., L.W., X.Z.; Performed the experiments. L.W., J.S.; Analyzed the data. J.S., M.Sh., X.Z.; Wrote the manuscript. All authors read and approved the final manuscript.

References

1. Bray F, Ferlay J, Soerjomataram I, Siegel RL, Torre LA, Jemal A. Global cancer statistics 2018: GLOBOCAN estimates of incidence and mortality worldwide for 36 cancers in 185 countries. CA Cancer J Clin. 2018; 68(6): 394-424.
2. Radovic M, Kanesvaran R, Rittmeyer A, Früh M, Minervini F, Glatzer M, et al. Multidisciplinary treatment of lung cancer in older patients: a review. J Geriatr Oncol. 2019; 10(3): 405-410.
3. Testa U, Castelli G, Pelosi E. Lung cancers: molecular characterization, clonal heterogeneity and evolution, and cancer stem cells. Cancers (Basel). 2018; 10(8): 248.
4. Meng S, Zhou H, Feng Z, Xu Z, Tang Y, Li P, et al. CircRNA: functions and properties of a novel potential biomarker for cancer. Mol Cancer. 2017; 16(1): 94.
5. Kulcheski FR, Christoff AP, Margis R. Circular RNAs are miRNA sponges and can be used as a new class of biomarker. J Biotechnol. 2016; 238: 42-51.
6. Liu T, Ye P, Ye Y, Lu S, Han B. Circular RNA hsa_circRNA_002178 silencing retards breast cancer progression via microRNA-328-3p-mediated inhibition of COL1A1. J Cell Mol Med. 2020; 24(3): 2189-2201.
7. Li X, Wang J, Zhang C, Lin C, Zhang J, Zhang W, et al. Circular RNA circITGA7 inhibits colorectal cancer growth and metastasis by modulating the Ras pathway and upregulating transcription of its host gene ITGA7. J Pathol. 2018; 246(2): 166-179.
8. AbouHaidar MG, Venkataraman S, Golshani A, Liu B, Ahmad T. Novel coding, translation, and gene expression of a replicating covalently closed circular RNA of 220 nt. Proc Natl Acad Sci USA. 2014; 111(40): 14542-14547.
9. Xu Q, Deng B, Li M, Chen Y, Zhuan L. circRNA-UBAP2 promotes the proliferation and inhibits apoptosis of ovarian cancer though miR-382-5p/PRPF8 axis. J Ovarian Res. 2020; 13(1): 81.
10. Wang K, Sun Y, Tao W, Fei X, Chang C. Androgen receptor (AR) promotes clear cell renal cell carcinoma (ccRCC) migration and invasion via altering the circHIAT1/miR-195-5p/29a-3p/29c-3p/CDC42 signals. Cancer Lett. 2017; 394: 1-12.
11. Fan L, Cao Q, Liu J, Zhang J, Li B. Circular RNA profiling and its potential for esophageal squamous cell cancer diagnosis and prognosis. Mol Cancer. 2019; 18(1): 16.
12. Yao Y, Hua Q, Zhou Y. CircRNA has_circ_0006427 suppresses the progression of lung adenocarcinoma by regulating miR-6783-3p/DKK1 axis and inactivating Wnt/β-catenin signaling pathway. Biochem Biophys Res Commun. 2019; 508(1): 37-45.
13. Thomson DW, Dinger ME. Endogenous microRNA sponges: evidence and controversy. Nat Rev Genet. 2016; 17(5): 272-283.
14. Long Z, Wang Y. miR-195-5p suppresses lung cancer cell proliferation, migration, and invasion Via FOXK1. Technol Cancer Res Treat. 2020; 19: 1533033820922587.
15. Guo Z, Li J, Sun J, Sun L, Zhou Y, Yu Z. miR-346 Promotes HCC progression by suppressing breast cancer metastasis suppressor 1 expression. Oncol Res. 2018; 26(7): 1073-1081.
16. Sun CC, Li SJ, Yuan ZP, Li DJ. MicroRNA-346 facilitates cell growth and metastasis, and suppresses cell apoptosis in human non-small cell lung cancer by regulation of XPC/ERK/Snail/E-cadherin pathway. Aging (Albany NY). 2016; 8(10): 2509-2524.
17. Lin Z, Guo H, Cao Y, Zohrabian S, Zhou P, Ma Q, et al. Acetylation of VGLL4 regulates hippo-YAP signaling and postnatal cardiac growth. Dev Cell. 2016; 39(4): 466-479.
18. Zhang W, Gao Y, Li P, Shi Z, Guo T, Li F, et al. VGLL4 functions as a new tumor suppressor in lung cancer by negatively regulat-

ing the YAP-TEAD transcriptional complex. Cell Res. 2014; 24(3): 331-343.
19. Zhou J, Wang H, Chu J, Huang Q, Li G, Yan Y, et al. Circular RNA hsa_circ_0008344 regulates glioblastoma cell proliferation, migration, invasion, and apoptosis. J Clin Lab Anal. 2018; 32(7): e22454.
20. Li X, Yang L, Chen LL. The biogenesis, functions, and challenges of circular RNAs. Mol Cell. 2018; 71(3): 428-442.
21. Dong Y, Xu T, Zhong S, Wang B, Zhang H, Wang X, et al. Circ_0076305 regulates cisplatin resistance of non-small cell lung cancer via positively modulating STAT3 by sponging miR-296-5p. Life Sci. 2019; 239: 116984.
22. Wang L, Tong X, Zhou Z, Wang S, Lei Z, Zhang T, et al. Circular RNA hsa_circ_0008305 (circPTK2) inhibits TGF-β-induced epithelial-mesenchymal transition and metastasis by controlling TIF1γ in non-small cell lung cancer. Mol Cancer. 2018; 17(1): 140.
23. Wang L, Tong X, Zhou Z, Wang S, Lei Z, Zhang T, et al. Circular RNA hsa_circ_0008305 (circPTK2) inhibits TGF-β-induced epithelial-mesenchymal transition and metastasis by controlling TIF1γ in non-small cell lung cancer. Mol Cancer. 2018; 17(1): 140.
24. Liang G, Meng W, Huang X, Zhu W, Yin C, Wang C, et al. miR-196b-5p-mediated downregulation of TSPAN12 and GATA6 promotes tumor progression in non-small cell lung cancer. Proc Natl Acad Sci U S A. 2020; 117(8): 4347-4357.
25. Khandelwal A, Seam RK, Gupta M, Rana MK, Prakash H, Vasquez KM, et al. Circulating microRNA-590-5p functions as a liquid biopsy marker in non-small cell lung cancer. Cancer Sci. 2020; 111(3): 826-839.
26. Li X, Chen SH, Zeng JW. MiR-421 is overexpressed and promotes cell proliferation in non-small cell lung cancer. Med Princ Pract. 2020; 29(1): 80-89.
27. Kim DH, Park S, Kim H, Choi YJ, Kim SY, Sung KJ, et al. Tumor-derived exosomal miR-619-5p promotes tumor angiogenesis and metastasis through the inhibition of RCAN1.4. Cancer Lett. 2020; 475: 2-13.
28. Wang Y, Xu R, Zhang D, Lu T, Yu W, Wo Y, et al. Circ-ZKSCAN1 regulates FAM83A expression and inactivates MAPK signaling by targeting miR-330-5p to promote non-small cell lung cancer progression. Transl Lung Cancer Res. 2019; 8(6): 862-875.
29. Li S, Niu X, Li H, Liang Y, Sun Z, Yan Y. Circ_0000003 promotes the proliferation and metastasis of non-small cell lung cancer cells via miR-338-3p/insulin receptor substrate 2. Cell Cycle. 2019; 18(24): 3525-3539.
30. Zhang E, Shen B, Mu X, Qin Y, Zhang F, Liu Y, et al. Ubiquitin-specific protease 11 (USP11) functions as a tumor suppressor through deubiquitinating and stabilizing VGLL4 protein. Am J Cancer Res. 2016; 6(12): 2901-2909.
31. Tajonar A, Maehr R, Hu G, Sneddon JB, Rivera-Feliciano J, Cohen DE, et al. Brief report: VGLL4 is a novel regulator of survival in human embryonic stem cells. Stem Cells. 2013; 31(12): 2833-2841.
32. Wu A, Wu Q, Deng Y, Liu Y, Lu J, Liu L, et al. Loss of VGLL4 suppresses tumor PD-L1 expression and immune evasion. EMBO J. 2019; 38(1): e99506.
33. Li H, Wang Z, Zhang W, Qian K, Liao G, Xu W, et al. VGLL4 inhibits EMT in part through suppressing Wnt/β-catenin signaling pathway in gastric cancer. Med Oncol. 2015; 32(3): 83.
34. Liu X, Kong C, Zhang Z. miR-130b promotes bladder cancer cell proliferation, migration and invasion by targeting VGLL4. Oncol Rep. 2018; 39(5): 2324-2332.
35. Deng X, Fang L. VGLL4 is a transcriptional cofactor acting as a novel tumor suppressor via interacting with TEADs. Am J Cancer Res. 2018; 8(6): 932-943.
36. Li N, Yu N, Wang J, Xi H, Lu W, Xu H, et al. miR-222/VGLL4/YAP-TEAD1 regulatory loop promotes proliferation and invasion of gastric cancer cells. Am J Cancer Res. 2015; 5(3): 1158-1168.
37. Shen S, Guo X, Yan H, Lu Y, Ji X, Li L, et al. A miR-130a-YAP positive feedback loop promotes organ size and tumorigenesis. Cell Res. 2015; 25(9): 997-1012.

Original Article

Cordycepin Suppresses The Malignant Phenotypes of Colon Cancer Cells through The GSK3ß/ß-catenin/cyclin D1 Signaling Pathway

Jie Xu, B.Sc.[1], Xia Shen, B.Sc.[2], Daozhong Sun, B.Sc.[1], Yanjie Zhu, B.Sc.[3]*

1. Department of General Surgery, Zhejiang Greentown Cardiovascular Hospital, Hangzhou, Zhejiang, China
2. Department of Emergency, Zhejiang Greentown Cardiovascular Hospital, Hangzhou, Zhejiang, China
3. Department of Dermatology, The Second People's Hospital of Yuhang District, Hangzhou, Zhejiang, China

**Corresponding Address: Department of Dermatology, The Second People's Hospital of Yuhang District, Hangzhou, Zhejiang, China*
Email: 1048950853@qq.com

Received: 04/August/2021, Accepted: 21/February/2022

Abstract

Objective: Cordycepin, also known as 3′-deoxyadenosine, is the main bioactive ingredient of *Cordyceps militaris* and possesses various pharmacological effects. This study was performed to investigate the role of cordycepin in regulating the biological behaviors of colon cancer cells and the potential mechanism behind it.

Materials and Methods: In this experimental study, after treatment of colon cancer cells with different concentrations of cordycepin, inhibition of proliferation was detected by the 3-(4,5-dimethythiazol-2-yl)-2,5-diphenyl tetrazolium bromide (MTT) assay. Colon cancer cell migration and invasion abilities were analyzed by wound healing and Transwell assays. Flow cytometry was performed to detect cell apoptosis. A lung metastasis model in nude mice was utilized to examine the effect of cordycepin on the metastasis of colon cancer cells *in vivo*. Western blot was used to quantify GSK3β, β-catenin and cyclin D1 expression levels.

Results: Cordycepin inhibited colon cancer cell proliferation, migration and invasion, induced apoptosis *in vitro*, and inhibited lung metastasis of colon cancer cells *in vivo*. GSK-3β inhibitor (CHIR99021) treatment abolished the effects of cordycepin on cell viability, migration, invasion and apoptosis. Additionally, cordycepin promoted the expressions of GSK3β, and inhibited β-catenin and cyclin D1 in colon cancer cells, while co-treatment with CHIR99021 reversed the above effects.

Conclusion: Cordycepin suppresses the malignant phenotypes of colon cancer through the GSK3β/β-catenin/cyclin D1 signaling pathway.

Keywords: Colon Cancer, Cordycepin, Cyclin D1, GSK3β, β-Catenin

Cell Journal(Yakhteh), Vol 24, No 5, May 2022, Pages: 255-260

Citation: Xu J, Shen X, Sun D, Zhu Y. Cordycepin suppresses the malignant phenotypes of colon cancer cells through the GSK3β/β-catenin/cyclin D1 signaling pathway. Cell J. 2022; 24(5): 255-260. doi: 10.22074/cellj.2022.8160.

Introduction

Colon cancer is one of the most common malignancies (1). Surgical resection, chemotherapy, and molecular targeted therapy are the main treatment strategies for colon cancer (2). Nonetheless, approximately 50% of colon cancer patients develop chemoresistance (3). Therefore, the search for possible therapeutic agents is important to improve the prognosis of colon cancer patients.

Natural products represent a rich source for the discovery and development of anti-cancer drugs (4-6). Cordycepin, also known as 3'-deoxyadenosine, is a kind of nucleoside analog, which is extracted from *Cordyceps militaris* (7, 8). Cordycepin has various pharmacological effects, including anti-tumor, anti-bacterial, and anti-aging activity, immunomodulation, scavenging of free radicals and anti-ischemia/reperfusion injury activity (8-10). Reportedly, cordycepin can inhibit the growth of colon cancer cells, suggesting that cordycepin is promising in the treatment of colon cancer (11). However, the detailed mechanism by which cordycepin exerts its tumor-suppressive functions is not clear.

Kinases play a critical role in cellular signal transduction, and many of them are associated with tumorigenesis and cancer progression (12). Glycogen synthase kinase 3 (GSK3), a serine/threonine kinase, which has two isoforms, GSK3α and GSK3β (13). GSK3β has been found to regulate the survival and proliferation of colon cancer cells (14). Interestingly, GSK3β is reported to be involved in the phosphorylation of β-catenin, thereby activating the E3 ubiquitin ligase subunit β-Trcp and inducing the proteasome degradation of β-catenin (15). In addition, elevated levels of nuclear β-catenin is considered to be a hallmark of aggressive colon cancer, which activates Wnt-related targets including c-myc, cyclin D1, MMP2 and MMP9, thereby promoting cell proliferation, invasion and migratory potential (16-19). The present study aimed to investigate the role and mechanism of GSK3β/β-catenin/cyclin D1 pathway in colon cancer.

Materials and Methods

Cell lines and cell culture

In this experimental study, Cordycepin (3′-deoxyadenosine, CAS: 73-03-0) was obtained from Sigma-Aldrich (St. Louis, MO, USA). Human immortalized colon mucosa cell line FHC, and human colon cancer cell lines (HT-29 and LoVo) were provided by the Shanghai Cell Bank of the Chinese Academy of Sciences (Shanghai, China), and the cells were cultured in Roswell Park Memorial Institute-1640 (RPMI-1640) medium (Gibco, Waltham, Waltham, MA, USA) supplemented with 10% fetal bovine serum (FBS, Gibco, Waltham, MA, USA), 0.1 mg/mL streptomycin (Gibco, Waltham, MA, USA) and 100 U/mL penicillin (Gibco, Waltham, MA, USA) at 37˚C in a humidified environment with 5% CO_2. The medium was changed every 1-2 days, and when the confluence reached 80%, 0.25% trypsin was used for trypsinization, and the cells were passaged.

3-(4,5-dimethythiazol-2-yl)-2,5-diphenyl tetrazolium bromide (MTT) assay

The cells were trypsinized, resuspended and then inoculated in 96-well plates at 5×10^3 cells/well, with 3 replicate wells for each group of cells. HT-29 and LoVo cells were treated with different concentrations of cordycepin (20, 40 and 80 μM) for 24 hours, respectively. Cells with no treatment served as the control group. After adding 10 μL of MTT (Sigma-Aldrich, St. Louis, MO, USA) per well, the cells were further incubated for 2 hours. Then dimethylsulfoxide (DMSO; Sigma-Aldrich, St. Louis, MO, USA) was added into the wells, and the crystals were dissolved, and the absorbance values were measured by a spectrophotometer at 490 nm.

Wound healing experiment

HT-29 and LoVo cells were inoculated into 6-well culture plates (5×10^5 cells/well) and cultured. When the confluency of the cells reached 90%, a scratch was made in the middle of the monolayer cells with a sterile 200 μL pipette tip. Then, the cells were gently washed 3 times with phosphate buffered saline (PBS), the width of the scratch was detected, and then the cells were cultured with serum-free medium. After 24 hours, the scratch was detected under the microscope again. Scratch healing rate (%)=(0 hours scratch width−24 hours scratch width)/0 h scratch width×100%.

Transwell assay

Cell invasion assays were performed with Transwell chambers (Corning, NY, USA). Matrigel (1:10; BD Biosciences, Franklin Lakes, NJ, USA) was used to cover the filter of Transwell chambers. The density of HT-29 cells was modulated to 1×10^6 cells/mL with serum-free medium, and 100 μL of cell suspension and 600 μL of the complete medium were supplemented to the upper compartment and lower compartment, respectively. After 2 days, the cells on the upper surface of the filter were removed, and the cells on the below surface of the filter were fixed with 4% paraformaldehyde, and subsequently stained with 0.1% crystal violet. The number of cells that passed through the filter were counted in five random fields of view, and the average was calculated to indicate the invasion ability of the cells.

Flow cytometry

The cells were trypsinized with EDTA-free trypsin, and the cells were collected by centrifugation. According to the manufacturer's instructions for Annexin V-FITC/PI Apoptosis Detection Kit (Yeasen Biotech Co., Ltd., Shanghai, China), the colon cells were washed twice with PBS and resuspended with 1× binding buffer and accordingly incubated with 5 μL of Annexin V-FITC staining solution and 10 μL of propidium iodide (PI) staining solution for 15 min at ambient temperature in the dark. After the cells were washed by PBS, a flow cytometer (BD Biosciences, San Jose, CA, USA) was used to quantify apoptosis within 1 hours.

Lung metastasis assay

All animal experiments were approved by the animal Ethical Committee of Zhejiang Greentown Cardiovascular Hospital (2017A044). 12 nude mice (6-week-old, male) weighing 12-15 g, purchased from the Experimental Animal Center of Zhejiang University, were randomly grouped into 2 groups (n=6 in each group). The mice in each group were injected with HT-29 cells (1×10^7 cells per mouse) via the caudal vein, and then treated with or without cordycepin (20 mg/kg). After 2 weeks, the mice were euthanized, and the fresh lung tissues were harvested for histopathology analysis. The number of metastatic nodules in the lung of each mouse was counted with naked eyes. Next, formalin-fixed and paraffin-embedded lung tissues were prepared, and 4 μm of thick sections were stained with hematoxylin and eosin and then observed under the microscope (NikonEclipseE600; Nikon, Thornwood, NY, USA).

Western blot

The colon cancer cells were lysed in RIPA lysis solution (Beyotime Biotechnology, Shanghai, China), and the BCA protein assay kit (Beyotime Institute of Biotechnology, Haimen, China) was utilized to quantify the protein concentration. After adding protein loading buffer and boiling to denaturation, sodium dodecyl sulfate polyacrylamide gel electrophoresis (SDS-PAGE) was performed. The protein samples were transferred onto the polyvinylidene fluoride

(PVDF) membranes, and then were blocked at ambient temperature for 1 hours using 5% skimmed milk. Then the membranes were incubated with the following primary antibodies: anti-GSK3β (1:2000, ab32391, Abcam, Shanghai, China), anti-β-catenin (1:2000, ab16051, Abcam, Shanghai, China) and anti-cyclin D1 (1:2000, ab16663, Abcam, Shanghai, China) overnight at 4˚C. The following day, the secondary antibody, Goat Anti-Rabbit IgG H&L (1:5000, ab6721, Abcam, Shanghai, China), was added, and the membrane was incubated for 1 hour at 37˚C. After the membranes were washed by tris buffered saline tween (TBST), the ECL chemiluminescence kit (Beyotime Biotechnology, Shanghai, China) was used for luminescence development, and an Odyssey imaging system was utilized to analyze the grayscale value of each band.

Statistical analysis

Statistical product and service solutions (SPSS) software (version 23.0, SPSS, Chicago, IL, USA) was adopted to process the data represented as "mean ± standard deviation". To make the comparison between two groups, a One-Sample Kolmogorov-Smirnov test was used to detect the normality of the data. If the data were normally distributed, an independent sample t test was utilized; paired sample Wilcoxon signed rank test was adopted to compare the data with skewed distribution. One-way ANOVA test was performed to make the comparison among three or more groups. If there was a significant difference, Newman-Keuls analysis was performed to make the comparison between 2 groups. The differences were considered statistically significant at P<0.05.

Results

Cordycepin suppresses the malignant phenotypes of colon cancer cells

The molecular structure of cordycepin is shown in Figure 1A. To probe the biological effect of cordycepin on the phenotypes of FHC and colon cancer cells, the proliferation of HT-29, LoVo and FHC cells was detected by the MTT method after treatment with different concentrations of cordycepin (20 μM, 40 μM and 80 μM). As shown, the viability of colon cancer cells was decreased by cordycepin treatment in a dose-dependent manner (P<0.05, Fig.1B); notably, only high doses of cordycepin (80 μM) could significantly suppress the viability of FHC cells (Fig.S1A, See Supplementary Online Information at www.celljournal.org), which suggested that cordycepin selectively kills cancer cells. The results of the scratch healing assay and Transwell assay showed that cordycepin treatment reduced the migration and invasion of HT-29 and LoVo cells compared with the control group (P<0.01, Fig.1C, D). In addition, flow cytometry revealed that cordycepin treatment promoted the apoptosis of HT-29 and LoVo cells compared with the control group (P<0.05, Fig.1E). Additionally, a lung metastasis model in nude mice was used to evaluate the metastasis of HT-29 cells *in vivo*, and it showed that cordycepin treatment inhibited the pulmonary metastasis of HT-29 cells *in vivo* (Fig.S1B, See Supplementary Online Information at www.celljournal.org).

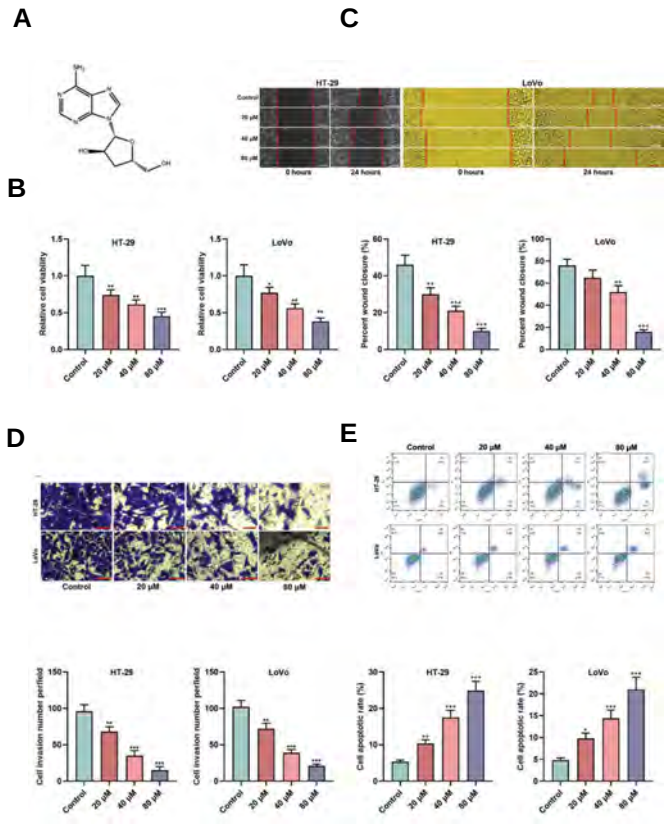

Fig.1: Effects of cordycepin on the biological behaviors of colon cancer cells**. A.** The molecular structure of cordycepin. **B.** Cell viability of HT-29 and LoVo cells was detected by MTT assay after treatment with different concentrations of cordycepin (control, 20 μM, 40 μM and 80 μM). **C.** Cell migration (scale bars: 50 μm) of HT-29 and LoVo cells was detected by scratch healing assay after treatment with different concentrations of cordycepin (control, 20 μM, 40 μM and 80 μM). **D.** Cell invasion (scale bars: 50 μm) of HT-29 and LoVo cells was detected by Transwell assay after treatment with different concentrations of cordycepin (control, 20 μM, 40 μM and 80 μM). **E.** Cell apoptosis of HT-29 and LoVo cells was detected by flow cytometry after treatment with different concentrations of cordycepin (control, 20 μM, 40 μM and 80 μM). All experiments were repeated at least 3 times and were performed in triplicates, and data were presented as mean ± SD. *; P<0.05, **; P<0.01, and ***; P<0.001.

Effects of cordycepin and GSK-3β inhibitor (CHIR99021) on GSK3β protein expression

To investigate the mechanism by which cordycepin suppresses the malignancy of colon cancer cells, Western blot was used to detect the expressions of GSK3β protein in colon cancer cells. Cordycepin treatment was found to promote GSK3β protein expression in HT-29 and LoVo cells in a dose-

dependent manner (P<0.001, Fig.2A). After the co-treatment with CHIR99021, the promoting effect of cordycpin on GSK-3β protein expression was reversed (P<0.001, Fig.2B).

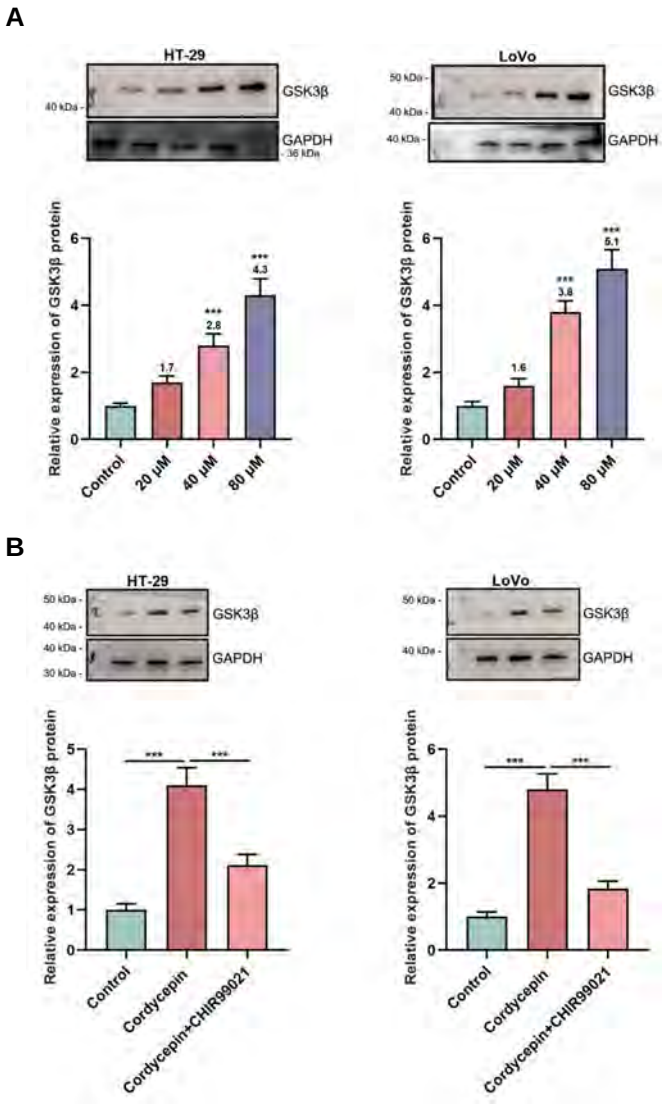

Fig.2: Effects of cordycepin and CHIR99021 on GSK3β expression**. A.** GSK3β protein expression in HT-29 and LoVo cells was detected by Western blot after treatment with different concentrations of cordycepin (control, 20 μM, 40 μM and 80 μM). **B.** GSK3β protein expression in HT-29 and LoVo cells was detected by Western blot after co-treatment with 80 μM cordycepin and 10 μM CHIR99021. All experiments were repeated at least 3 times and were performed in triplicates, and data were presented as mean ± SD. ***; P<0.001.

Effects of cordycepin and CHIR99021 on the biological behaviors of colon cancer cells

To investigate that whether the tumor-suppressive effects of cordycepin on colon cancer cells are dependent on GSK3β, after the HT-29 and LoVo cells were treated with cordycepin and CHIR99021, MTT assay, scratch healing assay, Transwell assay and flow cytometry were used to detect the viability, migration, invasion and apoptosis of the colon cells, repectively. It was found that, cordycepin treatment inhibited the viability, migration and invasion, and promoted apoptosis of HT-29 and LoVo cells; remarkably, co-treatment with CHIR99021 reversed the above effects of cordycepin (P<0.001, Fig.3A-D).

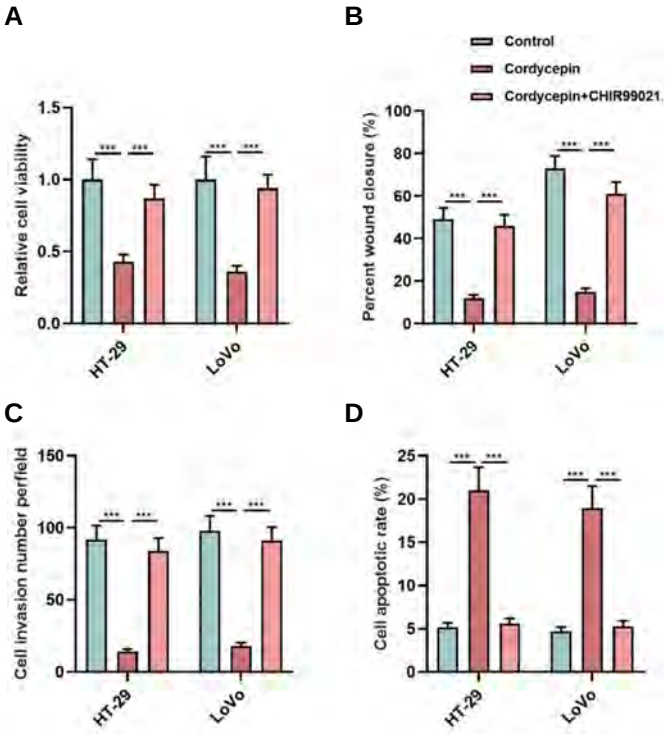

Fig.3: Effects of cordycepin and CHIR99021 on the viability, migration and apoptosis of colon cancer cells. **A.** Viability of HT-29 and LoVo cells was detected by MTT assay after treatment with 80 μM cordycepin and 10 μM CHIR99021 for 24 hours. **B.** Migration of HT-29 and LoVo cells was detected by scratch healing assay after treatment with 80 μM cordycepin and 10 μM CHIR99021 for 24 hours. **C.** Invasion of HT-29 and LoVo cells was detected by Transwell assay after treatment with 80 μM cordycepin and 10 μM CHIR99021 for 24 hours. **D.** Apoptosis of HT-29 and LoVo cells was detected by flow cytometry after treatment with 80 μM cordycepin and 10 μM CHIR99021 for 24 hours. All experiments were repeated at least 3 times and were performed in triplicates, and data were presented as mean ± SD. ***; P<0.001.

Effects of cordycepin and CHIR99021 on cyclin D1 and β-catenin protein expressions

Next, we investigated the regulatory effects of cordycepin and GSK3β on cyclin D1 and β-catenin, the expression levels of cyclin D1 and β-catenin proteins were detected by Western blot. The results showed that the expression levels of cyclin D1 and β-catenin protein were reduced upon cordycepin treatment; however, co-treatment with CHIR99021 inhibited the effects of cordycepin on cyclin D1 and β-catenin protein expression (P<0.001, Fig.4A, B). These data suggested that cordycepin could regulate the expression level of cyclin D1 and β-catenin in colon cancer cells via activating GSK3β.

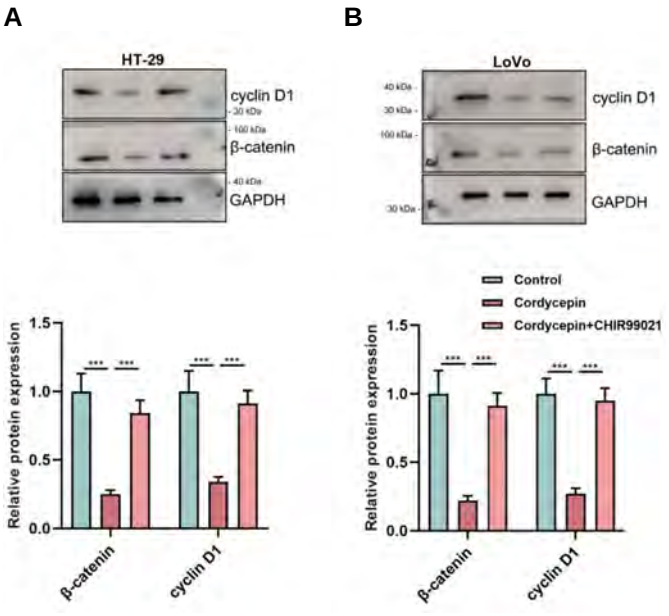

Fig.4: Effects of cordycepin and CHIR99021 on cyclin D1 and β-catenin protein expressions. **A, B.** Cyclin D1 and β-catenin protein expressions of HT-29 and LoVo cells were detected by Western blot after co-treatment with 80 μM cordycepin and 10 μM CHIR99021. All experiments were repeated at least 3 times and were performed in triplicates, and data were presented as mean ± SD. ***; P<0.001.

Discussion

Colon cancer patients with distant metastasis or recurrence after surgery have poor prognosis (20). In recent years, several studies have implied that cordycepin can induce apoptosis of cancer cells and promote DNA damage to inhibit the proliferation and metastasis of cancer cells, and it may also increase the chemosensitivity of cancer cells (21, 22). For example, cordycepin inhibits the proliferation of tongue cancer cells in a dose-dependent manner (23). Cordycepin can down-regulate the expression of C-X-C chemokine receptor type 4 in hepatocellular carcinoma cells in a dose-dependent manner, significantly inhibiting the migration and invasion of hepatocellular carcinoma cells (24). Another study shows that cordycepin can regulate the expressions of cyclin-dependent kinase 1 and cyclin B1, leading to cell cycle arrest of esophageal cancer cells (25). In addition, multiple previous studies report that cordycepin has the potential to block the progression of colon cancer (26-28). Specifically, cordycepin can inhibit the migration and invasion of HCT116 cells by regulating the expression of Prostaglandin E2 receptor 4 and the transduction of AMPK-CREB signaling pathway (27). Additionally, cordycepin can induce the activation of JNK1, leading to cell cycle arrest of HCT116 cells (28). Consistently, in the present study, cordycepin was found to significantly inhibit the proliferation, migration and invasion of colon cancer cells and promote their apoptosis.

GSK3β is a serine/threonine kinase partaking in modulating cell proliferation, DNA repair, cell cycle progression, signal transduction and metabolic pathways (29). Importantly, the dysfunction/dysregulation of GSK-3β is involved in tumorigenesis, and it may exert cancer-promoting function or tumor-suppressive function in different cancers (30-32). GSK3β promotes epithelial-mesenchymal transition (EMT) of triple-negative breast cancer cells, and GSK3β inhibitors selectively kill cancer cells with mesenchymal properties and are considered as potential therapeutic targets for triple-negative breast cancer (30). Resveratrol can inhibit the EMT of colon cancer through the AKT/GSK-3β/Snail signaling pathway (31). The occurrence, progression and drug resistance of pancreatic ductal carcinoma are thought to be related to the expression of GSK3β, and the inhibition of GSK3β induces apoptosis and slows the growth of tumors and metastases (32). β-catenin is a crucial component in Wnt signaling pathway; the abnormal activation of the Wnt/β-catenin signaling pathway facilitates the accumulation of β-catenin in the nucleus and the transcription of many oncogenes such as c-Myc and Cyclin D1, thereby contributing to the occurrence and development of a variety of cancers including colon cancer (33, 34). Importantly, GSK3β can phosphorylate β-catenin, leading to the ubiquitination and proteasomal-dependent degradation of β-catenin (15, 35). The dysregulation of the GSK3β/β-catenin pathway is involved in the regulation of the malignant biological behaviors of cancer cells (36-38). For instance, upregulated gene 4 can promote the proliferation of osteosarcoma cells through the GSK3β/β-catenin/cyclin D1 pathway (37). PIK3CD induces malignant phenotypes of colorectal cancer by activating AKT/GSK-3β/β-catenin signaling (38). Herein, we found that cordycepin could increase GSK3β expression and inhibit the expression levels of β-catenin and cyclin D1, which partly explains the mechanism of cordycepin's tumor-suppressive effects in colon cancer.

Conclusion

This study not only confirms the tumor-suppressive role of cordycepin in colon cancer, but also reports that the biological function of cordycepin on colon cancer cells is mediated by GSK3β/β-catenin/cyclin D1 pathway. It's worth noting that, even though cordycepin/*Cordyceps militaris* is widely used in traditional Chinese medicine, clinical trials are still needed to further validate its safety and efficacy in treating colon cancer.

Acknowledgments

This research was supported by Hangzhou Health and Family Planning Science and Technology Project (B20210003). We thank all those who provided any type of assistance in conducting this study. The authors declare that they have no competing interests. We also thank Hubei Yican Health Industry Co., Ltd. for its linguistic assistance during the preparation of this manuscript. The data used to support the findings of this study are available from the corresponding author upon request.

Authors' Contributions

Y.Z.; Conceived and designed the experiments. Y.Z.,

J.X., X.S., D.S.; Performed the experiments. Y.Z., J.X.; Analyzed the data. J.X.; Wrote the manuscript. All authors read and approved the final manuscript.

References

1. Zhang Q, Li S, Bai L, Yu D, Li H, Tong R. Self-delivery janus-prodrug for precise immuno-chemotherapy of colitis-associated colorectal cancer. ACS Appl Mater Interfaces. 2022; 14(1): 297-306.
2. Chen Y, Zhang F, Du Z, Xie J, Xia L, Hou X, et al. Proteome analysis of chi revealed its role in colon cancer through the apoptosis and ferroptosis pathway. Front Oncol. 2021; 11: 727130.
3. Wen J, Min X, Shen M, Hua Q, Han Y, Zhao L, et al. ACLY facilitates colon cancer cell metastasis by CTNNB1. J Exp Clin Cancer Res. 2019; 38(1): 401.
4. Adnan M, Siddiqui AJ, Hamadou WS, Patel M, Ashraf SA, Jamal A, et al. Phytochemistry, bioactivities, pharmacokinetics and toxicity prediction of with its anticancer potential against human lung, breast and colorectal carcinoma cell lines. Molecules. 2021; 26(3): 768.
5. Reddy MN, Adnan M, Alreshidi MM, Saeed M, Patel M. Evaluation of anticancer, antibacterial and antioxidant properties of a medicinally treasured fern tectaria coadunata with its Phytoconstituents analysis by HR-LCMS. Anticancer Agents Med Chem. 2020; 20(15): 1845-1856.
6. Adnan M, Siddiqui AJ, Arshad J, Hamadou WS, Awadelkareem AM, Sachidanandan M, et al. Evidence-based medicinal potential and possible role of Selaginella in the prevention of modern chronic diseases: ethnopharmacological and ethnobotanical perspective. Rec Nat Prod. 2021; 15(5): 355.
7. Jang HJ, Yang KE, Hwang IH, Huh YH, Kim DJ, Yoo HS, et al. Cordycepin inhibits human ovarian cancer by inducing autophagy and apoptosis through Dickkopf-related protein 1/β-catenin signaling. Am J Transl Res. 2019; 11(11): 6890-6906.
8. Khan MA, Tania M. Cordycepin in anticancer research: Molecular mechanism of therapeutic effects. Curr Med Chem. 2020; 27(6): 983-996.
9. Tan L, Song X, Ren Y, Wang M, Guo C, Guo D, et al. Anti-inflammatory effects of cordycepin: a review. Phytother Res. 2020.
10. Ashraf SA, Elkhalifa AEO, Siddiqui AJ, Patel M, Awadelkareem AM, Snoussi M, et al. Cordycepin for health and wellbeing: A potent bioactive metabolite of an entomopathogenic medicinal fungus and its nutraceutical and therapeutic potential. Molecules. 2020; 25(12): 2735.
11. Li SZ, Ren JW, Fei J, Zhang XD, Du RL. Cordycepin induces Bax-dependent apoptosis in colorectal cancer cells. Mol Med Rep. 2019; 19(2): 901-908.
12. Patel M, Sachidanandan M, Adnan M. Serine arginine protein kinase 1 (SRPK1): A moonlighting protein with theranostic ability in cancer prevention. Mol Biol Rep. 2019; 46(1): 1487-1497.
13. Han X, Zhang G, Chen G, Wu Y, Xu T, Xu H, et al. Buyang huanwu decoction promotes angiogenesis in myocardial infarction through suppression of PTEN and activation of the PI3K/Akt signalling pathway. J Ethnopharmacol. 2022; 287: 114929.
14. Yang MH, Ha IJ, Lee SG, Lee J, Um JY, Ahn KS. Ginkgolide C promotes apoptosis and abrogates metastasis of colorectal carcinoma cells by targeting Wnt/β-catenin signaling pathway. IUBMB Life. 2021; 73(10): 1222-1234.
15. Ren Y, Zhu F, Liu Z. Inhibitory effect of icariin on osteosarcoma cell proliferation via the Wnt/β-catenin signaling pathway. Oncol Lett. 2018; 16(2): 1405-1410.
16. Rappaport JA, Entezari AA, Caspi A, Caksa S, Jhaveri AV, Stanek TJ, et al. A β-catenin-TCF-sensitive locus control region mediates GUCY2C ligand loss in colorectal cancer. Cell Mol Gastroenterol Hepatol. 2022; 13(4): 1276-1296.
17. Shtutman M, Zhurinsky J, Simcha I, Albanese C, D'Amico M, Pestell R, et al. The cyclin D1 gene is a target of the beta-catenin/LEF-1 pathway. Proc Natl Acad Sci USA. 1999; 96(10): 5522-5527.
18. Bhatt M, Patel M, Adnan M, Reddy MN. Anti-metastatic effects of lupeol via the inhibition of MAPK/ERK pathway in lung cancer. Anticancer Agents Med Chem. 2021; 21(2): 201-206.
19. Adnan M, Siddiqui AJ, Hamadou WS, Snoussi M, Badraoui R, Ashraf SA, et al. Deciphering the molecular mechanism responsible for efficiently inhibiting metastasis of human non-small cell lung and colorectal cancer cells targeting the matrix metalloproteinases by Selaginella repanda. Plants (Basel). 2021; 10(5): 979.
20. Nguyen JQ, Irby RB. TRIM21 is a novel regulator of Par-4 in colon and pancreatic cancer cells. Cancer Biol Ther. 2017; 18(1): 16-25.
21. Yoon SY, Park SJ, Park YJ. The anticancer properties of cordycepin and their underlying mechanisms. Int J Mol Sci. 2018; 19(10): 3027.
22. Wang CY, Tsai SW, Chien HH, Chen TY, Sheu SY, So EC, et al. Cordycepin inhibits human gestational choriocarcinoma cell growth by disrupting centrosome homeostasis. Drug Des Devel Ther. 2020; 14: 2987-3000.
23. Zheng Q, Sun J, Li W, Li S, Zhang K. Cordycepin induces apoptosis in human tongue cancer cells in vitro and has antitumor effects in vivo. Arch Oral Biol. 2020; 118: 104846.
24. Guo Z, Chen W, Dai G, Huang Y. Cordycepin suppresses the migration and invasion of human liver cancer cells by downregulating the expression of CXCR4. Int J Mol Med. 2020; 45(1): 141-50.
25. Xu JC, Zhou XP, Wang XA, Xu MD, Chen T, Chen TY, et al. Cordycepin induces apoptosis and G2/M phase arrest through the ERK pathways in esophageal cancer cells. J Cancer. 2019; 10(11): 2415-2424.
26. Lee SY, Debnath T, Kim SK, Lim BO. Anti-cancer effect and apoptosis induction of cordycepin through DR3 pathway in the human colon cancer cell HT-29. Food Chem Toxicol. 2013; 60: 439-447.
27. Jeong JW, Park C, Cha HJ, Hong SH, Park SH, Kim GY, et al. Cordycepin inhibits lipopolysaccharide-induced cell migration and invasion in human colorectal carcinoma HCT-116 cells through down-regulation of prostaglandin E2 receptor EP4. BMB Rep. 2018; 51(10): 532-537.
28. Lee SJ, Moon GS, Jung KH, Kim WJ, Moon S-K. c-Jun N-terminal kinase 1 is required for cordycepin-mediated induction of G2/M cell-cycle arrest via p21WAF1 expression in human colon cancer cells. Food Chem Toxicol. 2010; 48(1): 277-283.
29. Lin J, Song T, Li C, Mao W. GSK-3β in DNA repair, apoptosis, and resistance of chemotherapy, radiotherapy of cancer. Biochim Biophys Acta Mol Cell Res. 2020; 1867(5): 118659.
30. Vijay GV, Zhao N, Den Hollander P, Toneff MJ, Joseph R, Pietila M, et al. GSK3β regulates epithelial-mesenchymal transition and cancer stem cell properties in triple-negative breast cancer. Breast Cancer Res. 2019; 21(1): 37.
31. Yuan L, Zhou M, Huang D, Wasan HS, Zhang K, Sun L, et al. Resveratrol inhibits the invasion and metastasis of colon cancer through reversal of epithelial- mesenchymal transition via the AKT/GSK-3β/Snail signaling pathway. Mol Med Rep. 2019; 20(3): 2783-2795.
32. Edderkaoui M, Chheda C, Soufi B, Zayou F, Hu RW, Ramanujan VK, et al. An inhibitor of GSK3B and HDACs kills pancreatic cancer cells and slows pancreatic tumor growth and metastasis in mice. Gastroenterology. 2018; 155(6): 1985-1998.
33. Yang M, Zhong WW, Srivastava N, Slavin A, Yang J, Hoey T, et al. G protein-coupled lysophosphatidic acid receptors stimulate proliferation of colon cancer cells through the {beta}-catenin pathway. Proc Natl Acad Sci USA. 2005; 102(17): 6027-6032.
34. Zhao Y, Li B, Wang G, Ge S, Lan X, Xu G, et al. Dendrobium officinale polysaccharides inhibit 1-Methyl-2-Nitro-1-Nitrosoguanidine induced precancerous lesions of gastric cancer in rats through regulating Wnt/β-Catenin pathway and altering serum endogenous metabolites. Molecules. 2019; 24(14): 2660.
35. Zheng Q, Yao D, Cai Y, Zhou T. NLRP3 augmented resistance to gemcitabine in triple-negative breast cancer cells via EMT/IL-1β/Wnt/β-catenin signaling pathway. Biosci Rep. 2020; 40(7): BSR20200730.
36. Dai J, Wei R, Zhang P, Kong B. Overexpression of microRNA-195-5p reduces cisplatin resistance and angiogenesis in ovarian cancer by inhibiting the PSAT1-dependent GSK3β/β-catenin signaling pathway. J Transl Med. 2019; 17(1): 190.
37. Liu Y, Xi Y, Chen G, Wu X, He M. URG4 mediates cell proliferation and cell cycle in osteosarcoma via GSK3β/β-catenin/cyclin D1 signaling pathway. J Orthop Surg Res. 2020; 15(1): 226.
38. Chen JS, Huang JQ, Luo B, Dong SH, Wang RC, Jiang ZK, et al. PIK3CD induces cell growth and invasion by activating AKT/GSK-3β/β-catenin signaling in colorectal cancer. Cancer Sci. 2019; 110(3): 997-1011.

Original Article

Ex vivo Optimization of Glucose-Regulated Protein 94/Glycoprotein 96 Expressions in Mammospheres; Implication for Breast Cancer Immunotherapy

Amirhossein Izadpanah, D.V.M.[1, 2], Nowruz Delirezh, Ph.D.[1]*, Rahim Mahmodlou, M.D.[3]

1. Department of Microbiology, Faculty of Veterinary Medicine, Urmia University, Urmia, Iran
2. Department of Stem cells and Developmental Biology, Cell Science Research Center, Royan Institute for Stem Cell Biology and Technology, Tehran, Iran
3. Department of Surgery, Emam Khomeini General Hospital, Urmia, Iran

Corresponding Address: P.O.Box: 165, Department of Microbiology, Faculty of Veterinary Medicine, Urmia University, Urmia, Iran
Email: n.delirezh@urmia.ac.ir

Received: 21/December/2020, Accepted: 22/June/2021

Abstract

Objective: The induction of immunity against cancer stem cells (CSCs) can boost the efficiency of cancer vaccines. Heat shock proteins (HSPs) are required for the successful activation of anti-tumor immune responses. Glycoprotein 96 (gp96) is a well-known HSP that promotes the cross-presentation of tumor antigens. The aim of the present study was to optimize the temperature for induction of gp96 in grade 3 breast cancer spheres.

Materials and Methods: In the experimental study, CSCs were enriched from breast tumor tissue samples and cultured in DMEM-F12 with epidermal growth factor (EGF), basic fibroblast growth factor (bFGF), B27, and bovine serum albumin (BSA) for 22 days. The expression level of CD24 and CD44 as CSC markers was measured by flow cytometry in secondary mammospheres, and the expression of *NANOG*, *SOX2*, and *OCT4* genes in CSCs was also analyzed using the real-time polymerase chain reaction (PCR). To find the optimal temperature regulation of gp96, the mammosphere was incubated at different temperatures for 1 hour, and gp96 expression was measured using the western blotting assay.

Results: Primary mammospheres were obtained after seven days of culture, and secondary spheres formed 22 days after passage. Flow cytometry analysis showed that cells with $CD24^{-}$ $CD44^{+}$ phenotype were enriched in the culture period (from 2.6% on day 1 to 32.6% on day 22). Real-time PCR indicated that *OCT4*, *NANOG*, and *SOX2* expression in mammospheres were increased by 3.8 ± 0.6, 17.8 ± 0.6, and 7.7 ± 0.8 fold respectively in comparison to the MCF-7 cell line. Western blot analysis showed that gp96 production was significantly upregulated when mammospheres were incubated at both 42°C and 43°C in comparison to the control group.

Conclusion: Altogether, we found that heat-induced upregulated expression of gp96 in CSCs enriched mammospheres from breast tumor tissue might be used as a complementary procedure to generate more immunogenic antigens in immunotherapy settings.

***Keywords*:** Breast Cancer, Cancer Stem Cells, Cellular Spheroid, Heat Shock Proteins

Cell Journal(Yakhteh), Vol 24, No 5, May 2022, Pages: 261-266

Citation: **Izadpanah A, Delirezh N, Mahmodlou R. Ex vivo optimization of glucose-regulated protein 94/glycoprotein 96 expressions in mammospheres; implication for breast cancer immunotherapy. Cell J. 2022; 24(5): 261-266. doi: 10.22074/cellj.2022.7908.**

Introduction

Four decades ago, the cancer stem cell (CSC) concept was proposed. It was stated that tumor growth, like the renewal of healthy tissues, is fueled by small numbers of so-called stem cells. It has gradually become clear that many tumors harbor CSCs in dedicated niches, and their identification has not been as obvious as was initially hoped. Recently developed lineage tracing has provided insights into CSC therapeutic response.

Breast cancer is the most common female neoplastic malignancy and the most important cause of female mortality in the world (1). Although this malignancy's highest incidence is in developed countries, studies showed that its incidence in developing countries has an increasing trend, and patients have a shorter life expectancy (2). Most of the deaths associated with breast cancer are due to metastasis and multiple drug resistance (3). Studies on the tumor microenvironment have revealed a rare cancer cell population with stemness features that seems to be the leading cause of the malignancy. This population is called CSCs, and they have the ability to self-renewal and differentiation into other progenies of cancer cells (4).

CSCs first were detected in acute myeloid leukemia (5), however, their footprint was discovered in all types of cancers later (6-9). They are assumed to be responsible for a tumor's main malignant characteristics, including invasion, metastasis, drug resistance, and relapse. Although CSCs can be distinguished by surface markers (e.g. CD24) and expression of stemness genes (e.g. OCT4, NANOG, SOX2), efforts to derivate a pure cell line of CSCs from tumor specimens have failed till now (10). Nevertheless, it has been proved that the culture of tumor cells in non-adherent vessels

would form spheroids, which are CSCs enriched, so, currently, tumor-derived spheres would prepare the most available models for CSCs examinations (11).

Heat shock proteins (HSPs) are necessary molecular chaperones that play an essential role in cells. They also play a crucial role in immunizing against tumors by interfering with the function of professional antigen-presenting cells (APCs), T lymphocytes, and NK cells (12-16). Hsp90B1 (gp96) is a type of HSP that plays a vital role in directing and delivering antigens through MHC class 1 and inducing $CD8^+$ T cells response. This role of HSPs has been used as a basis for clinical trials to develop anticancer vaccines (17, 18).

Despite the efforts that have been made to develop the cancer vaccines, reaching therapeutic success still is still far-fetched. In recent years, immunotherapy methods have hopefully increased the survival of patients (19). To improve the efficacy of these new treatments, boosting the immune response against cancer cells, specifically CSCs, is of the utmost importance. Therefore, upregulating the expression of HSPs in CSCs seems to increase the immunogenicity of these cells, and HSP-upregulated CSCs would be a better tumor antigen source for immunization and cancer vaccine production. In this study, we tried to set up an optimized protocol for the derivation of CSCs-enriched spheres from tumor tissue of breast cancer (which is called mammospheres) and upregulation of glycoprotein 96 (gp96) in these cells.

Materials and Methods

In the experimental study, the optimal temperature for induction of gp96 in grade 3 breast cancer spheres was investigated using mammosphere generation, immunohistochemistry, flow cytometry, real-time reverse transcription polymerase chain reaction (RT-PCR), and western blot techniques.

Preparing tumor sample and generation of mammospheres

Several biopsy samples of tumor tissue were obtained from a female patient with breast cancer during mastectomy and stored in sterile containers containing DMEM/F12 medium (Gibco, USA) with streptomycin-penicillin antibiotics (Sigma, USA), then delivered to the lab. Written consent was obtained from three patients before the surgery for using their tissue samples in the research. Approval of the ethics committee of Urmia University of Medical Sciences was obtained in advance (P6/97/4/25493). At least three tumor samples were applied to successfully generate mammospheres and the gp94 induction process as described below.

Breast tumor tissues were first minced mechanically by a scalpel and then digested enzymatically using collagenase type IV for 18 hours. Cells obtained from the digested tissue were cultured in 24-well plates (Biofil, China) coated with a thin layer of 1.5% agarose solution, in a low glucose DMEM (Dulbecco's Modified Eagle Medium) medium supplemented with epidermal growth factor (EGF, 20 ng/ml), basic fibroblast growth factor (bFGF, 20 ng/ml), B27 (2%), bovine serum albumin (BSA, 0.5 mg/ml) and penicillin-streptomycin at 37ºC and 5% CO_2 (20). The culture medium was refreshed every two days, and primary spheres were harvested on day 7, single cells of each sphere were then transferred into new 24-well plates to form secondary spheres which were then used to perform relevant tests on day 22.

Immunohistochemistry

For immunohistochemical (IHC) analysis tissue sections were cut at 6 µm thickness, mounted on slides, and antigen retrieval was performed. Endogenous peroxidase activity was blocked by immersing the slides in 1.0% H_2O_2, and 0.1% NaN3 in tris-buffered saline (TBS, Sigma, Germany) for 10 minutes. Nonspecific antibody binding was inhibited by incubating the sections in 4% commercial nonfat skim milk powder (Sigma, Germany) in TBS for 15 minutes; the slides were transferred to a humidified chamber and incubated with primary anti ER (2.5 µg/ml), PR (2.5 µg/ml) and Herr-2/neu (5 µg/ml) antibodies (Abcam, UK) overnight at room temperature. The sections were washed by TBS and incubated with biotinylated goat anti-mouse immunoglobulins (Abcam, UK) for 45 minutes and then with streptavidin-horseradish peroxidase conjugate (Abcam, UK) for 15 minutes. Antigenic sites were identified using 0.05% 3,3-diaminobenzidine with H_2O_2 (Sigma, Germany) as substrate and were then lightly counterstained with hematoxylin before being examined with light microscopy (21).

Flow cytometry

To confirm CSCs enrichment in mammospheres, the flow cytometry technique was used to determine the percentage of CSCs population in trypsinized secondary mammospheres on the 22^{nd} day of culture. For this assessment, $CD44^+CD24^-$ cells were considered as CSCs, and the percentage of this population was compared with single cells isolated from digested tumor tissue on the first day of culture.

Real-time reverse transcription polymerase chain reaction

Real-time RT-PCR was carried out according to the method described by Park et al. (22). Briefly, single cells of trypsinized secondary mammospheres were used for total RNA extraction by a commercially available kit (Qiagen, Valencia, CA, USA). Real-time RT-PCR was then performed on the synthesized cDNA to evaluate the expression level of stemness genes including *OCT4*, *NANOG*, and *SOX2*, resultant cDNA amplified by Taq DNA polymerase (Invitrogen, Germany) in a Rotor-gene 3000 thermal cycler device (Corbett, Australia). The Syber Green probe (Qiagen, Germany) was used for the detection of DNA amplification signals. The expression level of each gene was normalized to the *GAPDH* expression as a housekeeping gene, and breast cancer cell line (MCF7) as a control to calculate the relative expression ($2^{-\Delta\Delta Ct}$) of stemness genes.

Western blot

To induce upregulation of gp96 expression, mammospheres were incubated for 60 minutes at 42ºC and 43ºC in experimental groups and at 37ºC in the control group; these spheres were then trypsinized, and single cells were used for Western blot analysis. Cells were lysed with lysing buffer (50 mM Tris-HCl, pH=7.5, 150 mM NaCl, 0.5% sodium deoxycholate, 1% NP-40) supplemented with complete protease inhibitors (Roche Applied Science, Mannheim, Germany). Cell lysates (20 mg) were separated by electrophoresis on 10% sodium dodecyl-sulfate (SDS)-polyacrylamide gel and transferred to a nitrocellulose membrane. The blot was blocked with TBST (20 mM Tris-HCl, pH=7.6, 136 mM NaCl, and 0.1% Tween-20) containing 5% skim milk and then incubated with primary antibody against gp96 (2 µg, ml) and Actin (as a housekeeping protein, Santa Cruz, USA) at 4ºC overnight. The next day, after washing with TBST, the membrane was incubated with HRP-conjugated secondary antibody for 1 hour at room temperature. The bands were amplified using a chemiluminescent solution and photographed with the ECL kit (GE/Amersham Healthcare, UK) and Documentation Gel (SYNGENE, UK) (23).

Statistical analysis

Data from at least three independent experiments were expressed as means ± standard deviation, SD. Each data point of real-time PCR was run at least in triplicates and independent experiments were performed at least three times. Student's t tests or ANOVA (SPSS, version 21, IBM, USA) were used to determine statistically significant differences and $P<0.05$ was considered to be statistically significant unless otherwise specified.

Results

Immunohistochemistry characteristics of the tumor sample

The histopathology report of the tumor biopsy indicated that the patients had undergone a stage IV, grade 3 invasive ductal carcinoma breast cancer (data not shown). Tumor size was 3.5×2cm and involvement of axillary lymph node was reported. IHC study showed that the tumor was triple positive for Estrogen, Progesterone, and Her2-neu receptors (Fig.1).

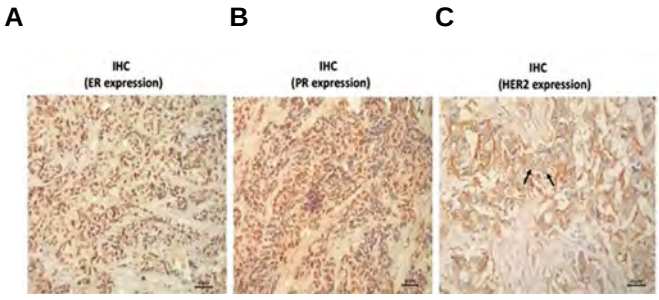

Fig.1: Immunohistochemical analysis. Tumor specimen was stained immunohistochemically using anti ER, PR and Her-2/neu monoclonal antibodies. From left to right presents the expression of ER, PR, and Her-2/neu receptors respectively (scale bar: 100 µm).

Tumor-derived mammospheres generation

The culture of tumor single cells with described protocol led to the formation of spheres after 7 days. The morphology of spheres was similar to what has been previously reported. The sphere trypsinized and passaged into subsequent plates, which led to the formation of secondary mammospheres on day 22 (Fig.2).

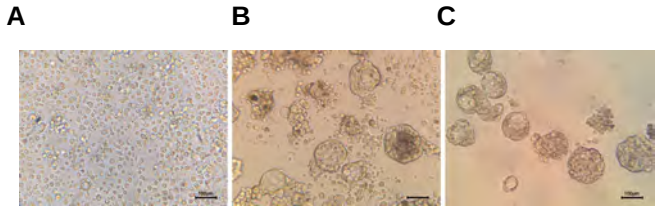

Fig.2: Mammospheres derived from tumor tissue. **A.** Cells isolated from digestion of tumor tissue samples on the first day of culture, **B.** Primary mammospheres on the 7th day of culture, and **C.** Secondary mammospheres formed from the passage of primary mammospheres on the 22nd day of culture (scale bar: 100 µm).

Flow cytometric analysis of cancer stem cells in tumor-derived spheres

To determine the percentage of CSCs among other cancer cells, the population of $CD44^{+}CD24^{-}$ cells as CSC phenotype was measured with flow cytometry. The percentage of CSCs on the first day of culture was 2.6%, whereas this population on the 22nd day of culture was 33.2% in trypsinized mammospheres (Fig.3).

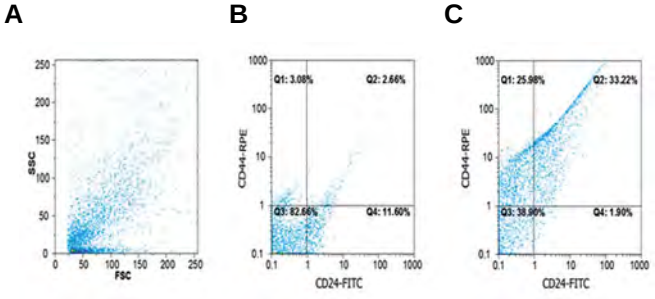

Fig.3: Phenotypic characterization of cancer stem cells (CSCs) enriched mammospheres. **A.** Flow cytometric analysis of CSCs was carried out using anti CD24 and anti CD44 monoclonal antibodies. Forward and side scatter analysis of cells are shown. **B.** Cells with $CD44^{+}CD24^{-}$ phenotype had a low percentage on the first day of culture, and **C.** But the population of these cells considerably increased in the 22nd day of culture in mammospheres.

Stemness genes expression

Relative expression of stemness genes, including *OCT-4*, *NANOG*, and *SOX2* were measured in trypsinized mammospheres in comparison with the MCF-7 breast cancer cell line as the control by real-time RT-PCR. Relative expression of these genes was significantly higher in mammospheres, which was 3.83 ± 0.62 fold for *OCT-4*, 17.83 ± 0.6 fold for *NANOG*, and 7.73 ± 0.78 fold for *SOX2* ($P\leq0.001$, Fig.4).

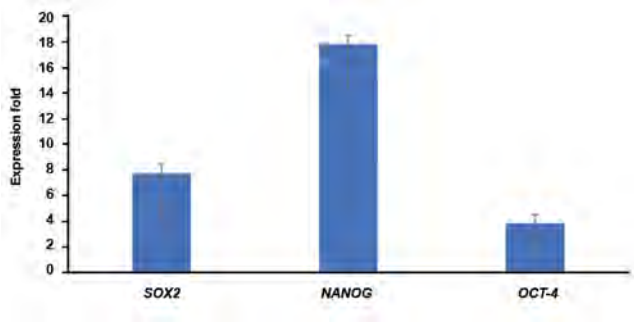

Fig.4: Stemness genes expressioin. Expression of *OCT-4*, *NANOG*, and *SOX2* was meassured in single cells of mammospheres in comparison to MCF-7 cell line. The expression level of genes in the MCF-7 cells was considered as 1 and the expression fold of them in single cells of cultured mammospheres was reported (P<0.001).

Glycoprotein 96 expression

Incubation of mammospheres for a short time (60 minutes) at 42°C and 43°C led to the upregulation of gp96 protein expression detected by Western blot. However, the viability of mammospheres did not decline after such incubation conditions. The sharpness of gp96 bands at 42°C and 43°C incubated mammospheres were significantly higher than 37°C (P≤0.001), but they have no considerable difference from each other (Fig.5).

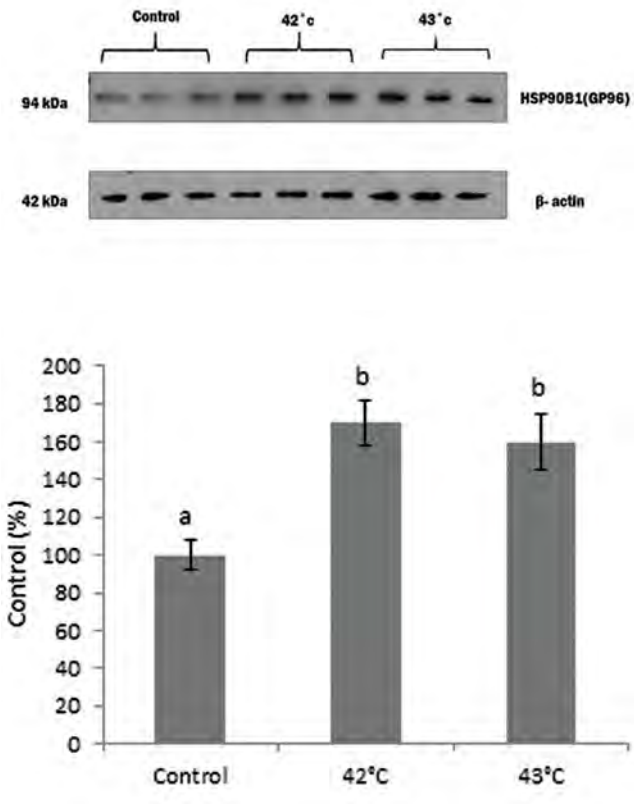

Fig.5: Expression levels of gp96 protein. Mammospheres were incubated in 42°C and 43°C as well as 37°C (control) for 1 hour and the expression of gp96 protein was measured using Western bloting test. Different letters indicate significant differences between mean values (P=0.03).

Discussion

CSCs are a group of cancerous cells within the tumor bulk with stem cell-like characteristics, including self-renewal properties, due to which the term Tumor Initiating Cells (TIC) has been used for them (11). It seems that the stemness properties of CSCs could be an explanation for cancer recurrence and chemoresistance. Among the other described characteristics for CSCs, the expression of some markers like CD44, CD133, and CD24, and on the transcription level, the expression of *SOX2*, *NANOG*, and *OCT4* is crucial (24).

One of the assays that can be applied to isolate CSCs, besides surface markers, is the Spheroid formation assay, which is based on the capability of these cells to generate multicellular three-dimensional (3D) spheres *in vitro* (25). So far, culture methods, including organotypic multicellular spheroid model, multicellular tumor spheroids, tissue-derived tumorspheres, and tumorspheres assay, have been developed (26). In this study, the tumorspheres assay was applied, which is based on dissociating tumor tissue to the suspension of single cells and culturing the obtained cellular suspension in a low adherent surface in a serum-free media which is supplemented with EGF and b-FGF growth factors to enrich CSCs. This condition can provide the establishment of spherical colonies. However, the formation of tumor structure cannot be fully mimicked by using this method (27).

In the present study, we successfully achieved mammospheres from breast tumor tissue. Our tumor-derived mammospheres were typical in morphology. We also passaged primary mammospheres to form secondary ones by trypsinization. The CSC population was enriched in mammospheres, which were 2.6% on the first day of culture compared to 33.2% on the 22nd day of culture.

SOX2 gene belongs to the family of SRY-related high mobility group (HMG) which is located on chorormose 3 and implicated in the cell development process by determining their fate and preserving stemness phenotype. It is well-known that *SOX2* takes part in different molecular mechanisms and states of diseases including cancer. It has been shown that dysregulated and increased expression of *SOX2* can impact proliferation, migration, invasion, resistance to apoptosis, and colony formation features in CSCs and tumor cells (28). *NANOG* is another master transcription factor of embryogenesis, located on chromosome 12, and engaged in conserving pluripotency and self-renewal potential in stem cells through the Insulin-like growth factor1 receptor (IGF1R) pathway. Overexpression of this transcription factor has been detected in different cancers, leading to inhibiting apoptosis and establishing chemoresistance (29). *OCT-4*, also recognized as POU5F1, belongs to the POU family of transcription factors on chromosome 6, and along with *NANOG* and *SOX2*, plays a vital role in developmental pathways and tumorigenesis. Since the enhanced expression of these genes has been linked to

poor prognosis in patients with cancer and resistance to chemotherapy (30), in the present study, we analyzed their expression levels in ex vivo generated mammospheres and found that stemness genes, including *OCT-4*, *NANOG*, and *SOX2*, overexpressed in mammospheres compared to a regular breast cancer cell line (MCF-7).

Another purpose of this study was to optimize incubation conditions for the upregulation of HSPs in mammospheres, which would lead to an increase in the immunogenicity of CSCs for immunotherapy settings. We showed that incubation of mammospheres for 60 minutes at 42-43°C upregulated GP96 protein expression (a member of the HSP90 family) without affecting the viability of mammospheres cells.

Homologous members of the HSP family are found in all parts of the cytosol, nucleus, mitochondria, endosomes, lysosomes, endoplasmic reticulum, intracellular membranes, and plasma membrane (31). Thus, HSPs isolated from tumor cells are potentially rich in tumor antigens (32). Given the role of HSP-peptide complexes in the activation and maturation of APCs, this complex may activate the polyclonal T lymphocyte response against tumor antigens. Under these conditions, even if the tumor loses some antigens under the selective pressure of the immune system, multiple T-cell clones will still be available to destroy the tumor cells (32, 33). The application of this approach makes it unnecessary to find tumor-specific antigens for each patient. Among the most critical tumor-derived HSPs facilitating the entry of antigenic peptides into MHC class I molecules are HSP70, and gp96 (17, 34, 35), however, the distribution of HSP molecules within the cell follows different prototypes. Gp96 molecules are typically present in the endoplasmic reticulum (36). Studies have shown that targeting HSPs, including HSP90, induces apoptosis in cancer cells (37), thus, it is necessary to evaluate the optimal conditions causing induction of these molecules to obtain the maximum potential of tumor antigenicity.

According to our findings, the best temperature and incubation time to induce maximal gp96 in breast cancer mammospheres were 42-43°C for 1 hour. In 1998, Madersbacher et al. (38) indicated that expression of HSP27 in LNCaP cells treated with heat shock from 43-49°C for 60min could increase in a temperature-dependent manner, though this study was performed on a cell line and expression of HSP27 was the primary purpose. Schueller et al. in 2001 showed that in hepatocellular carcinoma cell line HepG2, treating cells at 41.8°C for 60 minutes, increased the expression level of HSP70 and HSP90, which could substantially escalate the immunogenicity of the tumor, as well as the immune response to heat-shocked HepG2 cells Although the cell lines used in these two studies, were different, both of them had an epithelial origin and applying almost the same temperature resulted in rising expression levels of HSP70 and HSP90, which was consistent with the result of our study (39, 40).

This study had some limitations; first, the difficulty of preserving mammospheres for a more extended period without causing differentiation to investigate long term effects of heat treatment on the gp96 expression, Second, in this study, the samples were from the same patients of the same stage while obtaining tissue samples from patients of different stages could impact the percentage of the presence of CSCs and expression of gp96. Moreover, we did not study the influence of higher temperatures than 43°C on the structure and the expression of gp96.

Conclusion

In this study, we showed that tumor-derived mammospheres are CSCs-enriched, and the expression level of stemness genes is higher than regular breast cancer cell lines. It was also revealed that incubation of these mammospheres at a temperature between 42-43°C for 60 minutes would upregulate gp96 protein expression and make mammospheres a potent tool for preparing more immunogenic tumor antigens for use in immunotherapy modalities.

Acknowledgments

The authors thank the members of the Institute of Biotechnology of Urmia University for the discussions. In particular, they would like to thank Samira, Zand, Razieh Pak Tarmani, and Ashkan Basirnia for technical assistance and give special gratitude to Dr. Hamid Mehdizadeh for helpful comments on the manuscript. The study was funded by the Vice President of Research and Technology, Urmia University, Urmia, Iran (Grant no. 3.PD.462).The authors declare that they have no competing interests.

Authors' Contributions

N.D.; Designed this study and reviewed the manuscript. A.H.I.; Carried out laboratory management and technical procedures as well as statistical analysis. R.M.; Provided the clinical data and samples. All authors read and approved the final manuscript.

References

1. Siegel RL, Miller KD, Jemal A. Cancer statistics, 2019. CA Cancer J Clin. 2019; 69: 7-34.
2. Collaborative Group on Hormonal Factors in Breast Cancer. Type and timing of menopausal hormone therapy and breast cancer risk: individual participant meta-analysis of the worldwide epidemiological evidence. The Lancet. 2019; 394: 1159-1168.
3. Naser Al Deen N, Nassar F, Nasr R, Talhouk R. Cross-roads to drug resistance and metastasis in breast cancer: miRNAs regulatory function and biomarker capability. Adv Exp Med Biol. 2019; 1152: 335-364.
4. Sousa B, Ribeiro AS, Paredes J. Heterogeneity and plasticity of breast cancer stem cells. Adv Exp Med Biol. 2019; 1139: 83-103.
5. Bonnet D, Dick JE. Human acute myeloid leukemia is organized as a hierarchy that originates from a primitive hematopoietic cell. Nat Med. 1997; 3: 730-737.
6. Capp JP. Cancer Stem Cells: from historical roots to a new perspective. J Oncol. 2019; 2019: 5189232.
7. Al-Hajj M, Wicha MS, Benito-Hernandez A, Morrison SJ, Clarke MF. Prospective identification of tumorigenic breast cancer cells. Proc Natl Acad Sci USA. 2003; 100(7): 3983-3988.
8. Cammareri P LY, Francipane MG, Bonventre S, Todaro M, Stassi G. Isolation and culture of colon cancer stem cells. Methods Cell Biol. 2008; 86: 311-324.

9. Chen T, Yang K, Yu J, Meng W, Yuan D, Bi F, et al. Identification and expansion of cancer stem cells in tumor tissues and peripheral blood derived from gastric adenocarcinoma patients. Cell Res. 2012; 22(1): 248-258.
10. Batlle E, Clevers H. Cancer stem cells revisited. Nat Med. 2017; 23(10): 1124-1134.
11. Abbaszadegan MR, Bagheri V, Razavi MS, Momtazi AA, Sahebkar A, Gholamin M. Isolation, identification, and characterization of cancer stem cells: a review. J Cell Physiol. 2017; 232(8): 2008-2018.
12. Li R, Qian J, Zhang W, Fu W, Du J, Jiang H, et al. Human heat shock protein-specific cytotoxic T lymphocytes display potent antitumour immunity in multiple myeloma. Br J Haematol. 2014; 166(5): 690-701.
13. Shevtsov M, Pitkin E, Ischenko A, Stangl S, Khachatryan W, Galibin O, et al. Ex vivo Hsp70-activated nk cells in combination with pd-1 inhibition significantly increase overall survival in preclinical models of glioblastoma and lung cancer. Front Immunol. 2019; 10: 454.
14. Zhang Y, Zhang Y, Chen J, Liu Y, Luo W. Dendritic-tumor fusion cells derived heat shock protein70-peptide complex has enhanced immunogenicity. PLoS One. 2015; 10: e0126075.
15. Wu BX, Hong F, Zhang Y, Ansa-Addo E, Li Z. GRP94/gp96 in Cancer: Biology, Structure, Immunology, and Drug Development. Adv Cancer Res. 2016; 129: 165-90.
16. Wang Y, Sedlacek AL, Pawaria S, Xu H, Scott MJ, Binder RJ. Cutting Edge: the heat shock protein gp96 activates inflammasome-signaling platforms in APCs. J Immunol. 2018; 201(8): 2209-2214.
17. Strbo N, Garcia-Soto A, Schreiber TH, Podack ER. Secreted heat shock protein gp96-Ig: next-generation vaccines for cancer and infectious diseases. Immunol Res. 2013; 57(1-3): 311-25.
18. Wang S, Fan H, Li Y, Zheng H, Li X, Li C, et al. CD133 epitope vaccine with gp96 as adjuvant elicits an antitumor T cell response against leukemia. Sheng Wu Gong Cheng Xue Bao. 2017; 33(6): 1006-1017.
19. Sanmamed MF, Chen L. A Paradigm shift in cancer immunotherapy: from enhancement to normalization. Cell. 2018; 175(2): 313-326.
20. Dontu G, Abdallah WM, Foley JM, Jackson KW, Clarke MF, Kawamura MJ, et al. In vitro propagation and transcriptional profiling of human mammary stem/progenitor cells. Genes Dev. 2003; 17(10): 1253-1270.
21. Ruan S, Liu Y, Tang X, Yang Z, Huang J, Li X, et al. HER-2 status and its clinicopathologic significance in breast cancer in patients from southwest China: re-evaluation of correlation between results from FISH and IHC. Int J Clin Exp Pathol. 2017; 10(7): 7270-7276.
22. Park HS, Han HJ, Lee S, Kim GM, Park S, Choi YA, et al. Detection of circulating tumor cells in breast cancer patients using cytokeratin-19 real-time RT-PCR. Yonsei Med J. 2017; 58(1): 19-26.
23. Simsek BC, Turk BA, Ozen F, Tuzcu M, Kanters M. Investigation of telomerase activity and apoptosis on invasive ductal carcinoma of the breast using immunohistochemical and Western blot methods. Eur Rev Med Pharma Sci. 2015; 19(16): 3089-3099.
24. Zhao W, Li Y, and Zhang X. Stemness-related markers in cancer. Cancer Transl Med. 2017; 3(3): 87-95.
25. Amaral RLF, Miranda M, Marcato PD, Swiech K. Comparative analysis of 3D bladder tumor spheroids obtained by forced floating and hanging drop methods for drug screening. Front Physiol. 2017; 8: 605.
26. Weiswald LB, Bellet D, Dangles-Marie V. Spherical cancer models in tumor biology. Neoplasia. 2015; 17: 1-15.
27. Akbarzadeh M, Maroufi NF, Tazehkand AP, Akbarzadeh M, Bastani S, Safdari R, et al. Current approaches in identification and isolation of cancer stem cells. J Cell Physiol. 2019.
28. Novak D, Huser L, Elton JJ, Umansky V, Altevogt P, Utikal J. SOX2 in development and cancer biology. Semin Cancer Biol. 2019.
29. Gawlik-Rzemieniewska N, Bednarek I. The role of NANOG transcriptional factor in the development of malignant phenotype of cancer cells. Cancer Biol Ther. 2016; 17(1): 1-10.
30. Villodre ES, Kipper FC, Pereira MB, Lenz G. Roles of OCT4 in tumorigenesis, cancer therapy resistance and prognosis. Cancer Treat Rev. 2016; 51: 1-9.
31. De Maio A, Vazquez D. Extracellular heat shock proteins: a new location, a new function. Shock. 2013; 40(4): 239-246.
32. Kelly M, McNeel D, Fisch P, Malkovsky M. Immunological considerations underlying heat shock protein-mediated cancer vaccine strategies. Immunol Lett. 2018; 193: 1-10.
33. Yun CW, Kim HJ, Lim JH, Lee SH. Heat shock proteins: agents of cancer development and therapeutic targets in anti-cancer therapy. Cells. 2019; 9(1): 60.
34. Zeng Y, Graner MW, Katsanis E. Chaperone-rich cell lysates, immune activation and tumor vaccination. Cancer Immunol Immunother. 2006; 55: 329-338.
35. Binder RJ, Srivastava PK. Peptides chaperoned by heat-shock proteins are a necessary and sufficient source of antigen in the cross-priming of CD8+ T cells. Nat Immunol. 2005; 6: 593-599.
36. Ansa-Addo EA, Thaxton J, Hong F, Wu BX, Zhang Y, Fugle CW, et al. Clients and oncogenic roles of molecular chaperone gp96/grp94. Curr Top Med Chem. 2016; 16(25): 2765-2778.
37. Hoter A, El-Sabban ME, Naim HY. The HSP90 family: structure, regulation, function, and implications in health and disease. Int J Mol Sci. 2018; 19(9): 2560.
38. Madersbacher S, Groble M, Kramer G, Dirnhofer S, Steiner GE, Marberger M. Regulation of heat shock protein 27 expression of prostatic cells in response to heat treatment. Prostate. 1998; 37(3): 174-181.
39. Schueller G PP, Friedl J, Stift A, Dubsky P, Bachleitner-Hofmann T, Jakesz R, et al. Heat treatment of hepatocellular carcinoma cells: increased levels of heat shock proteins 70 and 90 correlate with cellular necrosis. Anticancer Res. 2001; 21(1A): 295-300.
40. Zaimoku R, Miyashita T, Tajima H, Takamura H, Harashima AI, Munesue S, et al. Monitoring of heat shock response and phenotypic changes in hepatocellular carcinoma after heat treatment. Anticancer Res. 2019; 39(10): 5393-5401.

Original Article

Quality Comparison of Decellularized Omentum Prepared by Different Protocols for Tissue Engineering Applications

Khatereh Fazelian-Dehkordi, Ph.D.[1], Sayed Fakhroddin Mesbah Ardekani, Ph.D.[1], Tahereh Talaei-Khozani, Ph.D.[2, 3*]

1. Department of Anatomical Sciences, Shiraz University of Medical Sciences, Shiraz, Iran
2. Histomorphometry and Stereology Research Center, Shiraz University of Medical Sciences, Shiraz, Iran
3. Tissue Engineering Lab, Anatomy Department, Shiraz University of Medical Sciences, Shiraz, Iran

Corresponding Address: P.O.Box: 7134845794, Histomorphometry and Stereology Research Center, Shiraz University of Medical Sciences, Shiraz, Iran
Email: talaeit@sums.ac.ir

Received: 07/February/2021, Accepted: 18/July/2021

Abstract

Objective: Decellularized greater omentum (GOM) is a good extracellular matrix (ECM) source for regenerative medicine applications. The aim of the current study was to compare the efficiency of three protocols for sheep GOM decellularization based on sufficient DNA depletion and ECM content retention for tissue engineering application.

Materials and Methods: In this experimental study, in the first protocol, low concentrations of sodium dodecyl sulfate (SDS 1%), hexane, acetone, ethylenediaminetetraacetic acid (EDTA), and ethanol were used. In the second one, a high concentration of SDS (4%) and ethanol, and in the last one sodium lauryl ether sulfate (SLES 1%) were used to decellularize the GOM. To evaluate the quality of scaffold prepared with various protocols, histochemical staining, DNA, and glycosaminoglycan (GAGs) quantification, scanning electron microscopy (SEM), Raman confocal microscopy, Bradford assay, and ELISA were performed.

Results: A comparison of DNA content showed that SDS-based protocols omitted DNA more efficiently than the SLES-based protocol. Histochemical staining showed that all protocols preserved the neutral carbohydrates, collagen, and elastic fibers; however, the SLES-based protocol removed the lipid droplets better than the SDS-based protocols. Although SEM images showed that all protocols preserved the ECM architecture, Raman microscopy, GAGs quantification, total protein, and vascular endothelial growth factor (VEGF) assessments revealed that SDS 1% preserved ECM more efficiently than the others.

Conclusion: The SDS 1% can be considered a superior protocol for decellularizing GOM in tissue engineering applications.

***Keywords**:* Decellularization, Extracellular Matrix, Greater Omentum, Scaffold, Tissue Engineering

Cell Journal(Yakhteh), Vol 24, No 5, May 2022, Pages: 267-276

Citation: **Fazelian-Dehkordi Kh, Mesbah Ardekani SF, Talaei-Khozani T. Quality comparison of decellularized omentum prepared by different protocols for tissue engineering applications. Cell J. 2022; 24(5): 267-276. doi: 10.22074/cellj.2022.7968.**

Introduction

Native autologous greater omentum (GOM) has been used as a flap in reconstructive surgery in many organs such as the esophagus, trachea, duodenum small intestine, and bladder. Native GOM has rich vascularity, high angiogenic activity, innate immune function, the capability to adhere to the surrounding structures, and high production sufficiency of growth factors (1). Omentum induces neovascularization; is involved in hemostasis, tissue healing, and regeneration; and acts as an *in vivo* incubator for culturing the cells and tissues (2). These properties make it a boon for regenerative medicine applications (3). As the GOM is used in many surgical reconstructions, transplantation of decellularized GOM decreases the chance of graft rejection (4).

Decellularized GOM has several applications in regenerative medicine. Autologous decellularized omentum provided appropriate structural and mechanical supports for the cardiac cells to generate contraction *in vitro* (5). Porcine decellularized GOM has been reported to support *in vitro* cell adhesion and growth (3). The metabolic rescue has been previously reported for human diabetic adipose-derived mesenchymal stem cells after culturing on decellularized GOM. The report indicates that the extracellular matrix (ECM) of the omentum has specific components with the capability to regulate cell functions. ECM of the omentum regulates adipocyte differentiation, glucose uptake, and lipolysis (6). Being decellularized with well-preserved architecture, including vessel framework, makes it a better choice for reconstructive surgery or tissue engineering. Due to the collagen and glycosaminoglycan (GAGs) content (3), decellularized tissues such as GOM can be gelatinized and form hydrogel for cell encapsulation (7). Recently, GOM-based 3D decellularized matrix has been used to fabricate the engineered cardiac tissue (8). Decellularized GOM has been used to prepare a hydrogel for cardiac cell encapsulation (5). Also, decellularized omentum was used as a platform for culturing the cells isolated from the human kidney,

urothelial cells, and endothelial cells (9).

The ECM, as an essential part of each tissue, has many bioactive macromolecules such as glycoproteins, GAGs, various growth factors, and cytokines. Natural scaffolds from decellularized tissues provide a biomimicry framework to protect cell adhesion, proliferation, migration, and functions; some of these decellularized scaffolds have been successfully transplanted in both animal models (10) and human clinical trials (11).

The target of the decellularization methods is to diminish any detrimental impact of decellularizing agents on the constitution and biological activity of the residual ECM along with cellular and nuclear material depletion. In the most common decellularization protocols, a combination of chemical, enzymatic, and physical approaches is used (11). These protocols are usually started with the cell membrane disruption using different physical treatments or ionic detergents, followed by washing the cellular debris with enzymes and detergents to solubilize and finally remove the cellular debris from the ECM (12). The freeze-thaw cycling is a useful method for disrupting the cell membranes (3); however, its administration alone cannot lead to the proper removal of all the nuclear material from the tissue (13). Therefore, its combination with other methods is used to remove cellular components more efficiently. Non-enzymatic agents such as ethylenediaminetetraacetic acid (EDTA) disrupt cell adhesion by chelating divalent cations such as Ca^{2+} and Mg^{2+}. These divalent ions are involved in attachment of cells to collagen and fibronectin (12). Also, treating the tissues with hyperosmolar and hypo-osmolar solutions (14) leads to cell lysis and disruption of DNA-proteins interaction (15). Ethanol and glycerol act as dehydrators in decellularization protocols and contribute to tissue dehydration and cell lysis. Acetone removes lipids from decellularized tissues (16).

The most popular protocols for GOM decellularization are based on the protocols used for adipose tissue decellularization (3). In the current study, we checked the mechanical, enzymatic, and lipid extractive mechanisms in the quality of cell lysis, DNA, GAGs, total protein, and vascular endothelial growth factor (VEGF) content to develop a proper scaffold for reconstructive surgery. Therefore, aims of this study was to evaluate the efficacy of three different protocols for GOM decellularization and compare the DNA depletion and ECM and ultra-structure retention for regenerative medicine application.

Materials and Methods

Experimental design

This experimental study was approved by the Ethics Committee of Shiraz University of Medical Sciences (IR.SUMS.REC.1396.S1013). The fresh GOM of healthy sheep was obtained from the city slaughterhouse. The tissues were washed with phosphate-buffered saline (PBS); after that, they were cut into small pieces (2×2 cm). Each piece (n=10-15) was treated with a specific decellularization protocol, as described in the following section. After lyophilizing the decellularized GOM, they were sterilized with UV light (wavelength: 253.7 nm) for 30 minutes. Finally, each piece (10 mg) was digested with 10 mg of pepsin [Biochemical (BDH), England] and 20 mL of 0.1 M Hydrochloric acid (HCL, pH=1.6-2.5) for 48-72 hours. All steps of the procedures were carried out at room temperature on an orbital shaker. Also, penicillin (100 IU/ml, Gibco, USA) and streptomycin (100 µg/Ml, Gibco, USA) were used to minimize microbial contamination.

Protocol-1 (sodium dodecyl sulfate [SDS 1%]): was based on the work done by Soffer-Tsur et al. (4) with some modifications. The osmotic shock was applied to fresh pieces of GOM by incubating in a hypotonic buffer containing 10 mM Tris and 5 mM EDTA for 24 hours (with three changes), followed by dehydrating in 70% and 100% ethanol for 30 minutes for each step. Then, lipid extraction was performed by incubation in 100% acetone for 24 hours (with three changes). Rehydration was performed by incubation the tissue pieces in 100% ethanol for 30 minutes, followed by overnight incubation in 70% ethanol at 4°C. After washing with PBS at pH=7.4, the samples were incubated again in the hypotonic solution for 2 hours. Further cell lysis was achieved by treating the pieces in 1% SDS dissolved in PBS for 24 hours (with 2 changes). Another hypotonic shock was done for 2 hours, and the samples were incubated again in 1% SDS and then in 2.5 mM sodium deoxycholate for the same period. The trace of detergents was washed by PBS and then by 50 mM Tris containing 1 mM $MgCl_2$ at pH 8.0 for 1 hour. Further lipid extraction and dehydration were performed with 70% and 100% ethanol for 30 minutes, followed by treating the samples in 100% acetone for 30 minutes (3 changes). Finally, 3-changes of hexane: acetone [60/40 (v/v)] for 24 hours were used to extract the polar lipid. The defatted tissues were rehydrated by treating the samples with decreasing ethanol concentration (100 and 70%) for 30 minutes at 4°C, followed by washing in PBS and double distilled water three times each. The decellularized tissue was frozen (-20°C) overnight and lyophilized by a freeze dryer (CHIRST, Alpha 1-2 LD plus, Germany, -50°C).

Protocol-2 (SDS 4%): freeze-thaw cycles (n=3) and mechanical rubbing of the pieces of GOM underwater were achieved for an hour. Subsequently, the samples were soaked in distilled water containing Penicillin (100 IU/mL, Gibco, USA) and Streptomycin (100 µg/mL, Gibco, USA) for 48 hours on a stirrer. After that, they were incubated in SDS 4% for 3 days under agitation using a stirrer and then rinsed in PBS. Rehydration and lipid extraction were done in the same way as performed for protocol-1. After washing with PBS and dehydrating

in 70% and 100% ethanol for 30 minutes, the samples were incubated in 2% SDS for 1 day. After another washing with PBS and distilled water, the pieces were finally lyophilized.

Protocol-3 [sodium lauryl ether sulfate (SLES 1%)]: freeze-thaw cycles and the mechanical rubbing were performed in the same condition as in SDS 4%. The GOM was cut into pieces and incubated in Sodium lauryl ether sulfate 1% (SLES, Kimia Sanaat Ataman Co. Tehran, Iran) for 72 hours at 18-20°C on a magnetic stirrer (with three changes). Subsequently, they were washed with PBS three times to remove the cell remnants and trace of chemical reagents. The decellularized tissue was frozen (-20°C) and lyophilized (17).

Decellularization efficiency

Pieces from intact and decellularized sheep omenta were fixed in formalin and prepared for paraffin-embedded histological sectioning. The samples were sectioned at a thickness of 5 µm and mounted on glass slides. The slides were stained with 0.1% Hoechst (33342, Sigma-Aldrich, USA) in PBS and H&E (Merck, Geneva, Switzerland) to assess the nuclear component removal.

DNA content analysis

DNA content of the intact and decellularized omenta (n=3) was assessed using dsDNA Assay Kit (Qiagen, Germany), according to the manufacturer's Guideline. Briefly, the lyophilized samples were cut into pieces. 25 mg of GOM was weighted and digested with proteinase K at 56°C. After washing, 200 µL of 96% ethanol was used to extract DNA; then, the pieces were transferred to DNeasy Mini spin column to elute DNA. The ratio of DNA to protein was assessed by a spectrophotometer (Nano drop Technologies Inc, Wilmington, USA) at 260/280 nm.

Retention of extracellular matrix content

Masson's Trichorom and aldehyde fuchsine staining were done to assess collagen and elastic fiber content preservation in intact and decellularized GOM. Images were acquired using standard bright field techniques (Olympus Japan).

To evaluate the retention of acidic GAGs and neutral carbohydrates, we stained the intact and decellularized tissues with Alcian blue and methylene blue (Sigma-Aldrich, USA) at pH=1 and Periodic acid–Schiff, respectively. Lipid removal was verified by staining the 5-µm frozen sections of intact and decellularized tissues with Oil Red-O Stain (Sigma-Aldrich, USA).

Quantification of glycosaminoglycan content

To determine the GAGs content of the intact and decellularized GOM, we performed a modified protocol prepared by Geerts et al. (18). About 100 mg of the lyophilized decellularized GOM was hydrolyzed using 0.25 mL of 6 M HCL (Fisher, Waltham, MA) for 20 hours at 95°C. After that, the samples were allowed to cool at room temperature. Subsequently, 250 mL methylene blue was added to 10 mL of the sample, and the optical absorbance was immediately evaluated at a wavelength of 510 nm. To measure the amount of GAG content, the optical density of the samples was compared with a calibration curve obtained by serial dilution of heparin in PBS.

Scanning electron microscopy

To evaluate the ultra-architecture of the decellularized GOM, we performed scanning electron microscopy (SEM). One part of each decellularized GOM was fixed with 2.5% glutaraldehyde (Sigma-Aldrich, St. Louis, MO, USA) in 0.2M PBS at pH=7.4 for 2 hours at 4°C. Subsequently, they were dehydrated in an increasing graded series of ethanol (50-100%). Finally, the samples were dried at the critical point and coated with gold by Q150R- ES sputter coater (QuorumTechnologies, UK); then, they were observed, and photography was taken by a VEGA3 microscope (TESCAN, Czech Republic).

Confocal Raman microscopy assessment

The Raman spectra of the GOM decellularized by three protocols and intact pieces were recorded. The laser power level was 50 mW using the excitation laser wavelength of 785 nm. In the current study, the samples were analyzed using Raman spectra in the range of 500 to 2000 cm^{-1} with a resolution of 4 cm^{-1}.

Quantitative Measurement of VEGF with sandwich-ELISA

The content of VEGF in the decellularized tissues was measured using Enzyme-Linked Immunosorbent Assay kit (ELISA, bioassay technology laboratory). The plate was pre-coated with sheep VEGF antibody. Forty µl pepsin-treated decellularized GOMs, and 10 µl anti-VEGF antibody were added to the sample wells. Moreover, 50 µl streptavidin-HRP was added to the sample and standard wells. Subsequently the wells were mixed and incubated for 60 minutes at 37°C. After washing the unbound Streptavidin-HRP, substrate solution was added to develop color. The reaction was terminated by adding an acidic stop solution, and the absorbance was measured at 450 nm. The amount of VEGF was also calibrated and normalized.

Protein assessment

The Bradford assay determined the total protein concentration of each decellularized sample and compared it with that intact GOM. Protein concentration measurement relies on the dye molecule, Coomassie brilliant blue G-250 (Fisher Scientific, USA), binding to basic amino acids such as lysine. The samples were digested using 0.25% pepsin in HCL (0.1 M) at a dilution

of 1:10 (gram of the pieces of GOM: pepsin). Subsequently, the protein content was measured by adding 50µL of each sample and a serial dilution of BSA, as standards, to 200 µL Bradford reagent in a 96 well micro-plate. Absorbance at 595 nm was recorded after 5 minutes by ELISA reader (Thermo Scientific Varioskan Flash Multimode Reader) (19).

MTT test on fibroblast cells

To evaluate the toxicity, we exposed the human fibroblast cells isolated from the gingiva at a density of 2×10^4 to decellularized GOM prepared with all three methods at concentrations of 0.5, 0.25, 0.125, and 0.625 mg/mL; the results were compared with the cells cultured in the absence of decellularized GOM as the control culture. Decellularized GOM was dissolved in Dulbecco's Modified Eagle Medium (DMEM, Gibco, USA) containing 15% fetal bovine ferum (FBS, Gibco Paisley, USA), 2 mL L-Glutamine 1%, 100 IU/mL penicillin, and 100 µg/mL Streptomycin. Cell viability was assessed by MTT method after 1, 3, and 7 days with 3 replications for each concentration. The supernatant was discarded, and MTT (1 mg/mL) was added to all wells and incubated for 3-4 hours. Then, Dimethyl sulfoxide (300 µL) (Sigma-Aldrich, USA) was added to the wells to dissolve the formazan crystals for 15 minutes. Finally, the optical density (OD) was evaluated at 595 nm with a spectrophotometer (Nanodrop Technologies Inc, Wilmington, USA).

Statistical analysis

The data were presented as mean ± standard error (SE). One-way ANOVA and the Tukey post hoc tests were used to compare the mean values. All analyses were performed using Graph Pad Prism version 6.00 For Windows (Graphpad, USA). A $P<0.0001$ was considered significant.

Results

Gross observation of the decellularized GOM revealed lipid loss, color change from yellow to colorless, and an increase in transparency. Although a slight decrease in consistency was detected, the shape of the decellularized pieces, vascular architecture, and homogeneity were preserved. There was no deformation or disintegration regardless of the protocol used for decellularization (Fig.1A-F).

Scanning electron microscopy microscopy

Scanning electron microscopy (SEM) evaluation confirmed the ultra-architecture integrity and efficiency of cell depletion after various decellularization processes. Lower magnification photomicrographs of decellularized GOM showed fibers that formed porous structures. The ultra-architecture of the decellularized GOM was similar in all pieces of GOM treated with different protocols (Fig.1G-I).

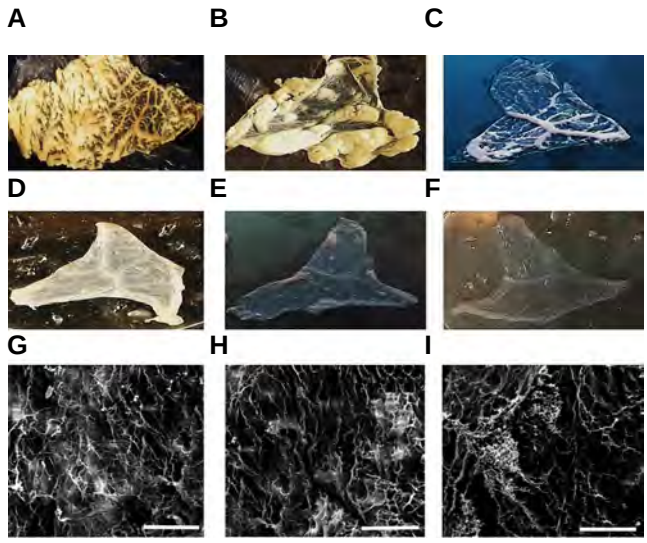

Fig.1: The gross morphology of the omentum in different decellularization phase and SEM images of the omentum decellularized by varous protocoles. **A-F.** As a result of lipid loss, the color of the GOM samples changed from yellow (undecellularized omentum) to colorless (decellularized omentum). SEM assessment showed ultra-architecture of the decellularized tissues was devoid of cells after decellularization by G. SDS 1%, H. SDS 4% and I. SLES 1% protocols (scale bar: 100 µm). SEM; Scanning electron microscope, GOM; Greater omentum, SDS; Sodium dodecyl sulfate, and SLES; Sodium lauryl ether sulfate.

Cell removal efficacy

Hoechst and H&E staining revealed that all protocols could remove the cells to an acceptable value because no cell nucleus was observed. The histological sections also showed some degree of morphological modifications of the processed tissues compared to native ones. In all decellularized tissues, fat extraction with polar and nonpolar solvents led to the absence of lipids and adipocytes; as a result, the honeycomb morphology, which can be observed in naïve tissue, was destroyed some extent. Accordingly, H&E staining revealed the presence of a few nuclei in the tissues processed by SLES 1%. Morphological comparison of the tissues prepared by various protocols revealed that all protocols showed a degree of destructive impact on ECM (Fig.2).

In all protocols, decellularization led to a significant decrease in the DNA content compared to intact GOM. Although a trace of DNA remained in all decellularized GOM, the amount of DNA was less than 50 ng/mg (standard rate). This amount is not enough to cause an immunological reaction after transplantation (20). A comparison of different protocols showed that DNA content was significantly less in the GOM prepared with SDS 1 and 4% than that prepared with SLES 1% ($P=0.05$, Fig.2A).

Glycosaminoglycan retention

Although Alcian blue and methylene blue staining

showed some extent of GAG retention in the omenta prepared with all protocols, quantification revealed a significant reduction in GAGs content in the decellularized omenta compared to the intact one (Fig.2). The best protocol for GAG retention was SDS 1%, while the amount of GAGs was significantly higher than the samples decellularized with the other two protocols. Overall, the SDS-based detergents showed a low degree of destruction for GAGs than SLES (Fig.2B).

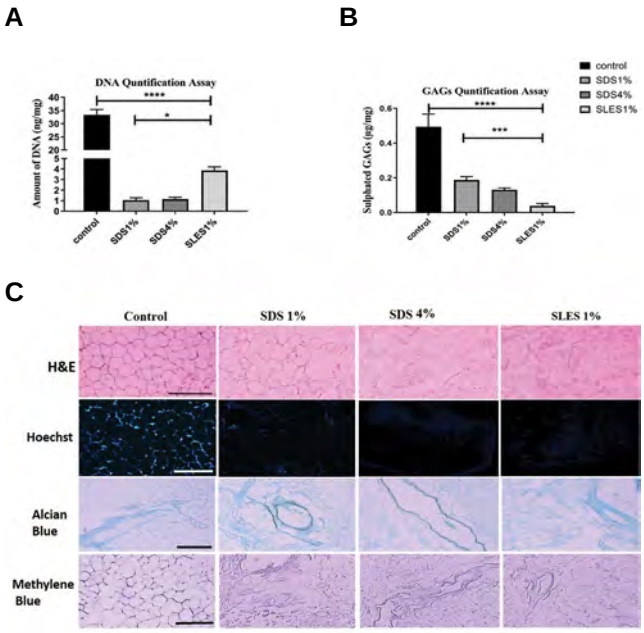

Fig.2: The graphs show the comparison of the DNA and GAGs quantification in different groups and micrographs show the decellularized GOM that stained by H&E, Hoechst, Acian blue and Methylen blue. **A.** The graph compares DNA quantification after decellularization with different methods and control**.** Data are expressed as the mean ± standard error of the mean (SEM), n=3 per group. ****; Indicates the significant difference with the control group (undecellularized tissue), (P<0.0001), *; Indicates the significant difference with SDS 1%, (P=0.044). **B.** The graph compares GAGs content of decellularized GOM with control. Graph showed that SDS 1% preserved the GAG content better than the other protocols. n=3 per group, ****; Indicates the significant difference with the control group, (P<0.0001), ***; Indicates the significant difference with using SDS 1%, (P=0.0061), **C**. Micrographs show H&E, Hoechst, Acian blue and Methylen blue staining of decellularized GOM (scale bar: 100 µm). GAGs; Glycosaminoglycans, GOM; Greater omentum, H&E; Hematoxylin and eosin, and SDS, Sodium dodecyl sulfate.

Retention of extracellular matrix contents

In all protocols, histochemical staining showed retention of ECM components after decellularization. Accordingly, periodic acid-schiff (PAS) staining showed the persistence of neutral carbohydrates. Masson's Trichrome and aldehyde fuchsine staining also demonstrated the retention of collagen and elastic fibers, respectively. All decellularization protocols showed an acceptable lipid removal, as indicated by Oil Red staining; however, lipid droplets were extracted more efficiently in SLES-treated scaffolds (SLES 1%). More similarity of the matrix structure in SLES-treated samples with native tissue, and sufficient fat removal, support the claim that a nonpolar solvent alone is more appropriate for fat removal (Fig.3).

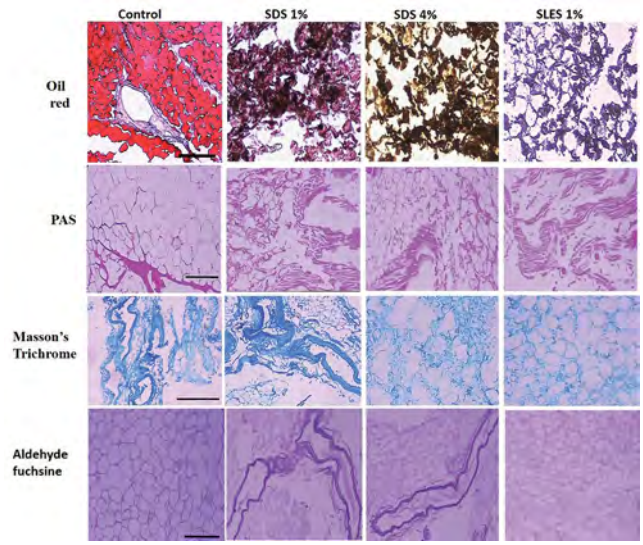

Fig.3: Histochemical assessments of decellularized omenta obtained by SDS 1%, SDS 4% and SLES 1% and undecellularized tissue (control) (scale bar: 100 µm). SDS; Sodium dodecyl sulfate and SLES; Sodium lauryl ether sulfate.

Bradford assay

Although the protein content of decellularized scaffolds was significantly washed out by the decellularization process regardless of the protocol (P<0.0001 for all), SDS 1% preserved the protein content significantly and more efficiently than the others (both P<0.0001). SLES showed a detrimental impact on the protein content so the pics of GOM treated with SLES 1% contained the least amount of protein compared to SDS-based protocols (P=0.0001, Fig.4A).

Quantitative measurement of VEGF concentration

VEGF, as the most abundant growth factor in the ECM of GOM, should be preserved after decellularization. To evaluate the preservation of this growth factor, we measured the level of VEGF as an example of growth factor content. Although VEGF was significantly washed in GOM treated by all protocols compared with the intact ones (control versus SDS 1% (P=0.0029), SDS 4% (P=0.0016), and SLES 1% (P=0.0003), VEGF was better preserved in the GOM prepared by SDS-based protocols compared to SLES-based ones (SDS 1% versus SLES 1%, P=0.0059) and SDS 4% versus SLES 1% (P=0.0139). VEGF washing off was significantly higher in the GOM prepared by SLES 1% (Fig.4B).

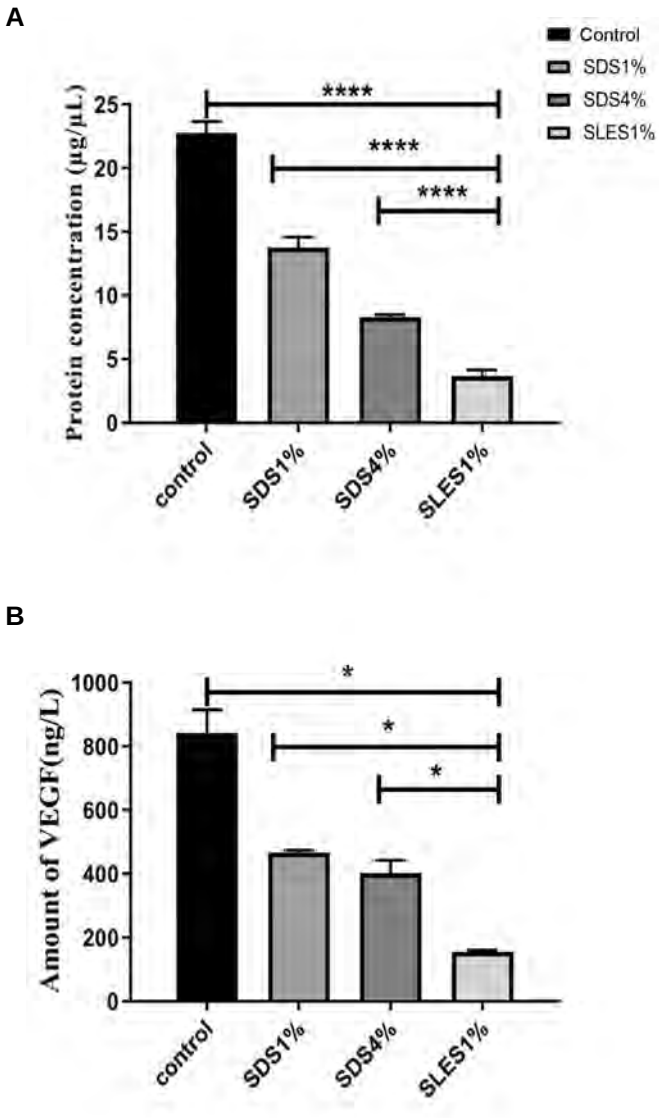

Fig.4: The graphs showed the protein and VEGF concentrations. **A.** Bradford assay showed a significant protein wash out after decellularization. Results are presented as mean µg protein per mg dry mass (n=3 per group), ****; Indicates the significant difference with the control group (P<0.0001), the omenta prepared by SDS 1% (P<0.0001), and SDS 4% (P=0.0001). **B.** ELISA assessment showed a significant decrease in the VEGF content after decellularization. Results are presented as the mean of VEGF (ng) per Liter dry mass (n=3 per group), *; Indicates the significant difference with the control group (P<0.05), SDS 1%, (P<0.05), and SDS 4%, (P<0.05). VEGF; Vascular endothelial growth factor , SDS; Sodium dodecyl sulfate, and ELISA; Enzyme-linked immunosorbent assay.

Raman spectrum

After normalization and baseline correction, both intact and decellularized omenta showed nearly similar Raman spectra. Peaks at 546 cm^{-1} and 607 cm^{-1} were assigned for Cholesterol. A peak at 1079 cm^{-1} signifies the triglycerides (fatty acids), and at 1100 cm^{-1} and 1129 cm^{-1} signifies the lipid. Bands at 862 cm^{-1} display phosphate groups, and the peak at 875 cm^{-1} expresses the stretch vibration of choline group N (CH 3)3, characteristic of phospholipids, phosphatidylcholine, and sphingomyelin. Bands at 1368 cm^{-1}, 1440 cm^{-1}, 1729, and 1742 cm^{-1} indicate phospholipids, lipid, and Ester group, respectively (21). Vibration at 1765 cm^{-1} for C = O stretch represents the lipid fraction. The intensity of all these bands decreased to a great extent in decellularized tissues, which indicated the successful lipid depletion by all protocols.

Bands assigned for protein were detected as well. Specific bands for amide I at 1655, 1667, and 1673 cm^{-1} and stretching vibration at 1544 cm^{-1} for Amide II was observed. Vibrations at 1250, 1253, 1267, and 1321 cm^{-1} determined amide III and peaks at 890 cm^{-1} and 963 cm^{-1} belong to protein content. A peak at 920 cm^{-1} assigned the C-C stretch of proline ring/glucose/lactic acid, and 938 cm-1 assigned the C-C stretch backbone (lipid and protein) (21).

The resonance at 818 cm^{-1} can be assigned for C-C stretching (collagen assignment). In addition, bands at 1004, 1036, 1067, 1451, 1587, and 1205 cm^{-1} represent phenylalanine presents in the collagen. Peaks for tryptophan and cytosine and guanine that indicate the presence of DNA can be found at 573, 1165, 1175, 1297 and 1548 cm^{-1}. Vibration at 940 cm^{-1} can be represented for carbohydrates as well. A peak at 1347 cm^{-1} represents an unknown mode. 1392 cm^{-1} C-N stretching represents the quinoid ring-benzoid ring-quinoid ring. Comparison of Raman spectra of intact and decellularized GOM revealed an impressive reduction in protein, collagen, and DNA content (22) (Fig.5).

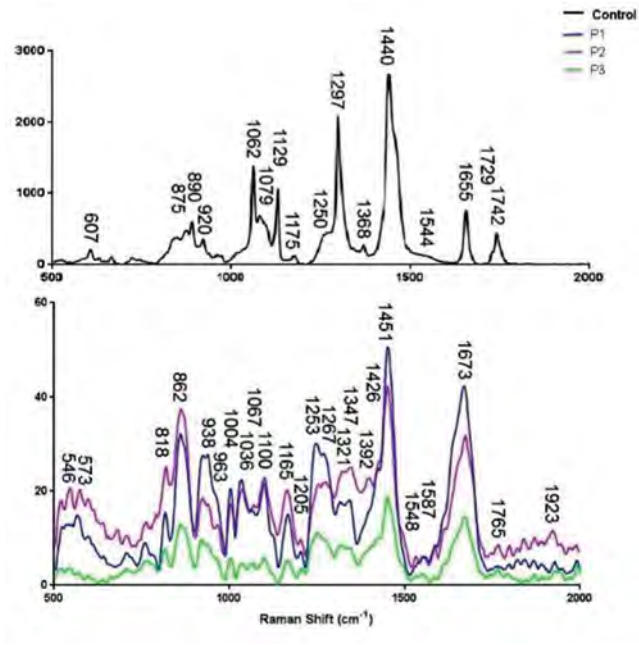

Fig.5: Raman spectra of native and decellularized omenta treatment using different decellularization protocols.

We also compared the intensity of the Raman spectra from the GOM prepared by various methods. Based on the Raman spectrum, SLES detergent decreased the amount

of lipid assigned at 862 and 1100 cm^{-1} compared to SDS detergent. A comparison of the intensity of the bands assigned for proteins at 1253 and 1267 cm^{-1} showed that the SDS 1% and SDS 4% better preserved these components than SLES 1%, a comparison of the band's intensity at 818 cm^{-1} also revealed better preservation of collagen by the SDS 4%. Besides, the Raman spectra showed that both SDS-based protocols retained collagen better than the SLES-based protocol. GAGs content was demonstrated in all decellularized scaffolds as indicated by vibration at 1062 cm^{-1}. Both SDS-based protocols preserved GAGs in the decellularized omenta better than the SLES-based protocols, and this finding confirmed the data obtained from the GAGs quantification assay. Furthermore, comparing the Raman spectra of commercially prepared SDS with SDS-treated samples revealed that SDS was completely washed out.

Overall, a comparison of various protocols showed that decellularization using SDS 1%, in combination with the other decellularization agents including EDTA, acetone-hexane, and ethanol, preserved collagen and protein better than the SLES-based protocol. Furthermore, administration of the higher SDS concentration in the SDS 4% extracted the lipid content more efficiently than SDS 1%, which used less amount of SDS (Fig.5).

Cytotoxicity of greater omentum

Cell viability was similar in all groups on the first day, regardless of the procedure. As the time progressed, the cell number increased in all conditions up to day 3; however, the cell viability remained constant up to day 7. In both SDS-treated cultures, the cell viability and proliferation significantly increased in the cultures exposed to 0.5% decellularized GOM compared to all the cultures exposed to lower concentrations as well as the control culture on day 3 (SDS 1% P=0.0001, P<0.0001 and SDS 4% P=0.0275, P<0.0001, P=0.0328). On day 7, cell viability was also significantly higher than all other groups in the cultures treated with 1% decellularized GOM treated groups (P=0.0454, P<0.0001, and P=0.0012). In the cultures treated with SDS 4%, a significant increase in cell viability was revealed in 0.5% decellularized GOM compared to 0.625% (P=0.0006).

In SLES-treated cultures, all concentrations of decellularized GOM had the same impact on the cell viability. However, cultures received 0.5% SLES, showed non-significant higher cell viability compared to all other groups on all days. Therefore, the data of this study showed that the influence of decellularized GOM on cell viability was depended on the type of detergent; however, SLES was not toxic for the cells as the cell viability in the cultures exposed to SLES-treated GOM was similar to the control culture (Fig.6).

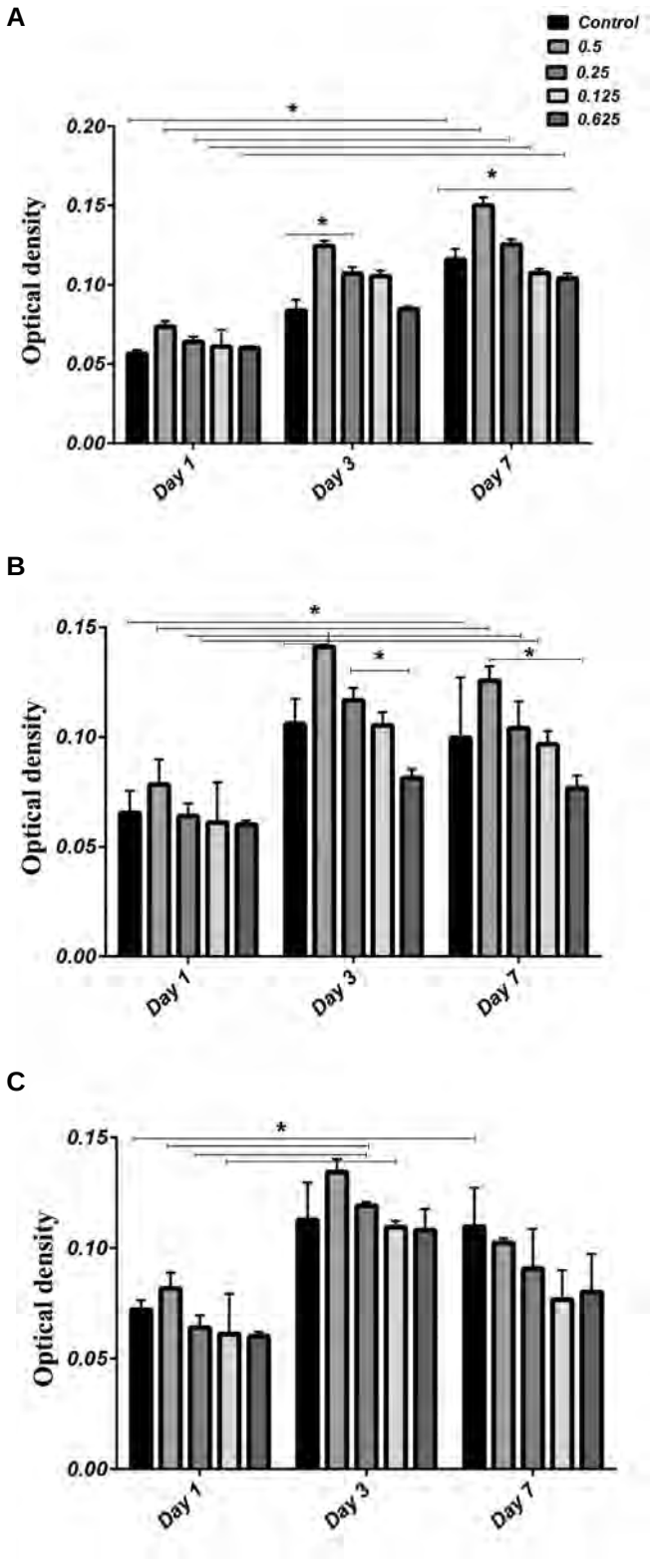

Fig.6: MTT test. Comparison of cell viability in the presence of different concentrations of decellularized GOM prepared with **A.** SDS 1%, **B.** SDS 4% and **C.** SLES (P<0.05).

Discussion

In the present research, we compared three protocols for decellularization of sheep GOM based on criteria such as damage to ECM constitutions, and ultra-architecture and efficient removal of cell and nuclear debris and lipid

extraction. Decellularization should ensure cellular and nuclear depletion and retain the ultra-architecture and composition of the ECM (20).

The data revealed that all protocols could remove DNA from the scaffolds to a great extent. The presence of DNA in the decellularized scaffolds can trigger inflammation; as a result, it can interfere with tissue repair (23). Regardless of the protocol, the DNA quantification assay revealed that the decellularized GOM contained less than 50 ng/mg dry weight (9), which has been reported as a safe DNA content that does not arouse inflammation after decellularized scaffold transplantation. However, previous works revealed mild inflammation after decellularized scaffold transplantation with the DNA content less than the allowed limit (24). Therefore, the recommended protocol is that which can minimize DNA remnant after decellularization. Our data showed that both SDS-containing protocols (SDS 1%, SDS 4%) significantly reduced the DNA content compared to the SLES-containing protocol (SLES 1%). Therefore, the decellularization method using SDS is better than SLES.

Besides DNA and cell debris removal, an appropriate decellularization protocol should retain the architecture and chemical structure of the ECM. H&E, aldehyde fuchsine, and Masson's Trichrome staining revealed that SDS and SLES-based protocols could preserve the tissue architecture. SEM images also confirmed ultra-architecture preservation after treatment with all protocols. SLES is a mild detergent (25) and has been previously used to decellularize organs such as the ovary (17), liver, and lung (25). The vascular architecture has been reported to be well preserved in SLES-treated scaffolds (26). Our Raman confocal microscopy and oil red staining confirmed that the best protocol for lipid extraction was the SLES-treated protocol; however, our data also indicated that SLES could wash out the protein, growth factors, and GAG content as well. Therefore, there should be a balance between the cell removal and ECM content retention for each recommended protocol.

GAGs, as the major components of the ECM, have numerous biological activities; they are involved in cell adhesion, cell growth regulation, and cell proliferation (27); therefore, the retention of GAGs can support the cell growth after recellularization of decellularized GOM. Our data showed that fat removal with SDS and hexane-acetone followed by mild detergents and hypertonic treatments had a less detrimental impact on the GAGs content than SLES. Sulfated GAGs carry negative charges, which stimulate the electrostatic interactions with growth factors and cytokines in ECM. Therefore, GAGs have roles in sequestration and controlled release of these factors into the cellular microenvironment.

Both SDS and SLES have detrimental impacts on protein and VEGF content; however, we showed that VEGF was better preserved in SDS-containing protocols. Previous studies have shown that SDS detergent disrupts the tissue ultrastructure (28) and growth factor deletion (29). On the other hand, SLES treatment has been shown to change the protein configuration (30); as a result, the antibodies cannot detect them properly in ELISA. Changes in the chemical configuration of proteins such as VEGF by SLES may also interfere with their functions. Better preservation of protein and VEGF by SDS-treated protocols may be due to the higher capability of SDS to preserve GAGs; as a result, the preserved GAGs may sequestrate the VEGF. Besides, some carbohydrates have been recommended to mitigate the cytotoxicity of biomaterial (31). The protocols retaining GAGs content may also help reduce the cytotoxicity of the trace of detergents used for decellularization. Therefore, GAGs retention within the ECM may be useful for engineering complex tissues (13). Confocal Raman spectroscopy can be considered a semi-quantitative method to characterize the biomolecular composition of native and decellularized tissues (32). Raman confocal microscopy confirmed extensive washout of GAGs by SLES-based protocol in our study.

In the current study, two SDS concentrations were used to show the optimal concentration of this detergent. SDS should remove the cells, and at the same time, it should retain the ECM content, including proteins such as VEGF. Our result showed higher concentration of SDS led to protein and VEGF washing. Along with our data, a study revealed that an increase in SDS concentration had harsh impacts on the matrix content of the decellularized kidney (33). In another study, two different SDS concentrations were used to decellularize ECM produced by the fibroblast sheet. It was found that a higher concentration of SDS increased the DNA depletion efficiency, although it accelerated the washing of the matrix and reduced mechanical properties of the decellularized sheet as well (23).

As GOM contains a large number of adipocytes, most of the protocols for GOM decellularization are based on the procedures for decellularization of the adipose tissue (32). Decellularization of GOM and adipose tissue has been obtained through some protocols which use cell rupture by mechanical procedures, solvent extraction, and enzymatic digestion (3, 6, 34). The protocols used in the current study provide a complex cell-free scaffold made up of a three-dimensional network of ECM, decellularized vascular bed, and preserved collagen and elastic fiber structure. A comparison of various protocols revealed that SDS-based protocols preserved GAGs and essential amino acids (phenylalanine, and hydroxyl proline) in the collagen structure better than SLES. However, SLES is a superior choice for lipid extraction. Previous studies on SDS have shown that long-term treatment with SDS has significant destructive effects on the natural ultrastructure of the ECM of the tissue and reduces GAGs and cytokines and has cytotoxic effects (35). However, the results of our study showed that the SDS detergent led to the preservation of the contents and structure of the ECM of grater omentum tissue. Based on the MTT test, SDS-based methods had a better impact on

the growth and survival of human gingival fibroblast cells without toxic effects than the SLES method.

GOM has often been used for angiogenic and regenerative properties (2). For instance, it has been used to coat the engineered colon, rectum, esophagus (36), stomach, and trachea. GOM has been used in osteochondral graft (37). Furthermore, autologous GOM has been used to treat perforated gastric/duodenal ulcers and decrease bleeding after hepatectomy or pancreaticoduodenectomy (38). Using allogeneic GOM that is more appropriate for standardizing the procedures and commercialization may arouse immunorejection. In decellularized GOM, the vascular architecture was preserved, and it might facilitate angiogenesis to the flaps (39). In this regard, SDS 1% is a superior choice as it can preserve VEGF better than other protocols. As decellularized GOM does not lead to inflammation, it could be taken from both living and decedent donors and then re-cellularized in vitro with autologous source of stem cells for soft tissue reconstruction.

Conclusion

Regardless of the protocols used for decellularization, the decellularized pieces of GOM preserved their shape, vascular architecture, and homogeneity with minimal deformation or disintegration. Although all the protocols showed the capability for a proper lipid removal and retention of neutral carbohydrate, collagen, and elastic fibers, SDS 1% (low concentration of SDS, hexane, acetone, EDTA, and ethanol) is considered the superior protocol for preservation of collagen and elastic fiber, protein, VEGF and GAGs.

Acknowledgments

The authors wish to thank the Research Deputy of Shiraz University of Medical Sciences for offering grant no 14418. This work was done by Kh.Fazelian-Dehkordi as a part of fulfillment for Ph.D. program. The authors would like to thank Shiraz University of Medical Sciences, Shiraz, Iran, and the Center for Development of Clinical Research of Nemazee Hospital and Dr. Nasrin Shokrpour for editorial assistance. The authors declare no conflict of interest.

Authors' Contributions

Kh.F.D.; Participated in all experimental work, data collection, evaluation, drafting, and statistical analysis. S.F.M.A.; Contributed to the study conception and design. T.T.-Kh.; Contributed extensively to the interpretation of the data, the conclusion, and revising of the draft. All authors read and approved the final manuscript.

References

1. Kim TH, Kim DY, Jung KH, Hong YS, Kim SY, Park JW, et al. The role of omental flap transposition in patients with locoregional recurrent rectal cancer treated with reirradiation. J Surg Oncol. 2010; 102(7): 789-795.
2. Di Nicola V. Omentum a powerful biological source in regenerative surgery. Regen Ther. 2019; 11: 182-191.
3. Porzionato A, Sfriso M, Macchi V, Rambaldo A, Lago G, Lancerotto L, et al. Decellularized omentum as novel biologic scaffold for reconstructive surgery and regenerative medicine. Eur J Histochem. 2013; 57(1): e4.
4. Soffer-Tsur N, Shevach M, Shapira A, Peer D, Dvir T. Optimizing the biofabrication process of omentum-based scaffolds for engineering autologous tissues. Biofabrication. 2014; 6(3): 035023.
5. Shevach M, Zax R, Abrahamov A, Fleischer S, Shapira A, Dvir T. Omentum ECM-based hydrogel as a platform for cardiac cell delivery. Biomed Mater. 2015; 10(3): 034106.
6. Baker NA, Muir LA, Washabaugh AR, Neeley CK, Chen SY-P, Flesher CG, et al. Diabetes-specific regulation of adipocyte metabolism by the adipose tissue extracellular matrix. J Clin Endocrinol Metab. 2017; 102(3): 1032-1043.
7. Lin T, Liu S, Chen S, Qiu S, Rao Z, Liu J, et al. Hydrogel derived from porcine decellularized nerve tissue as a promising biomaterial for repairing peripheral nerve defects. Acta Biomater. 2018; 73: 326-338.
8. Shevach M, Soffer-Tsur N, Fleischer S, Shapira A, Dvir T. Fabrication of omentum-based matrix for engineering vascularized cardiac tissues. Biofabrication. 2014; 6(2): 024101.
9. Loreto C, Leonardi R, Musumeci G, Pannone G, Castorina S. An ex vivo study on immunohistochemical localization of MMP-7 and MMP-9 in temporomandibular joint discs with internal derangement. Eur J Histochem. 2013; 57(2): e12.
10. Emami A, Talaei-Khozani T, Tavanafar S, Zareifard N, Azarpira N, Vojdani Z. Synergic effects of decellularized bone matrix, hydroxyapatite, and extracellular vesicles on repairing of the rabbit mandibular bone defect model. J Transl Med. 2020; 18(1): 1-18.
11. Porzionato A, Stocco E, Barbon S, Grandi F, Macchi V, De Caro R. Tissue-engineered grafts from human decellularized extracellular matrices: a systematic review and future perspectives. Int J Mol Sci. 2018; 19(12): 4117.
12. Crapo PM, Gilbert TW, Badylak SF. An overview of tissue and whole organ decellularization processes. Biomaterials. 2011; 32(12): 3233-3243.
13. Hoshiba T, Lu H, Kawazoe N, Chen G. Decellularized matrices for tissue engineering. Expert Opin Biol Ther. 2010; 10(12): 1717-1728.
14. Yang B, Zhang Y, Zhou L, Sun Z, Zheng J, Chen Y, et al. Development of a porcine bladder acellular matrix with well-preserved extracellular bioactive factors for tissue engineering. Tissue Eng Part C Methods. 2010; 16(5): 1201-1211.
15. Shupe T, Williams M, Brown A, Willenberg B, Petersen BE. Method for the decellularization of intact rat liver. Organogenesis. 2010; 6(2): 134-136.
16. Lumpkins SB, Pierre N, McFetridge PS. A mechanical evaluation of three decellularization methods in the design of a xenogeneic scaffold for tissue engineering the temporomandibular joint disc. Acta Biomater. 2008; 4(4): 808-816.
17. Hassanpour A, Talaei-Khozani T, Kargar-Abarghouei E, Razban V, Vojdani Z. Decellularized human ovarian scaffold based on a sodium lauryl ester sulfate (SLES)-treated protocol, as a natural three-dimensional scaffold for construction of bioengineered ovaries. Stem Cell Res Ther. 2018; 9(1): 252.
18. Geerts S, Ozer S, Jaramillo M, Yarmush ML, Uygun BE. Nondestructive methods for monitoring cell removal during rat liver decellularization. Tissue Eng Part C Methods. 2016; 22(7): 671-678.
19. Valipour Nouroozi R, Valipour Noroozi M, Ahmadizadeh M. Determination of protein concentration using bradford microplate protein quantification assay. Int Electron J Med. 2015; 4(1): 11-17.
20. Gilpin A, Yang Y. Decellularization strategies for regenerative medicine: from processing techniques to applications. Biomed Res Int. 2017; 2017: 9831534.
21. Talari ACS, Movasaghi Z, Rehman S, Rehman IU. Raman spectroscopy of biological tissues. Appl Spectrosc Rev. 2015; 50(1): 46-111.
22. Movasaghi Z, Rehman S, Rehman IU. Raman spectroscopy of biological tissues. Appl Spectrosc Rev. 2007; 42(5): 493-541.
23. Xing Q, Yates K, Tahtinen M, Shearier E, Qian Z, Zhao F. Decellularization of fibroblast cell sheets for natural extracellular matrix scaffold preparation. Tissue Eng Part C Methods. 2014; 21(1): 77-87.
24. Kargar-Abarghouei E, Vojdani Z, Hassanpour A, Alaee S, Talaei-Khozani T. Characterization, recellularization, and transplantation of rat decellularized testis scaffold with bone marrow-derived mesenchymal stem cells. Stem Cell Res Ther. 2018; 9(1): 1-16.
25. Ma J, Ju Z, Yu J, Qiao Y, Hou C, Wang C, et al. Decellularized rat

lung scaffolds using sodium lauryl ether sulfate for tissue engineering. Asaio J. 2018; 64(3): 406-414.
26. Naeem EM, Sajad D, Talaei-Khozani T, Khajeh S, Azarpira N, Alaei S, et al. Decellularized liver transplant could be recellularized in rat partial hepatectomy model. J Biomed Mater Res A. 2019; 107(11): 2576-2588.
27. Linhardt RJ, Toida T. Role of glycosaminoglycans in cellular communication. Acc Chem Res. 2004; 37(7): 431-438.
28. Ott HC, Clippinger B, Conrad C, Schuetz C, Pomerantseva I, Ikonomou L, et al. Regeneration and orthotopic transplantation of a bioartificial lung. Nat Med. 2010; 16(8): 927-933.
29. Reing JE, Brown BN, Daly KA, Freund JM, Gilbert TW, Hsiong SX, et al. The effects of processing methods upon mechanical and biologic properties of porcine dermal extracellular matrix scaffolds. Biomaterials. 2010; 31(33): 8626-8633.
30. Wang J, Jia R, Wang J, Sun Z, Wu Z, Liu R, et al. Investigation on the interaction of catalase with sodium lauryl sulfonate and the underlying mechanisms. J Biochem Mol Toxicol. 2018; 32(2): e22025.
31. Gholami M, Zare-Hoseinabadi A, Mohammadi M, Taghizadeh S, Behbahani AB, Amani AM, et al. Preparation of ZnXFe3-XO4@ chitosan nanoparticles as an adsorbent for methyl orange and phenol. J Environ Treat Tech. 2019; 7(3): 245-249.
32. Schwarz S, Koerber L, Elsaesser AF, Goldberg-Bockhorn E, Seitz AM, Dürselen L, et al. Decellularized cartilage matrix as a novel biomatrix for cartilage tissue-engineering applications. Tissue Eng Part A. 2012; 18(21-22): 2195-2209.
33. Schmitt A, Csiki R, Tron A, Saldamli B, Tübel J, Florian K, et al. Optimized protocol for whole organ decellularization. Eur J Med Res. 2017; 22(1): 1-9.
34. Omidi E, Fuetterer L, Mousavi SR, Armstrong RC, Flynn LE, Samani A. Characterization and assessment of hyperelastic and elastic properties of decellularized human adipose tissues. J Biomech. 2014; 47(15): 3657-3663.
35. Hassanpour A, Talaei-Khozani T, Kargar-Abarghouei E, Razban V, Vojdani Z. Decellularized human ovarian scaffold based on a sodium lauryl ester sulfate (SLES)-treated protocol, as a natural three-dimensional scaffold for construction of bioengineered ovaries. Stem Cell Res Ther. 2018; 9(1): 1-13.
36. Chung EJ, Ju HW, Yeon YK, Lee JS, Lee YJ, Seo YB, et al. Development of an omentum-cultured oesophageal scaffold reinforced by a 3D-printed ring: feasibility of an in vivo bioreactor. Artif Cells Nanomed Biotechnol. 2018; 46 Suppl1: 885-895.
37. Buyukdogan K, Doral MN, Bilge O, Turhan E, Huri G, Sargon MF. Peritoneum and omentum are natural reservoirs for chondrocytes of osteochondral autografts: a comparative animal study. Acta Orthop Traumatol Turc. 2016; 50(5): 539-543.
38. Collins D, Hogan AM, O'Shea D, Winter DC. The omentum: anatomical, metabolic, and surgical aspects. J Gastrointest Surg. 2009; 13(6): 1138-1146.
39. Kant RJ, Coulombe KL. Integrated approaches to spatiotemporally directing angiogenesis in host and engineered tissues. Acta Biomater. 2018; 69: 42-62.

Original Article

Mini Bioreactor Can Support *In Vitro* Spermatogenesis of Mouse Testicular Tissue

Zahra Amirkhani, Ph.D.[1], Mansoureh Movahedin, Ph.D.[1]*, Nafiseh Baheiraei, Ph.D.[2], Ali Ghiaseddin, Ph.D.[3]

1. Department of Anatomical Sciences, Faculty of Medical Sciences, Tarbiat Modares University, Tehran, Iran
2. Tissue Engineering and Applied Cell Sciences Division, Department of Anatomical Sciences, Faculty of Medical Sciences, Tarbiat Modares University, Tehran, Iran
3. Adjunct Research Associate Professor at Chemistry Department, Michigan State University, East Lansing, MI, USA

Corresponding Address: P.O.Box: 14115-331, Department of Anatomical Sciences, Faculty of Medical Sciences, Tarbiat Modares University, Tehran, Iran
Email: movahed.m@modares.ac.ir

Received: 20/April/2021, Accepted: 11/July/2021

Abstract

Objective: It was in the early 20th century when the quest for *in vitro* spermatogenesis started. *In vitro* spermatogenesis is critical for male cancer patients undergoing gonadotoxic treatment. Dynamic culture system creates *in vivo*-like conditions. In this study, it was intended to evaluate the progression of spermatogenesis after testicular tissue culture in mini-perfusion bioreactor.

Materials and Methods: In this experimental study, 12 six-day postpartum neonatal mouse testes were removed and fragmented, placed on an agarose gel in parallel to bioreactor culture, and incubated for 8 weeks. Histological, molecular and immunohistochemical evaluations were carried out after 8 weeks.

Results: Histological analysis suggested successful maintenance of spermatogenesis in tissues grown in the bioreactor but not on agarose gel, possibly because the central region did not receive sufficient oxygen and nutrients, which led to necrotic or degenerative changes. Molecular analysis indicated that Plzf, Tekt1 and *Tnp1* were expressed and that their expression did not differ significantly between the bioreactor and agarose gel. Immunohistochemical evaluation of testis fragments showed that PLZF, SCP3 and ACRBP proteins were expressed in spermatogonial cells, spermatocytes and spermatozoa. PLZF expression after 8 weeks was significantly lower ($P<0.05$) in tissues incubated on agarose gel than in the bioreactor, but there was no significant difference between SCP3 and ACRBP expression among the bioreactor and agarose gel culture systems.

Conclusion: This three-dimensional (3D) dynamic culture system can provide somewhat similar conditions to the physiological environment of the testis. Our findings suggest that the perfusion *bioreactor* supports induction of spermatogenesis for generation of haploid cells. Further studies will be needed to address the fertility of the sperm generated in the bioreactor system.

Keywords: Agarose Gel, Mouse, Perfusion Bioreactor, Spermatogenesis, Tissue Culture

Cell Journal(Yakhteh), Vol 24, No 5, May 2022, Pages: 277-284

Citation: **Amirkhani Z, Movahedin M, Baheiraei N, Ghiaseddin A. Mini bioreactor can support in vitro spermatogenesis of mouse testicular tissue. Cell J. 2022; 24(5): 277-284. doi: 10.22074/cellj.2022.8053.**

Introduction

Investigations into the progress of spermatogenesis *in vitro* began early last century (1), although the differentiation of spermatogonial stem cells (SSCs) into sperm cells remained a challenge. In the 1960s and 1970s, testis tissue culture was used to evaluate the process of spermatogenesis. In those experiments, spermatogenesis progressed as far as meiosis but haploid cells were never formed (2). In the 1980s, cell culture was used instead of tissue culture, but the development of fertile sperm cells remained problematic (3). Although there are many ways of culturing tissue fragments, the gold standard is the interphase method in which specimens are positioned at the interphase between the culture medium and a gas layer (4). By isolating seminiferous tubules acquired from immature mice, Sato et al. (5) generated fertile sperm using *ex vivo* culture. However, the overall duration and efficiency of spermatogenesis were not close to those reported *in vivo*.

Capillaries around a tissue provide oxygen and nutrients, as well as removing waste effectively, thereby supporting tissue homeostasis. Because it lacks such a microcirculatory network, the interphase method cannot provide the appropriate *in vivo*-like conditions. Researchers have tried innovative circulatory mechanisms to improve their culture systems (6, 7). To maintain physiological functions more efficient than conventional methods, microfluidic devices and bioreactors have been developed recently to culture testis tissue pieces (8-11). Different types of perfusion bioreactors have also been developed and have yielded more favourable results compared with static culture (12-14). In this study, a mini-perfusion bioreactor was designed that was capable of successfully sustaining spermatogenesis from immature mouse testis tissue fragments incubated for 8 weeks. This device provided sufficient nutrients and oxygen for tissue culture for having an *in vitro* model to study spermatogenesis progression during maturation of neonatal testicular tissue. The fertility of sperm generated in the bioreactor system will be addressed in future studies. Finally, the dynamic culture method described here must

be assessed in human testicular tissue culture to determine its potential utility in addressing male infertility.

Materials and Methods

Design of the mini-perfusion bioreactor system

In this experimental study, the mini-perfusion bioreactor system is composed of three polydimethylsiloxane (PDMS) layers (Sylgard 184, Dow Corning, Germany)-upper, middle and lower annular rings-with a central cylindrical cavity and a porous polyvinylidene fluoride membrane filter (pores size 0.22 μm, Millipore, Germany). The lower layer is composed of a medium flow chamber (5 mm wide and 5 mm high) and a channel for continuously supplying culture medium from a perfusion pump to an outlet. The middle layer comprises a tissue chamber of the same size. The culture medium was drawn through the inlet by a syringe pump at a rate of 15, 27, 50 and 100 μL/hour. The porous membrane was placed between the flow channel and the tissue chamber to separate sample tissues from the flowing medium. The upper layer was a waste material chamber. The thickness of the PDMS layers was 5 mm each (15).

Agarose support gel preparation for tissue culture

The method described by Yokonishi et al. (16) was used to prepare the agarose support gel. In brief, 1.5% w/v agarose solution (Carl Roth, Germany) was prepared and sterilised. Segments measuring 10×10×5 mm^3 were arranged using a scalpel blade under sterile conditions. The segments were then placed in a six-well plate containing alpha-minimum essential medium (αMEM; Bio-Ideal, Iran) supplemented by10% Knockout Serum Replacement (KSR, Gibco, UK), 60 ng/mL progesterone (Invitrogen, UK), 30 ng/mL beta-estradiol (PeproTech, Germany), 20 ng/mL epithelial growth factor (EGF, PeproTech), 10 ng/mL human basic fibroblast growth factor (bFGF, PeproTech), 10 ng/mL human glial cell line-derived neurotropic factor (GDNF, PeproTech) and 10 ng/mL leukemia inhibitory factor (LIF, Royan Institute, Iran) as the culture medium.

Animals

Six-day-old NMRI neonatal male mice provided by the Pasteur Institute of Iran were used as the source of testis tissue. The mice were maintained at an ambient temperature of 22°C and a 12/12 hours light/dark cycle. This study was approved by the Ethics Committee of Tarbiat Modares University, Tehran, Iran (IR.TMU.REC.1395.522).

Culture of testis tissues

Two groups of neonatal mouse testis were created for this study: tissue cultivated in the perfusion bioreactor and on agarose gel. For each group, 12 mouse pups were euthanised and the testes were removed, decapsulated, fragmented (1 mm^3 in size) and randomly allocated to either the bioreactor or the agarose gel. In the bioreactor group, the tissue was placed in the middle chamber. Assessments were performed after 2 and 8 weeks of culture. For static cultures, testis fragments were placed on agarose stands in a six-well culture plate, and medium was added to one-half to four-fifths the height of the agarose gel. The medium was changed twice a week. The culture incubator conditions were maintained under 5% CO_2 and 34°C temperature (5).

Viability test of the tissue during the culture

For checking the cytotoxic effects of the bioreactor components and accessories, the cell suspension was exposed to PTFE tubes, PDMS and bioreactor accessories for 72 hours under normal culture conditions. Cell viability was assessed at the beginning of culture and after 72 hours by Trypan blue staining. Moreover, after 8 weeks of culture by capturing multiple images, the viability of the cells in the tissue was assessed based on morphology.

Histology, morphology and functional examinations

Specimens were fixed with Bouin's fixative and embedded in paraffin wax. Sections were cut and stained with hematoxylin and eosin (H&E) or Weigert's hematoxylin and periodic acid-schiff (PAS, Merck, Germany). All sections were examined using a light microscope (Zeiss, Germany) (17). After 8 weeks of culture, the tissues were mechanically dissociated using needles to release the spermatid and sperm for evaluation on an inverted microscope (Zeiss Axiovert 40 CFL) (9).

Papanicolaou staining was performed to assess the sperm-like cell morphology (18). A Diff-Quick staining kit (Faradid Pardaz Pars Inc., Iran) was utilized to assess sperm morphology. Smears were firstly stained with Diff-Quick staining solutions I and II for 25 seconds. Afterwards, they were washed in distilled water. In the Diff-Quick smears, acrosomes stain pink or light purple, and the sperm nucleus, midpiece and tail stain dark purple (19). Double staining was performed to assess the acrosome reaction. Briefly, the smears were fixed with 3% glutaraldehyde for 30 minute, and the slides were stained with Bismarck brown (0.8% in deionised water, pH=1.8) for 10 minute and then with Rose Bengal (0.8% in 0.1 M Tris buffer, pH=5.3) for 25 minutes. Sperm-like cells with acrosomes that stained bright brown were considered to be sperm-like cells with an intact acrosome region (20).

Quantitative reverse transcription polymerase chain reaction analysis: gene expression quantitative analysis

Expression of promyelocytic leukaemia zinc finger (*Plzf*), *Tekt1* and *Tnp1* genes in testicular tissue fragments were evaluated after 2 and 8 weeks. Total RNA was extracted from the tissue fragments from both groups using RNX-Plus™ (CinnaGen, Iran) following the manufacturer's recommendation. The RNA concentration was then determined using an ultraviolet

spectrophotometer (Eppendorf Company, Germany). cDNA synthesis was performed using a RevertAid™ First Strand cDNA Synthesis kit (Fermentas, Germany) and oligo (dT) primers. For the polymerase chain reaction (PCR) reactions, primers for *Plzf, Tekt1* and *Tnp1* genes were designed. Designed primers were blasted using the NCBI website (https://www.ncbi.nlm.nih.gov/) (21) and were synthesised by a commercial source (CinnaGen, Iran) (Table S1, See Supplementary Online Information at www.celljournal.org). PCR was performed using Master Mix and SYBR Green I (Fluka, Switzerland) in an Applied Biosystems StepOne™ instrument (Applied Biosystems, UK). Melting curve analyses were used to confirm the quality of the PCR reactions. A standard curve was used to determine the efficiency for each gene (logarithmic dilution series of cDNA from the testes). The reference gene β-*actin* and the target genes were amplified in the same run. This process was repeated and duplicated three times for all target and reference genes. The reference genes were relatively equal, and the target gene expression levels were normalised to that of the reference gene.

Immunohistochemistry

The identity of SSCs, spermatocytes and sperm-like cells was verified by tracking the promyelocytic leukaemia zinc finger protein (PLZF), synaptonemal complex protein 3 (SCP3) and acrosin binding protein (ACRBP) (22-24). These markers were detected after 8 weeks of culture. For immunohistochemistry, primary antibody, mouse monoclonal anti-mouse antibody against PLZF, SCP3 or ACRBP (1:100, Santa Cruz Biotechnology, Germany) was added and the samples were incubated at 4°C overnight. The secondary antibody Alexa 488-conjugated anti-mouse IgG (1:200, Sigma, Germany) was added for 2 hours at 37°C in the dark. For nuclear staining 4′,6-diamidino-2-phenylindole (DAPI, 1:200, Sigma, Germany) was applied for 1 minute. The specimens were observed with a fluorescence microscope (Olympus, type CH2, Japan). To quantify the results, germ cells were defined as cells that stained positive for PLZF, SCP3 and ACRBP. The results are reported as the percentage of germ cells that were positive for the protein of interest relative to the entire population. From each sample, 5 sections were randomly selected and after high-magnification photography (magnification: x400), 5 fields from each section were analyzed by image-j software.

Statistical analysis

The data was analysed using one-way analysis of variance followed by Tukey's post hoc test and are shown as mean ± standard deviation (SD). Calculations were performed using SPSS (Version 15.0, SPSS Inc., USA). Each data point represents the average of three separate experiments, and five repeats were performed for each experiment. A $P \leq 0.05$ was considered to be significant.

Results

Organ culture

Neonatal mouse testicular tissue was cultured on agarose gel and in a mini-perfusion bioreactor (Fig.1A, B). The tissue samples were positioned on agarose gel and in the tissue chamber of the bioreactor (Fig.1C-F). In the agarose cultures, we observed necrotic changes, a hallmark of degenerative changes in the tissue, as darkened regions in the central parts (Fig.2B, (f) white arrow). In the bioreactor, the tissue samples were positioned in the tissue chamber. For the best flow rate, histological analyses were done (Fig.S1, See Supplementary Online Information at www.celljournal.org) and the best flow rate (27 µl/hour) was chosen for the tissue culture in the bioreactor, the central areas of the testicular tissue remained viable, which suggests that this tissue received vital ingredients from the medium.

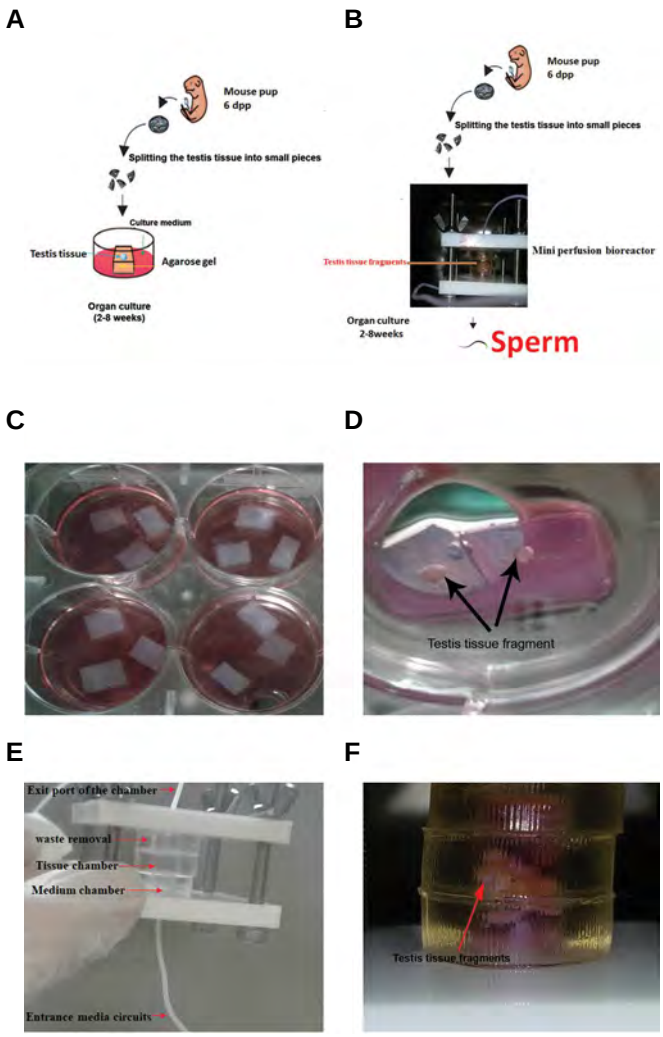

Fig.1: Schematic diagram of the neonatal mouse testicular tissue organ culture. **A.** Testicular tissue pieces placed on agarose gel, **B.** In the bioreactor. **C.** Agarose gel hexahedrons stand transferred to 6-well culture plates. **D.** Testicular tissue was cut to small pieces and placed on agarose gel (black arrows). **E.** Mini-perfusion bioreactor device. **F.** Testicular tissue fragments in the tissue chamber of the perfusion bioreactor system (red arrow).

Viability assessment of cells and tissues

Sertoli cells and spermatogonial cells were cultured with PTFE, PDMS and bioreactor accessories. After 72 hours, viability assay was done by Trypan blue staining, there was no cytotoxic reaction monitored after this co-culture (Fig.2A). Progression of spermatogenesis in organ culture was assessed by bright field and H&E staining for 8 weeks (Fig.2B). In the bioreactor, the central regions of the testicular tissue remained viable, and sperms were distinguished (Fig.2Bg, black arrows). Meanwhile in agarose culture, the central region was degenerated (Fig.2Bf, white arrow) and there was no evidence of existing sperm cells.

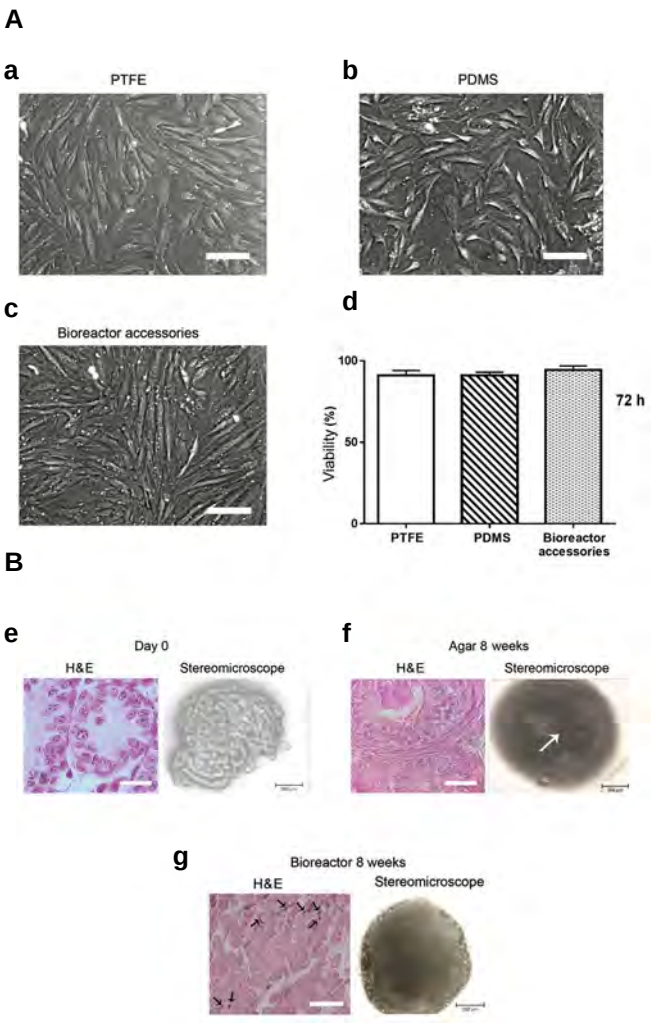

Fig.2: Results of viability assessment of cells, H&E staining and photomicrograph of the testicular sections. **A.** Cell suspension 3 days after culture with PTFE (a), PDMS (b), and bioreactor accessories (c). Viability assay graph of cells after 72 hours of this co-culture (d). **B.** H&E staining and photomicrographs of testicular tissue fragments day 0, 8 weeks of agarose gel and bioreactor culture (e-g). White arrow; Degenerative regions, Black arrows; Sperm cells. H&E images (scale bars e-g: 10 µm, magnification: x1000). PTFE; Polytetrafluoroethylene and PDMS; Polydimethylsiloxane.

Histology, morphology, and functional examinations

Spermatogenesis was maintained in the peripheral areas of the tissue samples cultured on agarose gel (Fig.3A, a, B, b). Histology showed seminiferous tubules exhibiting spermatogenesis in all tissue areas in the tissue cultured in the bioreactor. Different stages of spermatogenesis were seen in different regions of the tissue. Bioreactor cultures showed sperm-like cells after 8 weeks of culture (Fig.3C, c, D, d, Fig.4a). It is noteworthy that tissue integrity was preserved in both groups. In the tissue cultured on agarose gel, tubules were not observed centrally, probably because of the hypoxic conditions and limited access to nutrients. In the agarose gel cultures, no sperm cells were observed in the suspension produced by tissue dissociation (Fig.4b). By contrast, after removal of tissue from the bioreactor and mechanical dissociation, sperm-like cells were observed (Fig.4c), and staining showed that they appeared as normal sperm (Fig.4d-f).

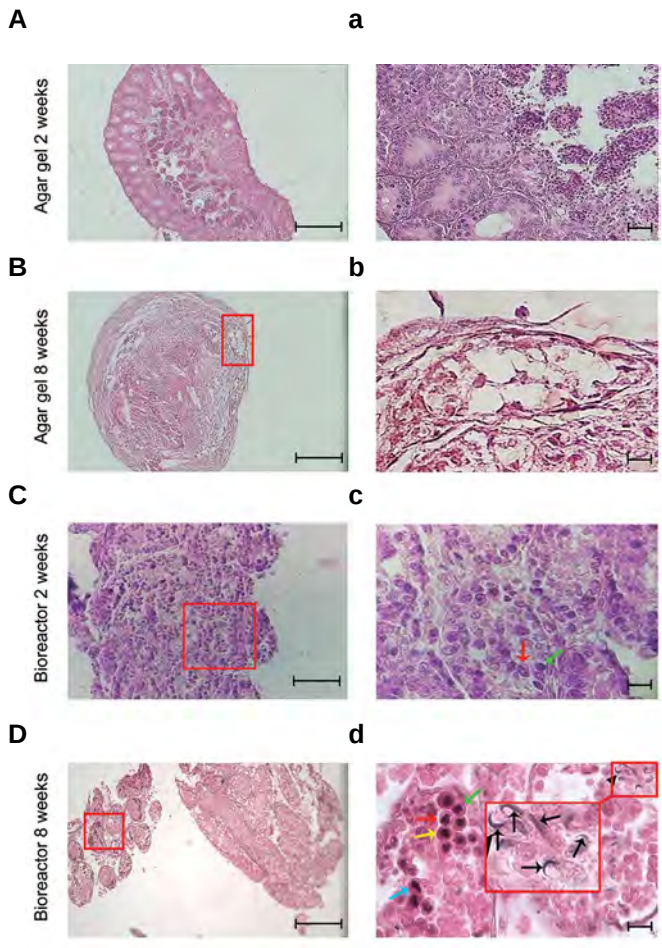

Fig.3: Progression of spermatogenesis in organ culture. **A, B.** H&E staining after 2 and 8 weeks of agarose gel culture, respectively. Higher magnification images of A and B (a, b). **C, D.** H&E staining after 2 and 8 weeks of bioreactor culture, respectively. Higher magnification images of C and D (c, d). Green arrow; Spermatogonia, Red arrow; Spermatocyte (c). Green arrow; Spermatogonia, Red arrow; Primary spermatocyte, Yellow arrow; Secondary spermatocyte, Blue arrow; Spermatid, Arrow head and black arrows; Long spermatids or sperm-like cells (d) [scale bars: 200 µm, magnification: x100 (A, B, D), 30 µm, magnification: x400 (C), 10 µm, magnification: x1000 (a-d)].

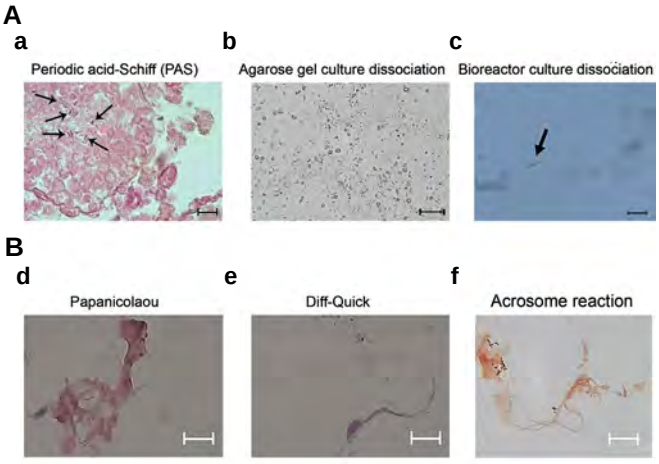

Fig.4: Staining to assess the morphology and function of sperm. After removal of testicular tissue from the bioreactor and mechanical dissociation, Papanicolaou and Diff-Quick staining were used to assess sperm morphology. Sperms were stained by a double staining protocol for acrosome reaction. **A.** Periodic acid-schiff (PAS) staining after 8 weeks of bioreactor culture (a). Black arrows in (a); Sperm cells. Agarose gel culture dissociation (b). Arrow indicates a sperm cell with flagella found in dissociated tissue in the bioreactor group (c). **B.** Papanicolaou staining (d). Diff-Quick staining (e). Acrosome reaction (f) (scale bars: 10 µm, magnification: x1000).

Molecular assessment

2 and 8 weeks after 3D culture, bioreactor and agarose gel groups were compared with neonatal testis. *Plzf* expression was significantly lower (P≤0.05) in both the bioreactor and agarose gel groups than in fresh neonatal testis. However, *Plzf* expression did not differ significantly between the bioreactor and agarose gel groups (Fig.5A, B). *Tekt1* and *Tnp1* expression also did not differ significantly between the groups after the 2-week culture period (Fig.5A). *Tekt1* and *Tnp1* expression after the 8-week culture was significantly higher (P≤0.05) in all groups compared with fresh neonatal testis (Fig.5B). 8 weeks after 3D culture, the bioreactor and agarose gel groups were compared with adult testis. Additionally, *Plzf* gene expression indicated that there was no significant difference between the groups. *Tekt1* expression was significantly lower in both culture groups than in adult mice testicular tissue but did not differ significantly between the two groups. *Tnp1* expression was significantly lower in the agarose group than in the adult mice testicular tissue after 8 weeks but did not differ significantly between the bioreactor culture and adult mouse testicular tissue (Fig.5C).

Immunohistochemistry

PLZF protein was expressed in the tissues that showed spermatogonial cells. SCP3 protein, was detected in the spermatocytes and in ACRBP-positive cells, indicating the existence of sperm-like cells (Fig.6). Quantification of the immunohistochemical staining indicated that PLZF expression was significantly lower (P<0.05) in adult tissue and both the bioreactor and agarose groups than in neonatal tissue. However, there was no difference at 8 weeks between the bioreactor culture and adult expression levels. At 8 weeks, PLZF expression was significantly reduced in the agarose gel group compared with that of the adult tissue and bioreactor groups. At 8 weeks, the SCP3 and ACRBP expression levels were significantly lower in both the agarose and bioreactor groups than in adult tissue but did not differ significantly between the bioreactor and agarose gel groups (Fig.6).

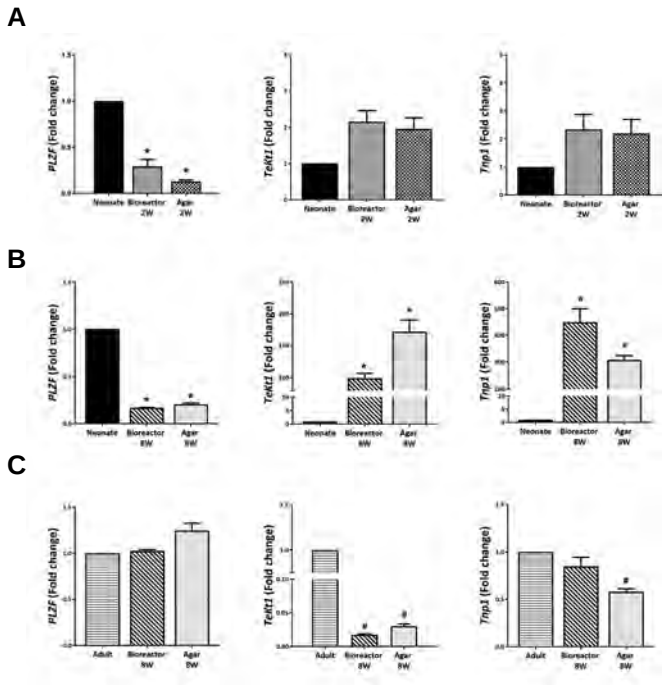

Fig.5: Gene expression in testicular tissue fragments in experimental groups. Expression of *Plzf*, *Tekt1* and *Tnp1* gene was assessed in tissues cultured in the bioreactor and on agarose gel for 2 and 8 weeks. **A-C.** Expression level was normalised to that of β-actin and is represented as mean ± SD after three repeats of the experiments. *; P<0.05 versus neonate and #; P<0.05 versus adult. Similar symbols indicate no significant differences between those groups.

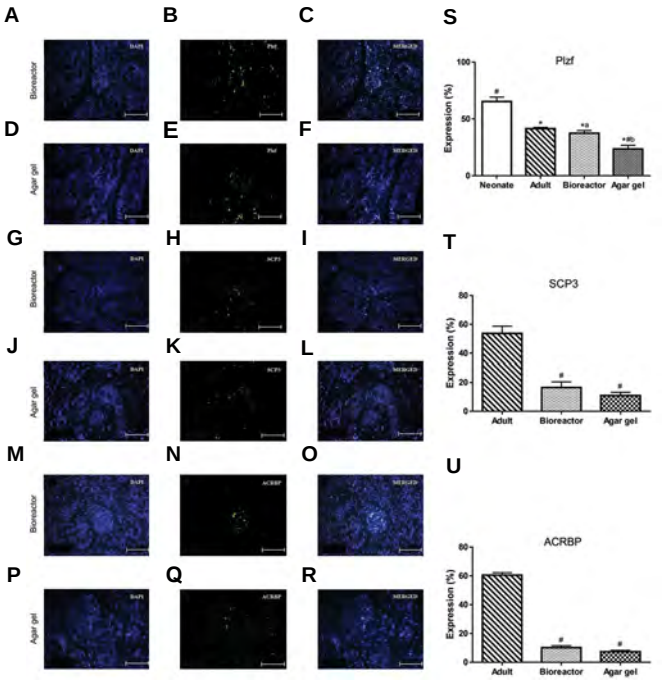

Fig.6: Immunohistochemistry of neonatal mouse testicular tissue after 8 weeks of organ culture. **B, H, N.** Expression of specific protein of spermatogonial cells (PLZF), spermatocytes (SCP3) and spermatozoa (ACRBP) in the bioreactor and **E, K, Q.** On agarose gel, respectively. **A-P.** Nuclei were stained by DAPI. **C-R.** The merged images. **S-U.** Expression of specific protein in experimental groups. Data are represented as mean ± SD of experiments performed in triplicate. #; P<0.05 versus adult and *; P<0.05 versus neonate. a and b indicate P<0.05 versus the respective between the bioreactor and agarose gel (scale bars: 10 µm).

Discussion

3D tissue culture is an effective technique for the preservation and development of various tissues, including germinal tissues. In this study, we developed a mini-scale perfusion bioreactor and compared it with agarose gel for 3D culture of immature mouse testicular tissue. Inside the body, capillaries around a tissue provide oxygen and nutrients and clear waste effectively, thereby supporting tissue homeostasis (9).

SSCs and A-pair/A-aligned spermatogonia have been suggested to be limited to the surrounding vasculature and interstitial tissue around the seminiferous tubules (25). A number of factors are responsible for diffusion within culture, such as cell density, tissue thickness and concentration of the materials on the tissue surface (26). In 3D cultures, static flow might lead to the formation of passive gradation of materials that will be equilibrated over the long term. Therefore, a forced but controlled culture medium perfusion is indispensable (27).

In the method using agarose gel, extensive induction of spermatogenesis did not happen because seminiferous tubules on the agarose gel merged to create a dome-shaped structure even if initially extended flat. As a result, the supply of nutrients and oxygen to the central region was insufficient, which led to necrotic and degenerative changes in the tissue (9). Thus, for the lack of microcirculatory system, the agarose gel method cannot provide conditions similar to those *in vivo*. Given the failure of the static culture methods, dynamic culture methods seem to be more effective in increasing spermatogenesis and producing haploid cells in a more effective 3D culture system that provides optimal conditions that simulate the physiological environment of the body. These conditions include temperature, oxygen and carbon dioxide content, mechanical, chemical and electrical stimulation, and improved access to nutrients and elimination of waste. Together, these factors should help to prevent necrosis in the central region of the tissue.

In this study, it was shown that the mini-perfusion bioreactor could induce more efficient spermatogenesis than the agarose gel method when loaded with mouse testis tissue and that this effect was consistent for 8 weeks. We had hypothesised that a dynamic culture system would adequately supply the tissue with oxygen and nutrients through the effective exchange of molecules in culture medium streaming across the tissue surface (28). Throughout the 8 weeks of culture on agarose gel, spermatogenesis was maintained only in the peripheral parts of the tissue. We suggest that, apart from the effective transfer of molecules between testis tissue and the culture medium, the tissues inside the mini-perfusion bioreactor were supplied with a greater amount of oxygen through the PDMS. If so, this would reduce oxygen toxicity in comparison with direct exposure (29-31).

It is also possible that the tissue chamber of the mini-perfusion bioreactor might also help to replicate the chemical environment of the body. For example, the porous membrane that disconnects the tissue chamber from the streaming medium, should increase the retention of the secreted molecules in the chamber. It is important to maintain efficient exchange and balance of molecules between the tissue and the medium (32). A dynamic system will achieve such a balance more easily than a static system, which is why it was suggested that the mini-perfusion bioreactor we used better fulfills this requirement compared with the agarose gel method.

The findings suggest that the mini-perfusion bioreactor can promote differentiation up to the stage of post-meiotic spermatozoa. It was concluded that the mini-perfusion bioreactor may be useful for developing a dynamic culture system for the maturation of premeiotic mouse germ cells to post-meiotic levels as well as morphologically normal spermatozoa. Such findings are consistent with those of Komeya et al. (9, 33).

Molecular changes in germ cells are useful for stimulating spermatogenesis. Our real-time PCR analysis of specific markers (*Plzf*, *Tekt1* and *Tnp1*) after 8 weeks of culture in the bioreactor and agarose gel revealed the presence of premeiotic, meiotic and post-meiotic cells, respectively. *Tnp1* expression after 8 weeks was significantly lower in the agarose group than in the adult mouse testicular tissue but did not differ significantly between the bioreactor culture and adult mouse testicular tissue. The mini-perfusion bioreactor provided sufficient nutrients and oxygen for tissue culture. In the tissue cultured on agarose gel, tubules were not observed centrally, probably because of the hypoxic conditions and limited access to nutrients. In the agarose cultures, we observed necrotic and degenerative changes in the central parts of tissue. Therefore, expression was lower in the agarose group after 8 weeks of culture compared to the bioreactor and adult groups. Yokonishi et al. (34) reported the presence of spermatid cells and sperm, which resulted in the formation of embryos. Aflatoonian et al. (35) reported the successful *in vitro* production of post-meiotic spermatid cells. Alrahel et al. (36) reported the expression of the post-meiotic gene, *Tnp1*, but only at the molecular scale and not beyond meiosis.

Immunohistochemical analyses have shown that epithelial cells express PLZF, SCP3, and ACRBP proteins, which are exclusive to SSCs, spermatocytes and spermatozoa, respectively. Our immunofluorescence analysis of the tissues after 8 weeks of culture in the bioreactor and agarose gel on these specific markers (PLZF, SCP3, ACRBP) showed the presence of premeiotic, meiotic, and post-meiotic cells.

Our results are in line with those of Mohaqiq et al. (37). Immunohistochemical studies of Rahmani et al. (38) showed the expression of the premeiotic marker PLZF in SSCs and undifferentiated spermatogonia. The immunohistochemical analysis of Gharenaz et al. (39) verified that PLZF-positive cells (spermatogonial stem cells) and SYCP3-positive cells (spermatocytes) exist

in the seminiferous tubules. Also in the agarose gel cultures, no sperm were observed in the suspension produced by tissue dissociation. By contrast, after removal of tissue from the bioreactor and mechanical dissociation, sperm- like cells were observed, suggesting that maturation to elongated spermatids is stopped on the agarose gel culture.

We were able to improve the culture conditions for testis tissues using our bioreactor for tissue culture. Bioreactor systems may prove valuable for preventing ischemia and facilitating the long-term culture of testis tissue. However, further research is needed to investigate the effects of enriching the culture medium with different supplements and growth factors. In the bioreactor system we are able to culture the tissue pieces (size 1 mm^3) but in the microscale dynamic culture systems only the seminiferous tubules can be cultured in the microchannels. Also at the end of the culture period, tissue removal from the middle chamber of the bioreactor is easily performed, but the extraction of the seminiferous tubules from the microchannels of other devices seems more complicated and difficult (40). Our bioreactor device is very simple, easy to use or user friendly, and more economically feasible than existing ones. Bioreactors can be optimised further by adjusting parameters including tissue chamber dimensions (particularly height), PDMS wall thickness, medium flow speed, and membrane porosity, and pore size. Such optimizations and other improvements of the culture medium could pave the way for developing new organ culture methods in the future.

Conclusion

The culture of testis tissues was improved by using a mini-perfusion bioreactor. Future studies are needed to determine the optimal culture conditions, for example the speed of flow of the medium and size of the tissue chamber. Optimisation of the culture conditions, including the culture medium may help to improve the methods for organ cultivation.

Acknowledgements

This study was supported by a grant from the Research Deputy of Tarbiat Modares University (TMU), Tehran, Iran. The authors declare no conflict of interest in this project.

Authors' Contributions

Z.A.; Performed all laboratory procedures, data collection, evaluation, statistical analysis, and drafted the manuscript. M.M.; Participated in the study design, revised the manuscript, contributed extensively in interpretation of the data and the conclusion. N.B.; Performed advising also performed editing the final version of this paper. A.Gh.; Designed the bioreactor, contributed to data and statistical analysis, and interpretation of data. All authors read and approved the final manuscript.

References

1. Champy C. Quelques résultats de la méthode de culture des tissus. Arch Zool Exp Gen. 1920; 60: 461-500.
2. Steinberger A, Steinberger E,Perloff W. Mammalian testes in organ culture. Exp Cell Res. 1964; 36(1): 19-27.
3. Staub C. A century of research on mammalian male germ cell meiotic differentiation in vitro. J Androl. 2001; 22(6): 911-926.
4. Trowell O. The culture of mature organs in a synthetic medium. Exp Cell Res. 1959; 16(1): 118-147.
5. Sato T, Katagiri K, Gohbara A, Inoue K, Ogonuki N, Ogura A, et al. In vitro production of functional sperm in cultured neonatal mouse testes. Nature. 2011; 471(7339): 504-507.
6. Chapin R E, Boekelheide K, Cortvrindt R, Van Duursen M B, Gant T, Jegou B, et al. Assuring safety without animal testing: the case for the human testis in vitro. Reprod Toxicol. 2013; 39: 63-68.
7. Perrard M-H, Sereni N, Schluth-Bolard C, Blondet A, d′ Estaing S G, Plotton I, et al. Complete human and rat ex vivo spermatogenesis from fresh or frozen testicular tissue. Biol Reprod. 2016; 95(4): 89, 81-10.
8. Komeya M, Hayashi K, Nakamura H, Yamanaka H, Sanjo H, Kojima K, et al. Pumpless microfluidic system driven by hydrostatic pressure induces and maintains mouse spermatogenesis in vitro. Sci Rep. 2017; 7(1): 1-8.
9. Komeya M, Kimura H, Nakamura H, Yokonishi T, Sato T, Kojima K, et al. Long-term ex vivo maintenance of testis tissues producing fertile sperm in a microfluidic device. Sci Rep. 2016; 6(1): 1-10.
10. Nowacki D, Klinger F, Mazur G, De Felici M. Effect of culture in simulated microgravity on the development of mouse embryonic testes. Adv Clin Exp Med. 2015; 24(5): 769-774.
11. Yamanaka H, Komeya M, Nakamura H, Sanjo H, Sato T, Yao M, et al. A monolayer microfluidic device supporting mouse spermatogenesis with improved visibility. Biochem Biophys Res Commun. 2018; 500(4): 885-891.
12. Garziano A, Urciuolo F, Imparato G, Martorina F, Corrado B,Netti P. A micro-perfusion bioreactor for on line investigation of ECM remodeling under hydrodynamic and biochemical stimulation. Lab Chip. 2016; 16(5): 855-867.
13. Gharravi A M, Orazizadeh M, Ansari-Asl K, Banoni S, Izadi S, Hashemitabar M. Design and fabrication of anatomical bioreactor systems containing alginate scaffolds for cartilage tissue engineering. Avicenna J Med Biotechnol. 2012; 4(2): 65-74.
14. Pazzano D, Mercier K A, Moran J M, Fong S S, DiBiasio D D, Rulfs J X, et al. Comparison of chondrogensis in static and perfused bioreactor culture. Biotechnol Prog. 2000; 16(5): 893-896.
15. Dadgar N, Ghiaseddin A, Irani S, Rabbani S, Tafti S H A, Soufizomorrod M, et al. Cartilage tissue engineering using injectable functionalized demineralized bone matrix scaffold with glucosamine in PVA carrier, cultured in microbioreactor prior to study in rabbit model. Mater Sci Eng C. 2021; 120: 1-10.
16. Yokonishi T, Sato T, Katagiri K, Ogawa T. In vitro spermatogenesis using an organ culture technique. Methods Mol Biol. 2013; 927: 479-488.
17. Russell LD, Ettlin RA, Hikim APS, Clegg ED. Histological and histopathological evaluation of the testis. Int J Androl. 1993; 16(1): 83.
18. World Health Organization. Examination and processing of human semen. 5th ed. Geneva: WHO Press; 2010.
19. Kruger T, Ackerman S, Simmons K, Swanson R, Brugo S, Acosta A. A quick, reliable staining technique for human sperm morphology. Arch Androl. 1987; 18(3): 275-277.
20. Köhn F, Mack S, Schill W, Zaneveld L. Detection of human sperm acrosome reaction: comparison between methods using double staining, Pisum sativum agglutinin, concanavalin A and transmission electron microscopy. Hum Reprod. 1997; 12(4): 714-721.
21. Nayernia K, Li M, Jaroszynski L, Khusainov R, Wulf G, Schwandt I, et al. Stem cell based therapeutical approach of male infertility by teratocarcinoma derived germ cells. Hum Mol Genet. 2004; 13(14): 1451-1460.
22. Ibtisham F, Wu J, Xiao M, An L, Banker Z, Nawab A, et al. Progress and future prospect of in vitro spermatogenesis. Oncotarget. 2017; 8(39): 66709-66727.
23. Lee WY, Lee R, Park HJ, Do JT, Park C, Kim JH, et al. Characterization of male germ cell markers in canine testis. Anim Reprod Sci. 2017; 182: 1-8.
24. Tardif S, Guyonnet B, Cormier N, Cornwall GA. Alteration in the processing of the ACRBP/sp32 protein and sperm head/acrosome

malformations in proprotein convertase 4 (PCSK4) null mice. Mol Hum Reprod. 2012; 18(6): 298-307.
25. Potter S J, DeFalco T. Role of the testis interstitial compartment in spermatogonial stem cell function. Reproduction. 2017; 153(4): R151-R162.
26. Griffith L G,Swartz M A. Capturing complex 3D tissue physiology in vitro. Nat Rev Mol Cell Biol. 2006; 7(3): 211-224.
27. Volkmer E, Drosse I, Otto S, Stangelmayer A, Stengele M, Kallukalam B C, et al. Hypoxia in static and dynamic 3D culture systems for tissue engineering of bone. Tissue Eng Part A. 2008; 14(8): 1331-1340.
28. Tehranirokh M, Kouzani A Z, Francis P S, Kanwar J R. Microfluidic devices for cell cultivation and proliferation. Biomicrofluidics. 2013; 7(5): 51502.
29. Kojima K, Nakamura H, Komeya M, Yamanaka H, Makino Y, Okada Y, et al. Neonatal testis growth recreated in vitro by two-dimensional organ spreading. Biotechnol Bioeng. 2018; 115(12): 3030-3041.
30. Komeya M, Yamanaka H, Sanjo H, Yao M, Nakamura H, Kimura H, et al. In vitro spermatogenesis in two-dimensionally spread mouse testis tissues. Reprod Med Biol. 2019; 18(4): 362-369.
31. Sharma S, Venzac B, Burgers T, Le Gac S, Schlatt S. Microfluidics in male reproduction: is ex vivo culture of primate testis tissue a future strategy for ART or toxicology research? Mol Hum Reprod. 2020; 26(3): 179-192.
32. Yu H, Alexander C M,Beebe D J. Understanding microchannel culture: parameters involved in soluble factor signaling. Lab Chip. 2007; 7(6): 726-730.
33. Komeya M, Sato T, Ogawa T. In vitro spermatogenesis: a century-long research journey, still half way around. Reprod Med Biol. 2018; 17(4): 407-420.
34. Yokonishi T, Sato T, Komeya M, Katagiri K, Kubota Y, Nakabayashi K, et al. Offspring production with sperm grown in vitro from cryopreserved testis tissues. Nat Commun. 2014; 5(1): 1-6.
35. Aflatoonian B, Ruban L, Jones M, Aflatoonian R, Fazeli A, Moore H. In vitro post-meiotic germ cell development from human embryonic stem cells. Hum Reprod. 2009; 24(12): 3150-3159.
36. Alrahel A, Movahedin M, Mazaheri Z, Amidi F. Study of Tnp1, Tekt1, and Plzf genes expression during an in vitro three-dimensional neonatal male mice testis culture. Iran Biomed J. 2018; 22(4): 258-263.
37. Mohaqiq M, Movahedin M, Mazaheri Z, Amirjannati N. In vitro transplantation of spermatogonial stem cells isolated from human frozen–thawed testis tissue can induce spermatogenesis under 3-dimensional tissue culture conditions. Biol Res. 2019; 52(1): 16.
38. Rahmani F, Movahedin M, Mazaheri Z, Soleimani M. Transplantation of mouse iPSCs into testis of azoospermic mouse model: in vivo and in vitro study. Artif Cells Nanomed Biotechnol. 2019; 47(1): 1585-1594.
39. Gharenaz NM, Movahedin M, Mazaheri Z. Three-dimensional culture of mouse spermatogonial stem cells using A decellularised testicular scaffold. Cell J. 2020; 21(4): 410-418.
40. Tokuoka Y, Kondo K, Nakaigawa N, Ishida T. Development of a microfluidic device to form a long chemical gradient in a tissue from both ends with an analysis of its appearance and content. Micromachines (Basel). 2021; 12(12): 1482.